Tidal analysis of the South China Sea

Prepared by:

Cemali Akdag
Delft, October 1996

Study tutors:

Prof. dr. ir. G.S. Stelling .....(Delft Hydraulics & Delft UT)
Prof. dr. ir. J.A. Battjes .....(Delft UT)
Ir. H.J.M.G. Steeghs .....(Delft Hydraulics)
Dr. ir. H. Gerritsen .....(Delft Hydraulics)
Dr. ir. N. Booij .....(Delft UT)

TU Delft

Delft University of Technology
Faculty of Civil Engineering
Group of Fluid Mechanics

Delft Hydraulics

Contents

Preface and Acknowledgements ... iii

Abstract ... vi

List of Symbols ... ix

1 Introduction ... *1–1*

2 The South China Sea ... *2–1*

2.1 Geography of the study area ... 2–1

2.2 Tides and Tidal Currents in the South China Sea ... 2–5
2.2.1 The semi-diurnal tidal constituents ... 2–8
2.2.2 The diurnal tidal constituents ... 2–10
2.2.3 Review of the tidal behaviour of the study area ... 2–11

2.3 Geographical distribution of tidal types ... 2–13

2.4 Tidal Currents and velocities ... 2–16

2.5 Additional remarks ... 2–18

3 Modelling the South China Sea ... *3–1*

3.1 South China Sea modelling in the past ... 3–1

3.2 The DELFT HYDRAULICS' South China Sea Model ... 3–3

3.3 How to go on with the South China Sea Model? ... 3–13
3.3.1 Sulu Sea ... 3–13
3.3.2 Java Sea ... 3–14
3.3.3 Malacca Strait ... 3–14
3.3.4 Gulf of Thailand ... 3–14
3.3.5 Possible incomplete modelling ... 3–15

3.4 Additional remarks ... 3–15

4 Problem analysis ... *4–1*

4.1 The Sulu Sea: an overview ... 4–1

4.2 Tides in the Sulu Sea ... 4–3
4.2.1 Analysis of tidal constituents from observations ... 4–5
4.2.2 Conclusions according to observed analyses ... 4–9

4.3 1-D TRISULA sensitivity analysis ... 4–9

4.4 The 1-D analytical model ... 4–11
4.4.1 Overview of the Sulu Sea as a basin system ... 4–12

4.5 Results of the 1-D harmonic analysis ... 4–13
4.5.1 Introduction ... 4–13
4.5.2 Discussion of the results ... 4–13

4.6 Development of water levels along the length axis ... 4–15

4.7 How to use the results of the 1-D analysis of the Sulu Sea? ... 4–17

4.8 Conclusions ... 4–19

5 TRISULA SCSM computations ... *5–1*

5.1 Introduction ... 5–1

5.2 Computation C01: tide generating forces 5–1
5.2.1 Semi-diurnal tides 5–1
5.2.2 The diurnal tides 5–3

5.3 Computation C02: exclusion of the Sulu Sea 5–4
5.3.1 Semi-diurnal tides 5–4
5.3.2 Diurnal tides 5–5

5.4 Computations C04 and C05 5–6

5.5 Conclusions of TRISULA computations 5–7

6 Conclusions and Recommendations 6–1

References xi

List of figures and tables xiii

Appendix 1: Introduction into tides 1

Appendix 2: Charts and Tidal data 15

Appendix 3: The 1-dimensional approach 26

Appendix 4: TRISULA computation results 71

Abstract

The region of South China Sea and the Indonesian waters, covering an area of about 9 million km^2, is characterised by a very complex tidal behaviour. This region, which will be called the South China Sea throughout this report, is entangled between the Pacific Ocean and the Indian Ocean. Therefore the tides in the South China Sea are driven by these two oceans.
Beside the co-oscillating nature of tides from two different oceans, the geography and the topography of the South China Sea are other essential elements in the complex tidal behaviour. Deep sea basins as well as shallow areas exist in the region. The geography is such, that the whole South China Sea can be thought of as existing of separate basins with each basin having its own tidal characteristics.
The complexity of the tides of the area is described by various authors. Tidal modelling of the area appears to be a hard task: no complete reliable hydraulic model of the area is constructed yet. Results of hydrodynamic models by different investigators seem to be widely different.
In June 1993, DELFT HYDRAULICS designed a tidal model of the South China Sea as well. The South China Sea Model, as it was called, comprised the southern parts of the South China Sea, the Sunda Shelf, Macassar Strait, Malacca Strait, Celebes Sea and the Sulu Sea. The results of this model so far are not completely satisfactory. So further calibration seems necessary.
One of the new topics of research that was suggested within the line of the South China Sea Model, was the construction of a more simplified representation of the study area. Before useful calibration of the model, this would help to study and understand basic mechanisms that control the tidal behaviour of this area. The representation should be as simple as possible but still incorporate the essential features of the hydrodynamic behaviour of the area. It should be suited as an analysis tool and produce insight into the elementary mechanisms at low expenditure in terms of time and computational effort.
This report describes a few steps to obtain this basic understanding. First the tidal behaviour of the South China Sea is thoroughly analysed once more, to get a clearer picture of the system's behaviour that has to be represented or reproduced. The complexity of the tides of the area and the reasons for this are summarised and, if possible, put into a figure.
Second the results of the various (numerical) models are discussed to find the reason for of difficulties with the tidal modelling. As described above, hydrodynamic modelling of the area turned out to be very difficult; results produced so far by different investigators do not always match. Even in the number of and rotating directions around amphidromic points sometimes differ. Also the "South China Sea Model" results until now were analysed in detail.

The main problem areas of the South China Sea Model are:

- *The Sulu Sea*: Tides enter this almost closed and rectangular basin from two opposite sides through narrow passages between tiny islands. The sizes of these passages are hard to be schematised in a relatively coarse numerical model. As the result of this, the modelling results for this sea and large parts of the neighbouring seas are insufficient.
- *The Malacca Strait*: the conic formed strait is characterised by extreme depth and width changes. There are lots of tiny islands at the mouth of this strait in the Java Sea, that negatively affect the modelling results. The extreme depth changes over relatively small distances and the tiny islands are difficult to schematise, in a relatively coarse grid. The results of this are affecting the large neighbouring areas, especially the Java Sea.
- *The Java Sea*: The model results for the Java Sea are insufficient as well. This is partly because of poor results originating from the Sulu Sea and the Malacca Strait. Moreover there are passages connecting the Java Sea with the Indian Ocean, which

are also hard to schematise because of their dimensions, but important enough to take into account the influence of tides from the Indian Ocean.

- *Possible modelling errors*: The tide generating forces were neglected in the past in all the model computations. Moreover, after studying the results of computations, the positioning of the model boundaries were doubted.

The third item of the study was an investigation of the applicability of a 1-D box model approach to stimulate the complex tidal behaviour of the study area. This approach was chosen in order to understand the sensitivity of the tidal behaviour in relation to various relevant parameters such as topography, modelling of passages, behaviour of some specific basins etceteras.
As a start this approach was applied to the Sulu Sea region only, leaving the total South China Sea area to be covered later once the method had shown its usefulness. The Sulu Sea was modelled as a connection of four basins, of which the outer basins represented the narrow passages, and the inside basins represented the deep sea basins of the Sulu Sea itself. At the open boundaries (at the two edges), water levels were given as boundary conditions and transition conditions of mass and momentum were prescribed between the basins. The reason for the choice of the Sulu Sea was a logical consequence of the major modelling difficulties there and its assumed influences for the rest of the South China Sea Model area.
Finally some new calculations were made with the South China Sea Model. These calculations were for some part the logical consequence of the study results of this project and for some part originating from ideas of former studies. One of the interesting calculations is for instance the model calculation with tide generating forces introduced in the model for the first time.

The study of the tidal behaviour of the South China Sea, as described in this report must be considered as not yet completed. There are lots of subjects, which still need to be looked into separately and thoroughly.
The results from the 1-D approach to the Sulu Sea indicate that it might be impossible to calibrate this model for three different stations to the desired outcomes, given two water level boundary conditions from two opposite sides. However this experiment underlined once more the sensitivity of this part of the model area to the schematization of the passages. This sensitivity is also underlined with a South China Sea Model computation excluding the Sulu Sea. The overall results, mainly of the areas neighbouring to Sulu Sea, were remarkably different.
The gridsize of the South China Sea Model in its final state (0.26`*0.26`), is too large to schematise the abrupt depth changes, small passages and the tiny islands. Problems due to this coarse grid for instance occur in the Malacca Strait, Sulu Sea, Lombok and Sape Straits and the Sunda Shelf edges.
Results of the first calculation of the model with tide generating forces fell short of expectations: the results showed some major differences with former model calculations and in general they could not be considered as improving the model. This leads to the conclusion that the difficulties with the South China Sea Model in its present state are not fully understood so far.
The location of the boundaries of the South China Sea Model must be reanalysed once more. Perhaps it would be advantageous to replace the positions of open boundaries at narrow passages of Lombok and Sape. In that case the grid enclosure should be enlarged to the south. In situations when the problems of the Sulu Sea and Malacca Strait seem not to be solved that easily, these areas could be excluded from the grid enclosure of the model as an attempt to set up the other parts of the model domain first.
Analysing the sensitivity problems, such as the Sulu Sea, the Malacca Strait and the Lombok and Sape Straits is still believed to be possible with a simplified model. An adapted version of the 1-dimensional method as used in this report or a 2-dimensional spectral or applied

harmonic analysis methods are suggested to future investigators. Also some of the interactive program packages of DELFT HYDRAULICS' can be thought of for the analysis of this problem.

List of Symbols

Symbol	Meaning	Dimension
a	Wave amplitude	m
b	Specific width; in chapter 4	m
B	Specific width	m
c	Wave celerity	m/s
f	Tide form number	-
g	Acceleration of gravity	m/s^2
h	Mean depth relative to reference water level	m
H	Water depth including elevation ($H=h+\xi$)	m
k	Wave number ($= {}^{2\pi}/_{L}$)	m^{-1}
l	Distance or length	m
L	Specific (basin) length	m
L_t	Total length (in chapter 4)	m
t	Time	s
Q	Discharge	m^3/s
T	Wave period	s
u	Velocity in x-direction	m/s
v	Velocity in y-direction	m/s
x	Distance along horizontal axis parallel to main flow direction	m
y	Distance along horizontal axis perpendicular to main flow direction	m
z	Water elevation in relation to reference level (used in graphs of the appendices)	m
Δ	Relative change or lag	-
λ	Wave length	m
ς	Water elevation in relation to reference level	m
θ	Resulting phase; in chapter 4	rad (or deg)
φ	Phase of propagating wave	rad (or deg)
ϕ	Phase of resulting wave; in chapter 4	rad (or deg)
ψ	Phase of reflected wave	rad (or deg)
ω	Angular frequency in waves ($= {}^{2\pi}/_{T}$)	s^{-1}

Special signs	
$\approx$	Almost equals
[ ]	Matrix notation
$\rightarrow$	Vector notation
<<	Much less than

1 Introduction

The tidal movements in the South China Sea and Indonesian waters are complex. One of the main reasons of this complexity is the geographical configuration of this area. The South China Sea together with the Indonesian waters, can be thought of as a system of several connected basins with each basin having its own characteristics. These characteristics are e.g. the coastal patterns and bottom topography. The bottom topography of the South China Sea together with the Indonesian waters are strongly varying: deep sea regions as well as shallow parts can be found in various basins.
As the result of the geographical positioning between the Indian and Pacific Oceans, the tides in the study area can be thought of co-oscillating tides from these two oceans. Tidal waves enter the study area from different directions. Combining this with the varying bottom topography and the presence of many tiny islands and small passages, the complexity of the tides can be explained.
This complexity is one of the main reasons that numerical modelling of the hydrodynamics in this area is puzzling. Different authors describe different results.
Within DELFT HYDRAULICS a tidal model of this area was constructed as well. This model is called the "South China Sea Model" and included the southern part of the South China Sea and the Indonesian Waters. The results of this model so far are not completely satisfactory. So further calibration seems necessary.
One of the new topics of research that was suggested within the line of the South China Sea Model, was the construction of a more simplified representation of the study area. Before useful calibration of the model, this would help to study and understand basic mechanisms that control the tidal behaviour of this area. It should be suitable as an analysis tool and produce insight into the elementary mechanisms at low expenditure in terms of time and computational effort.
As a first step an analytical (instead of numerical) approach for simplified equations was tested. The present report describes the masters degree study, that the author has performed at DELFT HYDRAULICS within the framework sketched above. His study covers the following items:

- First the tidal behaviour of the South China Sea is analysed again to establish a clearer picture of the system's behaviour.
- Second the results of the various (numerical) models are studied to find the reason why the tides in the area are that complicated that model representation is still limited. The search for the sensitivity of relevant parameters (such as topography, modelling of passages, behaviour of some specific basins) is one of the main goals of this part of the study.
- The third item is an investigation of the applicability of a 1-D box model approach to stimulate the complex tidal behaviour of the study areas. As a start this approach was applied to the Sulu Sea region only, leaving the total South China Sea area to be studied later once the method has shown its usefulness.

This report is built up in the following order:

In **chapter 1** the study area will be described. The geography of the area will be explained with the help of charts and an overview will be given of the observed tidal movements of the area.
In **chapter 2** a global view will be given of some previous efforts for modelling of the tides and detailed description will be made of the DELFT HYDRAULICS' South China Sea Model. In this same chapter the South China Sea Model will be split in elementary problem regions and

suggestions will be given for the solution of modelling problems regarding these regions. The South China Sea Model as it exists at the moment, will be discussed as well.

In **chapter 3** analyses will be made of two main regions of the model area: Malacca Strait and the Sulu Sea. These regions are believed to locally cause inaccurate modelling results, and these results are further believed to disturb modelling results in other neighbouring regions of the model domain. Therefore the tides in these two regions will be looked at separately.

Chapter 4, in which a 1-dimensional approach is chosen to discover the sensitivity of tidal waves in one of these regions: the Sulu Sea. First a 1-dimensional wave propagation approach of a simplified basin is made with TRISULA, DELFT HYDRAULICS' simulation program for hydrodynamic flows in two and three dimensions. Furthermore a computer program has been generated to envision the Sulu Sea as a connection of basins with tidal waves entering this system of basins from two opposite directions.

In **chapter 5**, discussions of the latest computations with the South China Sea Model will be made. A number of these computations is a logical consequence of the results of analyses described in this report. One of these computations for example, is a computation with tide generating forces introduced in the model for the first time. The results of these computations will be compared to the best made computation so far.

Final remarks and conclusions regarding this project will be given in **chapter 6**. The masters degree study reported here covers only part of the work that has been started to try and understand the difficulties in modelling the South China Sea area.

This report also contains a number of **appendices**. The *Appendix 1* contains a brief theory of the tides in general. In *Appendix 2*, there are maps of the study area with one of them containing the geographical names used throughout this report. Furthermore there are detail maps of the Malacca Strait and the Sulu Sea including a number of tidal stations identified in these regions. Tables with data consisting of the phases and amplitudes of the four most important tidal constituents for these stations are also included. *Appendix 3* contains the generation and validity tests of a self constructed 1-D model based on harmonic analysis. Furthermore it contains some results of the 1-dimensional TRISULA and 1-dimensional harmonic approaches. In this same appendix a printed output of one of the programmed files of the 1-D analysis is included as well. The last appendix, *Appendix 4*, contains the results of the latest South China Sea Model TRISULA computation results. Analyses of these runs were made with DELFT HYDRAULICS' TRIANA package, which are given in Appendix four, as are the observed values of the identified stations for the four determining tidal constituents.

2 The South China Sea

In this chapter the geographical aspects of the South China Sea and the Indonesian waters will be presented. After that, the general tidal movement in the area and some complicating elements will be dealt with.

Additional information which can be helpful with the study of this chapter, can be found in Appendices 1 and 2. Appendix 1 deals among others with general theory of tides and Appendix 2 contains some charts of the area. In Figure A 2.2 of Appendix 2, the topography of the area is presented with most of the geographical names used throughout this report.

2.1 Geography of the study area

The South China Sea together with the Indonesian waters constitute the area that can be found between the two continents Asia and Australasia and between the two oceans of Indian Ocean and Pacific Ocean. The study area, which will be called the South China Sea throughout this report, is shown in Figure 2.1. In this region extensive shallow water areas as well as deep oceanic basins exist as shown in Figure A2.1.
The study area is also an equatorial area (see Figure 2.2 on page 2–3 and Figures A2.1 & A2.2 of Appendix 2) including the South China Sea (southern part), the Sunda Shelf (including Java Sea), Malacca Strait, Sulu Sea, Celebes Sea, Flores Sea and Macassar Strait. It is not only an area which is the meeting point of two Oceans and two continents, but also an intersection point for humans of different cultures and religions. A wide and unique range of ecological beauties can be found in this region as well. Oceanographically, the region is considered to be part of the Pacific Ocean, geographically it is considered to be part of the Asian Continent.

Figure 2.1: Positioning of the study area in the world

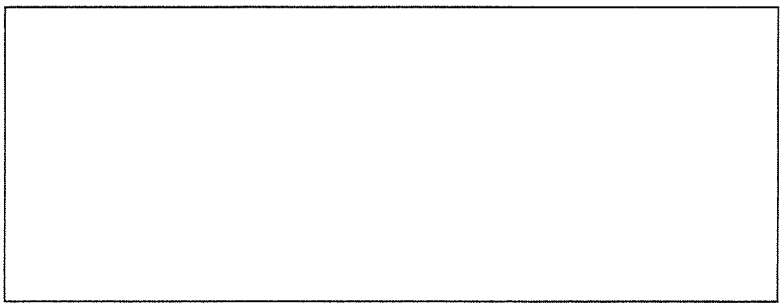

The South China Sea, with an extension of 2.4 Mil km^2 (about 4.5 times larger than the North Sea) is the largest single continuous body of water in the study area and can be found in the northern part. This sea is bounded by Taiwan Strait in the north, the Luzon Strait and Palawan Island (Philippines) in the east and north-east, by the Malaya Peninsula over Vietnam and Hong-Kong in the north-west and Kalimantan (better known as Borneo with an area of about 750000 km^2 which is about 3.3 times larger than Great Britain) in the south.
The South China Sea contains shelf areas as well as oceanic regions, in which numerous atolls and coral reefs are situated. An impression of this is given in Figure 2.3 on page 2–4, which is a depth profile chart of the sea bottom. The main topographical characteristic of oceanic regions in the northern and central parts of the South China Sea, is a V-shaped basin with a maximum depth of about 5000 m. Shelf areas of the South China Sea are the marine area, which stretches from the Taiwan Strait to Hainan Island, the Gulf of Tonkin and the northern part of the Sunda Shelf.

The main connection to the Pacific in the north-east is the very deep Luzon Strait, with depths from 1000 to 3000 m and width of about 350 km. South of Luzon Strait, the South China Sea is connected with the Sulu Sea by two main entrances. One of them is the Mindoro Strait, with about 100 km width and 300 m depth, and the second is the somewhat narrower Balabac Strait with about 60 km width and 80 m depth.

In the south-west there is a very shallow and broad shelf, which is the northern part of the Sunda Shelf, with depths generally less than 100 m. This region contains the Gulf of Thailand with a depth of about 70 m in the central parts. Also there is the region containing the shelf region between Borneo, Malaya Peninsula and Sumatra (Sumatra covers an area of about 525000 km^2, about 2.3 times larger than Great Britain), with depths less than 40 m at the equator.

The connection between the South China Sea and the Java Sea is formed by the Straits of Karimata, Gaspar and Bangka. with depths varying between 30 and 40 m. In the Java Sea, the depths vary from 20 m in the west off the south-east coast of Sumatra, to 60 m in the east at the entrance of Flores Sea. The Java Sea together with the southern parts of the South China Sea is called the Sunda Shelf.

The Sunda Strait, south-east of Sumatra, connects the Java Sea and the Indian Ocean. It has an irregular bottom topography. A small width of about 24 km and a depth of more than 60 m are the main characteristics. In the south of Java Sea there are two further passages which are of importance because of their connection function to the Indian Ocean. These are the Lombok Strait and Sape Strait. The Lombok Strait is about 800 m deep and 35 km wide in its largest part at the Java Sea side and is split in two passages in the southern side: of these the east passage is about 200 m deep and 20 km wide and the west passage is about 150 m deep and 15 km wide (Roberts et al.,-).

The Malacca Strait forms the connection between the Andaman Sea in the Indian Ocean and the Sunda Shelf. It has a depth of about 30 m and width of 35 km in its narrowest parts near Singapore. The depth increases gradually to 100 m in the north-west and its total length is about 800 km.

The eastern part of Java Sea is connected to the Macassar Strait in the north-east, through which the Java Sea is linked to Celebes Sea. Starting from the east of the Java Sea the depth increases immensely up to 4000 m maximum in the Flores Sea, which has a mean depth of 2000 m. The Macassar Strait is 600 km long and the width varies from 350 km in the South to about 150 km in the North. The eastern part of this Strait has a depth of about 1000 to 3000 m and the western part about 30 to 500 m.

Going to the north from Macassar Strait into the Celebes Sea, an extremely deep basin is encountered. The maximum depth in this almost circular basin is about 6000 m. The Celebes Sea is considered as the largest connection in the east, with the Pacific Ocean of the study area.

Through very narrow passages of the Sulu Archipelago in the north of the Celebes Sea, the Sulu Sea can be reached again. The Sulu Sea is a large nearly closed deep sea basin with a maximum depth of 5580 m and an almost quadric form. It is shallower in the west, with a mean depth of about 1000 to 1500 m and deeper in the east, with a mean depth of about 4000 m.

This little "journey" completes the study area of this report. It consists of an area of about 9 million km^2 in total. Compared to the North Sea, with its area of 525000 km^2 according to its International Hydrographic Bureau- Monaco boundaries (Becker, 1981), this area is about 17 times larger.

Figure 2.2: Area of interest

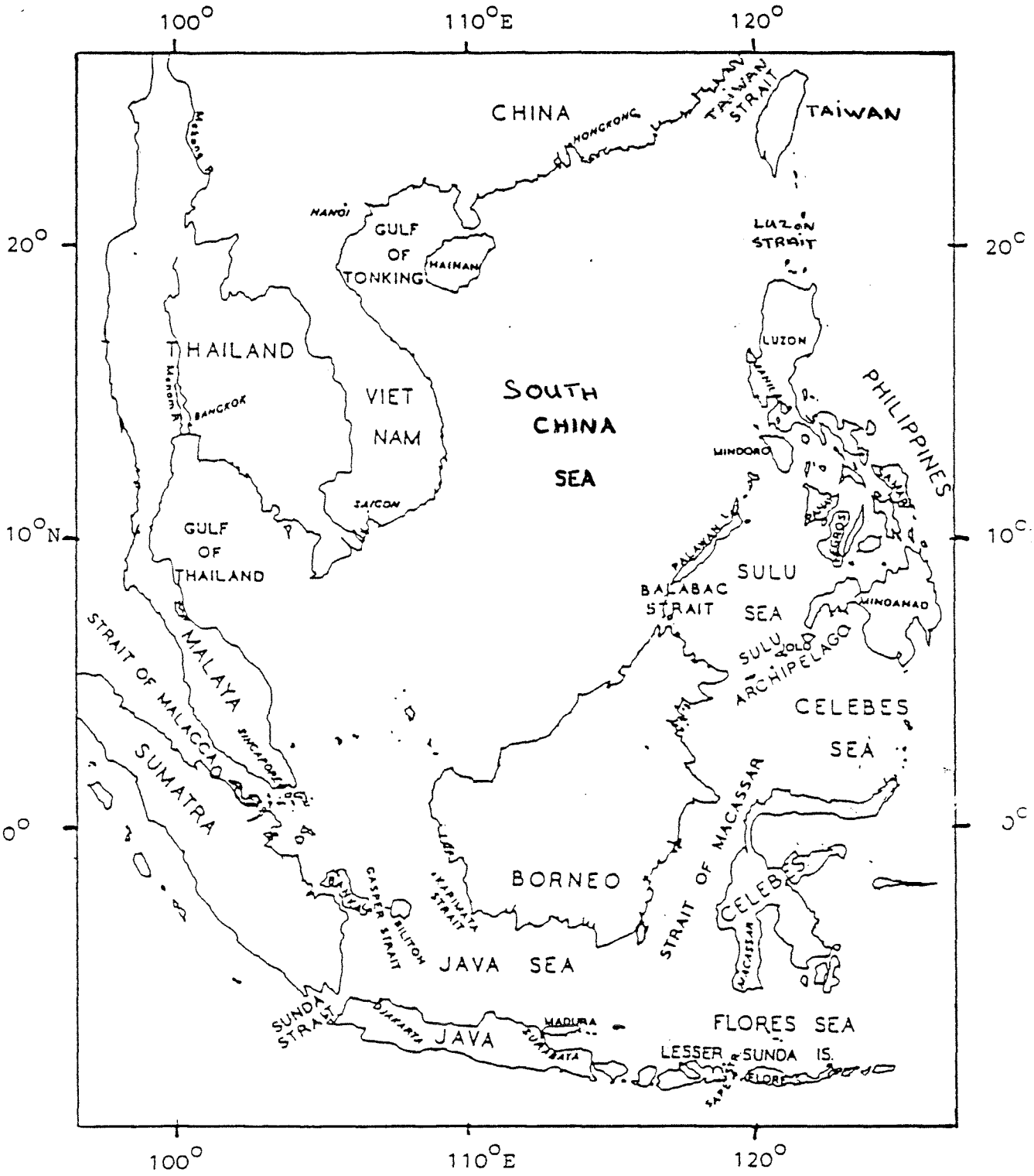

Figure 2.3: Bathymetry of the South China Sea; isolines in meters (*Zhou Di et al.*)

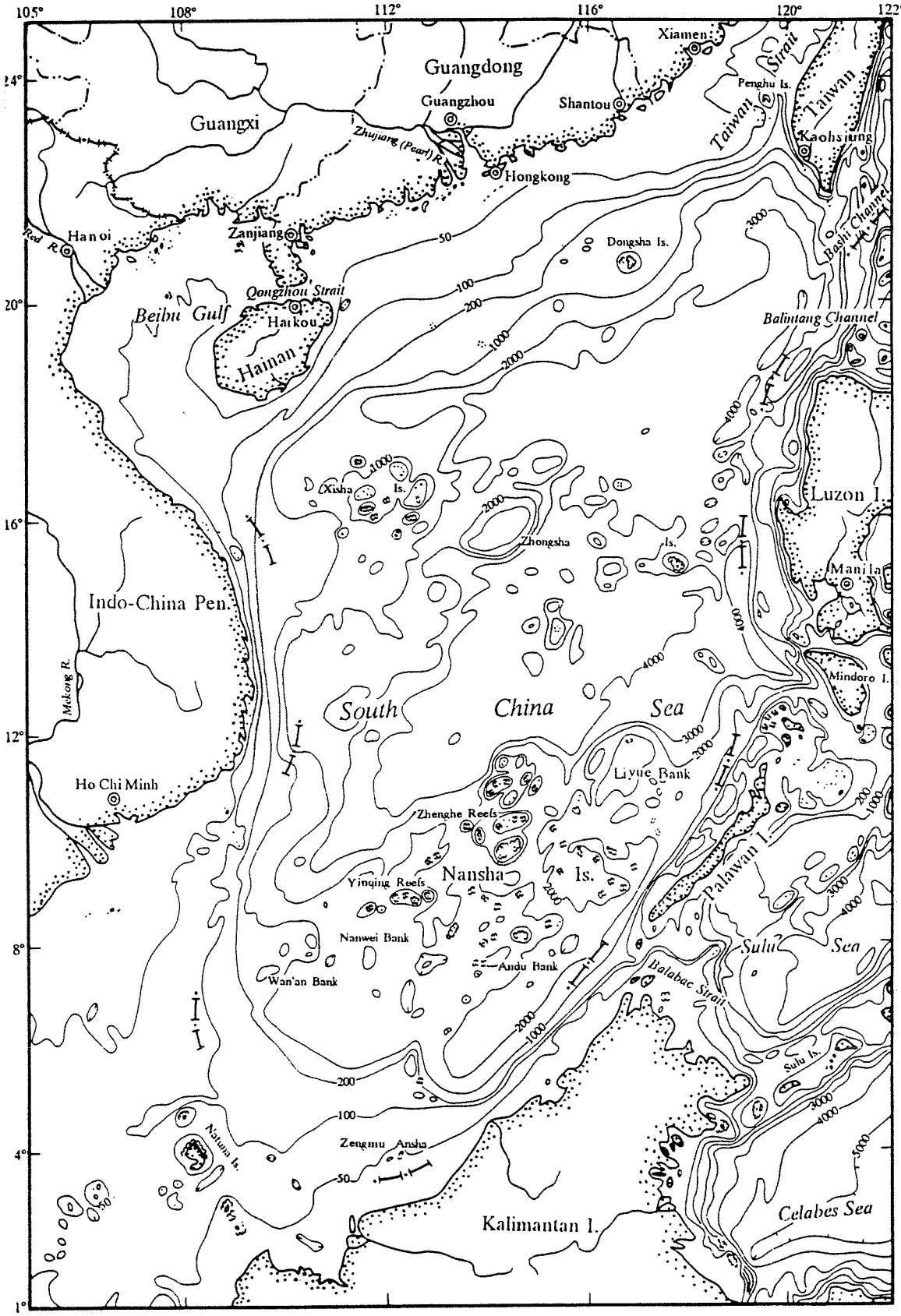

2.2 Tides and Tidal Currents in the South China Sea

Tidal oscillations in the South China Sea are mainly co-oscillating tides originating from tidal waves of the Pacific Ocean and the Indian Ocean. (Mihardja, 1991) The tide generated by the tide generating force of the moon and the sun is small, but remarkably important to the deeper area of the South China Sea and has strong effect on the semi-diurnal constituents. (Mihardja, 1991) Because of the extremely strong subdivision of the region into shelf regions and oceanic regions, the pattern is manifold and in each basin a different oscillation is dominant. (Wyrtki, 1961) The geographical distribution of tides within the study area will further be discussed in section 2.3.
According to Wyrtki (1961), The four most important tidal constituents give a relatively complete picture of the tidal pattern of the region and sufficient for a general description. These tides, with their periods T in hours are shown below in Table 2.1.

Table 2.1: List of tidal constituents

Tide	Description	Period (hrs)
M_2	semi-diurnal principal solar	12.42
S_2	semi-diurnal principal solar	12.00
K_1	diurnal luni-solar	23.93
O_1	diurnal principal lunar	25.82

For a geographical consideration of the tides however, the two diurnal and the two semi-diurnal tides can be dealt with together. According to the treatment of the tides of all oceans as given by Dietrich (1944) the following factors are presented and in the following pages these factors are illustrated.

- 1 M_2+S_2

  The sum of the amplitudes of the two most important semi-diurnal tides, indicating the amplitude of the semi-diurnal tide at spring tide. For the isoline figure of the amplitude of the semi-diurnal tides of the study area see Figure 2.4
- 2 K_1+O_1

  The sum of the amplitude of the two most important diurnal tides, indicating the amplitude of the diurnal tide at spring tide. For the isoline figure of the amplitude of the diurnal tides of the study area see Figure 2.5
- 3

  The phase of the M_2 tide, given by co-tidal lines related to Greenwich time. The phase of S_2 tide deviates from the M_2 tide less than 1.5 hours. For the figure of the of the study area see Figure 2.6: Co-tidal lines of the semi-diurnal tide M2 in lunar hours
- 4

  The phase of the K_1 tide, given by co-tidal lines related to Greenwich time. The phase of the O_1 tide deviates from the K_1 tide less than 2 hours. For the figure of the study area see Figure 2.7

Figure 2.4: Amplitude (cm) of the semi-diurnal tides (M2 +S2) (Wyrtki)

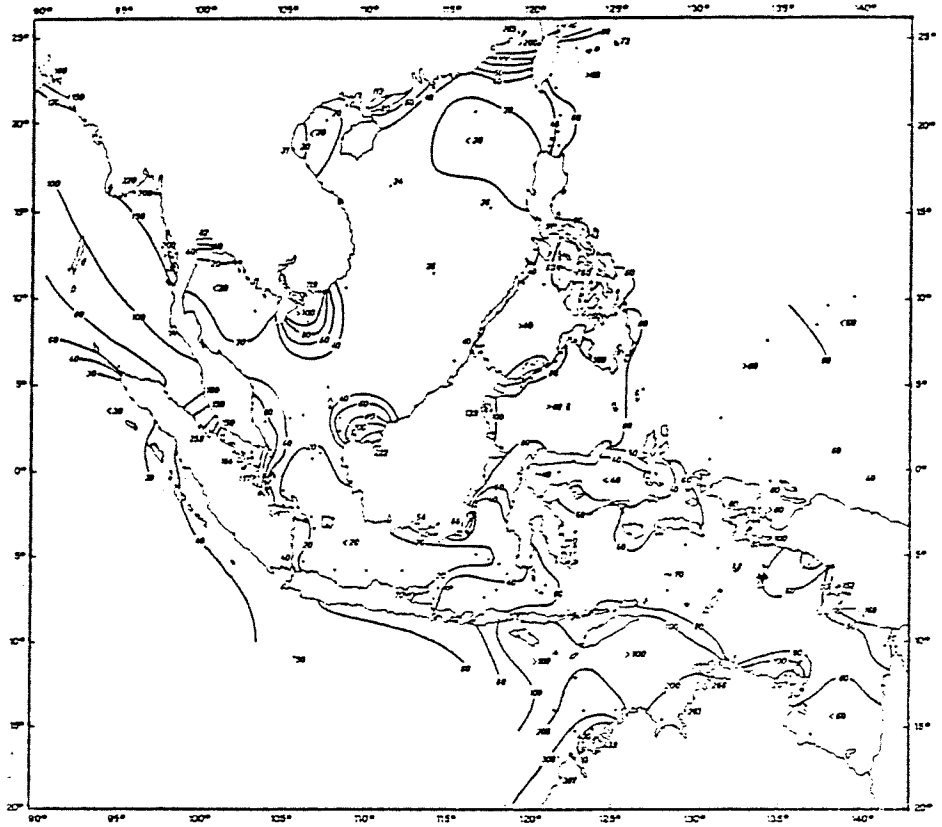

Figure 2.5: Amplitude (cm) of the diurnal tides (O1+K1) (Wyrtki)

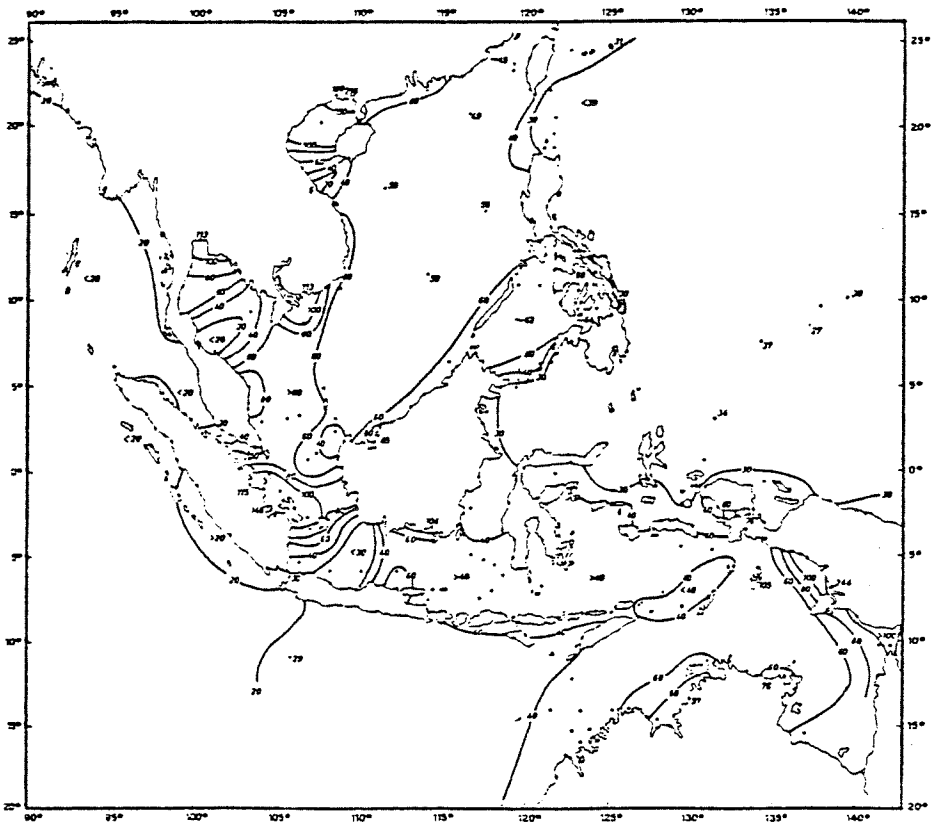

Figure 2.6: Co-tidal lines of the semi-diurnal tide M2 in lunar hours (Wyrtki)

Figure 2.7: Co-tidal lines of the diurnal tide K1 in lunar hours (Wyrtki)

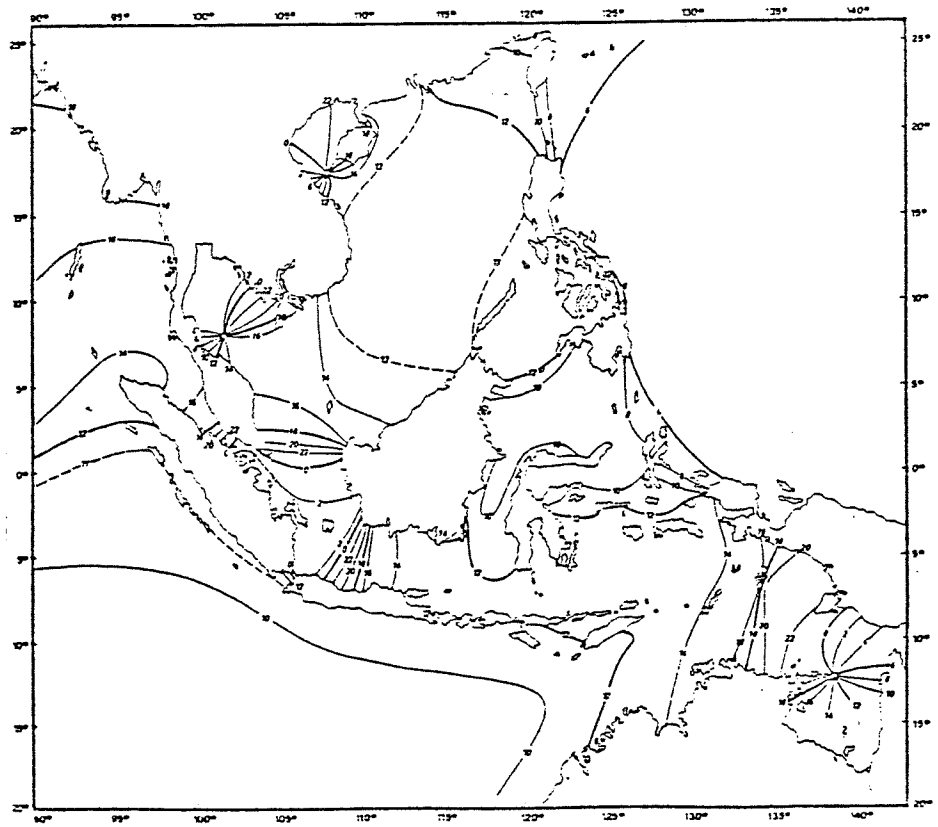

Based on these figures, the penetration of the tides from the two oceans into the South-east Asian Waters can be discussed. The geographical position of the names of bays, islands, lands etceteras are represented in a map (Figure A2.2) in *appendix 2.* In this same appendix, there is also a bottom profile chart (Figure A2.1) of the South China Sea.

2.2.1 The semi-diurnal tidal constituents

In Figure 2.4 and Figure 2.6 observed values of the sum of the amplitudes of both the semi-diurnal components and respectively the co-tidal lines of tidal component M_2 were represented. These figures together represent a global view of tidal movement of the semi-diurnal constituents in the region. In most parts of the study area, ratios of constituent amplitudes S_2/M_2 and the phase lag differences S_2-M_2 change slowly and slightly, except for areas very close to the amphidromic points. Therefore, the co-tidal charts of S_2 constituents are similar to those of M_2 constituent.

In the region between Japan and New Guinea the semi-diurnal tide is developed as a standing wave with a nodal line in north-south direction between 140^0 and 150^0 E (this can best be seen by looking at Figure 2.10 on page 2–12) The high water occurs simultaneously along the whole east coast of Taiwan and the Philippines with a phase of 9.5 hours. In the south of this region, in the vicinity of the Palau Islands, it occurs half an hour later, which leads to the conclusion that the wave is deflected and comes from the north. The amplitude of this wave is about 60 cm.

The semi-diurnal wave enters the South China Sea through the Bashi Channel, north of Luzon Strait, and spreads mainly south-westward, with a small branch entering the Taiwan Strait. Up north, on both sides of Taiwan, the wave is strongly refracted when coming into shallow water, so that it enters Taiwan Strait simultaneously from north and south. Consequently high amplitudes are caused in the centre of the shallow strait, exceeding 200 cm.

The south-westward going wave, advances into the South China Sea relatively slowly. In the northern coasts, the amplitudes first decrease from the east to the west, reaching a minimum west of Shantou (south-west of Taiwan Strait), and then increasing again to the west. The amplitude is less than 20 cm in the deep water areas of the South China Sea. The wave meets the Sunda Shelf exactly 7 hours after it was in Luzon Strait. A part of this wave, coming from Luzon Strait, enters the Gulf of Tonkin without forming an amphidromic region. The distribution of the co-tidal lines shows clearly a simple progressive wave reaching the edge of the shelf offshore Vietnam with a phase of 3 hours and the inner parts of the bay 9 hours later. The amplitudes rise up to 52 cm. Along the coasts of China, between Hong Kong and Hainan Strait, high amplitudes of more than 100 cm are found as an effect of the shelf (shoaling), which is met by the tidal wave almost under the same phase and causes a considerable increase of its amplitude.

When meeting the Sunda shelf, the propagation velocity of the tidal wave decreases. Especially off the coasts of Vietnam and Borneo the wave is refracted and high amplitudes develop. At the Mekong estuary in Vietnam, the amplitude reaches up to 119 cm and in the Datu Bay even to 222 cm. An interesting occurrence is, that the observations on islands off the coast show that the increase of the amplitude reaches far into the shelf and is not limited to a small region close the coast. The wave travels 7 hours from the time it passes the edge of the Sunda Shelf until it reaches the coasts of Malaya. There it splits into two branches, one moving northwards into the Gulf of Thailand and the other southwards and entering the Riau Archipelago region. The part of the wave entering the Gulf of Thailand forms an amphidromic region, with a clockwise circulation. Its centre is in $9^0$18' N, $103^0$28' E near the island of Palau Panjang. This point is much close to the east, which may be caused by the asymmetric arrival of the wave and by the loss of energy due to friction. The amplitudes are less than 20 cm in the whole amphidromic region. In the northern part a wave separates which does not participate in the amphidromic circulation, but moves directly towards the north. It causes strong tides at the northern coasts of the bay near Bangkok, reaching 82 cm.

The part of the wave moving southward in the South China Sea turns anticlockwise around an amphidromic point in $0^0$30'N, $106^0$30'E. Despite of this, the co-tidal lines are all concentrated west of this point leading to that the amphidromic region is developed asymmetrically. The wave begins its turn with a phase angle of 11 hours, reaches the Riau Archipelago with a phase of 4 hours and the Island of Bangka with 10 hours. Here it joins with the wave coming from the Java Sea and practically disappears. In the whole amphidromic region the amplitudes are small, only within the Riau Archipelago they are a little higher, but this seems to be partly an influence of the tidal wave entering through the Malacca Strait from the Indian Ocean. In the region between Borneo and Sumatra the influence of the tidal wave coming from the Pacific Ocean through the South China Sea practically ends for the reasons of friction and reflection.
South of Mindanao, another branch of the tides of the Pacific Ocean enters the study area via the Celebes Sea. The phase of this wave is about 10 hours and the amplitude is about 80 cm. In the Celebes Sea, off the coast of Borneo, the amplitudes increase up to 139 cm when the tidal wave reaches the shelf. To the north the tidal wave enters the Sulu Sea and needs 3 to 4 hours to pass the Sulu Archipelago[1]. In the whole Sulu Sea and in the Philippines the high water occurs practically simultaneously with a phase of 2 hours. This leads to the assumption that the tides in this region have the character of a standing wave. The amplitudes in the whole region are between 50 and 80 cm. The tidal wave of the South China Sea seems not to influence the tides in the Sulu Sea[2] (Wyrtki, 1961). The co-tidal lines of the small and shallow straits between Luzon and Mindanao are so strongly concentrated that a change of phase of nearly 5 hours occurs and strong tidal currents are the result. The waves entering from the Pacific have minor effect on the tide in Indonesian waters (like Java Sea), because most of them reflect from the western boundary back into the Pacific (Hatayama et al., 1996).

The semi-diurnal waves originating from the Indian Ocean reach the Lesser Sunda Islands with a phase of 3 hours and with amplitudes between 70 to 140 cm. A part of this strong wave passes the various narrow passages like Lombok Strait, Sape Strait and passages between the islands in the Flores Sea, to enter into the Java Sea and advances slowly northwards. Another part of the semi-diurnal wave from the Indian Ocean from the Flores Sea progresses into Java Sea without changing its direction to the west. The smaller northwards moving part advances further into the Macassar Strait, where it merges with the wave of the Pacific Ocean resulting to a phase of about 10 hours.
The wave deflected west into the Java Sea is weak and the amplitudes remain below 10 to 20 cm. (except for the south coast of Borneo where the amplitudes reach up to 40 cm) However a rapid change occurs in phases in the south-west coast of Borneo. According to Schwiderski (1979), a weak amphidromic point can be expected in such cases. As the result of this, Schwiderski (1979) detected two amphidromic points in Java Sea. The first is a clockwise one and lies in the middle. The second is counterclockwise and lies in the east, north of Madura Island. Wyrtki (1961) detected no amphidromic points in Java Sea.
A small part of the tidal wave from Indian Ocean also enters the South China Sea from the other side of the region. This wave enters via Andaman Sea into the Malacca Strait[3], where it advances slowly. The amplitudes rise from 80 cm at the entrance to 120 cm in the middle parts to more than 250 cm in the narrowest parts of Malacca Strait. This extreme increase of amplitude is a logical consequence of the conic shape of the Strait. No amphidromic point exists in this Strait and the tidal waves can be regarded as Kelvin waves [Pedlosky (1979), van Dantzig (1960), Dronkers (1961)] with a velocity of about 25 $^m/_s$. After passing the narrowest part the amplitude decreases again. A part of the wave passes over into the amphidromic region in southern South China Sea at which its influence almost vanishes. Other parts of the wave proceed into Java Sea and also become very weak.

---

[1] *Tides around the Sulu Sea will be dealt with in more detail in 4.1*
[2] *This is one of the major discussion points of this report*
[3] *Tides in Malacca Strait are considered in more detail in Appendix 1, section A1.6*

2.2.2 The diurnal tidal constituents

In Figure 2.5 summed amplitudes of the two diurnal constituents and in Figure 2.7 the co-tidal lines of the K_1 constituent were given. These figures should be studied together with this paragraph. The similarity between the diurnal constituents can also be assumed for the diurnal constituents of the study area. In most parts of, ratios of constituent amplitudes O_1/K_1 and the phase lag differences O_1-K_1 change slowly and slightly, except for areas very close to the amphidromic points. Therefore, the co-tidal charts of the O_1 constituent is similar to the K_1 constituent.
The diurnal constituents enter the South China Sea mainly through the Bashi Channel (north of Luzon Strait) and the Taiwan Strait. The tidal wave of the Pacific Ocean reaches the Philippines and New Guinea with a phase of 6 hours (related to its origin in the Pacific) and with amplitudes between 20 and 40 cm (see also Figure 2.10 on page 2–12).
When entering the China Sea high water occurs nearly simultaneously. The amplitudes of this standing wave are 50 to 60 cm. Contrary to the M_2 tide no intensification of the diurnal tides occur in Taiwan Strait, because the strait is directly passed from north to south by the tidal wave. The amplitudes increase gradually westward and southward, reaching a maximum in the Gulf of Tonkin, where diurnal constituents resonate. The diurnal tide develops an amphidromic region here, of which the circulation is counterclockwise and situated close to the coast of Vietnam. The whole northern part of the gulf has amplitudes above 100 cm which increase up to 216 cm in the north-eastern corner. This is a typical area of diurnal constituents, at which the amplitude of O_1 constituent is obviously larger than that of K_1.
High water reaches the Sunda Shelf in the South China Sea with a phase of 13 hours and the wave advances relatively fast. The amplitude of K_1 reaches 30 cm in the deep water areas of the South China Sea. Coming closer to the coast of Malaya it splits off, like the M_2 wave, into a north going and a south going branch. The branch moving into the Gulf of Thailand causes an amphidromic region with an anticlockwise circulation. The amphidromic point is displaced to the west close to the Malaya coast, where the amplitudes are smaller. The highest amplitudes are observed in the northern part of the gulf (113 cm). The part of the tidal wave moving southwards in the southern South China Sea advances slowly, but its amplitudes increase up to more than 100 cm along the coasts of Sumatra and Bangka. In the Gaspar and Karimata Straits this wave meets the wave coming from the Java Sea, and the amplitudes increase to 80 cm. An amphidromic region is not formed in southern South China Sea.
South of the Philippines the diurnal wave entering Celebes Sea is retarded, when it meets the first island groups, but advances quickly over the deep Celebes Sea. High water occurs simultaneously along all coasts of the Celebes with a phase of 10 hours, the amplitudes are about 30 cm. When passing the Sulu Archipelago the wave is retarded again like the M_2 tide. High water occurs in the whole Sulu Sea and in the Philippines simultaneously with a phase of 13 hours and the amplitudes are uniform almost everywhere at about 60 cm. No wave seems to penetrate directly from the Pacific Ocean through the Philippines nor does the wave of the South China Sea seem to have any influence in the Sulu Sea (Wyrtki, 1961).
Unlike the semi-diurnal tides, the diurnal tides in the Macassar Strait are determined rather by the tidal wave propagating from the Pacific. This is presumably due to weak diurnal tidal wave propagation from the Indian Ocean compared with that from the Pacific Ocean. Through the Macassar Strait the diurnal tidal wave penetrates into the Flores Sea and meets the wave of the Indian Ocean penetrating through the passages between the Lesser Sunda Islands. Thereby its amplitude reaches to 50 cm in the Flores Sea.

The diurnal wave of the Indian Ocean enters the region through the passages between the Lesser Sunda Islands and the Timor Sea into the Banda Sea and Flores Sea. In the Flores Sea the wave meets the stronger wave coming from the Macassar Strait, originating from the Pacific Ocean, where the two waves are refracted and enter the Java Sea. Here they advance at first quickly and later slowly, with the amplitudes reaching 80 cm on the north coast of Java up to 100 cm on the south coast of Borneo. In the range of the stronger concentration of

the co-tidal lines in the western Java Sea the amplitudes decrease to 20 cm. Later when approaching the Karimata Strait, between Borneo and Sumatra, this wave meets the wave coming from the South China Sea and the amplitudes rise again to 80 cm.
Diurnal tides also enter the region directly via the Malacca Strait. This part of the wave is however shielded by the strait because of its depth and width changes. In the Java Sea the wave originating from the Pacific Ocean is much more pronounced, so the wave from the Malacca Strait is not of importance anymore.

2.2.3 Review of the tidal behaviour of the study area

The tidal movement of the diurnal and semi -diurnal waves, as represented by the M_2 and the K_1 constituents are given one more time, in order to show the global tidal movement:

Figure 2.9: Schematic view of the wave propagation of the K1 tide (*Takaki et al.*)

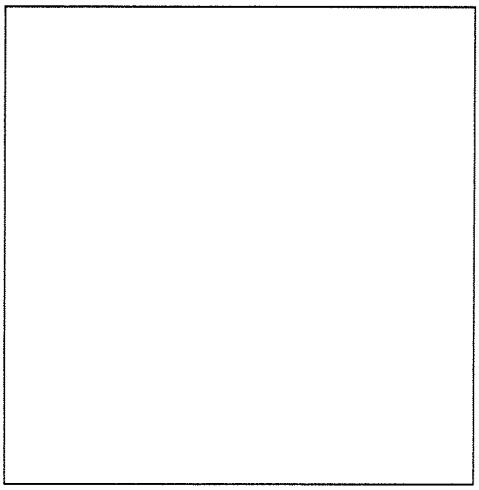

Figure 2.8: Schematic view of the wave propagation of the M2 tide (*Takaki et al.*)

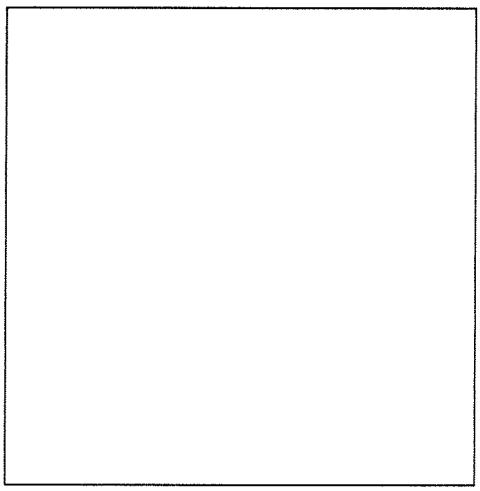

The semi-diurnal tides as well as the diurnal tides of the Pacific Ocean and the Indian Ocean penetrate deep into the South China Sea and the Indonesian Waters. The tides of the study area are therefore co-oscillating tides of the two oceans. Free oscillations due to direct influence of the moon and sun is negligible compared to the forced oscillations of the two Oceans (Mihardja, 1991). The tides of the Pacific Ocean govern the whole South China Sea, the Philippine Waters and the Celebes Sea, while those of the Indian Ocean govern the Timor Sea, the Banda Sea and the Sahul Shelf. The Molucca Sea, Macassar Strait and the Java Sea are the boundary regions between the tidal influence regions of the two oceans.
The areas in which the waves from the Indian Ocean are dominant are mostly out of the study area of this report. When only the study area is regarded, it can be concluded the waves from the Indian Ocean are less dominating than waves from the Pacific Ocean for the following reasons:

- Waves entering via the Andaman Sea undergo heavy resistance of the Malacca Strait. The width of Malacca Strait becomes very narrow near Singapore and the depth decreases as well. The entering waves have to push their way into the strait.
- South of Java the waves from the Indian Ocean are also expected to be shielded. First because of the various islands of Sumatra, Java, Lombok, Bali, Flores and so on. Second by strong decrease of the bottom profile south of Lesser Sunda Islands because of the Australian plates.
  Waves from the Indian Ocean enter the area mainly through Malacca Strait in the west, from the Flores Sea in the east and through various small passages between

southern Indonesian Islands of which Lombok, Sape and Sunda Strait are most known. In Java Sea the effects of waves from Indian Ocean are dominating.

Figure 2.10: Co-tidal lines of K1 and M2 tidal components (*Schiereck*)

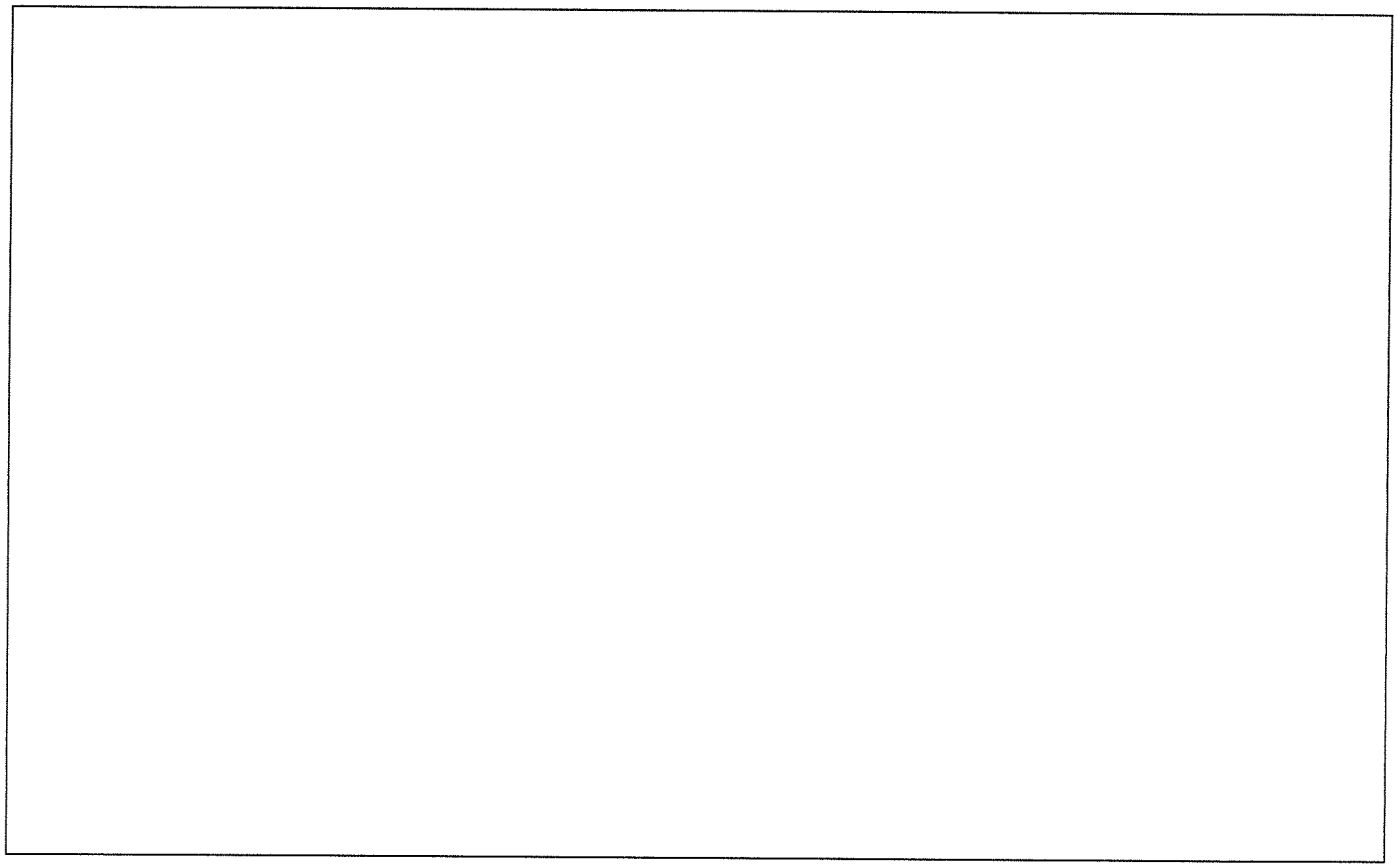

Remarkable too is the rotation directions of the amphidromic points within the study area. It should be counterclockwise in the northern and clockwise in the southern hemisphere (Murty&El-Sabh, 1989). However some examples are known of amphidromic points that do not match this rule. According to Murty&El-Sabh (1989), local peculiar topographic effects coupled with friction probably account for the exceptions to the rotation of amphidromic points of the co-oscillating tides in marginal seas. It is also noted that these points, that do not match this rule are geographically positioned not very far of the equator.
In the Gulf of Thailand the K_1 tide rotates counterclockwise according to expectation, but on the other hand the M_2 tide rotates clockwise. This seems to be caused, besides topographic and frictional effects, by the tidal wave coming from the South China Sea advancing almost as a progressive wave in the western parts of the gulf. It returns as a weak wave in the eastern parts of the gulf around the amphidromic point, which is much displaced to the east. The K_1 tide in the Gulf of Tonkin rotates counterclockwise according to the theory. The rotation of the M_2 tide around the amphidromic point, in the southern South China Sea just at the equator, is counterclockwise but the amphidromic region is developed asymmetrically which may be caused by the meeting of three different waves.
Beside the exceptions of rotation directions of observed amphidromic points, there are major differences of the positioning and the amount of calculated amphidromic points of different investigators. In
Table 3.1 on page 3–2 a table is given of the calculated M_2 amphidromic points by different investigators. Earlier it was noted that Schwiderski found two amphidromic points of the M_2 constituent in the Java Sea, while Wyrtki found none of them in that region.

2.3 Geographical distribution of tidal types

The tidal waves penetrate into the study area from opposite directions from the adjacent oceans. This can be seen by looking to co-tidal lines diagrams of the K1 and M2 tides given in Figure 2.6 and Figure 2.7. on page 2–7. To see this better, a global co-tidal lines diagram containing the Indian and Pacific Oceans of the K_1 and M_2 constituents is given in Figure 2.10.

Tidal waves are greatly affected by the depth and shape of the basins in which they are propagated. The friction because of the bathymetry, islands etceteras and the rotation of the earth because of Coriolis forces are further additional effects of tidal nature. Amplification of a wave occurs when the natural oscillation period of a basin approaches the period of the wave. The natural periods of oscillation[4] of the various basins in combination with natural periods of main constituents of the tide, are producing zones with predominantly diurnal tides and zones with predominantly semi-diurnal tides (see Figure 2.12 and Figure 2.13).

Classification of the tide can be made according to the relative importance of the four major constituents. This is most simply described by means of the quotient of their amplitudes (Wyrtki, 1961). For this the quotient of the sums of the amplitudes of the two diurnal and the two semi-diurnal tides is used.

tide form number:

$$f = \frac{H_{K1} + H_{O1}}{H_{M2} + H_{S2}} \qquad (2.1)$$

The tide form number can have values between zero and infinity, corresponding to a pure semi-diurnal and a pure diurnal tide respectively. According to Wyrtki (1961), for the presentation of the geographical distribution of the tidal types the division of Dietrich (1944) can be used again, which can be represented as follows:

- f = [0-0.25]
  - . Semi-diurnal tide
  - . Two high waters and two low waters of approximately the same height per day
- f = [0.25-1.5]
  - . Mixed tide, prevailing semi-diurnal
  - . Daily two high waters and two low waters, which show inequalities in height and time.
- f = [1.5-3.0]
  - . Mixed tide, prevailing diurnal
  - . Occasionally only one high water and one low water daily, but sometimes also two high waters and two low waters per day, showing strong inequalities in height and time.
- f = [3.0-~]
  - . Diurnal tide
  - . Only one high and one low water daily.

Examples of tidal motions according to their tide form number can be seen in Figure 2.11.

[4] *Natural periods and oscillations are explained in Appendix 1, section A1.5*

Figure 2.11: Typical tidal curves representing the four tidal types during a period of 16 days (*Wyrtki*)

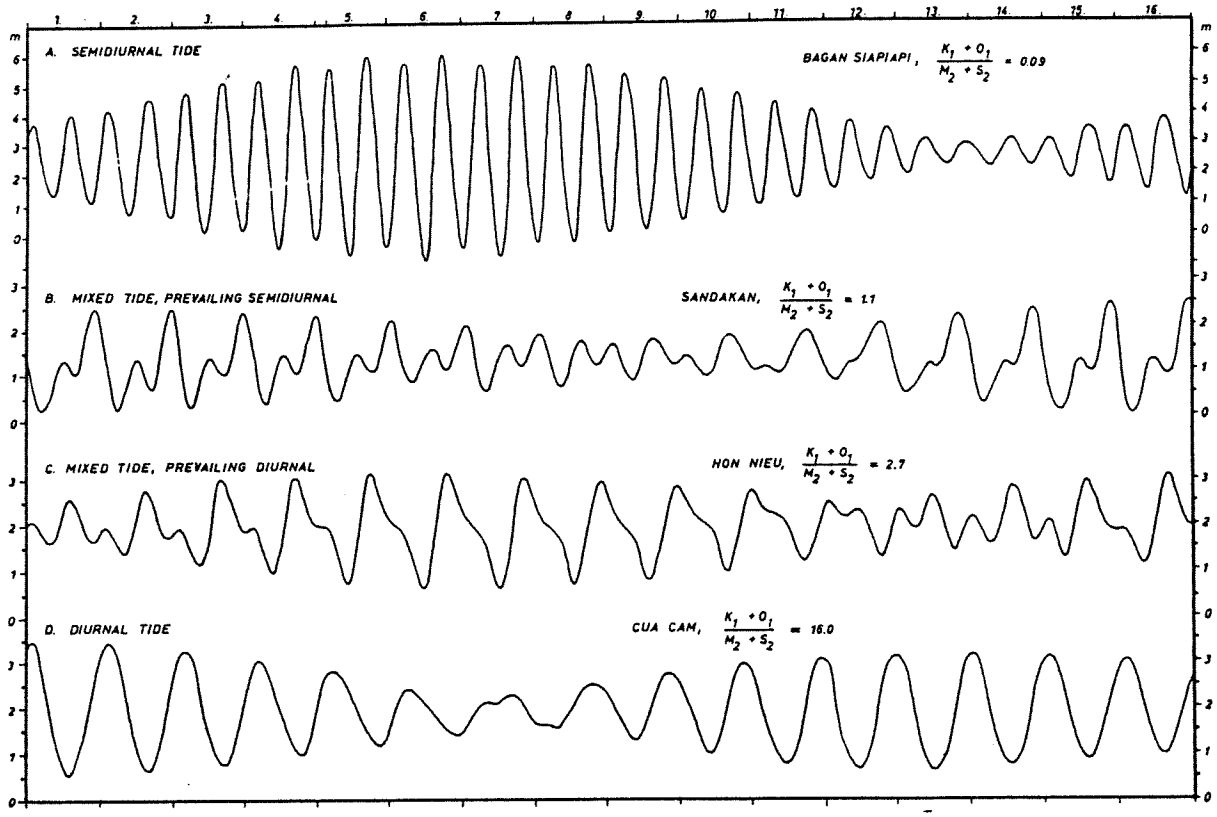

After the calculation of tide form numbers for the whole area of the South China Sea, a study on the geographical distribution of tidal types can be made. In this way the possibility is created to see what tidal type is dominant in which areas by one single look.
The geographical distribution of tidal forms as illustrated in Figure 2.12 and in Figure 2.13 by different investigators, show that the semi-diurnal tides are dominant in the regions connected directly to the Indian Ocean, such as Malacca Strait.

Figure 2.12: Geographical distribution of tidal types according to Cao&Fang (*Zhou Di et al.*)

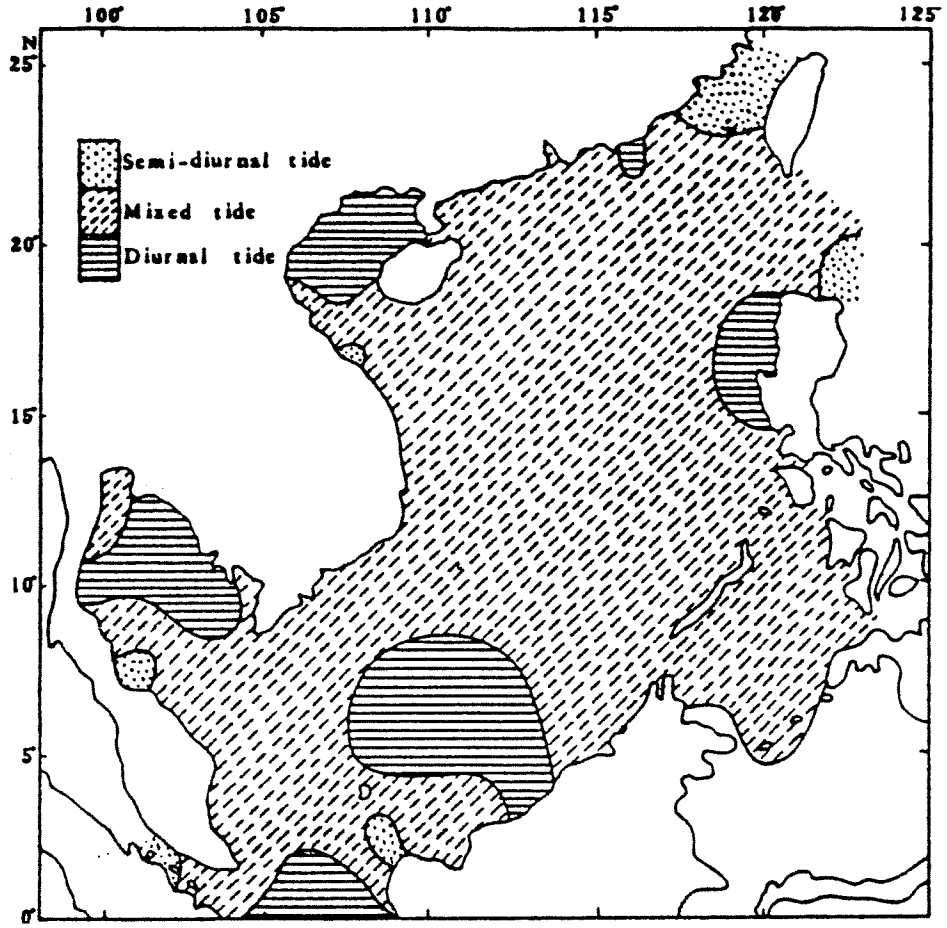

In the western Pacific Ocean the diurnal tide is more pronounced, but the semi-diurnal tide is still dominant giving a mixed prevailing semi-diurnal tide. This changes immediately when the tides enter the waters of the South China Sea. Almost the entire South China Sea has a mixed prevailing diurnal tide, because the amplitudes of the semi-diurnal tide are small. Only in Taiwan Strait, where local conditions cause a considerable strengthening of the M_2 tide, semi-diurnal tides are found to be dominant. In other regions the diurnal tide is amplified. Thus in the Gulf of Thailand, the Gulf of Tonkin and in waters between Sumatra and Borneo an almost pure diurnal tide is found. The Java Sea has a prevailing diurnal tide as well. In the eastern parts of the Indonesian waters, at the region of Lesser Sunda Islands, the mixed prevailing semi-diurnal tide is dominant by direct influence of the Indian Ocean. Near the Philippines, in the Sulu Archipelago region, development of prevailing diurnal tides can be seen due to local conditions.

Figure 2.13: Geographical distribution of tidal types according to Wyrtki (*Wyrtki*)

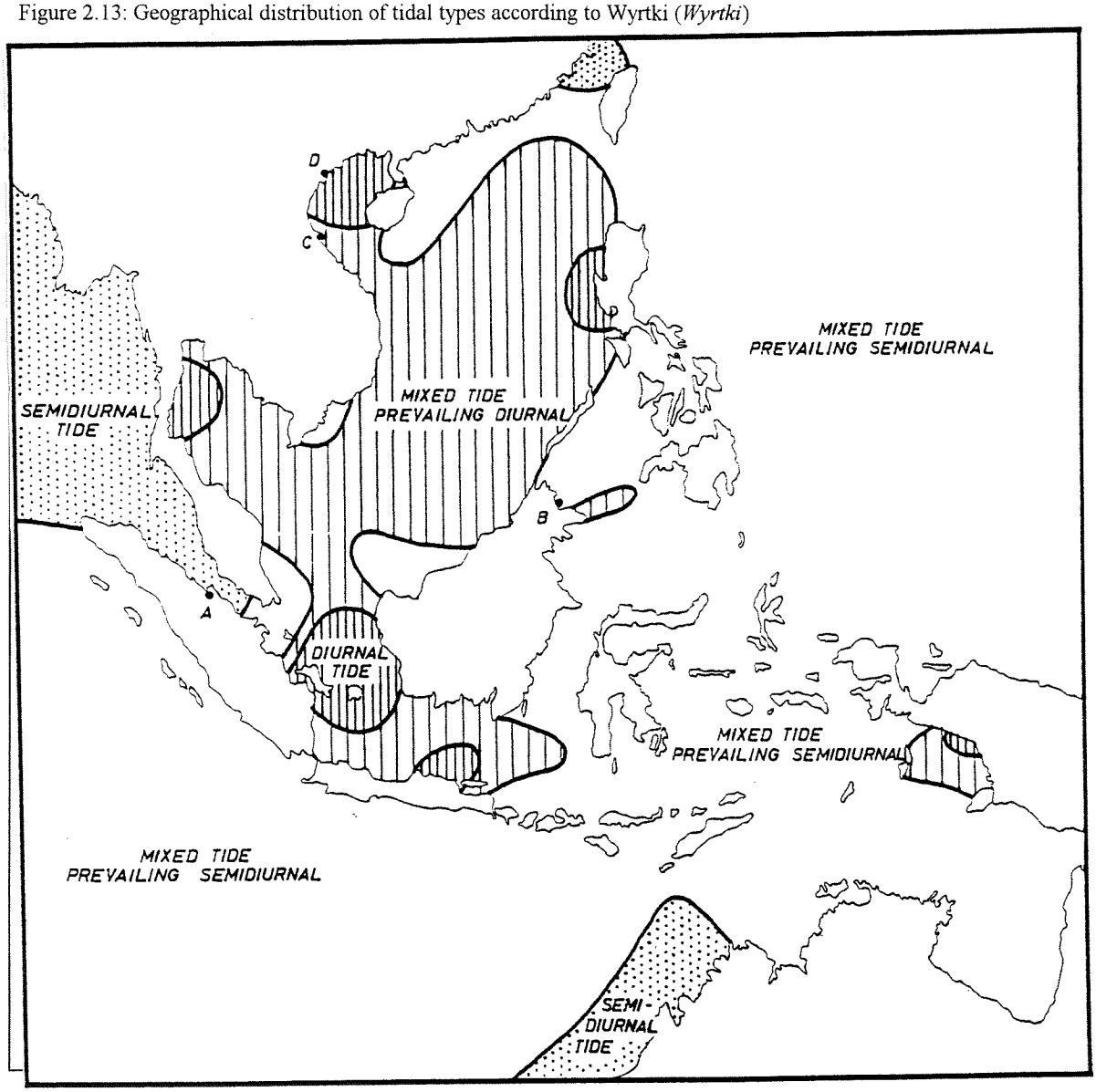

Between the last two figures there are beside obvious similarities also some obvious differences in distribution of tides. The tides in the Gulf of Thailand and the coastal region of Borneo in the South China Sea are some of the examples for this. This underlines once again that different investigators have different findings of the tides in these waters.

2.4 Tidal Currents and velocities

Unfortunately sufficient data to extensively discuss tidal currents of the four major constituents are lacking. Based on available data (for example of observations of the Snellius expedition (Wyrtki, 1961)) from the northern coastal areas of the South China Sea some discussions can be made for the K_1 diurnal constituent and the M_2 semi-diurnal constituent. The strongest tidal current due to K_1 (> 40 $^{cm}/_s$) appears in the Hainan Strait and the sea area south-west of the Hainan Island. The second strongest current (about 30 $^{cm}/_s$) occurs in the mouth of the Gulf of Thailand. There is a lag of about 12 hours for the appearing time of maximum current velocity of K_1 tidal current from the Taiwan Strait to the southern Hainan Island. Two counterclockwise tidal current amphidromic points of K_1 exist in the Gulf of Tonkin and the mouth of the Gulf of Thailand (see Figure 2.14). According to the modelling results of Cao&Fang, (Zhou Di et al., 1994), the maximum velocity of K_1 constituent in most areas of the South China Sea are less than 10 $^{cm}/_s$. Tidal amphidromic points of K_1

seem to appear east of the Hainan Island, east of the Paracel Island, in the western Balabac Strait, and in the north-western Datu Bay.

Observed maximum velocity and its occurrence time of the M_2 constituent, Figure 2.15, shows that the velocity of M_2 rises to a maximum over 100 $^{cm}/_s$ in the southern Taiwan Strait, over 40 $^{cm}/_s$ near the Mekong Estuary and the mouth of Gulf of Thailand, and 10 to 20 $^{cm}/_s$ along the Guangdong coast (near Hong Kong see Figure 2.3: Bathymetry of the South China Sea; isolines in meters *(Zhou Di et al.)*

on page 2–4) and in the Gulf of Tonkin and Gulf of Thailand. Two amphidromic points appear in the Gulf of Tonkin and three in the Gulf of Thailand. The phase lag of M_2 from the Taiwan Strait to the south, near Hainan Island, is about 6 hours.

Figure 2.14: Observed distributions of (absolute maximum value) velocity (cm/s) and (b) its appearing time of the K1 tidal constituent in the northern South China Sea and the Gulf of Thailand (*Zhou Di et al.*)

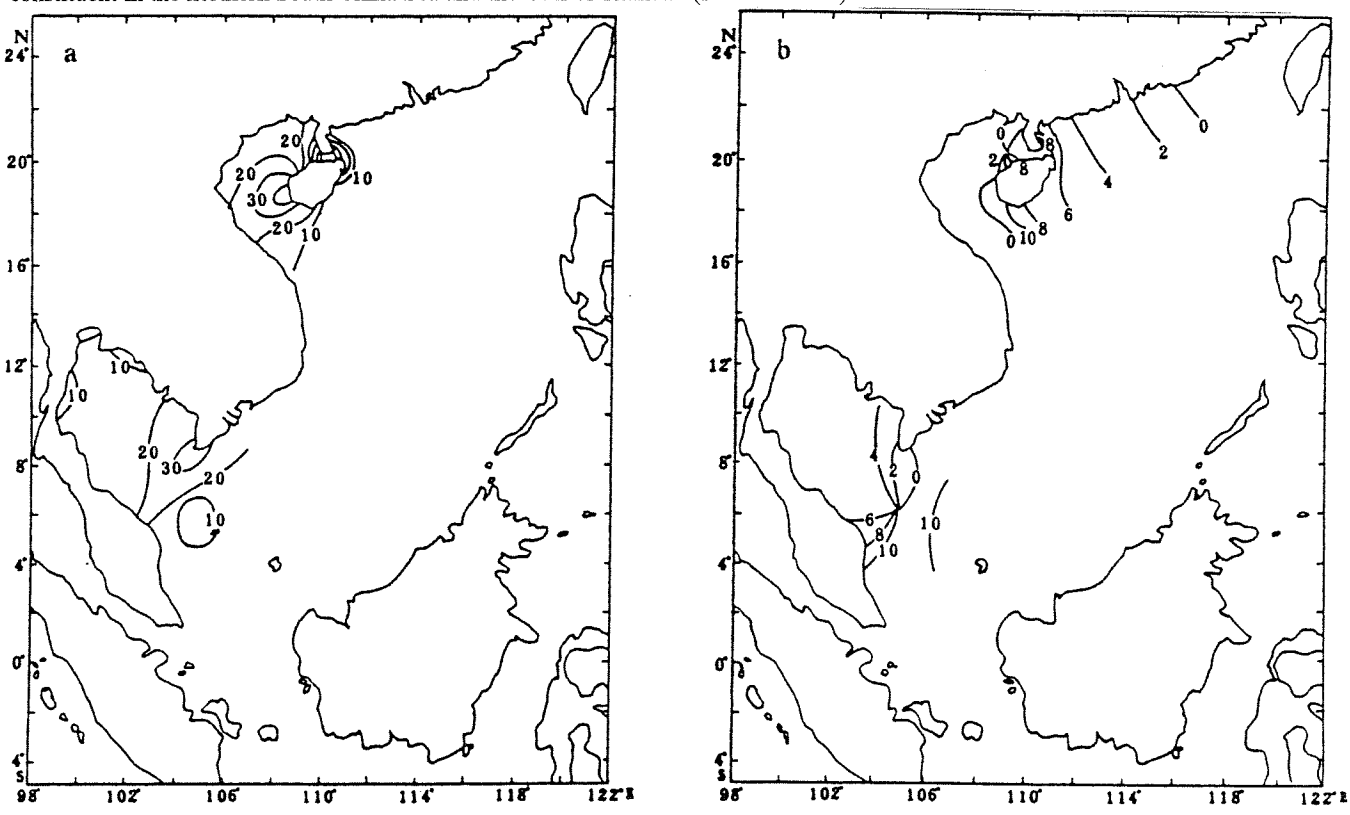

Simulated maximum velocity contours of M_2 tidal current and the distributions of cotidal hour lines in the South China Sea are basically consistent with observations. Simulation by Cao&Fang, (Zhou Di et al., 1994), gave a velocity of < 10 $^{cm}/_s$ for the M_2 tidal current in other areas of South China Sea. One amphidromic point appeared in the Gulf of Thailand, and seven more in the area from the southern Taiwan Strait to the mouth of the Gulf of Thailand.

Figure 2.15: Observed distributions of (absolute maximum value) velocity (cm/s) and (b) its appearing time of the M2 tidal constituent in the northern South China Sea and the Gulf of Thailand (*Zhou Di et al.*)

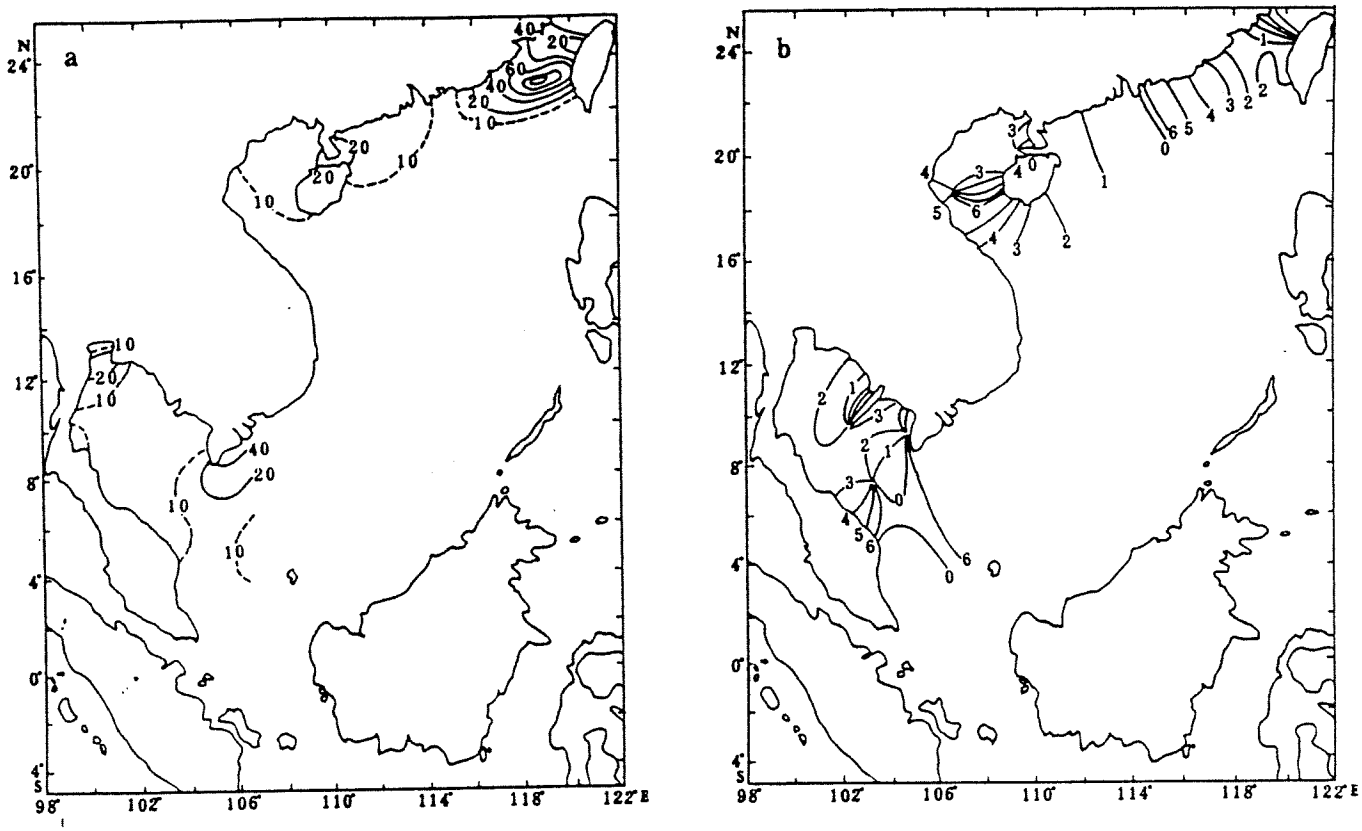

The South China Sea Model constructed by DELFT HYDRAULICS (This model will be discussed in more detail in section 3.2) also showed comparable results. High velocities were noticed locally in the Malacca Strait, on the north-western and south-eastern coasts of Borneo and through some passages to the Sulu Sea.
Available observations show that the long axis of the ellipse of tidal constituents is roughly parallel to the coastline in the northern and southern South China Sea, and affected by the basin topography in the central South China Sea (Wyrtki, 1961). Tidal observations at the Ren'ai Reef passage-way of the Nancha Islands showed that in reef areas the tidal velocities are much higher than that in open sea, and the current direction is strongly affected by topography.

Summarising, in open sea and especially over the shelves, tidal currents are observed but they normally do not exceed velocities of 50 $^{cm}/_{s}$. Over the deeper regions, these velocities are even smaller. Measurements of semi-diurnal tidal currents at the surface showed amplitudes between 3 and 25 cm/s and for diurnal tides between 6 and 27 cm/s.
In chapter 3, modelling results for water elevation caused by tides will be discussed.

2.5 Additional remarks

In this chapter, a first introduction is made in the geography of the study area together with its tidal behaviour. This is done by findings from literature of measurement or simulations. The similarities and the differences of the findings on tidal behaviour of the study area by these different investigators is shown in this chapter as well. The significant differences in the findings of the investigators underline the complexity of the tidal behaviour of the South China Sea area.
It should also be noted that the tides of the study area are influenced by natural conditions like the ocean currents and seasonal monsoon winds [(Wyrtki, 1961), (Takaki et al., 1996)].

The monsoon winds are westerly during the winter months and easterly during the summer months. The monsoons and surface currents will not further be dealt with in this report.
Before presenting further investigations, first a brief overview will be given of the investigations by numerical modelling of the tides of the South China Sea region in the next chapter.

3 Modelling the South China Sea

This chapter mainly deals with the efforts made on tidal modelling of the South China Sea region in the past. It would be outside the field of interest and the goals of this report to thoroughly present the results of all the investigations made so far. Therefore only some of them are presented here. This presentation is made to see whether different authors come up with the same or seemingly the same conclusions or whether they widely differ in their findings.
DELFT HYDRAULICS also generated a model for modelling the tide of the South China Sea. The South China Sea Model, as this model was named, will also be described in this chapter. At the end of this chapter an overview will be given of the results of the computations that were previously made with this model. The problems of the model will be presented and the main problem parts or areas will be summed up. Furthermore the question will be raised whether the South China Sea Model produced results of sufficient accuracy and if not, suggestions will be made of alterations in the model in order to improve these results.

3.1 South China Sea modelling in the past

Modelling the South China Sea has proved itself as a tough numerical challenge in the past. In order to improve the understanding of the hydrodynamics of the South China Sea Model many hydraulic models have been constructed of (parts of) the South China Sea. Up to now however, investigators have failed to construct completely reliable hydrodynamic model. This can be explained by the occurrence of some difficult elements for tidal modelling in this area. As demonstrated in the previous chapter, the tidal behaviour of the area is quite complex and the bathymetry is such (see section 2.1) that both a shelf sea and a deep ocean model are required.
One of the most up to date modelling results that are known in literature are those of the South China Sea model of Cao&Fang (Zhou Di et al., 1994). The similarity in tidal patterns of K_1 and M_2 constituents with O_1 and S_2 constituents respectively is highly supported by numerical simulations of Cao&Fang (Zhou Di et al., 1994). Some results of this simulation is given in Figure 3.1.
As demonstrated in the previous section, the amplitude of O_1 is slightly less than that of K_1 except in the Gulf of Tonkin. Two counterclockwise tide amphidromic points appear respectively in the western mouth of the Gulf of Tonkin and in the Gulf of Thailand. In the Gulf of Thailand, the counterclockwise tide amphidromic point of O_1 tidal wave does not form an amphidromic system. The co-tidal charts of simulation results by different authors of the diurnal K_1 and O_1 constituents are rather consistent in these two gulfs, but unfortunately numerical results for the open part of the South China Sea seem not to be similar.
In the northern South China Sea, the distribution of M_2 constituent obtained by numerical simulation by different authors are relatively consistent. The propagation process and distribution trend of S_2 tidal wave is identical to that of M_2, but its amplitude is less than a half of M_2 amplitude within most parts of the study area.
In the south-western shelf however, including Gulf of Thailand, results by different authors M_2 constituent are not similar. Some examples of computed amphidromic points of the M_2 constituent (amounts and positioning) by different authors are shown in Table 3.1.
In Table 3.1 the amphidromic points are numbered and these numbers are geographically placed in a detailed map in order to get a clearer picture.

Figure 3.1: Iso-amplitude contours (dashed line in cm) and iso-phase-lag contours (solid line, in degree, for (a) the K1 constituent and (b) the M2 constituent according to Cao&Fang. (*Zhou Di et al.*)

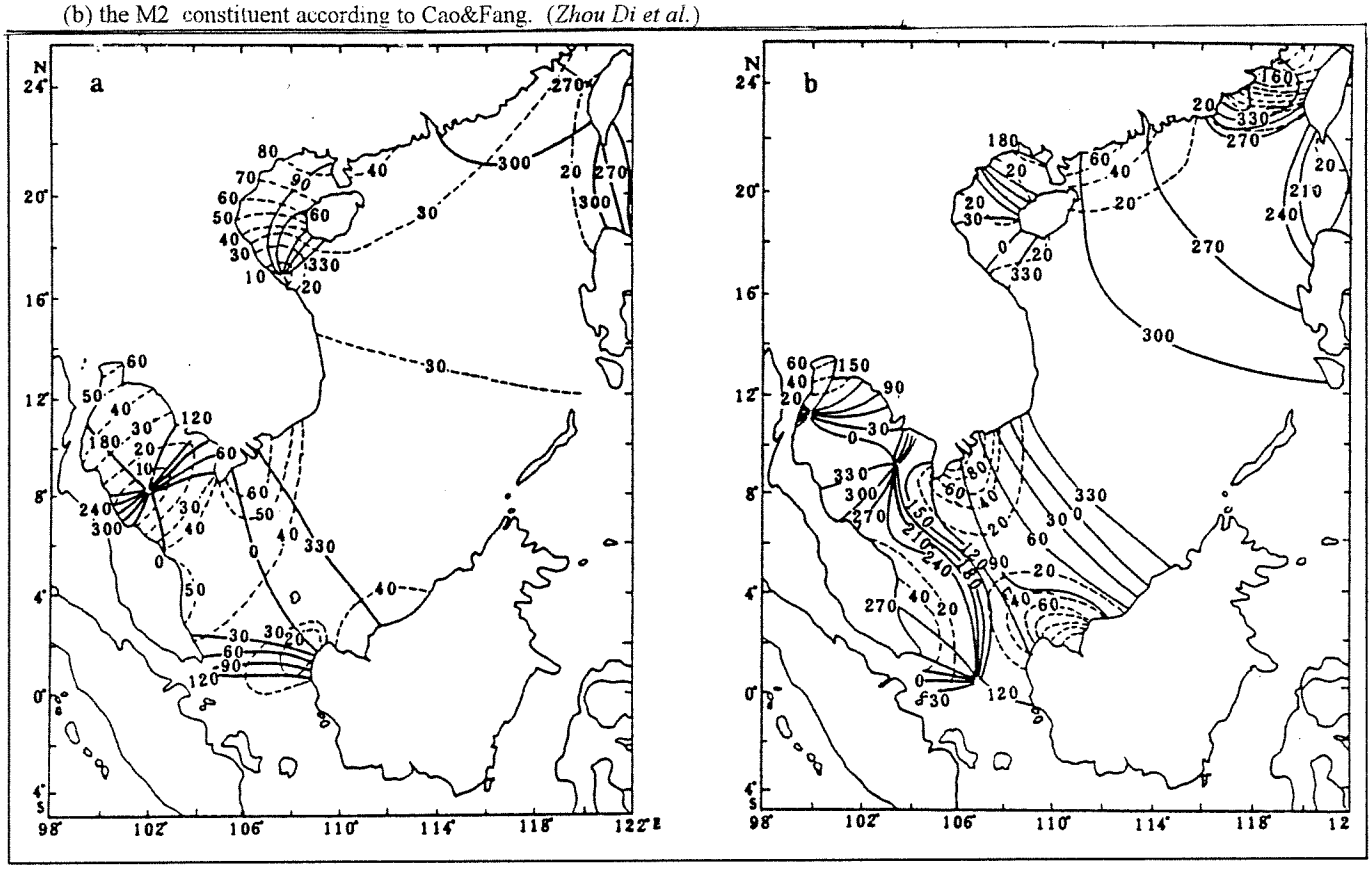

Table 3.1: List of M2 Constituent amphidromic points obtained by numerical simulations for the South China Sea (*Zhou Di et al.*)

Author	*no in*	*Latitude*	*Longitude*	*Phase rotation direction*
	1	10°47'N	100°51'	Left
Sergeev (1964)	2	7°30'N	104°03'	Right
	3	0°16'N	106°33'	Left
	4	11°10'N	100°40'	Left
Thuy (1969)	5	8°30'N	104°00'	Right
	6	2°40'N	107°00'	Right
	7	11°22'N	100°40'	Left
Minh (1975)	8	6°00'N	104°40'	Right
	9	2°30'N	107°50'	Left
Ye and Robinson	10	9°19'N	99°58'	Left
(1983)	11	8°27'N	104°07'	Right
	12	11°12'N	100°30'	Left
Shen et al. (1985)	13	7°36'N	105°00'	Right
	14	2°30'N	106°36'	Left
	15	11°15'N	99°30'	Left
Cao&Fang	16	8°30'N	103°30'	Right
(1993)	17	4°30'N	106°15'	Left
	18	2°30'N	106°30'	Right

In this table, it can be seen that there are in most cases three different amphidromic points are found by the authors:

- along the longitude of about 100^0
- along the longitude of about 104^0
- along the longitude of about 107^0

Figure 3.2: Geographical positioning of the amphidromic points, as given in Table 3.1

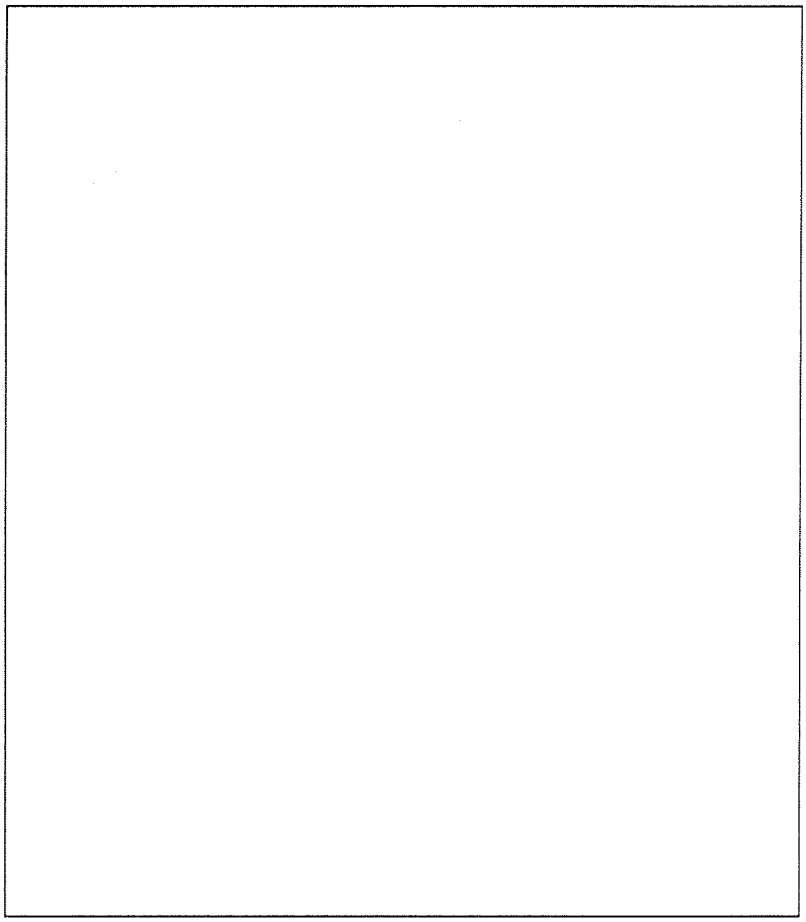

After studying Table 3.1 and Figure 3.2 it can obviously be seen that not every author finds the same number of amphidromic points. The exact positioning of the amphidromic points differ as well. Furthermore the rotation direction of the amphidromic points, indicated as number 3, 9, 6, 14, 18, 17 above, are varying between different authors although these points are close to each other. This leads to the assumption, that model representation at this region of the South China Sea has been and is still limited.
Up to the moment, observed data of tidal velocities are not extensively known. Discussion of tidal velocities of the study area can therefore only be based on modelling results of different authors. This was the reason that modelling results of tidal velocities were already discussed in section 2.4. In the following paragraphs a detailed analysis will be made of the DELFT HYDRAULICS' South China Sea Model.

3.2 The DELFT HYDRAULICS' South China Sea Model

The South China Sea Model is based on TRISULA, DELFT HYDRAULICS' simulation program for hydrodynamic flows in two and three dimensions. The model was constructed with the

depth averaged version of TRISULA. The depth schematization of the model was based on bathymetric information as digitised from Admiralty Charts (edition 1992). The initial model covered an area of approximately 9 million km^2 with rectangular grids, sized 25×25 km^2.
The governing equations were the equation of mass and the shallow water equations with hydrostatic equilibrium. The tidal dynamics were driven by prescribing the water level variations along the open sea boundaries of the representative tidal constituents. For the generation of these conditions, use was made of the Global Ocean Tide model of Schwiderski (1978) in combination with the Admiralty Tide Tables. At closed boundaries a perfect-slip condition was applied. The initial conditions were zero currents and a flat sea surface.
In Figure 3.3 the grid enclosure of the DELFT HYDRAULICS' South China Sea Model is given. The boundary conditions of the model are given at the following locations:

- 1- In the Northwest: where the Andaman Sea flows into the Strait of Malacca.
- 2 - In the North: the middle part of South China Sea.
- 3 - In the East:
  - 3.1 in the Celebes Sea
  - 3.2 in the Flores Sea.
- 4 - In the South: at a number of straits which connect the Indonesian Seas (Java Sea) with the Indian Ocean. These straits are:
  - 4.1 Sunda Strait
  - 4.2 Lombok Strait
  - 4.3 Sape Strait

Figure 3.3: Delft hydraulics' South China Sea Model.

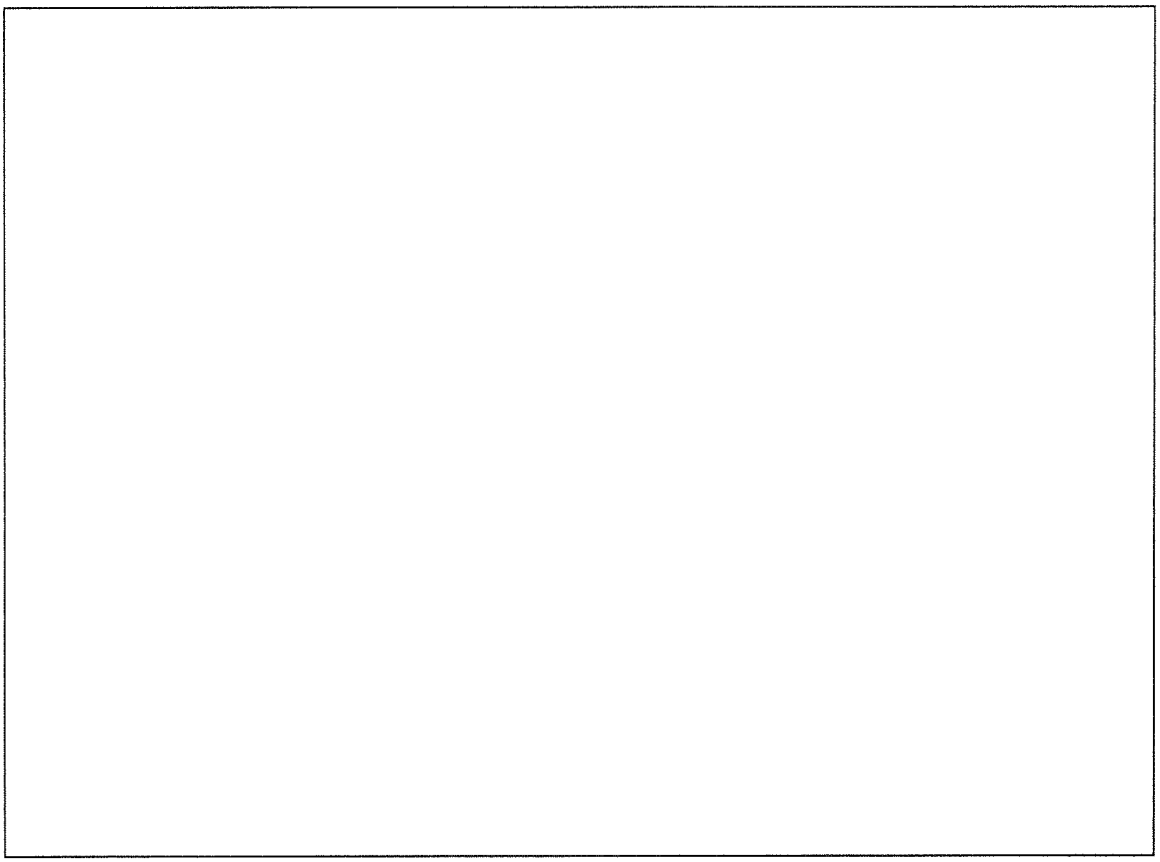

The model is calibrated by comparing the computational results with measurements. The time series for some specific amount of tidal stations were analysed with DELFT HYDRAULICS' TRIANA package. The computations were made in -7 UTM time zone, which means that some measurements of tidal stations in -8 time zone had to be shifted.

In June 1993 the first run (identification number S08) of the model was made. The results of this first computation were promising. Close to open boundaries and within the central parts of the model area the results were however far from observed values.
In this state the model could only be used to create boundary conditions for more detailed models and not for large scale hydraulic motion, or transport of material computations.

Some first remarks considering the model were:

- Although the rectangular grid modelling produced some appreciable results, question was raised whether a spherical grid modelling would yield better results.
- The Coriolis parameter was taken constant for the whole area.
- The tide generating forces were neglected.

Given the first results, it was soon concluded that the model was not satisfactory yet. In an effort to improve the model, a calculation with spherical grids was suggested to be the next step. This computation was given the identification number of S11.
No alterations to the bottom profile were suggested, because this was assumed to be well schematised. Tide generating forces were possibly one of the many alterations for improving the model. Their effect to the solutions was however believed to be minor, so they were still neglected. Improvement of the model results should be searched for in other more important aspects first.
The computation with spherical grids (S11) showed no major differences compared to the first run (S08). The expected improvement of the model results did not occur. Locally, especially for semi-diurnal components, there were some slight improvements. (for example in Java Sea and near Singapore). One of the major errors that occurred in computations S11 as well as S08 was the amount of amphidromic points of the M_2 constituent. Both computations showed only one amphidromic point while Schwiderski detected two of them in the same area. (one between Cambodia and Malaya Peninsula and one in Java Sea near Singapore)
It was suspected, that the model included a systematic error in the results. Suggestions were made to make the model smaller near Malacca Strait by "cutting it off" near Singapore. This was suggested in order to be able to analyse whether the disappointing results in Java Sea were caused by a too roughly schematization of Malacca Strait.
A re-analysis of S11 with 94 monitoring stations (instead of 27 used before), with the help of TRIANA, showed that the semi-diurnal components (especially M_2) still showed too much differences between the computed results and measured results. Especially the results of phases were very disappointing. It was interesting that all the calculated values of the amplitudes were larger than observed values. This led to the conclusion that the simulation should be done with a smaller time step in order to achieve more accuracy of the results.
A new calculation with a smaller time step, in an effort to improve the results of the semi-diurnal components was then suggested. This was given identification number S12. Also a calculation ignoring advective terms together with less time step, identification number S13, was suggested. If the advective terms could be neglected, some credit could be gained in computing time.
Calculation S12, with time step of 5 minutes instead of 15 minutes, showed significantly better results for the M_2 component. Given these results, it was concluded the time step of 15 minutes was too large. However, whether the time step of 5 minutes was still not too large also, could not be discovered from this run. The representation of the results for diurnal tides with less time step were acceptable. This could however not be said for semi-diurnal tides. The semi-diurnal tides were differing up to 20^0 in phase and 20% in amplitude.
Computation S13, identical to S11 except for leaving out of the advective terms, showed no significant differences in results. It was then concluded the advective terms could be neglected in future runs. This resulted to a considerable credit in computing time.

To discover whether the time step of 5 minutes was still too large, a new run was made with identification number S14. This run was similar to S12 except the time step of 1 minute. For the four most important tidal constituents (M_2, S_2, K_1, O_1) there were no further changes in results. This led to the conclusion that the time step of the calculations could be taken as 5 minutes and smaller time steps would not lead to better results. Computation of the model with the exclusion of the Malacca Strait has never been made so far.
As there was not sufficient improvement in the results of the model so far, it was refined to half the gridsize, by interpolating the original bottom profile. During the run that was made with refined grid dimensions, the computation was terminated because of occurring instabilities. To prevent these instabilities, two straits (Lombok Strait and Sape Strait) were closed. The computation that then was made was given the identification number T03.
Computation T03 showed results of the diurnal tides (for phases and amplitudes), which were almost the same as in computation S12, except for the Sulu Sea area. The results of semi-diurnal tides were completely different.

Some interesting remarks that were made looking at the results of the semi-diurnal components (T03 compared to S12) were:

- The results in Java Sea and Macassar Strait of computation T03 showed not any significance with S12. This is probably due to the closing of the Lombok and Sape Straits.
- In the finer model, the amplitudes of all tidal components were larger than those in S12 in the Sulu Sea. The passages of the Sulu Sea were apparently less disturbing to the results in this case.
- The phase-lines in the South China Sea for semi-diurnal tides were comparable to observational phases. There was however a strong resonance (too little dissipation) to be seen at the coasts of Borneo, and Vietnam. This has become visible more strongly since the refinement of the grid size.
- Results in Celebes Sea were comparable to the observed values.

After the results of T03, the following alterations were suggested to further improve the results:

- One calculation with the original coarse model with closed boundaries at the positions of Lombok Strait and Sape Strait. After this calculation it would be possible to see whether the results of the coarse model resembled the results of the finer model with identical boundaries.
- One calculation with the finer model, with much larger viscosity coefficient (500 m^2/s) than was assumed in earlier calculations. This suggestion was made as an attempt to stabilise the calculation with the finer model and open boundaries Sape and Lombok Strait by suppressing instabilities.
- Double-check of the schematization of the bottom topography of the area with detailed admiralty charts and with the ETOPO 5 bottom file.
- Schematization of narrow straits with lots of tiny islands with much larger bottom roughness parameter than assumed up to the moment.

The results following of the suggested alterations were the following:

1• Calculation of the coarse model with closed boundaries at Sape and Lombok Straits.
The results of the diurnal tides were indeed resembling the results of the finer model. There were similarities in Java Sea but also some major differences in the outer parts of the model. The results of the semi-diurnal tides however, were significantly different from the finer model.

In the finer model there was stronger resonance at the coasts, especially at the coasts of Northwest Borneo and at Mekong Estuary in Vietnam. This could be explained by noticing that the two models were differing in schematization of the coasts, the bottom profiles and roughness parameter in those areas.
While verifying the bottom schematization, it turned out that a significant error had been made with the interpolation of the bottom profiles from the coarser to the finer model. Also some errors were made on the modelling of the coastal lines. This was noticed to be one of the reasons for the differences between the results of the two models.

For the time being, the following conclusions were made:

- the finer model as well as the coarse model showed some schematization errors at the coastal zones and bottom profiles.
- There still existed large discrepancies between model results and measurement data for both the coarse and finer models.
- Given the results of both models, the conclusion was drawn that a finer model for the area was needed.
- Comparing the results of S12 to S16 (see Table 3.2) it was concluded that Sape Strait and Lombok Strait were of huge importance for the results of the semi-diurnal tides in Java Sea.

2• Calculation of the finer model with larger viscosity parameters:
This turned out not to be successful, because of persistent occurrences of instabilities at Sape Strait.

3• Verifying used bottom schematization:
The schematization used until the last calculation showed some major errors. One of the main errors for instance was that the distance between the coasts of Borneo and Vietnam was not correctly implemented. Because of this, it was wise to reconsider the bottom schematization for the whole model area.

Two options were given to choose from:

- Set up of a new model with new bottom schematization of 15` grid (about 27*27 km^2)
- Set up of a new model with new bottom schematization of 5` grid (about 9*9` km^2)

Before discussing the newly developed SCSM first all the computations so far will be summarised in Table 3.2. Not all calculations shown in this table is considered in detail in the former and following notes.

Table 3.2: Overview of calculations with the first version of the South China Sea Model

RUN id.	SPECIFICATION
S08	• rectangular grids, one grid size 25x25 km^2 • constant Coriolis parameter and no tide generating forces • time step of 15 minutes • 27 measurement stations in model area
S11	As S08 except for: • spherical grids with varying Coriolis parameter • 94 measurement stations, with results optimised by TRIANA
S12	As S11 except for: • time step of 5 minutes (was 15 minutes)
S13	As S11 except: • no advective terms
S14	As S11 except for: • time step of 1 minute • initial height (a_0) of 0 m (was 1,5 m) • Calculation is done 5 days longer than in S11
S16	As S12 except: • no advection and a_0=0
T03	As S12 except for: • grid size ≈ 10x10 km^2 $(0,10)^0$x$(0,10)^0$ • Lombok Strait and Sape Strait are changed into closed boundaries to prevent instabilities
G01	• reschematization of the basin and coastal areas in the whole model • spherical grids of 0.15' by 0.15' • time step of 10 minutes
G02	As G01 except: • a time step of 5 minutes
G03	As G01 except: • a time step of 2,5 minutes

The choice was made on setting up of a new model (with grid size 15'×15') and new bottom schematization derived from ETOPO 5 and GED database systems. In this new model, the model area is enlarged to the North. The reason given for this was the expectation that a bigger and coarser model would better suite into the goals of an overall model for the area. One of the reasons for deciding on a coarse model was that future (possibly to undertaken) 3-D advanced TRISULA computations are viable more likely when using a coarser model.

Before application of the model in the larger area, first a calculation with new bottom and coastal schematization in the older, not enlarged, area was suggested for verification of the effects of the new schematizations on the previous results.

Table 3.3 gives a short description of the finally developed South China Sea Model:

Table 3.3: The final version of the SCSM, with rearranged bottom profile and new gridsize

Grid Type	Spherical grid modelling
Model Area	Taiwan Strait (boundary) Luzon Strait (boundary) South China Sea Sulu Sea Celebes Sea Macassar Strait Malacca Strait Java Sea Flores Sea
Origin (1,1] ζ-point)	-8,875N 95,125E
Grid distance	15 minutes
Geometrical Schematization	GED coastal data
Depth Schematization	Based on ETOPO 5 data. In narrow passages depths are averaged from detailed admiralty charts.
Boundary conditions	Identical to boundary conditions of the former model.
Roughness parameter	Uniform Manning parameter of 0,026 $m^{1/2}/s$ for the whole area.
Viscosity parameter	Uniform parameter of 250 $m^{1/2}/s$

With this latest model (the northern boundaries in the South China Sea were kept in old position) three calculations with computation time of 20 days each were suggested in order to determine the optimal time step:

- identification number G01 with a time step of 10 minutes.
- identification number G02 with a time step of 5 minutes
- identification number G03 with a time step of 2,5 minutes

The time integration method is of the ADI-type [Kuipers&Vreugdenhil, 1973; Stelling 1983]. The wave propagation is related to the Courant number (Stelling&Booij, 1993), defined for a staggered orthogonal curvilinear grid as given by TRISULA user-guide (release 2, May 1995):

$$C_f = 2\Delta t\sqrt{g\,h}\sqrt{\frac{1}{\sqrt{G_{\xi\xi}}^2}+\frac{1}{\sqrt{G_{\eta\eta}}^2}} \qquad (3.1)$$

in which $\sqrt{G_{\xi\xi}}$ and $\sqrt{G_{\eta\eta}}$ are coefficients to transform curvi-linear to rectangular coordinates in latitude and longitude direction respectively.

$\sqrt{\frac{1}{\sqrt{G_{\xi\xi}}^2}+\frac{1}{\sqrt{G_{\eta\eta}}^2}}$ is also the specific (grid) length in meters.

Theoretically the CFL condition is not a compulsory element within the calculations for stability, because water levels and velocities are implicitly solved along grid lines. However, the CFL condition is still considered because of accuracy of solutions (Stelling&Booij, 1993). It is noted that for irregular boundaries (islands, channels, etc.) where the grid lines do not smoothly follow the geometry, Courant numbers larger than $4\sqrt{2}$, may lead to badly predicted flow patterns.
With computations G01, G02 and G03, it turned out that a time step of 5 minutes was needed. This time step corresponded with a mean Courant number of 1,4 and a maximum Courant number of 3,7.

After comparing the results of G02 to the results of S12 the following comments could be given:

- The new model with calculation G02 resulted into considerably worse results, when compared with G01.
- Locally there were some relatively more accurate results.
- The schematization of the narrow passages to the Sulu Sea is decisive for the results of the eastern part of the model area. In the newly developed model, these passages were probably schematised too deep and/or too smooth.
- Schematization of other narrow passages Sape, Lombok and Malacca Strait, are also of much importance to the results.
- The results for the diurnal tides are less influenced by schematization of details, like narrow passages and little island groups, than the results of the semi-diurnal tides.

To achieve better results, it was suggested that the schematization of the narrow passages should first be re-analysed. The passages to the Sulu Sea should be altered by changing the depths and roughness parameter locally. This should also be done for the passages at Sape Strait and Lombok Strait. The depth values of Sunda Strait and Malacca Strait should also be reanalysed. These narrow passages were believed to be the key elements of the model.
To improve the results of the model several more attempts have been made. The calculations are however all made with the modified older model: which is as shown in Figure 3.3 and with gridsize of 0.26`×0.26`, but with modified bottom schematization and geometrical schematization. Only one single run was made with the model as described in Table 3.3 which produced disappointing results. The strategy was to set up the older model first before setting up the enlarged finer model for setting up of the larger model seemed even a harder task. Therefore all the discussions of results and the calculations of South China Sea Model are based on the older model further in this report.
An overview of all the attempts made to set up the model is briefly given below in Table 3.4. These runs will not be discussed in detail any further in this report.

Table 3.4: Overview of calculations with the modified version of the SCSM

Run Id	Alteration related to G02	Purpose	Result
G04	Boundary conditions semi-diurnal tides Sape Strait	improve the results of the Java Sea	only some local improvements of amplitudes and phases
G05	Less depth at Sunda Strait	improve the results of the Java Sea	only some local improvements in Java Sea
G07	Adjustment of depths at Palawan Archipelago	improve results in Sulu Sea	Slightly better results in Sulu Sea, at the coast of southern Borneo worse results
G08	viscosity parameter of 750 (was 250)		no effects except for stability
G09	former RWS depth schematization at Sulu Archipelago	improve the results of the semi-diurnal tides in Sulu Sea	no significant changes, slightly better results in Celebes Sea
G10	Depth schematization in whole Sulu Sea including neighbouring Archipelago's changing to RWS schematization.	improvement of semi-diurnal components in Sulu Sea	More accurate results in Sulu Sea, however less accurate results at southern and western coasts of Borneo.
G11	As G10, but depth schematization in Sulu Sea differently interpolated		comparing to G10 slightly less accurate results in Sulu Sea
G12	As G10, except for roughness parameter changed to 0,05 (was Manning 0.026)		almost no effect, very little improvement of results
G13	As G10, but this time an exceptional Manning parameter of 0,5 at Sulu Archipelago passages.		Amplitudes in Sulu Sea almost as observed, but phases on average 90^0 out of phase
G15	As in G13, but with extreme low Manning parameter of 0,001 (was 0,026)		No differences comparing to G13.
G17	As G13, but depths at Palawan passages 1,5 times deeper.	improvement of phases in Sulu Sea	Comparing to G13, phases even more out of phase.

From these computations, the following conclusions were drawn:

- Schematization of the narrow passages to the Java Sea, often no larger than 1 to 2 grids, is of much importance for local results in Java Sea.
- In general, tidal currents are extremely influenced by the basin schematization of the Java Sea.
- The results of almost every run were strongly influenced by the schematization of the Sulu Sea and the narrow passages at the two sides of this sea. Modelling errors caused by this area are considered to affect the results of the model up to the western parts of Java Sea.

The results of computation G13 are briefly presented in the figure on the next page. Values given are the differences of the computed values from the observed values, H_c means computed amplitude, φ_c means computed phase.

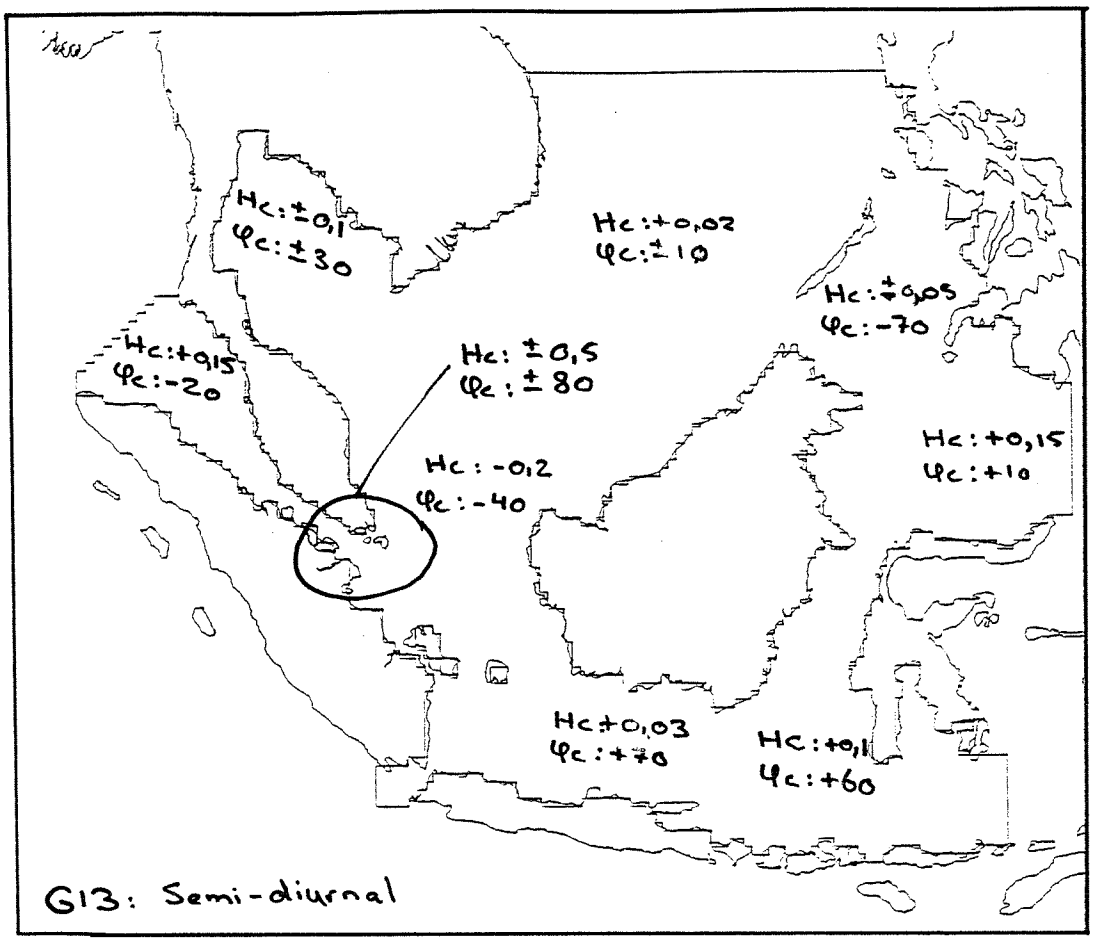
Hc: ±0,1
φc: ±30
Hc: +0,02
φc: ±10
Hc: ±0,05
φc: -70
Hc: +0,15
φc: -20
Hc: ±0,5
φc: ±80
Hc: +0,15
φc: +10
Hc: -0,2
φc: -40
Hc: +0,03
φc: +70
Hc: +0,1
φc: +60
G13: Semi-diurnal

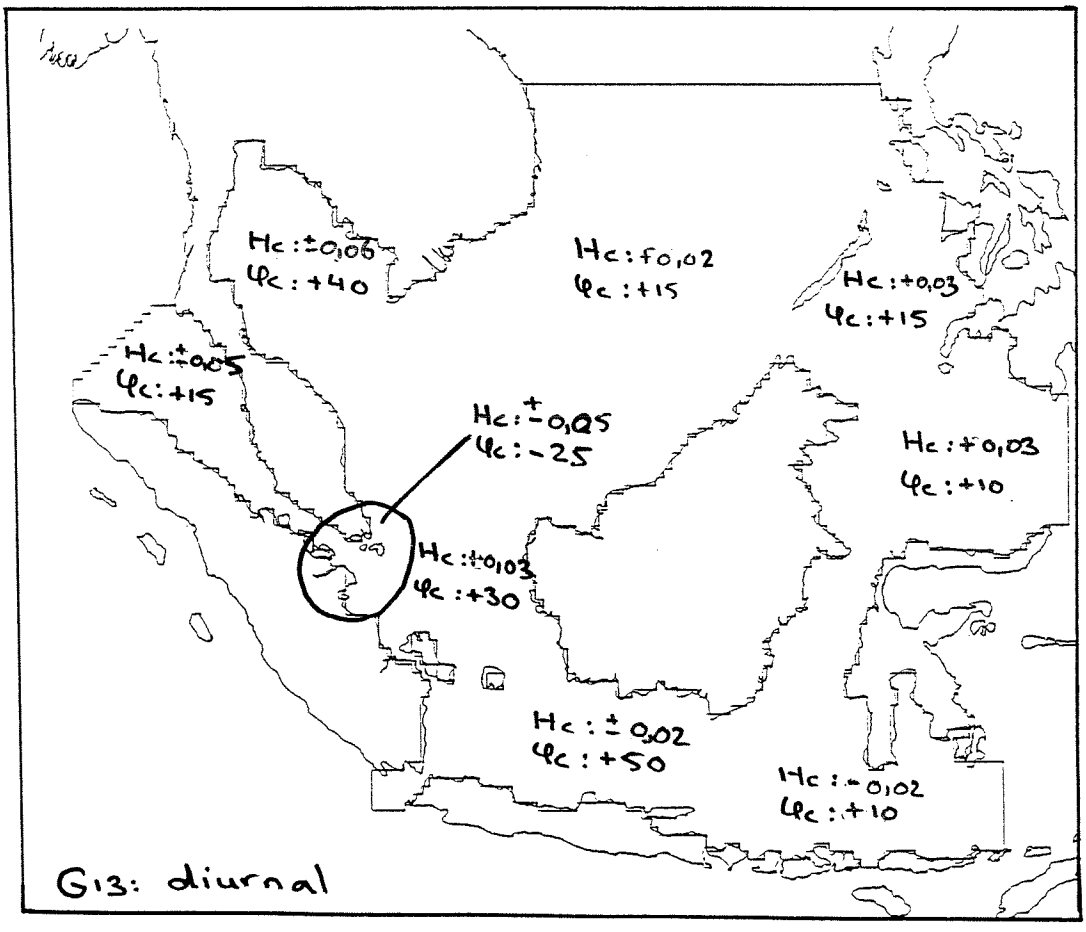
Hc: ±0,06
φc: +40
Hc: +0,02
φc: +15
Hc: +0,03
φc: +15
Hc: ±0,05
φc: +15
Hc: ±0,05
φc: -25
Hc: +0,03
φc: +10
Hc: ±0,03
φc: +30
Hc: ±0,02
φc: +50
Hc: -0,02
φc: +10
G13: diurnal

3.3 How to go on with the South China Sea Model?

The section above was a brief summary of the development of the South China Sea Model between June 1993 and June 1995. The conclusions and recommendations described in that section were for most part as represented in the notes made during the South China Sea Model project during 1993-1995. Further supplement on the conclusions after the study of the tides of the study area can be given as follows:
It is obvious that even after many attempts, the South China Sea Model shows many complications. To achieve acceptable results of the model, it is needed that the major problems are split in parts and that each problem part be solved on its own.
First there are some major schematization problems. In the study area there are lots of little islands and narrow water passages, which are of great importance for the results. However, the dimensions of these passages and tiny islands are such, that they are hard to schematise in the model. The schematization of the sea basin and coastal lines also has major effect on the results and needs thorough analysis. The geometry of the model domain is very important for tidal movements: the presence of shelf areas as well as deep sea basins within the study area increases the geometrical problems even more. Transition between relatively sharp frontiers of deep to shallow areas seems to be a major problem (over a small distance) and in such conditions the grids are too coarse.
Difficulties of bottom schematization are even strengthened by the geographical positioning of the study area. Because the South China Sea area is located in low latitudes the frictional terms get an increasing importance as the Coriolis parameter and advective terms are reduced near the equator (Pohlmann, 1987). The advective terms can even be neglected in the case of the South China Sea Model as demonstrated with computation S13. The frictional terms are known to be extremely sensitive to bottom schematizations.
Combined with complicated tidal movement in the large modelling area a difficult numerical modelling environment is created with all the complexities mentioned above.
Although much work has been done to achieve better results, there is still a lot to do before it can be assumed there is a suitable model. To further tackle the problem, the major issues can be addressed separately. Subdivision in more or less separate problems can be made when the earlier mentioned complexities and the notes of the last section are considered together. Each sub-problem will be considered apart in the following sub-sections.

3.3.1 Sulu Sea[5]

First the Sulu Sea area can be considered as a problem area. The former calculations made so far with the South China Sea Model demonstrated that the results of the Sulu Sea were far from accurate. This sea is very deep in the middle parts and both to the Celebes Sea and the South China Sea, it is separated by lots of islands, shallow reefs and some deeper water passages. Because of the dimensions of the islands and passages the Palawan and Sulu Archipelago's are very hard to schematise in the model.
A first suggestion to study the effect of the Sulu Sea is the computation of the model with the Sulu Sea excluded of the model domain. This has been done in the past by other researchers already. Pohlmann (1987), made a baroclinic model of almost the same area as the South China Sea Model but the Sulu Sea. Unfortunately reasons for the choice of his boundaries are lacking, but it might be the disturbing effect of this sea in his modelling results. With implementing boundary conditions at the position of the two shallow archipelago's, the solution of the problems of the model might be reached without any possible disturbance by the Sulu Sea. In this way verification can be made whether the insufficient results in Sulu Sea

[5] *The Sulu Sea will be dealt with in section 4.1*

really affect a huge part of the model domain and the extent of the area in which these results possibly have any influence.
About the effect of the passages of Palawan and Sulu Archipelago's to the Sulu Sea different authors have different opinions. Wyrtki (1961) suggests the tides from the Pacific Ocean do not reach the Sulu Sea through the Palawan Archipelago. The modelling results of the Sunda Model (van Berk, 1986) demonstrated that the effect of Palawan Archipelago is moderate on the tides in Sulu Sea as well.
There have been earlier approaches to the modelling of the South China Sea by foreign oceanographers using a closed boundary at the Sulu Archipelago (so the Palawan Archipelago section open). Also approaches with a closed boundary at Palawan archipelago (and Sulu Archipelago open) are known. These approaches deserve to be given some more attention to, given the modelling problems of the Sulu Sea. Verification of both these approaches with the SCSM could help to define the effects of both these Archipelago's to the South China Sea Model. Later in this report, in section 5, more attention will be given to these approaches.

3.3.2 Java Sea

Second there are some major problems in the modelling results of the Java Sea. The reason for this is believed to be the result of the conditions at the open boundaries. The model results are sensitive to the schematization narrow passages like Lombok Strait and Sape. Instabilities of modelling results occurred in previous calculations due to these sensitivities. There must still be put much effort in finding the most optimal schematizations (size and roughness) for these passages. The schematization of the sea basin in Java Sea can be given some more attention too, for this turns out to be extremely influential because of its shallow depth.
The poor results in the Java Sea are for some part also caused by other neighbouring problem areas, like Sulu Sea and Malacca Strait. Reverse influence, which means that the poor results of for instance the Sulu Sea and the Malacca Strait are for some part caused by poor results of the Java Sea, is unlikely because of the movement directions and intensities of the tides. For the results of Java Sea, it is seems therefore to be a good cause to solve the modelling problems of these areas, the Sulu Sea and the Malacca Strait, first.

3.3.3 Malacca Strait[6]

Third there is the area of the Malacca Strait, with also many little islands at its end, see also sections 2.2.1 and 2.2.2. The amount of tides entering the South China Sea from the Indian Ocean through the Malacca Strait, is highly depending on the schematization of the Malacca Strait. Especially at the narrow end near Singapore and the Riau Archipelago, the results of the several earlier computations with the South China Sea Model were not satisfying. The reason of this is believed to be the geometrical schematization problems of the passages, islands etc. within the Riau Archipelago area and the depth schematization problems. This problem seems therefore to be similar with the problem of the Sulu Sea.

3.3.4 Gulf of Thailand

Fourth there is the problem of resonance occurrences, especially at the coasts of Vietnam and in the north-western areas of Borneo. There are also some local disturbances within the region of the Gulf of Thailand. This seems to be the result of the presence of shallow depths and the abrupt change of depth from very deep to shallow. In sections 2.2.1 and 2.2.2, it was noted that both reflection and refraction compared with shoaling occurs in these areas. The solution of the problems in these areas might also be found in local adaptations to depth schematizations. Locally adapting the depth (shallower or deeper), the coastline and the

[6] *The Malacca Strait is considered in more detail in Appendix 1, section A1.6*

bottom roughness (adaptation to the Manning coefficient regarding of local conditions) are the main aspects that can be thought of.
The insufficient results of Gulf of Thailand can not be the consequence of the results of Malacca Strait, Sulu Sea and small passages to Java Sea, because these areas are quite far from the Gulf of Thailand.

3.3.5 Possible incomplete modelling

The tide generating forces were neglected, because they were assumed to be not significant for model results. It is questionable whether this assumption is true.
The question arises whether the gridsize of the model should not be refined, because of the many small islands and passages (this has already been tried see Table 3.4). It might even be sensitive, given the occurring problems at some specific locations of the model, that the model area should be adapted as well.

With respect to the adaptation to the model area the following alternatives can be thought of:

- Is the Sulu Sea really necessary in the model? If this marginal Sea could be excluded, this would possibly prevent some modelling difficulties. Pohlmann (1987) and Cao&Fang (Zhou Di et al., 1994) set up models of the South China Sea area without the Sulu Sea before.
- The same question for Sulu Sea can also be asked for Malacca Strait.
- What is the effect of closing both the passages of Sape and Lombok or only one of them? A first computation with closing of both these passages was made with T03 (see Table 3.2), but the aim of that computation was different by then. Pohlmann (1987), set up a baroclinic model of almost the same area as the DELFT HYDRAULICS' South China Sea Model, except for closed boundaries at the positions of these straits. Mihardja (1993), set up an enlarged South China Sea model with only Lombok Strait closed (also Sape Strait open).
- Should the model area be enlarged to the south and cover some part of the Indian Ocean and Timor Sea also? In this way the problems of boundary conditions at the narrow passages of Sape and Lombok might be avoided. In the several runs that were made in the past, the schematization of these narrow passages and their boundary conditions appeared to be one of the major problems. There are examples of models of this area like that of Mihardja (1993), and Takaki et al. (1996), of which the authors are confident of the obtained results. At the beginning of generation of the South China Sea Model, there was awareness of this problem, but the choice is still made on open boundaries at the positioning of these passages, because tidal data was otherwise not available in open side of the Indian Ocean in the south (only use of Schwiderski's Global Tide Model could be made then).

3.4 Additional remarks

Tidal models of the South China Sea do not show acceptable accuracy. Different investigators seem to have significant different findings of the tides within the area.

Also the results of DELFT HYDRAULICS' South China Sea Model are not yet sufficiently accurate and problems of the model arise in different locations. The problems of the South China Sea Model can be separated in parts. Explanation of the occurrence of each of the problem parts and the search of solutions for them separately must then be the next step. In the previous section, this separation and suggestions for the solution of each separated part has been made. In the following chapters some of the separate problems will be analysed.

4 Problem analysis

The inaccuracies of the South China Sea Model are fundamental, for example sometimes there is a phase lag of more than three hours (90°). Before further tuning of any parameters, basic insight in the fundamental mechanisms that determine the tidal behaviour of the area is crucial.
For understanding the mechanisms involved, one of the major problem areas of the South China Sea Model will be considered apart. The area chosen for this consideration is the Sulu Sea. This sea is believed to significantly disturb the global results of the South China Sea Model. Also the tidal behaviour of the Sulu Sea itself is not well understood. For a proper representation in a tidal model it is needed to try to understand this.

First a brief description will be given of this area. Then its tidal behaviour will be discussed with the help of tidal data from the Admiralty Tide Tables. Thereafter calculations will be made with a 1-D TRISULA application. Further analytical approach will be made by studying the results of a 1-D model based on harmonic analysis. In this model the Sulu Sea is represented as a system of connected basins.
If this approach proves itself to be successful the method will be applied later for the rest or other specific areas of the model domain. The calculations will be restricted to semi-diurnal tides (M_2), leaving the other constituents open for future calculations.

Appendix 2 and Appendix 3, at the end of this chapter, are important supplements of this chapter. Appendix 2 contains charts of among others the Sulu Sea and also charts presenting numbered tidal stations. In addition tables with tidal data and tables with self calculated variables, which help to explain the tidal behaviour of the area, is given in the same Appendix 2 as well.
Paragraph A3.1 of Appendix 3, contains the underlying theory behind the analytical model and the demonstration of the generation of the model in steps. Paragraph A3.2 of Appendix 3 contains the testing of the validity of the model and A3.3 contains one copy of one of the programmes. Finally A3.4 contains some result plots of the TRISULA 1-D model and the 1-D model based on harmonic analysis as well as the test results of the last model.

4.1 The Sulu Sea: an overview

The Sulu Sea, see Figure A2.3, is a mediterranean sea with roughly a rectangular form. It extends north-eastward from Sabah (Malaysian Borneo) and is bounded to the north-west by Palawan, to the north-east by Panay and Negros and to the south-east by the Zomboanga peninsula on Mindanao Island and the islands of the Sulu Archipelago. It covers an area of about 250000 km^2 and is up to 5000 m deep (Apel et al., 1985). Several shallow straits connect the Sulu Sea to the Celebes Sea, the South China Sea and the Pacific Ocean.
The bathynetry of the Sulu Sea shows three general depth regimes, one shallow and two deep, as it can be seen in Figure 4.1 (note that 1 fathom equals 1.825 m).
Three detailed bathymetric profiles of the sea are given as indicated in Figure 4.1. The bottom profile found along the connecting line of the stations SS1, SS2 and SS3 is shown in Figure 4.2. The profiles along the other lines are called 102 and line 111 and are shown in Figure 4.3. Tidal characteristics of the Sulu Sea area will be discussed in detail in the following section 4.2.
In the paragraphs 2.2.1 and further, it was already mentioned that mixed semi-diurnal and diurnal tides dominate the Sulu Sea and that there is an approximate 4-hour phase shift in tides across the Sulu Archipelago.

Figure 4.1: Bathymetry of Sulu Sea, showing locations of stations SS1, SS2 and SS3 (*Apel et al.*)

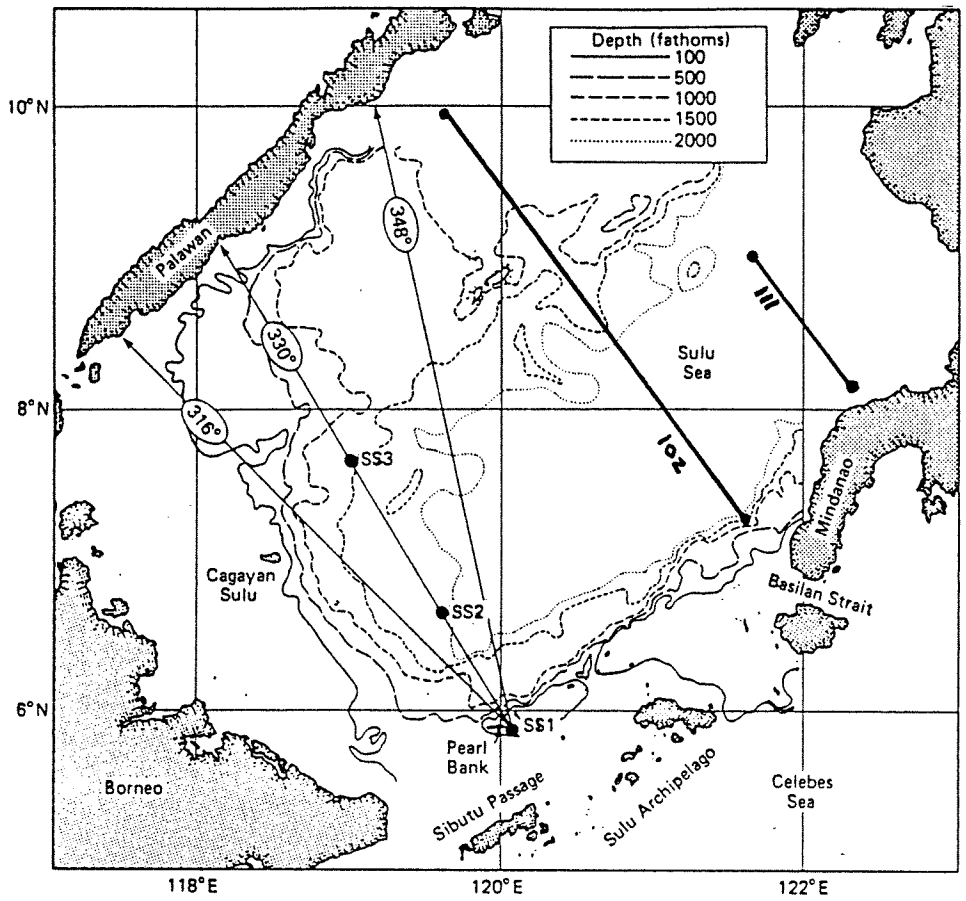

Figure 4.2: Bottom topography of the Sulu Sea across the stations SS1, SS2 and SS3 (*Apel et al.*)

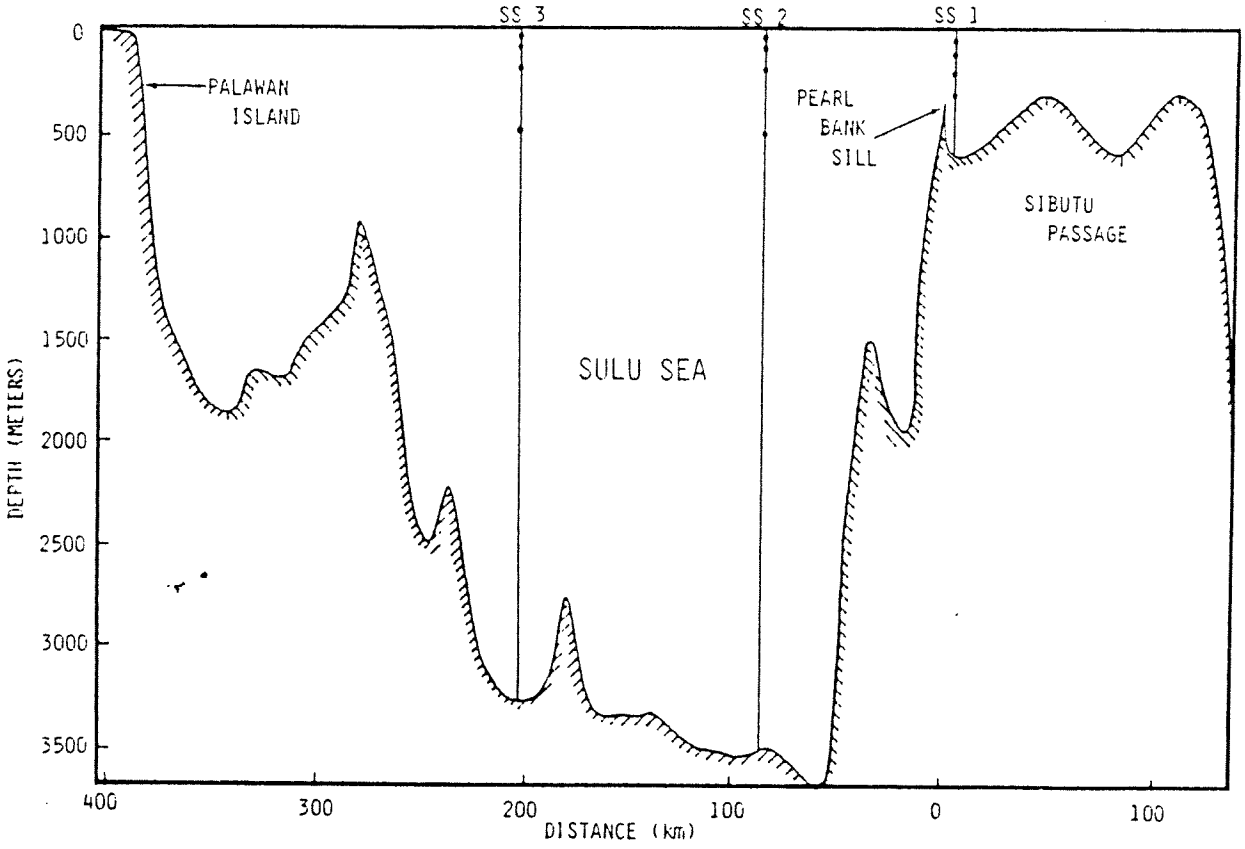

Figure 4.3: Bottom profiles across the lines 102 and 111 (*Exon et al.*)

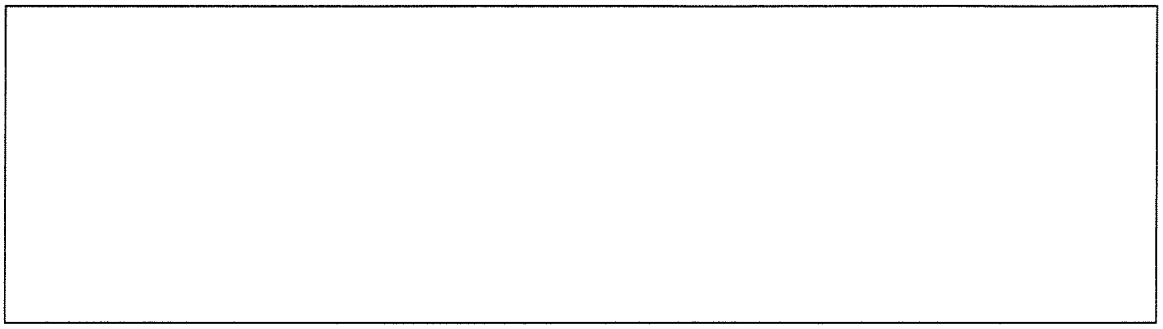

4.2 Tides in the Sulu Sea

In Figure 4.4 a detailed tidal flow diagram is given of the tidal movements in the Philippine Islands region.
Two flood tidal streams enter Sulu Sea from opposite directions. One of them is originating from the South China Sea through the openings of the Palawan Archipelago, the other from the Pacific Ocean mostly through Basilan Strait and Sibutu Passage. Tides from San Bernardino Strait and Surigao Strait seem not to reach the Sulu Sea, they are mostly shielded within the major Philippine Islands.
The stream from the South China Sea passes from north to south along the west coasts of Luzon and Palawan and through Verde Island Passage, Mindoro Strait, Linapacan Strait and Balabac Strait. That part of the stream, which enters by Mindoro Strait follows the coast of Mindoro, part of it continuing round the coast of that island. The rest of the stream sets south-east and splits at the north-west point of Panay. Part of this flow turns south from the north-west point of Panay.
The east going stream, entering through Balabac Strait, turns north-north-east along the east coast of Palawan and spreads itself like a fan over the Sulu Sea in a north-east and east direction. It forms an east going stream between Cuyo Islands and Panay, and a stream which sets south of the Cagayan Islands, where it is reported to meet the stream from Surigao Strait approximately on the meridian of Cagayan Island.
In Sibutu Passage the flood stream sets north-west. Also in the Sulu Archipelago the flood stream sets generally north and west, but takes many local directions between the islands, where it also appears to be influenced by the monsoon currents. In the channels between the islands of the Sulu Archipelago the tidal streams are strong and irregular. Through Basilan Strait the west going stream moves along the west coast of Mindanao northward until it meets the south going stream from Surigao Strait somewhere midway off the coast.

As indicated above, the tides enter the Sulu Sea from two main directions. In the Sulu Sea itself tides from these two main directions meet and tidal movement can be noticed to all directions. Tidal velocities in the narrow passages of the Sulu Archipelago and the Palawan Archipelago are higher than open sea and in some cases much higher.

Figure 4.4: Direction of the main flood stream in Philippine waters[8&9] (*Heslam*)

[8] *Numerals indicate the rate of tidal streams in knots (1 knot equals about 0.51 m/s)*

[9] *Ebb streams generally set in the opposite direction at the same rate as the flood unless otherwise indicated.*

4.2.1 Analysis of tidal constituents from observations

The amplitudes and phases of the four major tidal constituents from tidal stations in the Sulu Sea have been investigated in order to find any consistency in the propagation and behaviour of the tides. Values of amplitudes and phases (according to the Admiralty Tide Tables, edition 1996) of the M_2 and K_1 tidal components, are depicted on a chart of the Sulu Sea at known tidal stations. An overview of used stations (Figure A2.5), together with a table consisting data of amplitudes and phases of the four major tidal constituents (Table A2.1) is given in Appendix 2.
The dominating semi-diurnal tidal constituent of the area is the M_2 constituent and the diurnal constituent the K_1 constituent. This can be seen by looking at Table A2.2 of Appendix 2, in column 4.
Before discussing the observational data, the Sulu Sea is simplified into a basin with mean dimensions, in order to calculate average wavelengths and velocities. As the result of this the following picture can be drawn, in which the Sulu Sea simplified into a rectangular basin with length l, width b and depth h (note that the length of the basin is shorter than the width):

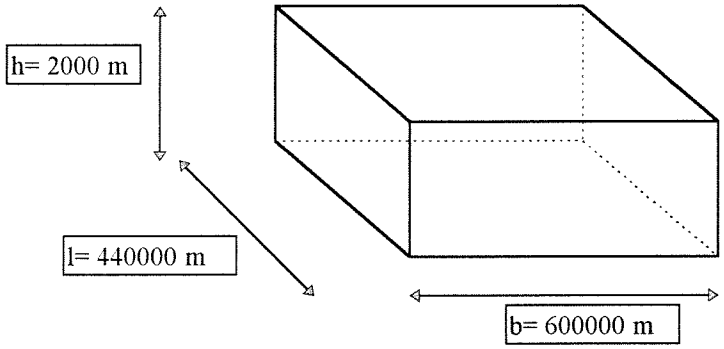

Given this approximation estimations can be made of the tidal waves in this basin, when use is made of the shallow water flow approximation:

$$\lambda = cT \ (\mathrm{m}) \quad \text{and}$$

$$c = \sqrt{gh} \quad \left(\frac{\mathrm{m}}{\mathrm{s}}\right)$$

Wave velocity $\mathbf{c \approx 140\ ^{m}/_{s}}$ in the whole basin (with g= 10 m/s^2)
wavelength $\mathbf{M_2}$: $\mathbf{\lambda \approx 6.25 \times 10^6\ m}$ (with T = 44700 s)
wavelength $\mathbf{K_1}$: $\mathbf{\lambda \approx 12.1 \times 10^6\ m}$ (with T = 86150 s)

Observation of semi-diurnal tides in the Sulu Sea

The semi-diurnal tidal behaviour of the Sulu Sea can be described with tidal constituent M_2, because this constituent is obviously the significant semi-diurnal constituent within the area (Takaki et al., 1996) which is also justified by looking at column 4 of table A2.2 of Appendix 2. The tidal movement of both the M_2 and S_2 constituents are quite the same however, and therefore an analysis based on M_2 is also valid for the S_2 constituent.
The ratio *basin length : wavelength* for the M_2 tidal wave is:

$$^{l}/_{\lambda} = 0.07 \approx {}^{1}/_{14}$$

The wave will cross the length of the basin in $^{440000}/_{140} \approx 3100$ seconds, or about 50 minutes resulting in a M_2 phase difference of about 25° between the both sides of the basin.

Assuming that the waves in the Sulu Sea basin are of standing wave type, significant basin length needed for the existence of resonance can be calculated as follows (at least a quarter of λ must equal L):

$$L = \frac{41}{2(n+1)} \qquad \text{with } n=\{0,1,2,3...\} \qquad (4.1)$$

Considering the semi-diurnal constituent M_2, L=880000 can be calculated. As is can be seen, $^{L}/_{\lambda} < 1$ so resonance will not occur in the Sulu Sea. Resonance would occur in the Sulu Sea when the period of the M_2 tidal wave equals the resonance period. The resonance period of a specific basin can be calculated as follows:

$$T_{res} = \frac{41}{2(n+1)\sqrt{gh}} \qquad (4.2)$$

For the resonance period of the Sulu Sea over the length about 6300 s can be calculated, which is far less than 44700 s of the M_2 tidal wave, so resonance will not occur as well.
Seen the approximate 50 minutes the wave takes to propagate from one end to the other, it can be said that high (or low) water levels occur at almost the same time at both ends of the basin.
Of course the real situation is much more complicated because of the depth profile and the coastline contours and the presence of many islands and passages. However still some similarity can be discovered between the real situation and this simplified analysis.

After analysing the observed amplitudes and phases of the tidal constituents of 51 tidal stations (see Tables A2.1 and A2.2), the following remarks can be made:

- Along the coasts of the Philippine Islands neighbouring the Pacific Ocean the amplitudes are about 0.6 m and the phases about 131°. The influence of this Pacific Ocean wave stretches from the Luzon Strait in the north to the Zomboanga Peninsula in the south (so along the eastern side of the Philippine Islands), but nowhere in the Sulu Sea and the adjacent seas like the Bohol Sea. In the Bohol Sea, until Surigao, the amplitudes are about 0.3 m and the phases about 276°, almost the same as in the Sulu Sea and much different than those in the Pacific. There is a phase difference of 150° between the Sulu Sea and the Pacific, which equals about 5 hours. This indicates that it is unlikely, that the waves from the Pacific penetrate into the Sulu Sea directly through the narrow straits between Luzon and Mindanao. The bottom profile in the Pacific Ocean, just at the east side of the Philippines (see coloured map A2.1 in Appendix 2), also justifies this. The Philippine trench with depths ranging up to 10 km can be found there and the narrow straits of the Philippines can be regarded as reflecting bodies because of the huge and abrupt depth change. The passages of the Philippine Islands between the Pacific Ocean and the Sulu Sea are also very narrow and many tiny islands are situated in these passages. This means that the waves undergo too heavy resistance to pass directly from the Pacific Ocean to the Sulu Sea.
- Through the Sulu Archipelago, it seems that waves enter the Sulu Sea mainly in two different ways. First through the Basilan Strait and Pilas Channel: the amplitudes of the waves at this location are about 0.3 m and the phases about 150°. The second way is through the passages between the Tawi Tawi Islands, like the Sibutu Passage in which the amplitudes are about 0.2 m and the phases about 180°. It seems however, that the Sulu Archipelago has a very retarding effect on the movement of the waves, which can be concluded by looking at the phase figures on both sides of the Archipelago. There is a phase difference of about 110°, about 4 hours, and high waters seem to occur earlier on the Sulu Sea side rather than on the Celebes Sea side.

- Through the Palawan Archipelago there are also two main entrances for the tidal waves of M_2. First there are the passages in the north-east like Mindoro Strait and Linapacan Strait. The phases of the M_2 tidal wave at the location of these straits are about 275° and the amplitudes about 0.2 to 0.3 m. Second come the entrances in the south-west of which the Balabac Strait is the most important. The amplitudes there are about 0.3 m and the phases are about 285°. Of these entrances, those in the north-east seem to be the most important for the whole area. The phase figures seem to increase slowly going down from the north-east to the south-west (which means there is a systematic phase lag between tidal stations) and then to the Sulu Archipelago. The amplitude and phase of the Scarborough Shoal, station 50 in the Table A2.1 of Appendix 2, is characteristic for the phase and amplitude of the Palawan Archipelago at the South China Sea side. Like in the north-east, the amplitude on this position is 0.2 m and the phase is 276^0. A high phase lag as through the Sulu Archipelago does not occur here. This leads to the conclusion that the waves have the ability to move much easier through the Palawan Archipelago and do not undergo heavy friction as through the Sulu Archipelago.
- In the middle parts of the Sulu Sea, along the coasts of Borneo and Philippines the amplitudes are about 0.45 m and the phases about 290°. The high amplitudes in this area could be the result of the more or less abrupt change of the mean depth with factor 3 in the middle parts of the Sulu Sea. Unfortunately no observed values in middle parts of the Sulu Sea, except for coastal zones, are available, so no further remarks about these areas can be made.
- If the Sulu Sea is regarded as a basin with one single opening at the position of the Palawan Archipelago or only at the Position of the Sulu Archipelago (and other openings closed for simplicity), the amount of water flushing through this opening and its velocity can roughly be calculated with the channel detention method (Verspuy, 1987). When the sum of amplitudes of both the semi-diurnal tides M_2 and S_2 is taken as 0.5 m, the following quick calculation can be made:

  At the closed end of the basin Q = 0. The maximum amount of water flushing through the open end by M_2+S_2 is then:

$$Q_{max} = \omega \times b \times l \times \zeta_{max} \qquad (4.3)$$
$$\approx \omega \times 440000 \text{ m} \times 600000 \times 0.5 \text{ m} \approx 18{,}6 \times 10^6 \text{ m}^3/\text{s}$$
$$\text{with: } \omega = 1{,}42 \times 10^{-4}$$

  In terms of velocities, the maximum velocity through the open passage due to semi-diurnal tidal constituents is:

$$u = {}^{Q}/_{b\,h} \qquad (4.4)$$

  When the Palawan Archipelago is considered open and if the mean width of the passages of the Palawan Archipelago is considered as 200 km and the mean depth as 250 m this results into a velocity of about 0.4 $^{m}/_{s}$, which is about 0.8 knots (1 knot equals 0.51 $^{m}/_{s}$).
  On the other hand if only the Sulu Archipelago is open and if the mean width of the passages of the Sulu Archipelago is considered as 120 km and the mean depth as 80 m this results into a velocity of about 2 $^{m}/_{s}$, which is about 4 knots (1 knot equals 0.51 $^{m}/_{s}$).

It should be noticed that the channel detention method is theoretically not allowed for a basin of such dimension as used above for the Sulu Sea (see Verspuy, 1987). However for a first impression with no high accuracy needed, this method is used here anyway.

Observation of diurnal tides in the Sulu Sea

The same approach, analysis of the amplitudes and phases in several tidal stations in the Sulu Sea, is made for a diurnal tidal constituent as well. The K_1 constituent is obviously more dominating in the Sulu Sea than the other constituent O_1. This can be justified by looking at column 6 of Table A2.2 of Appendix 2. Again the same suggestion as it was made between M_2 and S_2 can be made for the diurnal tides: analysis of the behaviour of the K_1 constituent is also valid for the behaviour of the O_1 constituent. The tidal movements of both these diurnal constituents are quite the same.
As already calculated, the wave velocity is about 140 $^m/_s$ and the wavelength is about 12.1×10^6 m. This means that the waves, crossing the Sulu Sea in about 50 minutes time, would result in a phase difference between the two edges, (Palawan Archipelago-Sulu Archipelago) of about 12.5°. Again with a quick calculation with (4.1), it can be seen that no resonance occurs in the basin. At least one quarter of the wavelength is still much more greater than the width or the length of the basin.

Further remarks that can be made after the analysis of the diurnal coefficient K_1 are:

- Again, it can be said that it is unlikely that the tides from the Pacific enter the area directly through passages between Luzon and Mindanao. The phase lag between the Bohol Sea and the Pacific Ocean is considerably high. In the Pacific the phases are about 185°-235° while just the other side in the Bohol Sea phases are about 305°-315°. This means a phase difference of about 70°-80°, which equals about 5 hours.
- At the Palawan Archipelago, the values of the phases and the amplitudes are about the same on both sides of the South China Sea and the Sulu Sea. The amplitudes are about 0.3 m and the phases about 305°. The waves apparently can pass the straits of Palawan Archipelago, without being disturbed. It can also be seen, that the Mindoro Strait in the north-east is the major passage of the Palawan Archipelago. Going south-west from this strait the amplitudes are almost the same and there is a systematic phase lag between tidal stations.
- Along the coasts of Borneo and the Philippine Islands like Panay and Negros, there is some increase in the amplitudes and the presence of a certain phase lag again, going from Palawan Archipelago to the Sulu Archipelago direction. The amplitudes of the K_1 wave increase up to 0.35 m and the phases are then about 310° (which means 5° phase lag). These increases are however not that significant like those for the semi-diurnal waves. This increase might again be the result of abrupt depth profile change with a factor 3 in the centre parts of the Sulu Sea.
- Along the Sulu Archipelago there are some differences between the figures on the amplitudes and phases, depending on the side (the Sulu Sea and the Celebes Sea) the analysis is made. On the Celebes Sea side, the phases are about 245° and the amplitudes are about 0.15 to 0.2 m. On Sulu Sea side the phases are about 295° and the amplitudes about 0.25 to 0.3 m. Apparently there is a phase difference of about 50°, about 3.5 hours, and high waters seem to occur earlier on Sulu Sea side rather than on the Celebes Sea side. Also the amplitudes in the Sulu Sea side are larger than those of the Celebes Sea side. The waves from the Celebes Sea seem not to have big influence on the waves in Sulu Sea .
- The phase difference between the Palawan Archipelago and the Sulu Archipelago, is remarkably close to 12.5° and high waters occur earlier at the Palawan Archipelago side. The waves, mainly entering through Mindoro Strait seem to cross over the Sulu Sea from north to south.
- With (4.3) and (4.4), again the maximum water displacement can be calculated, this time caused by diurnal tides. The maximum amplitude of the diurnal tides $K_1 + O_1$ can be taken as 0,6 m.

Using (4.3) with $\omega = 7{,}3\times10^{-5}$ gives: $Q = 11{,}5\times10^{6}$ m^3/s
When only Palawan Archipelago is considered to be open: u = 0.23 m/s ≈ 0,5 knot
When only Sulu Archipelago is considered to be open: u = 1,2 m/s ≈ 2,4 knots

4.2.2 Conclusions according to observed analyses

In Table A2.2 of Appendix 2, the tide form number (see equation (2.1)) of each tidal station is calculated. When the same subdivision of tidal types as in section 2.3 is made, the tide distribution according to Wyrtki (see Figure 2.13) can be drawn rather than that of Cao&Fang (see Figure 2.12).
Wyrtki (1961), briefly stated that the tidal waves from the South China Sea do not enter the Sulu Sea. In the notes of van Berk (1986), the same is suggested: the tides in the Sulu Sea are supposed to be directed only through the passages of the Sulu Archipelago with a phase lag of about 4 hours.
In the sections before, the conclusion is drawn that the waves enter the area mainly from the South China Sea through the passages of the Palawan Archipelago. This is contrary to the assumptions made by Wyrtki and van Berk stated above.
For the semi-diurnal waves Wyrtki (1961) assumed that the waves were of standing type, with a phase of approximately 2 hours which equals to 60°. The analysis in the former section showed that the phases are about 270°. Resonance of (standing) waves does not occur because of the small distances between the edges and the relatively large depths of most of the basins.
For the diurnal tides, Wyrtki (1961) gave an identical description. No possibility of resonance of standing waves, and a phase of about 195°. In the analysis above a phase of 295° is stated. The phase numbers of both Wyrtki and the observed analysis of this section are in fact the same: Wyrtki uses the time zone of 0 (UTM) instead of -7 used in this section.
The modelling results so far and the question what errors the Sulu Sea probably causes in them is discussed in detail in paragraph 3.2. As seen in the sections before, the Sulu and Palawan Archipelago's consist of many tiny islands and small channels. The tidal waves enter the Sulu Sea from both sides with different amounts. The effect of these channels on tidal movements are not exactly known. It is however certain that these channels are the determining factors for the tidal movements, so it is needed to discover or try to understand their effects. Therefore the behaviour and movement of the tides in the Sulu Sea demands a thorough analysis. This sea apparently has a very complicated tidal behaviour and its topography is obviously very hard to schematise in a model with relatively coarse grids.

It is chosen that the Sulu Sea will first be analysed by a 1-D and if desired later with a 2-D analytical model in order to find the sensitivity of the geometrical dimensions and their effects on modelling results
The modelling of these archipelago's can be achieved by modelling the whole length of the archipelago's as a passage with a mean depth and locally adapted bottom friction. This will be the basis of the 1-D approach.

4.3 1-D TRISULA sensitivity analysis

The Sulu Sea can be considered as a linkage of several basins with considerable depth and width changes. To understand the behaviour of waves travelling through two deep sea basins with a relatively shallow passage a 1-dimensional test model was created with TRISULA. The boundary relations of this test model were zero elevation at one end and a specific water elevation at the other end. From this approach, it was found that oscillations occurred when the shallow basin was relatively deep, deeper than about 100 m, without occurrence of phase

lags. When the shallow passage was chosen relatively shallow, shallower than about 50 m, no oscillations but phase lags occurred.

An other one dimensional test case was created in order to examine the influence of the Sulu and Palawan passages to the enclosed Sulu Sea during this study as well. This analysis was based on rectangular grids with two shallow passages both connecting two deep seas. The dimension of the test case was 3 gridcells in x-direction and 40 gridcells in y-direction, with the y-direction positioned from north to south. The gridsize was 27 km. Actually the shallow passages represented the passages between the Palawan Archipelago, taken at the position of Balabac Strait and the passages between the Sulu Archipelago, taken at the position of Sibutu Passage (see chart in Appendix 2). The depth values were generated from depth charts of the area.
At the positions of (1,2) and (40,2) two water level conditions, amplitudes 0.40 m and 0.20 m respectively and phases both 0, were given. Several stations were positioned on the test case geometry in order to generate history plots of water elevations. The mean depth between St.1 and St.1a was about 3500 m, between St.1a and St.2 2000 m, between St.2 and St.3 about 150 m in its initial state, between St.3 and St.5 1880 m and finally between St.5 and St.6 110 m in its initial state. With this model the effects of depth changes of the shallow passages and friction was mainly looked at . Therefore the depth of the two shallow passages and the Manning coefficient were varied in several computations.

This TRISULA 1-D model schematization is shown in the drawing below. (Note that station 6 is positioned just inside the shallow passage at the SE end)

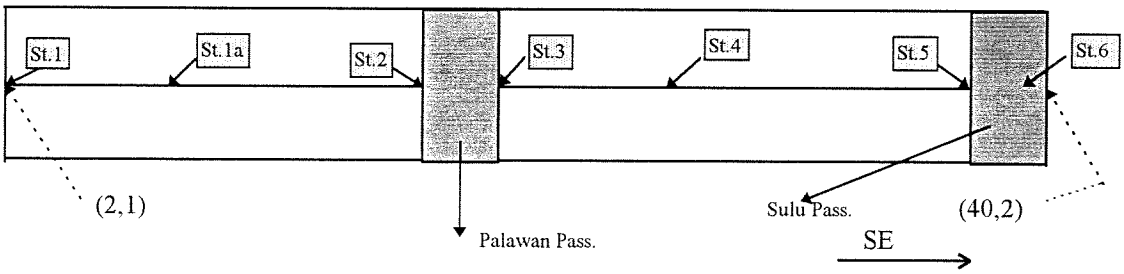

The first computation of the test case with its initial situation, with depths as estimated from charts, showed a standing wave character. This is shown in Figure A3.1 of Appendix 3.
Varying the depth of the Palawan Passage (first shallow part) two values seemed not to influence the character of the test case. This is shown in Figure A3.2 in which the elevations are presented of a computation with a mean depth of 200 m for Palawan Passage and 70 m for the Sulu Passage.
On the other hand, increasing the mean depth of the second shallow passage (this should be Sulu Passage) to more than 120 m had major influence on the water elevations of the stations. This is shown in Figure A3.3, in which a computation is presented with a mean depth of 250 m for Palawan Passage and 150 m for the Sulu Passage. The vulnerability for the increase of depth of the second shallow passage (at 40,2) can be explained by mentioning that the boundary level is imposed on the shallow part itself there. The waves are not driven by a deep basin first at that end.
With depths less than 100 m for both shallow passages the water elevations are less disturbed and a clear standing wave appearance is detected. In figure A3.4 a water elevation diagram is given for the depth of 70 m of both passages and in figure A3.5 another plot with Palawan Passage kept at 70 m and the Sulu Passage with 95 m.
It was remarkable to see, that the elevation of stations 5 and 6, St.5 and St.6 (all close to the (40,2) end), were all obviously higher than the boundary elevation of 0.2 m, so these stations are influenced strongly by the boundary elevation of the other edge (1,2). It could also be seen that the smaller the Manning coefficient was, the more the waves were disturbed within the

system. This is of course not very surprising; the disturbing effects are damped out more quickly the more friction is imposed.

This 1-D TRISULA model eventually gave no extensive insight in the sensitivity of the processes involved. It was necessary to make a lot of different runs in order to see any systematic in outcome by comparing the large amount of computation results.
A bird eye view of the effect of one single variable within the whole system would be more pleasant. Therefore the decision was made to examine the sensibility of these passages with an other analytical approach. In order to accomplish this, a 1-D harmonic model was made as a first step towards a fully 2-D analytical model to analyse the tidal behaviour.

4.4 The 1-D analytical model

For a better understanding of the behaviour of a complicated system of several basins, an analytical 1-dimensional calculation is generated based on harmonic analysis. At the front and rear end of this system, the water levels are given as harmonic functions. Between two basins, at the boundaries of which one basin meets the other, it is assumed that the water level is the same for both basins. Moreover, the water discharge is linked by the continuity of mass.
Before discussing the results of this analysis, it should be noticed that a detailed explanation of how the system is set up and how the solutions are obtained are discussed in Appendix 3, paragraph A3.1. This explanation also includes an example of such an application: a system related to the area of the Sulu Sea near the Philippines, of which the tidal behaviour is complicated and not well understood. Test results of the reliability and validity of the generated 1-D model can also be found in paragraph A3.2 of Appendix 3.
The picture presented in the next page is a global view of the system, containing the various basins with each its own dimension of depth, width and length. A number of monitoring stations are created (at the connection of basins and at begin and end of the system), in order to locally calculate and make graphical presentations of water levels. These stations are given their index figures and are presented in the picture as well.

4.4.1 Overview of the Sulu Sea as a basin system

(not in scale)

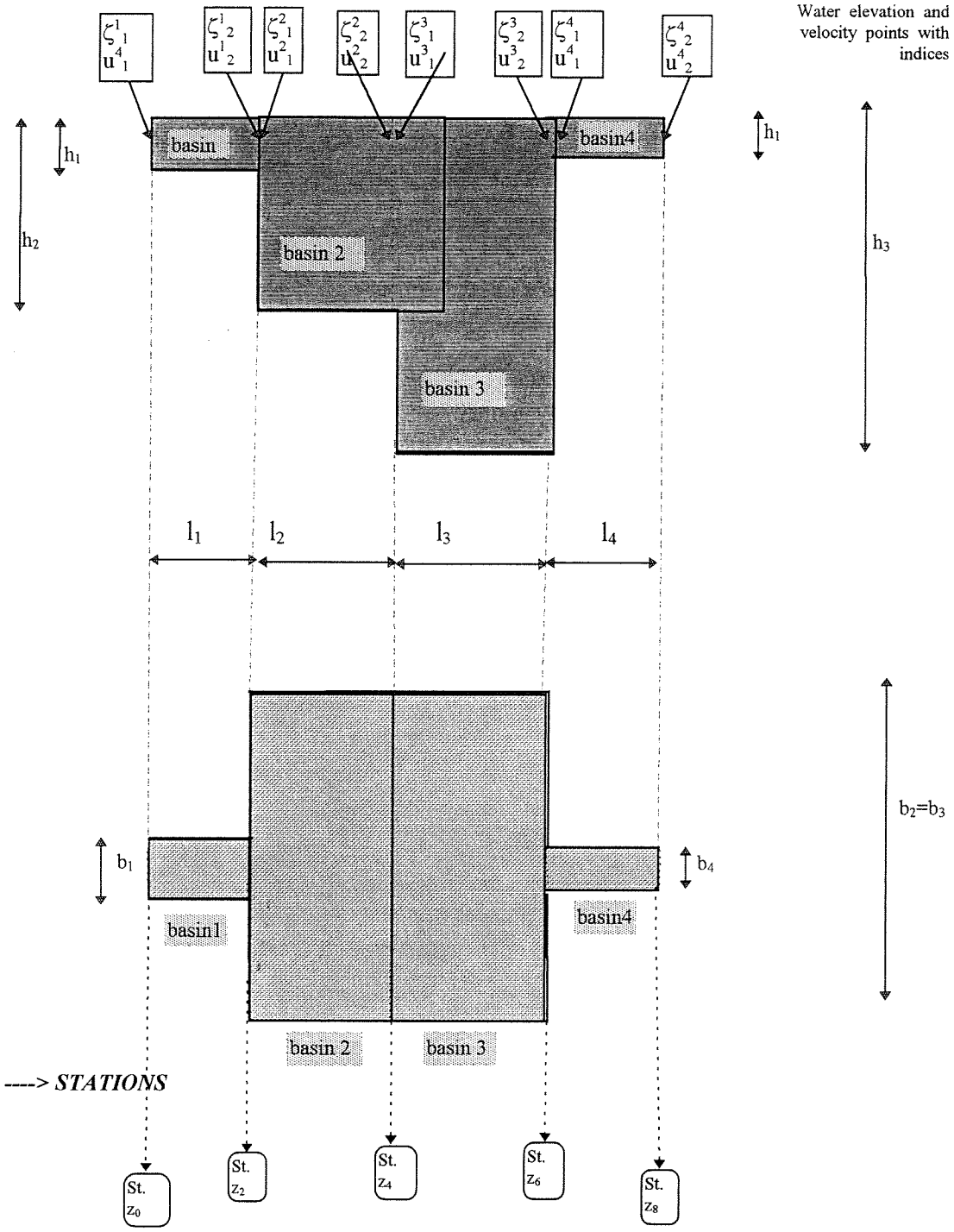

4.5 Results of the 1-D harmonic analysis

4.5.1 Introduction

The system of four basins, depicted on page 4–12, is used to have an insight in the way the several variables (depth d, width b, and length l) of the two narrow openings at the begin and the end of the system are influencing the results within the whole system. It is further interesting how the dimensions of the two outer basins, basin 1 and 4, affect the water elevations and phases within the constantly sized basins 2 and 3.
The 8 steps approach, as given in paragraph A3.1.2 of Appendix 3, has been the basis to of generated computer program(s) in which a set of calculations are made of the system of equations (A3.14) and (A3.15) as given in Appendix 3. The results of the calculations (the amplitudes and phases) are plotted as isoline diagrams for selected stations. A number of these plots are included in Appendix 3 and will be explained in later sections.
In this way a complete overview can be achieved of the effect of ratio of basin dimensions 1 and 4, given the constant basin dimensions of basin 2 respectively 3. Isolines of phases for instance generated as the result of various combinations of basin 1 and basin 4 width sizes, show the areas at which the results of phases are sensitive to small changes of width or areas at which the model produces stable results with no huge changes in a large range of width combinations of both basins. Such plots are also possible for combinations of varying depths and lengths of the two basins 1 and 4.
The conditions for the occurrence of resonance and oscillations is dealt with in earlier sections and in Appendix 1. The different programs that have been generated can also serve to see whether any of these characteristics occur, and if so the combination of dimensions of basins 1 and 4 of these occurrences. Each program is designed to examine the effects of the change(s) of one single dimension parameter of the outer basins to the middle basins. The computations made and results of them will be presented in following sections.
It is also interesting how the water elevation of the system of basins develop along the length axis of the system. By given dimensions for all basins and after having calculated other necessary variables, a diagram showing the actual water elevation or amplitude development along the length axis, can give an additional insight of the behaviour of tidal waves given as boundary conditions. A number of diagrams of this kind are also included in Appendix 3.

4.5.2 Discussion of the results

Before discussing the results and having a look at the isoline plots first, the values will be given for all the basin dimensions, which were taken constant during the computations. These dimensions were chosen as much in accordance as their real (mean) values obtained from charts. Then an overview of the calculations made will be given. All calculations are based on the variation of one of the dimensions of basin 1 and basin 4 together. Per group of calculations, these outer basins are varied 15 times each, resulting to a combination of 225 computations each time.

With all calculations:

Basin no	depth (h)	length (l)	width (b)
2	1000 m	220 km	600 km
3	3000 m	220 km	600 km

The values presented for basins 2 and 3 in this table are unchanged throughout the calculations.

Computation 1: Depth variation of outer basins: see Figure A3.6 up to Figure A3.11 of Appendix 3.

Basin no	depth (15 steps)	length	width
1	50..750 m	80 km	240 km
4	10..150 m	100 km	360 km

1 depth index for basin 1 equals 50 m depth.
1 depth index for basin 4 equals 10 m depth.

Computation 2: Width variation of outer basins: see Figures A3.12 up to Figure A3.17 of Appendix 3.

Basin no	depth	length	width (15 steps)
1	250 m	80 km	40..600 km
4	80 m	100 km	40..600 km

1 width index for basin 1 equals 40 km width.
1 width index for basin 4 equals 40 km width

Computation 3: Length variation of outer basins: see Figures A3.18 up to Figure A3.23 of Appendix 3.

Basin no	depth	length (15 steps)	width
1	250 m	8..120 km	240 km
4	80 m	10..150 km	360 km

1 length index for basin 1 equals 8 km length
1 length index for basin 4 equals 10 km length

The Amplitudes

Below 200 m (height index of 4) for H_1, *computation 1* reveals 'hot spots' areas (or disturbed areas) in the isoline plots of amplitudes for stations Z_2 (Figure A3.6), Z_4 (Figure A3.9) and Z_6 (Figure A3.10). These areas can be discovered for all the results containing a water depth of approximately 0 to 200 m water depth of basin 1. Apparently it is an instable area in which oscillations occur. Other depth combinations of basins 1 and 4 (so those not containing depths of basin 1 between 0 to 200 m) the amplitude isolines show an appreciable sight.
It can also be seen that the higher the two indices get (differently formulated: the deeper both the outer basins are) the lower the amplitude in one station gets moving to the value of station Z_0.

With *computation 2*, width indices plots for Z_2 (Figure A3.12), Z_4 (Figure A3.14) and Z_6 (Figure A3.16), a same kind of unstable area is seen in which the amplitudes apparently oscillate. This is the area between the width indices 5 and 8 of basin 1, also widths between 150 and 240 km. Out of this area the amplitude isolines are linear and the more the indices are away from the trouble area the less the amplitudes get.

Computation 3, the length variation of the outer basins for Z_2 (Figure A3.18), Z_4 (Figure A3.20) and Z_6 (Figure A3.22), shows no disturbed isoline patterns. It seems that the longer both the basins get the higher the amplitudes get as well. For smaller values of the length of basin 1, the isolines are curved. For higher values for the length of both basins 1 and 4 the isolines are linear.

The phases

The most remarkable feature of the phase isolines is, that the 'disturbed' areas of oscillations, which have been noticed with the amplitude isolines, are also disturbed areas with the isoline plots of phases. In these disturbed areas the phase lines are very closely situated to each other. In fact this is not a phase disturbance area, but an area at which a phase alteration of 180° occurs (the availability of many isolines close to each other is caused

by the automatic interpolation of phases of the program used), which can be explained by a complete reflection of the waves in some specific basin dimensions. The dimensions at this area is such, that the wavelengths have the possibility to be in phase and as the result of this high oscillations occur.
The occurrence of oscillations is for instance shown in Figure A3.24 and Figure A3.25. Figure A3.25 is the same plot as Figure A3.27 and Figure A3.25 is the same plot as Figure A3.27, but in both these figures, this time water elevations above 1 m is plotted. It can be seen that on some spots elevations up to 20 m exist with certain combinations of basins 1 and 4 dimensions.

With the dimensions given in the tables presented before, *computation 1* (depth variations) shows [Z_2 (Figure A3.7), Z_4 (Figure A3.8) and Z_6 (Figure A3.11)] outside the disturbed areas, a parabolic kind of isolines of phases ranging from 300° for small H_4 indices to 180° for large H_4 indices. In most of the depth indices combinations, except for small indices of H_1, the phases are mainly determined by the basin index H_4 (depth of basin 4). The phase isolines of stations Z_4 and Z_6 are almost the same and the only difference with the phase isolines of Z_2 is, that the Z_2 isolines are more linear and shifted more to the right.

Computation 2 (width variation of basins 1 and 4) isoline plots for Z_2 (Figure A3.13), Z_4 (Figure A3.15) and Z_6 (Figure A3.17) reveal a disturbance area at the same areas as in the amplitude isoline plots as well. Again two totally different phase occurrences appear above and below this disturbance area. Above this, the phases are almost linear and range from 120° for small B_4 indices to 0° for large B_4 indices. Below the disturbed area, with increasing B_4 indices the phases range from 300° to 200°. In the disturbed phase area, a phase shift of 180° occurs again. In this case the phases are viable more sensitive and determined by the dimensions of basin 4 rather than basin 1.
From both computations discussed above, it can be concluded that the smaller the depth and width of basin 4 gets the larger the phase lag at a certain station gets. The same can also be said of basin 1. Furthermore the dimensions of basin 4 seem to be more determining for the results. This should be the Sulu Archipelago in real situation.

Computation 3, the length variations of the two outer basins, seems to have no 'disturbed' areas of amplitudes and phases. The results of Z_2 (Figure A3.19), Z_4 (Figure A3.21) and Z_6 (Figure A3.23) all reveal the same pattern. Moreover the length effect of the outer basins on phases are linear and can be explained by the increase of the phase lag at a basin with increasing length of it. It turns out that the longer basin 4 is, the higher the phase at Z_6 is and also that the longer basin 1 is the higher the phase at Z_2.

4.6 Development of water levels along the length axis

Beside the study of the development of amplitudes and phases of identified points in the basins system, a look at the development of variables over the length axis (starting from basin 1 to basin 4) will probably give additional insight to the behaviour of the tides in the basins. Therefore the development of the amplitudes and the actual water levels over the length axis will be examined in this paragraph. A number of plots showing these developments are included in Appendix 3.

Starting with Figure A3.29 and A3.30, the development of the amplitudes of water elevation over the basin length can be seen for given basin dimensions.

The dimensions of A3.30 include the solutions of dimensions of station Z_2 as given in Table 4.2 for computation 1:

basin 1: l = 80 km, b = 240 km, h = 350 m
basin 2: l = 220 km, b = 600 km, h = 1000 m
basin 3: l = 220 km, b = 600 km, h = 3000 m
basin 4: l = 100 km, b = 360 km, h = 20 m

The dimensions of A3.29 include the solutions of dimensions of station Z_6 as given in Table 4.2 for computation 1:

basin 1: l = 80 km, b = 240 km, h = 750 m
basin 2: l = 220 km, b = 600 km, h = 1000 m
basin 3: l = 220 km, b = 600 km, h = 3000 m
basin 4: l = 100 km, b = 360 km, h = 50 m

In Figure A3.29, it can be seen that the basins 1, 2 and 3 behave almost the same in their sinusoidal movement in vertical direction. These basins are relatively deep and the width change (factor b1/b2 = 0.4) is apparently not disturbing the waves. In basin 4 however, there is a relatively sharp drop of water level. This can be explained by the extreme depth and width changes between basin 3 and basin 4 (h3/h4 = 60; b3/b4 = 1.7) In basin 4 the amplitude decreases sharply because of the relatively short wavelength this small and narrow basin has in relation to its length than the other basins. The wave amplitudes decrease because a considerable part of a sinusoide for water elevations can exist in this basin.
In Figure A3.30 the picture is almost the same. In basin 4 (still narrow and relatively shallow) there is still a heavily decrease of amplitudes for the same reason as in Figure A3.29. Between basins 1 and basin 2, this time there is also a relatively sharp depth change (h1/h2 = 0.35). The waves in basin 2 and 3 are this time enclosed between basin 1 and 4. Because of the width and depth changes (between basin 1 and 2 and between basin 3 and 4) the waves are mostly reflected at the position of these boundaries. Once the waves in basins 2 and 3 are initiated by waves originating from basin 1 and 4, the waves grow stronger in these basins because of reflection. The depth change between basins 2 and 3 seem only to have a slight effect: a small rise in amplitude can be detected going from basin 2 to 3. There is a relatively heavy drop of amplitude in basin 1 this time as well. This can also be explained by the relatively short wavelength this basin has in relation to its length.
Figure A3.31 shows an identically shaped picture as Figure A3.30. The difference in values can be explained by the change in dimension parameters of basin 1 and 4 (h1 = 300 m, h4 = 30 m, b1 = 360 km, b4 = 240 km, other values the same as in Figure A3.30). The explanation given for Figure A3.30 is therefore also valid for Figure A3.31.
In Figure A3.32 a picture of a basin system is presented in which the strengthening of the waves in basins 2 and 3 is so immense that oscillation occurs. The dimensions that are changed in relation to Figure A3.30 is given at the top of the picture. This basin system combination is one of the points that can be found in isoline plots, as discussed in the paragraph before, in the 'disturbance areas'. The specific combination of basin dimensions is such that oscillation of water elevations occurs.
What happens if one of the end basins (Basin 1 and basin 4) is completely closed? To investigate this, first the water elevations at specific stations of a basin system with three combinations is looked at. These three combinations are:

- A system of four basins with both the end basins open.
- A system of three basins in which the first end of the basins is a closed boundary.
- A system of three basins with the last end a closed boundary.

The following basin dimensions were given (combination 1):

basin 1: l = 80 km, b = 360 km, h = 300 m
basin 2: l = 220 km, b = 600 km, h = 1000 m

basin 3: l = 220 km, b = 600 km, h = 3000 m
basin 4: l = 100 km, b = 240 km, h = 60 m

Basin 1 is absent in combination 2 and basin 4 is absent in combination 3. Combination 1, 2 and 3 is given in Figure A3.33 (in the same order) as water elevations of specific stations in time. The following boundary conditions were given for the three combinations:

- combination 1: ζ_0 (of Z^1_1) = 0.2 cos (ωt + 305) and ζ_8 (of Z^4_2) = 0.5 cos (ωt + 160)
- combination 2: u_0 (of Z^1_1) = 0 and ζ_8 (of Z^4_2) = 0.5 cos (ωt + 160)
- combination 3: ζ_0 (of Z^1_1) = 0.2 cos (ωt + 305) and u_8 (of Z^4_2) = 0

In Figure A3.33, it can be seen that in case the both end basins are open, there is a significant phase lag between the stations. In case one of the end basins is closed the waves are of standing type with all stations being in phase. The rise and fall of water levels almost occurs simultaneously for the whole system in that case.
The actual water levels, at a given time, of combination 1 and 2 are also given in the next following figures of Appendix 3. In Figures A3.34, A3.35, A3.36 and A3.37 the actual water levels at t=0, t=T/4, t=3T/4, and t=T respectively of combination 1 above are given. In Figures A3.38, A3.39, A3.40 and A3.41 the actual water levels of combination 2 above at t=0, t=T/4, t=T/2 and t=3T/4 respectively are given. These pictures confirm the conclusions that were already drawn above for combinations 1 and 2.

4.7 How to use the results of the 1-D analysis of the Sulu Sea?

From the programs made to calculate this 'four basin linkage system', bird eye views in the form of isoline plots of amplitudes and phases have been generated. For an arbitrary station the possibility is achieved by this to choose the combination of dimensions of basins 1 and 4 in order to obtain desired values; amplitude and phase of this station. When this choice is made the development of water levels over the length axis of the basins system can be looked at, as was done with some examples, in order to see the development of water levels in the complete system. This can be a long and iterative process because the combination of dimensions obtained from the calculations at station 2 is not necessarily the same combination from the calculations of for example station 6.
What are the desired values? These are the values for amplitudes and phases of the M_2 tidal coefficients given in Admiralty Tide Tables for tidal stations near the computed points. A number of such stations can be found in Table A2.1 of Appendix 2. Note however that in the calculations of the 1-dimensional model, the phase of the stations is used for the time zone -8, while the tables of Appendix 2 are designed for phases of time zone -7. For the M_2 constituent this will result to a difference of about 29^0. The desired solutions, for M_2 are for instance (with $|\zeta|$ the amplitude and φ_0 initial phase):

Table 4.1: Desired solutions of the stations

pos.	$\|\zeta\|$ (m)	φ_0 (degree)	geography	remarks
z^1_1 (Z_0)	0.2	305	Scarborough Shoal	boundary condition
z^1_2 (Z_2)	0.3	301	Puerto Princesca	station no 9
z^2_2 (Z_4)	0.45	320	Cagayan Islands	mean of no 16 and 43
z^4_1 (Z_6)	0.2	290	Pearl Bank	station no 22
z^4_2 (Z_8)	0.5	160	Balut Island	boundary condition

When the phase and amplitude isolines of stations Z_2, Z_4, and Z_6 each laid upon each other, the intersection of the two desired isolines according to the values of Table 4.1 are the solutions of the regarded station. Arriving at the same combination of basin 1 and 4

dimensions belonging to the three different stations Z_2, Z_4 and Z_6 is a very tough task and can take lot of repetition of computations.
As an example the depth and width solution combinations of the three stations is given in the following table (note that Z_2, Z_4, Z_6 are in fact equal to the positions z^1_2, z^3_2, and z^4_1). The results of computation 3 are no further analysed because the length of the basins seems not to be further important for the moment.

Table 4.2: Overview of computed basin dimensions in stations

station	computation 1		computation 2	
	h_1	h_4	b_1	b_4
Z_2	350	20	480	240
Z_4	xx	xx	xx	xx
Z_6	750	50	480	420

In this table xx means there was no solution possible according to the combination searched for as given in Table 4.1. So the centre of the system produces results which are not in accordance with the desired values under given circumstances. Furthermore, as expected the solution of station Z_2 is not the solution of station Z_4. Recalculations with new parameters is therefore needed in order to obtain solutions which are not widely differing between the relevant stations.
To achieve some sort of calibration, it is needed that the goals of calibration (desired solutions for three stations in one time as given in Table 4.1) are more restricted, because calibration for three different stations together at the same time seems an impossible task.
The aim to calibrate three stations at one time should be set aside. Station Z_4 can for instance be neglected, because the desired solutions as given in Table 4.1 for Cagayan Islands is not a set of observed values at this point, but an interpolation of two stations on the coast sideways of it. Observed values in the centre parts of the Sulu Sea do not exist. From the two stations that are left, one can be chosen as representative for the calibration of the whole Sulu Sea. (such an approximation has also been done by van Berk, (1986)). Following on this, the choice is made on Puerta Pricesca because this station gave the most inaccurate results with former South China Sea Model computations. This will also be position z^1_2 or station Z_2.
It is important to discover the effect of the change of one parameter in the isoline plots and this can be achieved by repeating of many computations and by thoroughly analysing the results of them. The earlier results, showed that the depth and width of basin 1 must be larger than those of basin 4. According to the results of computations, as given in Table 4.2 two new computations 4 and 5 can be made in the following form:

computation 4		computation 5	
h_1	h_4	b_1	b_4
300	30	360	240

Computation 4 is based on the width variation of the outer basins with only the values h_1 and h_4 changed as given in the table (only the result of the amplitude at Z_2 is given in figure A3.25). Computation 5 on the other hand is based on depth variation of the outer basins with only the widths of b_1 and b_4 changed (only the result of the amplitude at Z_2 is given in figure A3.24). The result of computation 4 was that the phase isolines were shifted more to the right, which means that the desired phase of 300^0 could be chosen for less depth of basin 1 and less depth of basin 4. Still no calibration could be made however of all the three stations together.

4.8 Conclusions

The tidal behaviour of the Sulu Sea region is investigated with data originating of Admiralty Tide Tables. In this region, a complex tidal behaviour is present. Tidal waves seem mainly to enter this almost rectangular Sulu Sea from two directions: through tiny islands and passages of the Sulu archipelago and through the passages of the Palawan Archipelago. According to the phase lags between tidal stations, tidal waves entering the Sulu Sea from the South China Sea through the Palawan Archipelago undergo much less resistance than waves entering through the Sulu Archipelago. Therefore it was then concluded that the tidal waves enter the Sulu Sea mainly through the passages of the Palawan Archipelago.
However this conclusion is contrary to the findings of some scientists among which Wyrtki is one of them. Tide form numbers calculated for a number of tidal stations of the Sulu Sea are in accordance with the figures as drawn by Wyrtki for the geographical spreading of the tides in these regions.
So according to phase lags, mean wave celerities and geography, the waves of the Sulu Sea seem apparently to be originating mainly from the South China Sea via the Palawan Archipelago. This is overruled however, when tide form numbers of tidal stations are geographically looked at: the tides in this case seem mainly to be originating from the Celebes Sea through the passages of the Sulu Archipelago. This conclusion is of course made on the assumption that the approximation of the tide form number and its distribution domains are undoubted and 'water-tight'. Although the tide form numbers in the Sulu Sea and the Celebes Sea obviously differ, they are of the same tidal distribution type.

To understand the basic mechanisms of the Sulu Sea 1-D tidal studies are made. A first analysis with TRISULA gave the impression that the whole sea reveals a standing wave character and the water elevations are more or less simultaneous everywhere. This analysis did however not produce a global picture of the processes involved (that was searched for) and therefore a 1-D analysis based on harmonic analysis is generated by programming.
A model is developed, by assuming that the Sulu Sea is a 'black box' in which two signals are sent. To discover the possible kinds of output and the sensitivity of the two outer basin dimensions (due to specific dimension changes and boundary conditions), on the results within the 'black box' was the main purpose of the model. This black box model was used to give a first insight in the sensitivities and help to understand the problems with the South China Sea Model.
However the model in this state proved itself not to be applicable on a large scale, because setting up of the model for more stations together seemed to be an impossible task. It turned out that the application of the model in this state, has to be modified. Modification of the implementation of boundary conditions can for instance be thought of. But given the results with this approximation, the systems involved in the Sulu Sea are proved themselves far too complex to be represented 1-dimensional.
The development of the water levels along the length axis showed that waves in the middle parts of the basin system can oscillate when the outer basins are relatively shallow and/or narrow. In such cases the waves, once initiated, are 'trapped' in the middle parts between the outer basins and resonate as the result of reflections. When one of the outer basin is very shallow and/or narrow, it seems there is a relatively sharp drop of water level in the basin, which increases at the other end again to achieve the water elevation at the boundary with its neighbouring basin (the water levels at this points must be equal according to the transition condition, see Appendix 3). In that case, at the intersection point with the neighbouring basin, there is then a sharp angle of water level. This sight is the reason of doubt whether the condition of water levels equality is well assumed, in case two neighbouring basins are very much differing in their dimensions. In nature it is possible that there is an occurrence of a discontinuity of water level at the transition of a very large basin with a very small basin. (this is called the harbour paradox). In such cases it should be more sensitive to handle an

energy balance between the two basins rather than equality of water levels. However a balance based on energy conversation introduces other difficulties, because this would not be a linear condition.

In a 1-D modelling of this system, by nature no provisions can be made for sideways variation of the calculated variables. This will get important however, especially when large widths are involved. With large widths the Coriolis forces also become an important factor. To achieve a more convincing analytical model, it is needed to modify the model into a 2-D model with Coriolis force and if desired with bottom friction. Probably it will then be possible to better represent the tidal mechanisms of the Sulu Sea.

The 1-D approach can of course still be used to examine the sensitivity of other regions of the South China Sea Model domain, like the Malacca Strait. The tidal movement in the Malacca Strait itself, is at first sight much less complicated than in the Sulu Sea, because tidal movement in Malacca Strait is almost clearly 1-dimensional. Because the application of a 1-D model is described in detail for the more complicated Sulu Sea region, the application for the Malacca Strait will be left for future investigators. But initial steps for this study are already made during this study and represented in section A1.6 of Appendix 1 and with tables in Appendix 2.

5 TRISULA SCSM computations

During this study some additional computations were made with the South China Sea Model as well, in order to understand the behaviour of the model with some major alterations. In this chapter, discussions will be made of these computations. Some of these computations are for some part a logical consequence of the conclusions made in earlier notes, but some are also computations that were thought of two years ago, but for some reason never have been performed so far.
Each of these new runs will mainly be compared to run G13 of two years ago unless otherwise indicated. By then G13 was pointed out as the calculation with statistically best results for the complete model domain. The computations of tidal stations of the South China Sea Model will be compared to their observed values to see local differences between computed and real values. In Appendix 4, these tidal stations are given together with their observed values for phase and amplitude of each component. Thereafter, the results of computation G13 are given (of each component) together with TRIANA analyses. All computation results described in this chapter can also be found in Appendix 4.
At the end of this chapter a brief overview will be given of the new made calculations in tabular form as it has been made in Table 3.4, for the runs of two years ago. Following this table, an other table in which a statistically analysis of the results of these latest runs will be presented as well.

5.1 Introduction

The last computation runs of the South China Sea Model (SCSM) are already from two years ago. A discussion of most of the runs is already made in section 3.2. Best results achieved by then were assumed to be the results of the computation with identification number G13. G13 was based on modelling of the narrow openings to the Sulu Sea with extreme bottom roughness coefficient. A Manning coefficient of 0.05 was taken to achieve this. This was especially done to improve the results of the semi-diurnal components in the Sulu Sea.
As the results of this, the amplitudes showed some improvement of accuracy. In most stations of the Sulu Sea however, the computed phases still showed huge errors compared to the observed values. Phase lags of 90° were no exception at some stations.

5.2 Computation C01: tide generating forces

The main new element in this computation is the introduction of the tide generating forces in the SCSM for the first time. It was always assumed that the tide generating forces would not make much difference on the overall results. This was assumed because the model produced many different kind of errors and the tide generating forces would not be the only and the most important solution for them. It is also known that the tides in the South China Sea region are forced oscillations driven by the Pacific and Indian Ocean and the energy budget of the tides generated by direct influence of the moon and the sun is much lower than the energy budget of the tides by forced oscillations. (Mihardja, 1991). Therefore the introduction of tide- generating forces should not lead to much difference in results.

5.2.1 Semi-diurnal tides

For this section he the following figures of Appendix 4 have to be studied:

Figure A4.1: Observed values of phase and amplitude of the M_2 component.
Figure A4.3: Observed values for the phase and amplitude of the S_2 component.
Figure A4.4: Computations of G13 concerning the M_2 component.
Figure A4.6: Computations of G13 concerning the S_2 component.

Figure A4.7: Computations of C01 concerning the M_2 component.

The first impression after a global view of the results is that the results of C01 are, contrary to the expectations, significantly different in results compared to the results of G13. This is especially the case within the deeper parts of the model area.
Significant improvements, the phases are much less out of phase and the amplitudes are more accurate, (especially for the phases) apparently occur within the deeper parts because of the introduction of the tide generating forces. These are the waters of the northern parts of the South China Sea (the areas between north-eastern coasts of Borneo and Mekong Estuary and areas between Luzon and Vietnam) and the waters of the Celebes Sea and Macassar Strait.
In the Celebes Sea and Macassar Strait the phases show decreased values and in the South China Sea increased phases compared to G13. Although the phases are less out of phase, the improved results of phases are accompanied by worsened, less accurate, values of amplitudes. In the Celebes Sea and Macassar Strait more accurate phases are accompanied by increased and deteriorated amplitudes. The situation is reverse in the South China Sea: improved phases are accompanied with less satisfying amplitude values.
In Java Sea the results are still disappointing. In most stations, the amplitudes and phases (with some local exclusions) are larger than the observed values. The phases in C01 have even become more out of phase. In Macassar Strait the phases are slightly more accurate.
In the waters surrounding the Malaya Peninsula the phases and amplitudes are exactly the same as in G13. In the Gulf of Thailand each station needs to be looked at separately. Locally the results are better: some stations show exactly the same calculated values as are the observed values, however some stations show results far from observed values as well.
In the Sulu Sea, the results still do not show acceptable accuracy. In most stations the amplitudes are computed too large and the phases too low.

The results are briefly shown in the figure below. (Values given are the differences of the computed values from the observed values, H_c means computed amplitude, φ_c means computed phase):

5.2.2 The diurnal tides

For this section he the following figures of Appendix 4 have to be studied:

Figure A4.2: Observed values for the phase and amplitude of the K_1 component.
Figure A4.5: Computations of G13 concerning the K_1 component.
Figure A4.8: Computations of C01 concerning the K_1 component.
Figure A4.10: Computations of C01 concerning the O_1 component.

In the whole South China Sea the phases show appreciable and better results. However this is seemingly not the case for the amplitudes: the amplitude results are less accurate for the whole model area. Along the coasts of Borneo and in the Gulf of Thailand, (except for some local stations) the improvement of the results of phases is not to be seen as in the rest of the South China Sea. The phases there are even more out of phase than the results of G13. The amplitudes are lower than G13 in deeper parts and higher than G13 in shallower parts of the South China Sea (which in both cases means less accuracy).
In the Celebes Sea and Macassar Strait, the phases are more closer to the observed values. In Malacca Strait, the amplitudes have are a little more accurate along the coasts of Sumatra and the phases have remained almost the same.
More disappointing results can be seen again in the Sulu Sea and the Java Sea. In the Sulu Sea the amplitudes are all higher than the observed values (with a ratio of about 1.5) and the phases are all less than the observed values (worst result is a phase difference of -93°, in G13 the worst difference was 17°). The worst results in phases as well as amplitudes are in the middle parts of the Sulu Sea.
Almost for all stations, (except for some peculiar stations) of the Java Sea, the calculated amplitude values are only approximately 60% of the observed values. The phases are, especially in southern parts, up to 170° out of phase and in the northern parts up to 45° out of phase. At the Riau Archipelago region the amplitudes have the value of about 45% of the observed values and the phases are 160° out of phase.

The results are briefly shown in the figure below. (Values given are the differences of the computed values from the observed values, H_c means computed amplitude, φ_c means computed phase):

5.3 Computation C02: exclusion of the Sulu Sea

The Sulu Sea has already been mentioned as being one of the major problems of the South China Sea Model throughout this report. Therefore a summary of the problems and the reason of errors because of the Sulu Sea will not be made here once more.
One of the main questions that occurred, for instance in section 3.3.1 was: can the problems of the South China Sea Model because of the Sulu Sea, simply not be avoided by exclusion of this sea from the model domain? If the model seems to be able to produce far better results without this sea, the occurring problems in other areas could be solved first without the interference of the Sulu Sea.
This computation was therefore mainly designed to get a first impression of the changes of the computation results without the Sulu Sea. The South China Sea Model was therefore disposed of this sea, by introducing dry points at the positions of the Palawan and the Sulu Archipelago's. The Sulu Sea is then transformed into a lake.
It should be noted that for a more detailed look, it is better to exclude the Sulu Sea from the model by the alteration of the grid enclosure of the model and cut off the Sulu Sea in this way. In this way boundary conditions can be given at the positions of the Sulu and Palawan Archipelago's and the model could be directed better in its computation. This is not done in C02, because the main goal was to have a quick look at the possibly systematic change of the model without the Sulu Sea in the first place.

5.3.1 Semi-diurnal tides

For this section he the following figures of Appendix 4 have to be studied:

Figure A4.1: Observed values of phase and amplitude of the M_2 component.
Figure A4.3: Observed values for the phase and amplitude of the S_2 component.
Figure A4.4: Computations of G13 concerning the M_2 component.
Figure A4.6: Computations of G13 concerning the S_2 component.
Figure A4.11 and Figure A4.12: Computations of C02 concerning the M_2 component.
Figure A4.15: Computations of C02 concerning the S_2 component.

The most significant change in results (in relation to G13) because of the exclusion of the Sulu Sea can be seen in the Celebes Sea. The effects appearing in the Celebes Sea make the amplitudes and phases differently develop in Macassar Strait and Java Sea.
In the Celebes Sea and the Macassar Strait, the phases have decreased to more accurate values relative to measurements. The amplitudes have however increased, which is less accurate from the observed values. In the Java Sea, the phases all have increased systematically almost 10°, which means they are 10° even more out of phase. The amplitudes remained mostly the same. It can therefore be said that there are only minor consequences of closing the Sulu Sea within the Java Sea. Any systematic change of results in Java Sea seems to be the result of differences in Macassar Strait. An area in which also not any significant change can be seen is the Malacca Strait. This is not surprising because this region is far away from the Sulu Sea.
In the South China Sea and Gulf of Thailand, there are some slight changes in results. In open sea regions the phases change about 3° and no changes can be seen in results of the amplitudes. At coastal regions (except for the direct neighbourhood of the Palawan Archipelago), there are also no or very little changes in amplitudes and some slight change in phases.
It can therefore be said that the exclusion of the Sulu Sea has little consequences to the results at the South China Sea side but relatively major consequences at Celebes Sea side. The obvious changes at the Celebes Sea side results to changes in the Java Sea, but the Java Sea itself shows no further influence. Although the phases positively develop in the Celebes Sea and the Macassar strait, the overall results of the model do not show any progress, because of

the worsening of the amplitudes in Celebes Sea and Macassar Strait and the systematic worsening of the results in Java Sea.

The results are briefly shown in the figure below. (Values given are the differences of the computed values from the observed values, H_c means computed amplitude, φ_c means computed phase):

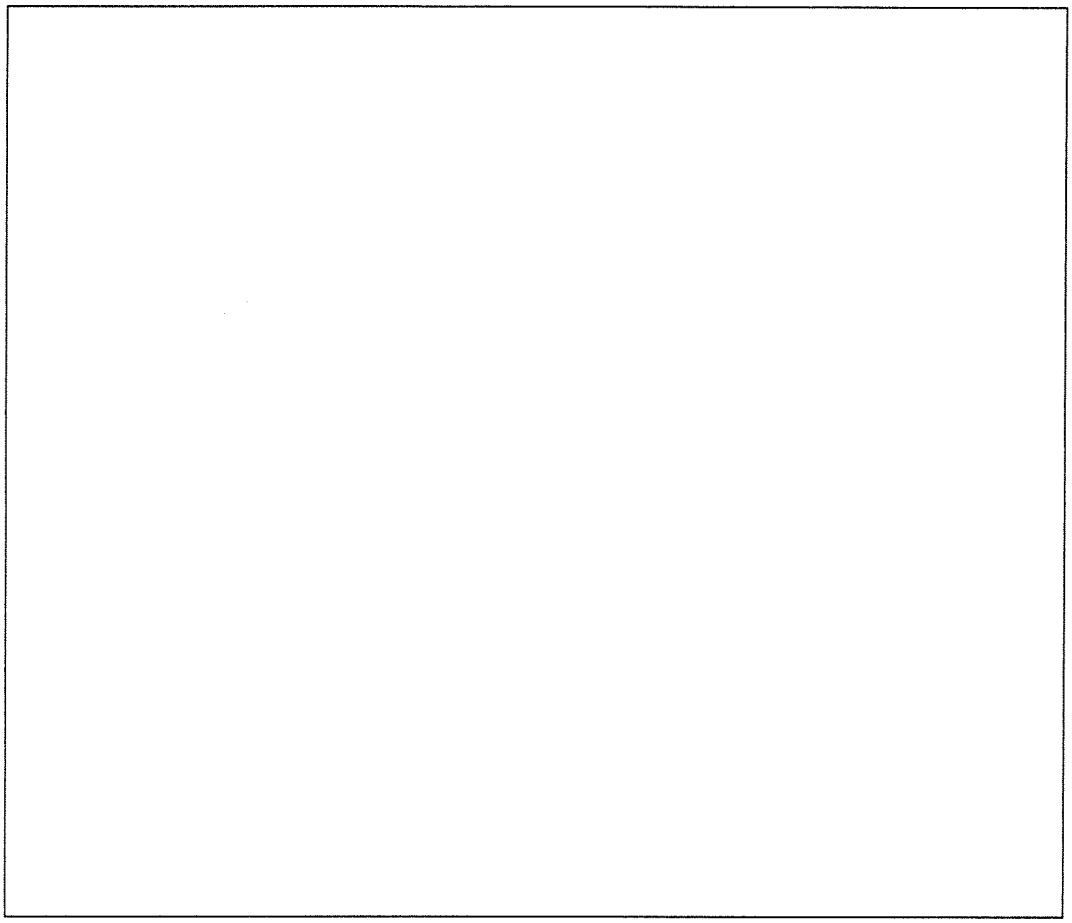

5.3.2 Diurnal tides

For this section he the following figures of Appendix 4 have to be studied:

Figure A4.2: Observed values for the phase and amplitude of the K_1 component.
Figure A4.5: Computations of G13 concerning the K_1 component.
Figure A4.13 and Figure A4.14: Computations of C02 concerning the K_1 component.
Figure A4.16: Computations of C02 concerning the O_1 component.

The effect of the exclusion of the Sulu Sea at the South China Sea side is a little bit more than that for the semi-diurnal tides. In the whole region of the South China Sea until the area between Singapore and Borneo the phases improve extraordinarily. However no improvement can be noticed in amplitudes. Only on the Vietnamese coasts the amplitudes improve almost presenting the observed values, but in other areas results are more disappointing.
In the Celebes Sea and Macassar Strait the phases also get more accurate compared to the observed values. However, the amplitudes do not show any progress again. In Java Sea the phases decrease in the northern region and increase in the southern region. As the result of this, the phases are less out of phase on the southern coasts of Borneo but a lot more out of

phase on the coasts of Java. The amplitudes are less accurate in relation to observed values in the Java Sea as well.
The results are briefly shown in the figure below. (Values given are the differences of the computed values from the observed values, H_c means computed amplitude, φ_c means computed phase):

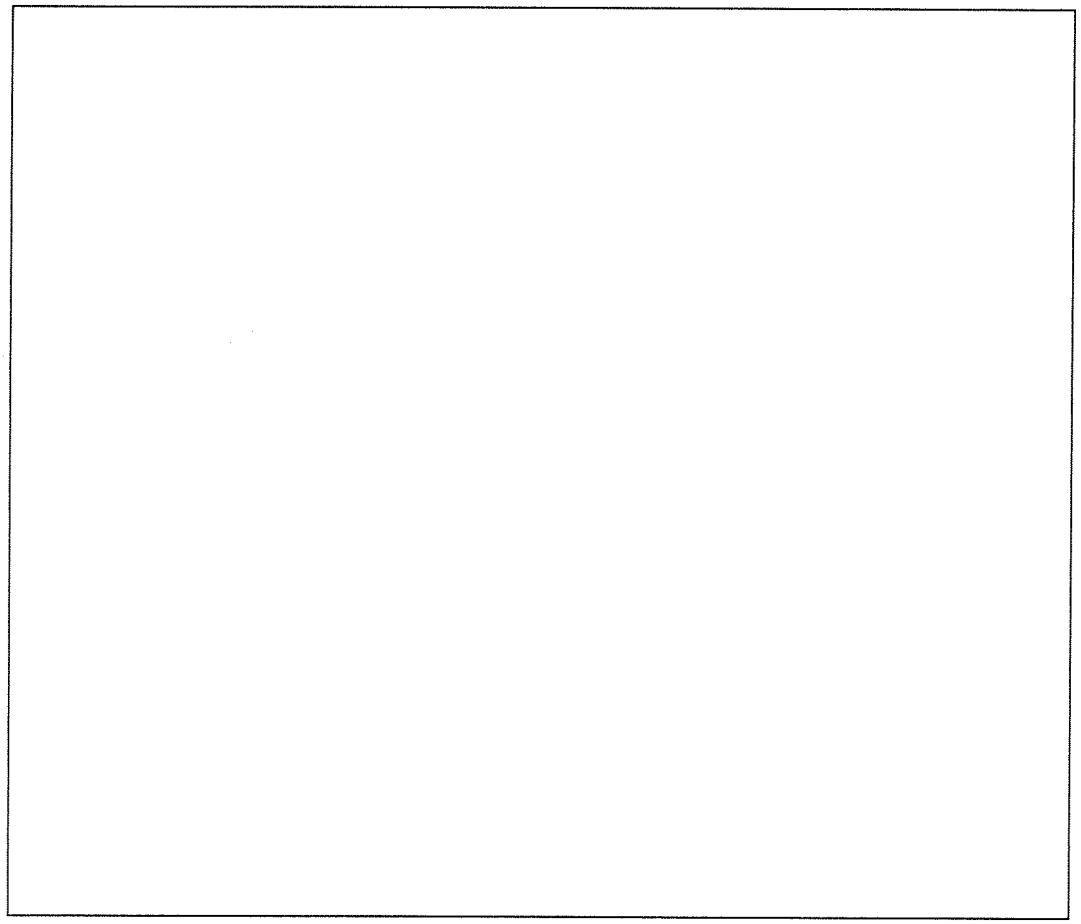

5.4 Computations C04 and C05

Calculation C04 is based on closing the Palawan Archipelago of the Sulu Sea while the Sulu Archipelago is schematised with its passages open.
Calculation C05 is based on closing of the Sulu Archipelago passages, while the passages of the Palawan Archipelago are schematised as natural.
The aim of C04 was to have a global look on the effect of the tides of the South China Sea to the tides in the Sulu Sea and the closure of the passages of Palawan Archipelago to the complete model domain. On the other hand, C05 had the aim to get an impression of the effect of the tides from the Celebes Sea to the tides of the Sulu Sea and the effect of closing the Sulu Archipelago on the global results of the complete model domain.
By the time of completing this report, only statistical data considering the global effects to the complete model domain were available, so only considerations of global effects of these runs will be considered in these sections.
The conclusions that in global can be drawn of these runs can be found in the next section.

5.5 Conclusions of TRISULA computations

Before presenting the conclusions an overview will be given of the new made calculations in tabular form as it has been made in Table 3.4 of two years ago:

Run Id	Alteration related to G13	Purpose	Result
C01	introduction of tide generating forces	analysis of the effect of tide generating forces	significant different results; in general less accurate than results of G13 except for deep parts
C02	Sulu Sea excluded	analysis of the effect of the Sulu Sea on model results	different results in seas neighbouring the Sulu Sea
C03	Malacca Sea excluded	analysis of the effect of Malacca Strait	run not made
C04	Palawan Archipelago closed	analysis of the effect of Palawan Archipelago passages	globally statistically more accurate model results than G13
C05	Sulu Archipelago closed	analysis of the effect of Sulu Archipelago passages	globally statistically less accurate model results in than G13

Introducing the tide generating forces has severe effects in the results but it is not a progress in general. The produced results were contrary to the expectations much more different than obtained results so far. Moreover, considering the results with tide generating forces, they were globally seen more disappointing in most areas and especially the shallower parts.
This would mean that the modelling difficulties of the South China Sea Model is even more serious than was assumed so far. The tide generating forces should lead to better general results, for these forces ought to be more perfecting of modelling: representing the real situation as much as possible. Not using the tide generating forces in the future computations can under these circumstances only be justified considering the computation time savings.
The advise of a critical look at all aspects of the model, such as its domain and boundaries, is however highly well placed here and a serious warning must be given that future runs of the South China Sea Model in this state is not representative for the real situation.
The exclusion of the Sulu Sea generally leads to better appreciable results of phases but more disappointing results of amplitudes. However as it has been mentioned earlier: the results of amplitudes might be improved by not closing the Sulu and Palawan Archipelago's with dry points, as it has been done in C02, but with adaptation of grid enclosure in the Sulu Sea neighbourhood.
It is remarkable to see, that the exclusion of Sulu Sea has far more prominent effect on the Celebes Sea side than the South China Sea side. This would mean the dimensioning of the Palawan Archipelago (between the South China Sea and the Sulu Sea) has not any effect on the results of South China Sea.
Because the closure of the both archipelago's of the Sulu Sea on their turn is worth to be looked at separately new runs, by only closing the Palawan Archipelago respectively the Sulu Archipelago of the Sulu Sea are made as well. However of these two runs (C04 and C05) only statistical data for discussion of the global model results is available. These are presented and discussed below.

Here are some statistics of the two runs together with G13:

Table 5.1: Run statistics

	M_2			S_2			K_1			O_1		
RUN	G13	C01	C02	G13	C01	C02	G13	C01	C02	G13	C01	C02
H_c-H_0	0.00	0.006	-0.01	0.01	0.003	-0.01	0.00	0.00	-0.02	0.00	0.012	-0.02
$\|H_c$-$H_0\|$	0.11	0.127	0.137	0.06	0.073	0.082	0.05	0.05	0.065	0.03	0.039	0.055
RMS- error	0.02	0.022	0.023	0.01	0.011	0.013	0.01	0.008	0.011	0.00	0.006	0.01
G_c-G_0	5.42	4.42	17.77	-7.30	-1.96	-1.73	16.88	13.44	25.0	5.36	7.60	9.91
$\|G_c$-$G_0\|$	37.92	40.83	38.76	33.39	43.77	42.62	20.77	18.60	29.4	15.04	14.85	18.27
RMS- error	5.74	6.29	6.47	5.41	6.79	7.031	3.13	2.89	5.36	2.49	2.37	2.72
	M_2			S_2			K_1			O_1		
RUN	C03	C04	C05	C03	C04	C05	C03	C04	C05	C03	C04	C05
H_c-H_0		0.00	-0.01		-0.01	-0.01		-0.01	0.02		-0.00	0.017
$\|H_c$-$H_0\|$		0.107	0.13		0.066	0.079		0.057	0.061		0.048	0.048
RMS- error		0.18	0.2		0.096	0.11		0.081	0.094		0.066	0.066
G_c-G_0		11.41	21.94		5.23	9.22		16.84	15.28		12.2	9.58
$\|G_c$-$G_0\|$		33.92	41.87		35.26	47.29		20.88	19.63		18.05	16.33
RMS- error		49.55	64.54		54.92	71.49		29.12	28.54		24.27	23.04

in which:

H_c-H_0 : computed amplitude minus observed amplitude
$|H_c$-$H_0|$: computed amplitude minus observed amplitude; absolute value
RMS- error : Root Mean Square of the computed amplitude minus observed amplitude
G_c-G_0 : computed phase minus observed phase
$|G_c$-$G_0|$: computed phase minus observed phase; absolute value
RMS- error : Root Mean Square of the computed phase minus observed phase

Under ideal circumstances H_c-H_0, $|H_c$-$H_0|$, G_c-G_0, and $|G_c$-$G_0|$ should lead to a value of 0. In some TRIANA presentations of Appendix 4, analyses are made of computations with H_c/H_0 values of tidal stations. In that case, the ideal situation can be pointed out as a value of 1.

From Table 5.1, it can be seen that both the computations C01 and C02 do not show any improvement of results compared to G13. Computation C01 only shows some slight improvement of the results of the diurnal constituents.

The computation in which the Palawan Archipelago is closed (C04) leads to better results of the model in general contrary to the computation in which the Sulu Archipelago (C05) is closed. This means that the influence of the passages of the Palawan Archipelago on the tides in the Sulu Sea is little compared to the influence of the passages between the Sulu Archipelago.

Finally one final remark of measured data of the tidal stations of the South China Sea Model: Comparing of data, which were used in computations with TRISULA and data of Admiralty Tide Tables showed some significant differences for tidal stations in the Malacca Strait and Sulu Sea regions. The tidal data used in TRISULA computations is based on the findings of the Admiralty Tide Tables edition 1992. Comparison was made with the Admiralty Tide Table data edition 1996. For some tidal stations differences of phases and amplitudes up to 15% were noticed for especially in the region of Singapore. The considerable differences in just four years of some stations one more time underline the complicated nature of the tides of the region.

6 Conclusions and Recommendations

In this report a study on the tides of the South China Sea region has been made. The tidal movements as they exist are analysed and the abilities or the inability's to represent these tidal movements with a hydrodynamic model are discussed. This section deals with the conclusions that can be drawn of this study and the recommendations that can be given for future research.
Unfortunately the study can not be regarded as completed yet. Although many 'hot items' have been investigated, there are still lots of question marks left: dealing with all the aspects of the problems would be out of the aim of this study.
Future research is therefore still needed. Hopefully the reader of the report in this state, can get enough imagination of the tidal behaviour of the area and can understand its problem areas together with their sensitivities. The problem analysis as it is drawn in this report has to be continued.
The study area has a very complicated tidal behaviour. This complexity is caused by the effects of extreme natural conditions of the region. The excitation of the tides within the area by two different oceans from different sides, the complicated geography, bathymetry and influences of ocean currents and monsoons are some of the examples of these natural conditions. The geography contains shelf areas with very shallow depths as well as very deep basins, and there are also lots of tiny islands and small passages. The total of these conditions together with the large size of the area (the South China Sea 17 times larger than the North Sea) is the consequence for the creation of a hard modelling environment.
The difficulty of creating a model which reliably represents the real situation, appears also from the lack of confidential hydraulic models of the area. The DELFT HYDRAULICS' model, which was constructed during June 1993 and June 1995, also identified itself not to be reliable yet.

Conclusions of the analysis of the separate problem areas of the South China Sea Model were mentioned as follows:

- Sulu Sea

  The tides enter this almost rectangular sea basin from two opposite sides through narrow passages and tiny islands. The amount of the tides entering from both sides and the effective dimensions of the passages they enter through are puzzling. It has been demonstrated with model runs in the past and the model runs during this study, that this sea is of extreme importance for the global results of the complete South China Sea Model. The poor results of the Sulu Sea apparently disturb the results of parts of the South China Sea, Celebes Sea and the Java Sea. This was shown in a model run with the Sulu Sea removed of the model: it resulted in very different results in the Celebes Sea, Java Sea and the South China Sea. Two other runs considering the analysis of the importance of the passages at the Palawan and Sulu Archipelago's of the Sulu Sea were made. Closing the Palawan Archipelago resulted into overall better accuracy of the results than former model calculations with open Palawan Archipelago boundaries. On the contrary, closing the Sulu Archipelago resulted into more insufficiently results.
  The complexity of the Sulu Sea is also underlined with a 1-dimensional analysis based on harmonic analysis. With this 1-dimensional analysis, it was seen that calibration of the results of different stations together in the Sulu Sea in desired solutions (of natural occurrence) is a very hard or impossible task. The processes involved in the Sulu Sea proved themselves to be too complicated to be represented with a 1-dimensional representation.

- Malacca Strait

  The problem of the Malacca Strait can be compared to that of the Sulu Sea: the results of the end part of region neighbouring the Java Sea are very disappointing and these results affect the results of the Java Sea. The tides mainly enter from one side of the strait and are influenced by the geometrical changes going from north-west to south-east and the tiny islands at the south-east end. Model representation of this area is hard, not only by the geometry and the islands (the islands are tiny and the depth variations are very extreme and abrupt), but also because the area in the south-east is the meeting point of tides from three different directions.

- Java Sea

  The results of Java Sea are disappointing as well. This is partly because of the negative influences of the results of the Sulu Sea and Malacca Strait, but also because of Java Sea's own modelling difficulties. The bottom schematization of the Java Sea proved itself extreme sensitive for modelling results because of its shallow depth. Difficulties also occur because of the two narrow passages Lombok Strait and Sape Strait, both modelled as open boundaries. These two straits determine the amount of tides entering the area from the Indian Ocean. The modelling results of two years ago already demonstrated, that the representation of these passages strongly influences the results within the Java Sea.

- Gulf of Thailand

  In the Gulf of Thailand the results are locally very disappointing but locally very appreciable as well. This is the result of the shallowness of the area and the strange behaviour of the tides mainly coming from two different sides. The problems in this part of the model are local and compared to the other problem areas less severe.

Because of the relatively coarse grid size, the modelling of some specific areas of the model is very difficult. The narrow passages of Lombok and Sape (this was already demonstrated in modelling results in the past), the Malacca Strait and the passages of the Sulu and the Palawan Archipelago's of the Sulu Sea are examples for this. Also there are some tiny island which can not be ignored and that are hard to schematise with the current coarse model (examples are the islands in the Sulu Sea region and the Riau Archipelago region). The depth variations are very extreme and abrupt in some parts of the study area: Malacca Strait, Sulu Sea and the edges of the Sunda shelf are some examples for this. Under these circumstances it seems to be that the gridsize of the current model is too coarse.

Recommendations for future investigators considering the problems of tidal modelling of the South China Sea can be described as follows:

By introducing the tide generating force for the first time in model computations, it was seen the model results were globally less appreciable contrary to the exceptions. Therefore a critical advise to once more consider all aspects of the model, especially its domain and boundaries, is highly recommended.
The problem of the Java Sea originating from Lombok and Sape Straits can probably be solved when the model is refined in its grid. The possibility to better schematise not only these passages but the passages between tiny islands and the abrupt depth changes as well is then achieved. The refinement of the gridsize is also believed to be advantageous for the results in the Malacca Strait (especially near Singapore) and the Sulu Sea.
The Gulf of Thailand is, as mentioned before, a local problem. Local adaptations to the bottom profile and coastlines are therefore needed to solve these problems. Some examples:

locally shallower or deeper areas, locally adapted coastlines and locally more or less bottom friction. On this manner, the results can better be directed to desired solutions.

The Sulu Sea and Malacca Strait reveal the same kind of problem: The tidal behaviour can not be modelled as desired because of schematization difficulties of some passages. For the case of Sulu Sea, a first attempt to analyse this problem with a 1-dimensional analysis showed no satisfying results. However it is still believed, one must be able to tackle the sensitivity problems, such as in Sulu Sea and Malacca Strait, by simplified analytical methods. The 1-dimensional method could still be useful when adapted. Differently implementation of boundary and transition conditions or implementation of energy conservation between separate basins are some adaptations that can be thought of.
If the 1-dimensional method still proves itself as not sufficient, the use of a different analytical approach can be considered. Examples of some different approaches are for instance a 2-dimensional analytical method or a (semi- numerical) spectral method.
The solution for the problems can also be searched for from numerical point of view. For example: the Sulu Sea and Malacca Strait can be 'cut off' the model and each solved on its own with a 2-dimensional numerical approach. Varying schematization possibilities can be tried, when for instance use is made with DELFT HYDRAULICS' RGFGRID and QUICKIN program facilities. These are packages to easily produce or adapt grids and grid resolutions and easily adapt the depth profiles locally. Another possibility of an interactive numerical approach is the use of PHAROS package. PHAROS is an extremely useful 2-dimensional program facility, when the behaviour of single harmonic constituents is looked at, in areas with varying depth and friction. This package proved itself to be extremely useful in the past with project concerning tidal basins and bays.

References

van AKEN, H.M., PUNJANAN, J., SAIMINA, S., 1988, Physical aspects of the flushing of the East Indonesian basins, *Netherlands Journal of Sea Research*, Vol.22(1988), No 4, pp 315-339.

APEL, J.R., HOLBROOK, J.R., LIU, A.K., TSAI, J.J., 1985, The Sulu Sea Internal Soliton Experiment, *Journal of Physical Oceanography*, Vol. 15(1985), pp 1625-1650

BECKER, G.A., 1981, Beiträge zur Hydrogrphie und wärmebilanz der Nordsee (in German), In Deutsche Hydrographische Zeitschrift, Heft 5, Hamburg, Deutsches Hydrographisches Institut, 1981.

van BERK, 1986, Damping of the Sulu Sea in Sunda Model (in Dutch), In notes of Rijkswaterstaat, Tidal Waters dep., Note DDWT- 86.202, the Hague, 1986.

BROWN, J., COLLINS, A., PARK, D., PHILIPS, J., ROTHERY, D., WRIGHT, J., 1989, Waves tides and shallow- water processes, lectures of the Open University, Pergamon Press, Oxford, 1989.

van DANTZIG, D., 1960, Free oscillations in a rotating rectangular basin (in Dutch), In Report of the Delta Committee, Part 3, Contributions II, the Hague, Mathematical Centre, 1960.

DRONKERS, J.J., 1960, Methods of tidal computation (in Dutch), In Report of the Delta Committee, Part 4, Contributions III, the Hague, Rijkswaterstaat, 1960.

DRONKERS, J.J., 1961, The effect of the Delta Works on the tides and the storm-surge levels along the coast of the south-western part of the Netherlands (in Dutch), In Report of the Delta Committee, Part 5, Contributions IV, the Hague, Rijkswaterstaat, 1961.

EXON, N.F., HAAKE, F.W., HARTMANN, M., KÖGLER, F.C., MÜLLER, P.J., WHITICAR, 1981, M.J., Morphology, water characteristics and sedimentation in the Silled Sulu Sea, Southeast Asia, *Marine Geology*, Vol. 20(1981), pp 165-195

GERRITSEN, H., 1993, Calibration of numerical flow-models in practical applications, In DELFT HYDRAULICS course guide of December 1993, Delft

GIESE, G.S., HOLLANDER, R.B., FANCHER, J.F., GIESE, B.S., 1982, Evidence of coastal seiche excitation by tide-generated internal solitary waves, *Geophysical research letters*, Vol. 9(1982), No 12, pp 1305-1308

HALL, G.P.D., 1975 ed. Indonesia pilot, Vol. 1, ed. 1, Taunton, England, 1975.

HESLAM, D.W. 1976 ed. Indonesia pilot, Vol. 2, ed. 1, Taunton, England 1976.

HESLAM, D.W., ed. 1978, Philippine Islands pilot, ed. 1, Taunton, England 1978.

HOLTHUIJSEN, L.H., ed. 1993, Applied Physical Oceanography (in Dutch), In lectures on the subject x2CT1 of Delft University of Technology, Civil Engineering dep., Delft, December 1993.

KOWALIK, Z., MURTY, T.S., 1993, Numerical modelling of Ocean Dynamics, 1993.

KUIPERS, J., VREUGDENHILL, C.B., 1973, Calculations of two-dimensional horizontal flow, Report on basic research S163, Part 1, DELFT HYDRAULICS, Delft, 1973.

LIU, A.K., HOLBROOK, J.R., APEL, J.R., 1985, Non-linear internal wave evolution in the Sulu Sea, *Journal of Physical Oceanography*, Vol. 15(1985), pp 1613-1624

MA HONG, 1987, On the winter circulation of the northern South China Sea and its relation to the large scale oceanic current, In Part 1 of: Nonwind-driven circulation of the northern South China Sea and numerical experiments, *Chinese Journal of Oceanology and Limnology*, Vol.5(1987), pp 10-20

MIHARDJA, D.K., 1991, Energy and momentum budget of the tides in Indonesian waters, Berichte aus dem Zentrum für Meeres- und Klimaforschung der Universität Hamburg, No 14, Hamburg, 1991.

MURRAY, S.P., ARIEF, D., KINDLE, J.C., HURLBURT, H.E., ed. L.J. PRATT, 1990, Characteristics of circulation in an Indonesian Archipelago Strait from hydrography, current measurements and Modelling results, The physical oceanography of sea straits, In NATO ASI Series, Vol. C, Kluwer Academic Publishers, Dordrecht 1990.

MURTY, T.S., El-SABH, M.I., 1989, Sense of rotation around tidal amphidromic points in the Northern and Southern hemispheres, *Marine Geodesy*, Vol.13(1989), No 1, pp 67-71

PAN HAI, LIU FENG-SHU, 1994, A numerical study of the tide-surge interaction in the East China Sea and the South China Sea, *Chinese Journal of Oceanology and Limnology*, Vol.12(1994), No 1, pp 13-21

PEDLOSKY, J., 1979, Geophysical Fluid dynamics, Springer-Verlag, New York, 1979.

POHLMANN, T., 1987, A three dimensional circulation model of the South China Sea, Institut für Meereskunde der Universität Hamburg, In ed. J.C.J. NIHOUL and B.E.M. JAMART, Three dimensional models of marine and estuarine dynamics, Elsevier Oceanography Series, Vol. 45, Elsevier, Amsterdam, 1987.

van RIJN, L.C., 1990, Principles of fluid flow and surface waves in rivers, estuaries, seas and oceans, Vol. 1, Aqua Publications, Amsterdam, 1990.

ROBERTS, H.H., MURRAY, S.P., HSU SHIN-A, Marine meteorology, physical oceanography and sedimentary dynamics of a back-arc basin and linking strait: Java Sea and Lombok Strait, In Draft proposal of Coastal Studies Institute, Louisiana State University, Baton Rouge, Louisiana 70803.

SCHIERECK, G.J., 1978, lectures of Tides, pys/BTA-60, Delft, October 1978.

SCHIJF, J.B., 1960, Tidal computations & hydraulic and electric models from a general point of view (in Dutch), In Report of the Delta Committee, Part 4, Contributions III, the Hague, Rijkswaterstaat, 1960.

SCHWIDERSKI, E.W., 1979, Global ocean tides part II, Technical report NSWC-TR 79-414, USA, 1979.

STELLING, G.S., BOOIJ, N., 1993, Computational modelling in open channel hydraulics, manual on the lectures of B84, Delft University of Technology, Delft, 1993.

TAKAKI, H., TOSHIYUKI, A., KAZUNORI, A., 1996, Tidal currents in the Indonesian Seas and their effect on transport and mixing, *Journal of Geophysical Research*, Vol. 101(1996), No C5, pp 12353-12373

VERSPUY, C., 1987, Long Waves (in Dutch), manual on the lectures of Long waves B73, Vol. 3, Delft University of Technology, Delft, 1987.

WYRTKI, K., 1961, Scientific results of marine investigations of the South China Sea and the Gulf of Thailand, In NAGA Report, Vol. 2, The University of California, Scripps Institution of Oceanography, La Jolla, California 1961.

ZHOU Di, LIANG YUAN-BO, ZENG-KUI, 1994, Oceanology of China Seas, Vol. 1&2, Kluwer Academic Publishers, Dordrecht 1994.

List of figures and tables

List of Figures

Figure 2.1: Positioning of the study area in the world 2–1
Figure 2.2: Area of interest 2–3
Figure 2.3: Bathymetry of the South China Sea; isolines in meters (Zhou Di et al.) 2–4
Figure 2.4: Amplitude (cm) of the semi-diurnal tides (M2 +S2) (Wyrtki) 2–6
Figure 2.5: Amplitude (cm) of the diurnal tides (O1+K1) (Wyrtki) 2–6
Figure 2.6: Co-tidal lines of the semi-diurnal tide M2 in lunar hours (Wyrtki) 2–7
Figure 2.7: Co-tidal lines of the diurnal tide K1 in lunar hours (Wyrtki) 2–7
Figure 2.8: Schematic view of the wave propagation of the M2 tide (Takaki et al.) 2–11
Figure 2.9: Schematic view of the wave propagation of the K1 tide (Takaki et al.) 2–11
Figure 2.10: Co-tidal lines of K1 and M2 tidal components (Schiereck) 2–12
Figure 2.11: Typical tidal curves representing the four tidal types during a period of 16 days (Wyrtki) 2–14
Figure 2.12: Geographical distribution of tidal types according to Cao&Fang (Zhou Di et al.) . 2–15
Figure 2.13: Geographical distribution of tidal types according to Wyrtki (Wyrtki) 2–16
Figure 2.14: Observed distributions of (absolute maximum value) velocity (cm/s) and (b) its appearing time of the K1 tidal constituent in the northern South China Sea and the Gulf of Thailand (Zhou Di et al.) 2–17
Figure 2.15: Observed distributions of (absolute maximum value) velocity (cm/s) and (b) its appearing time of the M2 tidal constituent in the northern South China Sea and the Gulf of Thailand (Zhou Di et al.) 2–18
Figure 3.1: Iso-amplitude contours (dashed line in cm) and iso-phase-lag contours (solid line, in degree, for (a) the K1 constituent and (b) the M2 constituent according to Cao&Fang. (Zhou Di et al.) 3–2
Figure 3.2: Geographical positioning of the amphidromic points, as given in Table 3.1 3–3
Figure 3.3: Delft hydraulics' South China Sea Model 3–4
Figure 4.1: Bathymetry of Sulu Sea, showing locations of stations SS1, SS2 and SS3 (Apel et al.) 4–2
Figure 4.2: Bottom topography of the Sulu Sea across the stations SS1, SS2 and SS3 (Apel et al.) 4–2
Figure 4.3: Bottom profiles across the lines 102 and 111 (Exon et al.) 4–3
Figure 4.4: Direction of the main flood stream in Philippine waters (Heslam) 4–4

List of Tables

Table 2.1: List of tidal constituents 2–5
Table 3.1: List of M2 Constituent amphidromic points obtained by numerical simulations for the South China Sea (Zhou Di et al.) 3–2
Table 3.2: Overview of calculations with the first version of the South China Sea Model 3–8
Table 3.3: The final version of the SCSM, with rearranged bottom profile and new gridsize 3–9
Table 3.4: Overview of calculations with the modified version of the SCSM 3–10
Table 4.1: Desired solutions of the stations 4–17
Table 4.2: Overview of computed basin dimensions in stations 4–18
Table 5.1: Run statistics 5–8

Appendix 1: Introduction into tides

This Appendix contains general theories or findings of the following subjects:

A1.1 Tidal Forces
A1.2 The equilibrium tidal theory
A1.3 Prediction of tides
A1.4 Tides in seas and oceans
A1.5 Standing waves: reflection, free and forced oscillations
A1.6 Tides of the Malacca Strait

A1.1 Tidal Forces

Tides are characterised by the rhythmic rise and fall of sea-level over a period of several hours. The rising tide is usually referred to as the flow or the flood, whereas the falling tide is called the ebb. This ebb and flow of the tide is manifested in tidal currents, which can be powerful, especially where the water is constrained by shallow depth or adjacent land masses. From the earliest times, it has been realised that there is some connection between the tides, the Sun and the Moon. Tides are highest when the moon is full (full moon) or new (new moon), and the times of high tide at any given location can be approximately related to the position of the Moon in the sky. Because the relative motions of the Earth, the Sun and the Moon are complicated, it follows that their influence on tidal events results in an equally complicated pattern. Nevertheless the magnitude of the tide- generating forces can be precisely formulated, although the response of the oceans to these forces is modified by permanent effects of topography and transient effects of weather patterns (Brown et al., 1989). In Figure A1.1 the orbits are given of the Sun, Moon and Earth system.

Figure A1.1: Orbital planes of the Sun, Moon and the Earth

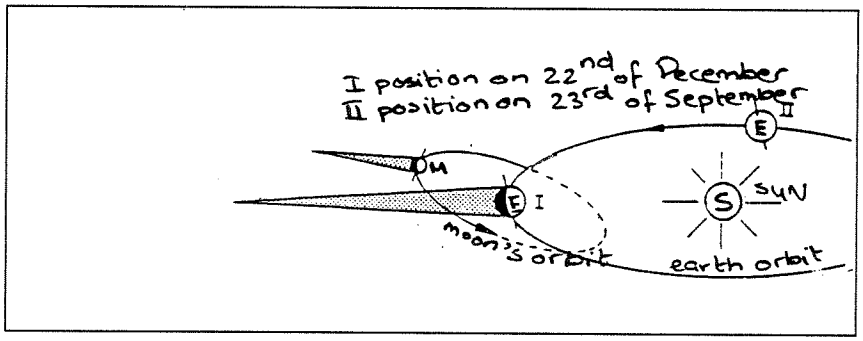

The tides following from the combined gravity forces of earth, moon and the sun are called the astronomical tides. The strength of astronomical tides is dependent of meteorological and topographical variations on the earth. The tide that would result if the whole earth was covered with a deep layer of water is called the equilibrium tide.
The observed astronomical tide is however much different from the equilibrium tide. The reason for this is the occurrence of continents and the natural shape of the ocean basins. The tide at any spot on the earth at any given time can therefore not be calculated simply from the equilibrium tide. With the equilibrium tide however, understanding of varying aspects of the real tide can be obtained.
When the influence of the sun is neglected, the earth and the moon would form a single system with their resulting centre of mass Z. The water masses of the earth would deform into an ellipsoid because of gravity forces between the earth and the moon and their rotation around their mutual mass point. The total centrifugal force within the earth moon system exactly balances the forces due to their gravitational attraction. The centrifugal forces are directed latitude to a line, joining the centres of the earth and the moon.
When for instance the moon is moving through a certain latitude of an arbitrary spot on the earth, or positioned at the highest point possible for this spot, it is then called the moon is culminating for this point and for all the other points on the same latitude line. For those points from where at the time of culmination the moon can be seen, there is an upper culmination and for all the points on the same latitude from where the planet or the moon can not be seen there is a lower culmination. (for example: the sun has an upper culmination on 12 o'clock and a lower culmination on 24 o'clock). While the earth rotates 'under' the watershield, two high-waters per day (24 hrs) occur on a given spot of the earth during the two moon culmination's and two low-waterlevels between these culmination's. This earth

moon interaction tidal type is generally called the M_2 tide. (M of Moon and 2 because two maximum and minimum levels occur per day)
The earth orbital plane (including equator plane of the earth) and the moon orbital plane are not always on the same level. These two planes always cross each other, but the angle between them is variable. With daily differences this inequality results to that the high and low waters are not repeatedly the same. The angle between midpoint earth and midpoint moon is called the earth-moon declination. (See Figure A1.2) Regarding the tides between the earth and the moon, there is an angle between the long axis of the ellipsoid and the equator because of moon declination. Because of this, especially at higher latitudes, the difference between two following high water levels (and two low water levels) can be daily different. This is called a diurnal inequality and its effect depends of the earth positioning.

Figure A1.2: Production of unequal tides due to Moon's declination

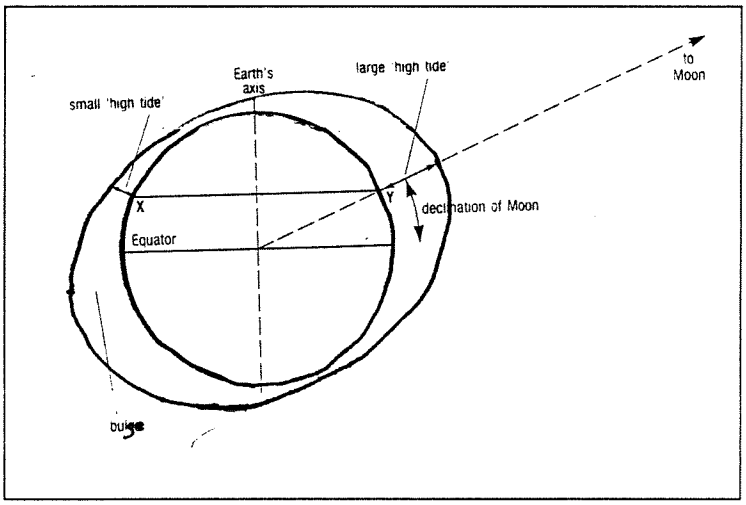

The sun has an essential part in the tidal motion on the earth as well. When the sun is on the same line as the moon (New Moon and Full Moon), the system of sun, moon and earth is in a linear position and the tidal influences of the moon and the sun strengthen each other. However, if the sun is in such a position, that it is positioned 90^0 from the moon (First Quarter and Last Quarter) the tidal effects are disturbing each other. The resulting tidal effect is then less than expected. These inequalities are called spring tide respectively neap tide. This can be seen in Figure A1.3.

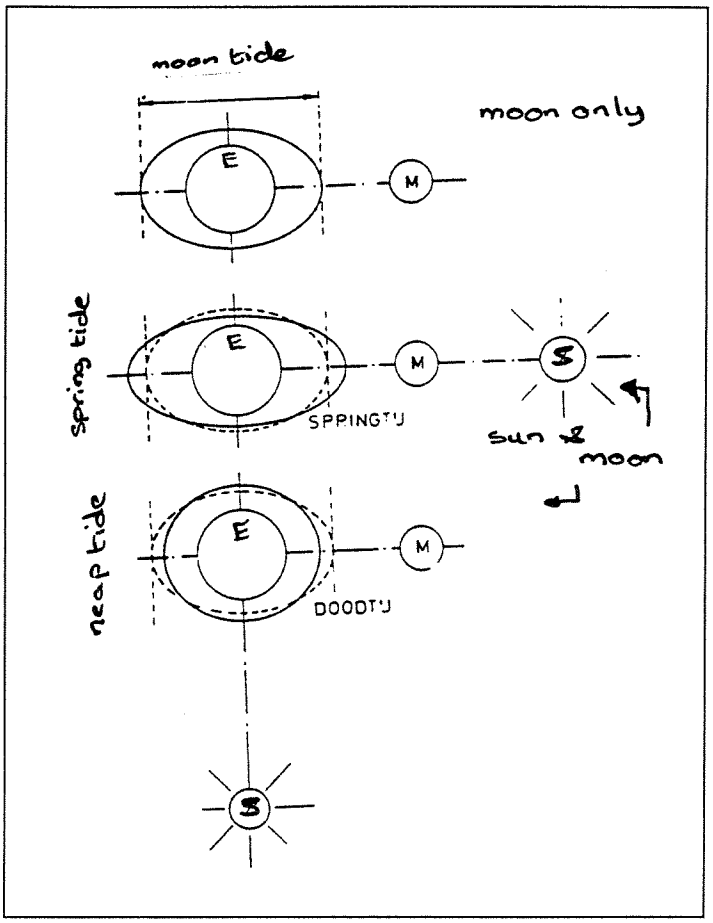

Figure A13: spring tide and neap tide due to Sun and Moon interaction

Apart from inequalities like neap tide and spring tide and the daily inequalities, there are other kinds of inequalities affecting tidal movements. One of these is inequality in the periodicity of interdependent movement of the earth, the sun and the moon.
The moon completes one turn around the earth in 27.32 days (one sidereal month) and the earth completes its movement around the sun in one year or in 365.2564 days. During one orbit of the moon around the earth, the earth has changed its position because of its own orbital movement around the sun. Because of this, the moon does not reach the same position on its orbit around the earth that it had one sidereal month earlier. For reaching the same position the moon has to proceed its movement until 29.53 days. This is called one synodical month. The time proceeded between two succeeding spring tides or between two succeeding neap tides is therefore 14.76 days. Following from this, the time between two high water levels or two low water levels on a certain point of the earth is not 12 hours but 12.42 hours, which equals to 12 hours and 25 minutes.
The distance between the moon and the earth is not constant, because the moon's is an ellipsoid with a given eccentricity. (e=0,055) The variation in distance from Earth to Moon results in corresponding variations in the tide-producing forces. When the moon is closest to the earth, it is said to be in its perigee. The moons tide-producing force is then increased by 20% during new moon or full moon compared to the tides resulting of the mean distance between earth and the moon. When the moon is in its apogee position, which is the furthest distance between the moon and the earth, there is a relatively low spring tide with relatively 20% less tide-producing force. After nearly one quarter of a year, from when the moon is in its apogee or perigee during new moon or full moon, the distance between the earth and the moon is on its average. The tides during neap tide and spring tide will then be close to their average values. The time passing between two apogees or perigees is about 0.56 year, not exactly 0.5 year as it might be expected, because the perigee position itself (regarded to the stars) is rotating around the earth in 8,85 years.
The declination of the sun is the angle between the sun mass point and the equator plane. This declination varies between $+23,5^0$ on 21st of June and $-23,5^0$ on 22nd of December each year. (on 21st of march and 23rd of September mean declination of 0^0) The plane level of the sun orbit around the earth is called the ecliptic. The equator level of the moon on its turn makes an angle between $+5^0$ and -5^0 with the ecliptic plane. The cutting line between the two levels is called the nodal line.
The moon also varies in its declination regarded to the earth. In 27,55 days the declination varies between $23,5^0$ and $-23,5^0$, because of its movement around the earth. Apart from this, the angle between the moon and the sun varies $+5^0$ and -5^0 in 18,6 years. As the result of this the moon declination in fact varies between $^+/_- 18,5^0$ and $^+/_- 28,5^0$.

Summarising the following table can be made of the different periodicity's:

Table A1.1: Periodicity's of diverse orbital movements

Planet	Periodicity	Period	Rotation)[1]
moon	• orbital movement around the earth	27,32 days	+
	• returning time of diverse moon sights (NM, FQ, FM, LQ)	29,53 days	+
	• variance of the ellipsoidal orbit	8,85 years	+
	• variance of the moon-sun flat	18,6 years	-
earth	• orbital movement around own axis	23 h. 56 min. 4,1 s.	+
	• orbital movement around the sun	365,26 days	+
	• variance of the angle of the earth axis)[2]	40000 years	
	• variance of the eccentricity of earth ellipsoidal orbit)[2]	95000 years	
	• turning of the ellipsoidal orbit, around the sun.)[2]	108000 years	+

[1] a positive turn means anticlockwise turn seen from the Polar star.
[2] not dealt with in these notes

A1.2 The equilibrium tidal theory

Attraction between two different bodies can be described by the gravity force law of Newton. This theorem is valid for the sun, the moon and the earth system as well. The gravity theorem can be described by the formula:

$$K = f\frac{M_1 M_2}{d^2} \qquad \text{(A1.1)}$$

in which: f = Newton's gravity constant
M_1, M_2 = elementary masses
d = distance between the mass-points of the two elements

Besides the gravity forces there are centrifugal forces, due to orbital movements of the concerned celestial bodies.
These two different forces results, for a given spot on the earth surface, in a specific total force. This resulting force is variable: it depends of the latitude of the considered point and is called the tide generating force. This force varies inversely with the cube of the distance from the moon. This is shown in Figure A1.4.

Figure A1.4: The derivation of tide generating forces.

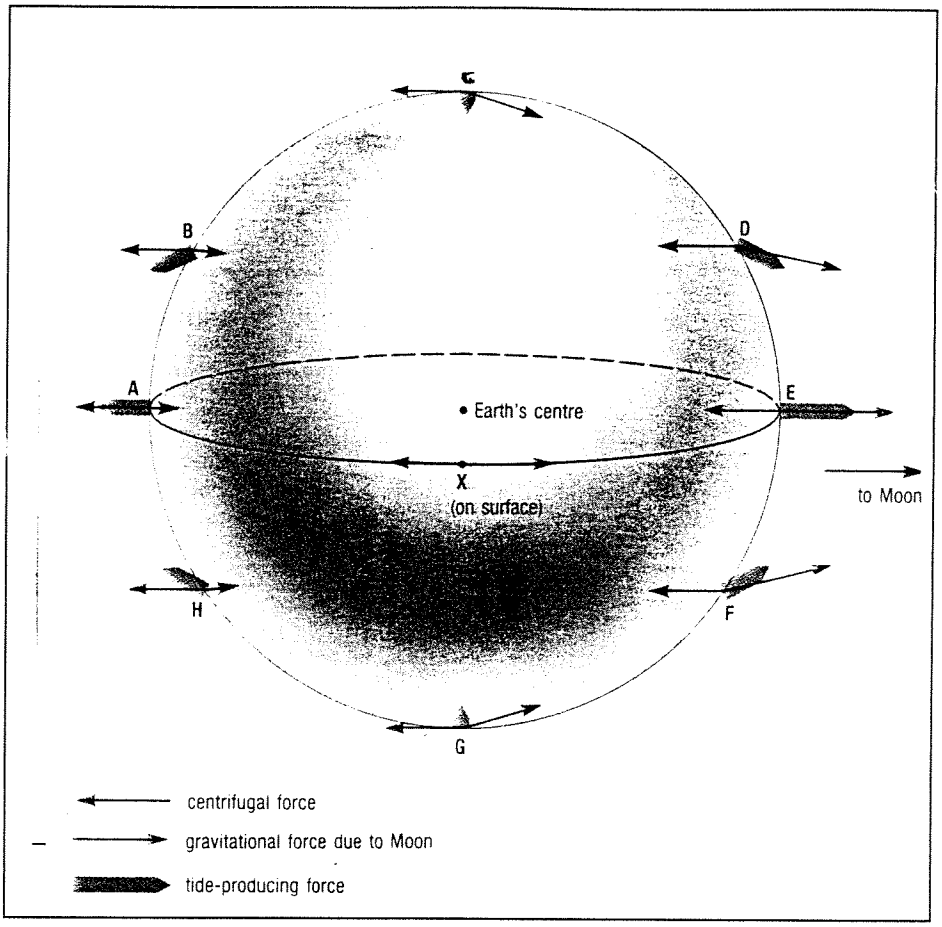

A1.2.1 The Earth-Moon system

The tide generating force for an arbitrary spot on the earth can be determined as follows:

1 The force resulting from the rotation of the two bodies, which is constant for all points on earth (or the centrifugal force):

$$F_a = f\frac{m1M}{d^2} \qquad \text{(A1.1).a}$$

2 Each point on the earth surface undergoes attraction force F_m of the moon. This force is also resulting from the attraction or gravity of the two bodies: the earth and the moon. On an arbitrary unit of mass m1, this force is depending of the actual distance (or the gravity force):

$$F_m = f\frac{m1M}{L^2} \qquad \text{(A1.2)}$$

3 A third, but very important force is the attraction of the earth (F_g) on an arbitrary mass unit on its surface:

$$F_g = f\frac{m1A}{r^2} = mg \qquad \text{(A1.3)}$$

with: g = gravity acceleration (9,81 in the Netherlands)
m1 = an arbitrary mass unit
A= earth mass; $5{,}98*10^{24}$ kg.
M= moon mass
d = mean distance between mass middle points between the earth and the moon, 384000 km

r= earth radius, 6370 km
L= distance of an arbitrary point on earth surface to the moon mass centre
($L \approx d - r\cos(\theta)$) ($\theta$:latitude)

It should be noted that the centrifugal force F_a is constant for any point on earth surface and that the gravity force of the moon F_m relies on the latitude. The forces F_a , F_m and F_g are balancing each other on earth surface with a resulting force. This resulting force is known as the tide generating force F_t. On any spot on earth, it is now possible to calculate the resulting force F_t. See Figure A1.5 below.

Figure A1.5: Centrifugal and attraction forces of the earth-moon system

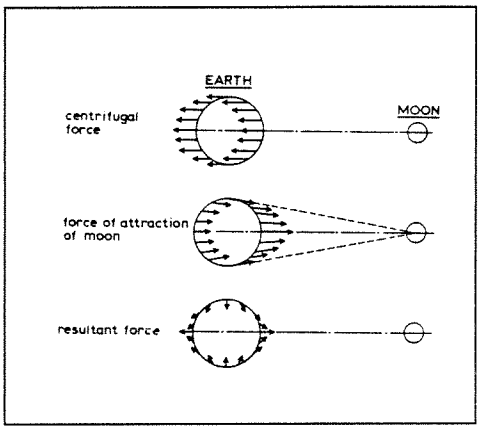

The tide generating force can further be split in two components:

- a horizontal component F_s, which is called the tractive force, directed tangential to earth surface.
- a vertical component F_v, which is directed in the same direction as the gravity force.

In mathematical form, these two forces can be written as:

(1.4) $$F_s = 1.5f\frac{Mr\sin(2\theta)}{d^3} \qquad F_v = 3f\frac{Mr\cos^2(\theta - 1/3)}{d^3}$$ (A1.5)

The same formulations can be made for the Sun and Earth system as well. The proportions of tides generated by the sun and the moon can be determined as:

$$Sun : Moon = 1 : 2.18$$

As it can be seen, tides generated by the moon are more important, because of the less earth to moon distance, although the sun mass is much more as the moon mass.

A1.3 Prediction of tides

For prediction of the tide in an arbitrary spot on the earth, the equilibrium tide as it is observed on the meridian of Greenwich, is used.

$$h = h_0 + \Sigma f_n H_n \cos(\omega_n t + V_n + u_n)$$ (A1.6)

in which: h= tide (horizontally or vertically)
h_0= mean tide
H_n= astronomical amplitude, is a constant value for different tidal components
ω_n= angle velocity
t= GMT (Greenwich Mean Time)
V_n+u_n= astronomical argument, of which:
V_n= uniformly changing part of the astronomical argument because, each day starts with t=0 again; each tidal constituents has also a new argument every day.

f_n, u_n= correction for the positions of the nodes, f_n is derived of astronomical analysis and presumed to be constant over a year

For a spot L degrees westerly of Greenwich, the equilibrium tide with t in GMT (nowadays UTM) is:

$$h= h_0 +\Sigma f_n H_n \cos(\omega_n t+V_n+u_n-pL) \quad \text{(A1.7)}$$

with p= 0,1,2....depending of return period of the tide per day.

This spot is in an other time zone than Greenwich. Supposing that the spot is in a time zone, in which it is S hours earlier than in Greenwich, the equilibrium tide can be written as:

$$h= h_0 +\Sigma f_n H_n \cos(\omega_n t+V_n+u_n-pL+\omega_n S) \quad \text{(A1.8)}$$

In the real tide, h_0 and H_n are presumed to be the mean depth and mean amplitude. For an arbitrary tidal component however, there will be a difference in phase with respect to the equilibrium tide, so the real tide will be given by:

$$h= h_0 +\Sigma f_n H_n \cos(\omega_n t+V_n+u_n-pL+\omega_n S-\kappa_n) \quad \text{with: } \kappa_n \text{= kappa-value} \quad \text{(A1.9)}$$

Most times this is written as:

$$h= h_0 +\Sigma f_n H_n \cos(\omega_n t+V_n+u_n-g_n) \quad \text{with: } g_n = pL+\omega_n S-\kappa_n \quad \text{(A1.10)}$$

the modified kappa-value

From this last equation, it can be seen that tides are summation of several sinusoidal expressions each with its own amplitude, angular velocity and phase at a given time. A measurement of actual water level h(t) will comprise all these sinusoids and if there is enough information available of the different constituents it will be possible to determine each of them. The only unknown parameters are H_n and g_n , other parameters can be measured. The method used to determine the separate constituents out of the measurement is done with the so called harmonic analysis or Fourier analysis [Dronkers (1961), Holthuijsen (1993)].

A1.4 Tides in seas and oceans

Tides can be separated in components of which the amplitudes and frequencies are known. The tide for a given area can be calculated from the summation of the determining components. Most of the time however, this summation does not result in the measured tide level. The reason for this is the non-linear interactions of tidal components in the linearized tidal equations.

The occurring non-linear interactions can for example be the result of:

- varying water depth
- bottom friction (non-linear)
- non-linear water movement, especially with high velocities (advective terms)
- varying wave celerities resulting of depth changes

In tidal computations with open seas, tides at a certain location can be calculated with the values of neighbouring spots. Calculations are made with equations in which all the tide determining effects are to be found. These equations are the equation of continuity and equations of momentum. For two-dimensional tidal computations the following set of equations can be used [Gerritsen (1993), Kowalik&Murty (1993), Pedlosky (1979), van Rijn (1979)]:

1• equation of mass:

$$\frac{\delta h}{\delta t}+(h+\zeta)\frac{\delta u}{\delta x}+(h+\zeta)\frac{\delta v}{\delta y}=0 \quad \text{(A1.11)}$$

2• equations of momentum in x and y direction:

$$\text{x-direction: } \frac{\delta u}{\delta t}+u\frac{\delta u}{\delta x}+v\frac{\delta u}{\delta y}+g\frac{\delta \zeta}{\delta x}-fv+\frac{gu\sqrt{u^2+v^2}}{C^2(h+\zeta)}-\frac{\tau_{wx}}{\rho(h+\zeta)}=F_s \qquad \text{(A1.12)}$$

$$\text{y-direction: } \frac{\delta v}{\delta t}+u\frac{\delta v}{\delta x}+v\frac{\delta v}{\delta y}+g\frac{\delta \zeta}{\delta y}+fu+\frac{gv\sqrt{u^2+v^2}}{C^2(h+\zeta)}-\frac{\tau_{wy}}{\rho(h+\zeta)}=F_v \qquad \text{(A1.13)}$$

in which:

x= horizontal, x-axis direction (in latitudes direction on the earth and positive to the east)
y = vertical, y-axis direction (in meridian direction and positive to the north t = time)
g = earth gravity acceleration
ς = water level regarded to reference level
h = distance between (mean) bottom level to reference level
u = depth averaged velocity in x-direction
v = depth averaged velocity in y- direction
f = Coriolis force parameter: $f=2\Omega\sin\varphi$, with $\Omega = 0{,}73*10^{-4}$ and φ angle position on the earth; φ= 0 at the equator and $^{+}/_{-}\,90^0$ at poles.
C= Chézy coefficient of bottom roughness
τ_{wx}, τ_{wy} = Wind drag coefficients for the x and y directions
F_s, F_v= Components of tide generating forces in horizontal and vertical directions

A1.5 Standing waves: reflection, free and forced oscillations

When a progressive wave comes to a wall it will be reflected. The reflected wave will travel in opposite direction with the same speed and can be constructed, thinking of the wall being a mirror. The result of the two waves is the so called standing wave. The resulting wave celerity has now become zero (+c and -c), hence the name standing. The water goes now up and down only in the so called anti-nodes, while in the nodes there is no vertical movement. However in the nodes the horizontal velocity is maximal. By complete reflection at the wall, velocity and water level are 90 degrees out of phase.

A particle moving on the earth's surface will get an acceleration perpendicular to its movement. This is called the gyroscopic acceleration or Coriolis force. This acceleration is maximal on the poles and zero on the equator. On the northern hemisphere it works to the right on the southern hemisphere to the left. The effect of gyroscopic acceleration on standing waves in closed basins is, that the waves do not travel linearly to and fro, but circle around.

This effect is figured in the drawing below:

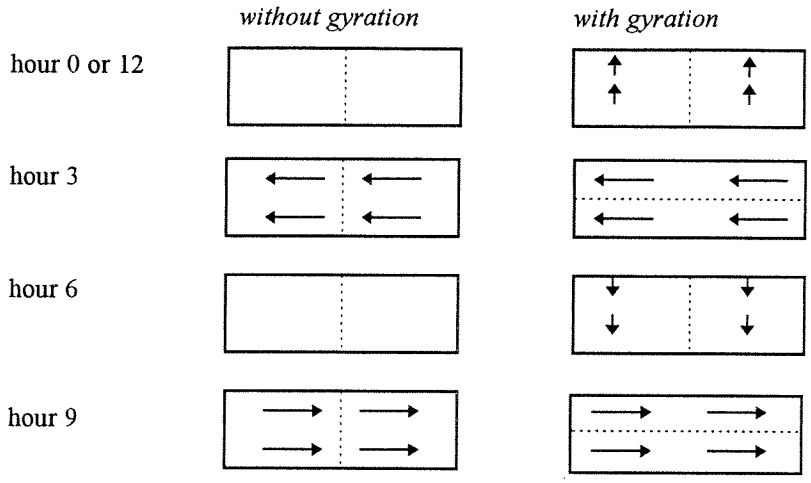

The effect of the Coriolis force is very obvious when significantly large areas are calculated. Coriolis force caused by the rotation of the earth around its own axis, is the reason for development of tangential currents.
The result with gyration is a rotating wave. When two oscillations come together, patterns occur like the waves rotate around one point. These points are very often to be seen, when single tidal constituents are regarded and they are called amphidromic points.
Bays and seas have natural periods, which is the period of a free oscillation of water in that bay or sea. The period of the first harmonic or fundamental mode of a closed bay or basin can be calculated as follows:

fundamental mode: $$T_n = \frac{2l}{\sqrt{gd}} \qquad \text{(A1.14)}$$

in which l is the length of the closed bay or sea.

This formula is in fact the time needed for a wave to travel to and fro once. At both ends the water velocity must be zero, because of the end walls, so an anti-node will occur at the walls. In the middle a node will occur.
It is also possible that more than one node occurs between the two walls, as long as anti-nodes exist at both ends. This is the case for the so called upper harmonics and can be represented as:

$$T_n = \frac{2l}{n\sqrt{gd}} \qquad \text{in which n = 1,2,3,.....} \qquad \text{(A1.15)}$$

In open bays the situation will be different. A node will occur and at the opening and the fundamental node can be represented as:

$$T_n = \frac{4l}{\sqrt{gd}} \qquad \text{or more general with upper harmonics:} \qquad \text{(A1.16)}$$

$$T_n = \frac{4l}{n\sqrt{gd}} \qquad \text{with n = 1,3,5,7.....} \qquad \text{(A1.17)}$$

The fundamental modes and higher harmonics given above are the so called free oscillations. When there is a strong force from outside, the movement will have the period of that force. This is called a forced oscillation. Forced oscillations can be the direct influence of the moon or sun, or a wave coming from the ocean.

An interesting phenomenon occurs when the period of the forced oscillation is equal to one natural period of a system. Then supposing friction is absent or limited, the movements become theoretically infinite. This is called resonance. Fortunately due to friction resonance never becomes infinite, however it can still be spectacular.
Forced oscillation (or excitation) in a closed basin can only come from the moon, sun or wind directly, because no other waves can enter the basin. This is also true for all the oceans.

A1.6.1 Schematic view of the Malacca Strait

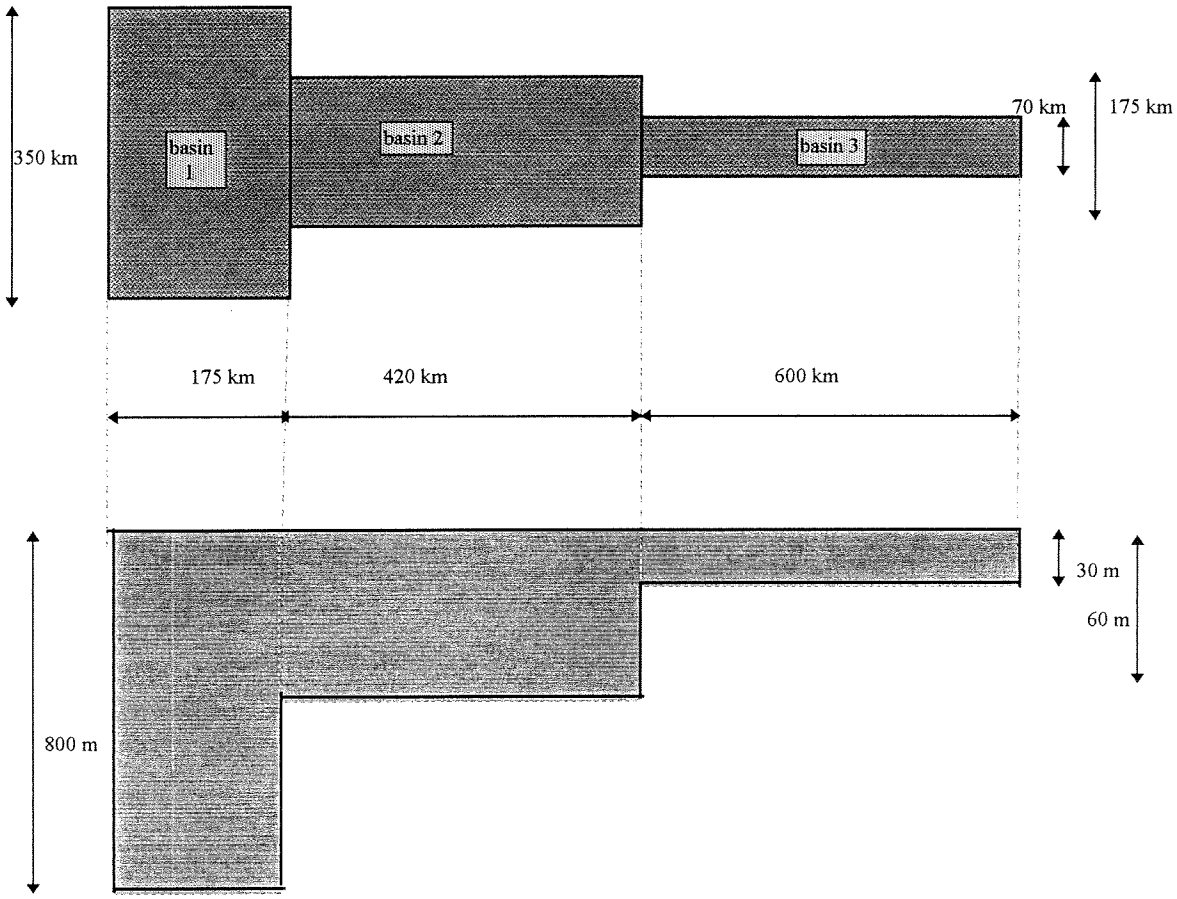

The transition of widths between basin 1 to basin 2 and between basin 2 and basin 3 is not abrupt but smooth. The Strait has roughly a conic form. The transition in depths between different basins are however more or less abrupt. This can also be seen by looking at the maps of Appendix 2 (Figure A2.1 and Figure A2.4).

A1.6.2 Analysis of the tides from observed data

The M_2 tidal wave is widely dominating the area. Because of this the tidal analysis will be restricted to this component.

Given the three basins the following table can be made:

with: $c = \sqrt{g\,h}$ $\Delta t = \frac{l}{c}$ $\Delta\varphi = \frac{\Delta t}{12.42}360$

Table A1.2: calculated phase lags in Malacca Strait

basin no	wave vel. c (m/s)	length, l (km)	time lag, Δt (hrs)	phase lag, Δφ (deg)
1	90	175	~ 0.54	~ 16°
2	25	420	~ 4.67	~ 135°
3	17	600	~ 9.8	~ 280°
total	-	1195	~ 15	~ 431°

After studying the phases of some stations of the M_2 constituent with the help of Table A2.3 and included map with tidal stations (Figure A2.6), Table A1.2 can be justified.

- Basin 1:
  - Starting from a phase of 280°, approximately between stations 31 and 32, and ending at a phase of 300° approximately between stations 29 and 30, a phase lag of 20° can be found. In Table A1.2, a phase lag of 16° is calculated.
- Basin 2:
  - Starting from 300°, at the end of basin 1, and ending at a phase of 156°, approximately the phase figure of station 6, a phase lag of 144° can be found. In Table A1.2 a phase lag of 135° is calculated.
- Basin 3:
  - Starting from a phase of 156°, at the end of basin 2, a phase lag of 265° can be found, if the end of basin 3 is laid at the position of station 21. In Table A1.2, a phase lag of 280° is calculated. The depth in this basin is quite constant so no major fault could have been made in the approximation of the average depth of this basin.

The observed phase lags are also not very far from the roughly calculated phase lags. It can also be seen, that the tides travel from basin 1 to basin 3 because the phases gradually increase starting from basin 1 to the end of basin 3. Oscillation of amplitude seems not to occur in all the three basins, because the fundamental node (see Appendix 1 section A1.5), is not fully enclosed in neither of the basins and the resonance period according to equation (4.2) of neither of the basins equals the wave period. The change in amplitudes are therefore only the result of geometrical changes (shoaling and reflection) and friction.
In basin 1 the amplitudes are about 0.4 m at the begin and are increased to about 0.6 m at the end. This increase is the result of the decrease of the mean depth in basin 1 itself and the change of width with factor 2 between basin 1 and basin 2. The waves increase in amplitude because of shoaling and the geometrical change in width. Starting at the begin of basin 2, there is also an amplitude of approximately 0.6 m and a mean depth of about 60 m, which is about 13 times shallower than basin 1. At the end of the same basin this amplitude is increased up to 1.3 m. This immensely increase is probably the result of change of depth with factor 2.5 between basin 2 and 3 and change of width with factor 2. The waves are pushed

higher as the result of this and the reflected waves in basin 2 probably strengthen the resulting amplitude height as well. At the begin of basin 3, a wave amplitude of 1.4 m is available as well. At the end of this basin the amplitude is decreased to about 0.5 m. This must be the result of friction compared with reflection. The mean depth is shallow: 30 m, and there are the islands of the Riau Archipelago which strengthen the friction effects. Amphidromic points do not occur in whole Malacca Strait. The waves can be regarded to travel mainly in a one way direction. According to Mihardja (1991), the waves in Malacca Strait can be regarded as Kelvin waves.

In the third column of Table A2.4, calculated tide form numbers can be found. Given the geographical spreading of these tide form numbers, the similarity with Figure 2.13: Geographical distribution of tidal types according to Wyrtki, can be discovered.

Appendix 2: Charts and Tidal data

This Appendix contains some specific charts of the study area and tidal data of the Sulu Sea and the Malacca Strait regions. Four tables containing tidal data of the Sulu Sea and the Malacca Strait can be found in this Appendix as well.

- The following charts can be found in this Appendix:

  — Figure A2.1: Coloured bottom profile chart of the study area.
  — Figure A2.2: 'Geography of the study area', topographical chart of the study area.
  — Figure A2.3: Detail chart of the Sulu Sea
  — Figure A2.4: Detail chart of the Malacca Strait
  — Figure A2.5: Chart of the Sulu Sea containing numbered tidal stations
  — Figure A2.6: Chart of the Malacca Strait containing numbered tidal stations

- The following tables are included in this Appendix:

  — Table A2.1: Overview of tidal constituents in the Sulu Sea related to time zone -7 UTM
  — Table A2.4: Overview of calculated tidal data of the Sulu Sea
  — Table A2.4: Overview of tidal constituents in the Malacca Strait related to time zone -7 UTM
  — Table A2.4: Overview of calculated tidal data of the Malacca Strait

Figure A2.1 Depth profile chart of the study area (+ means height, - means depth) Values in meters.

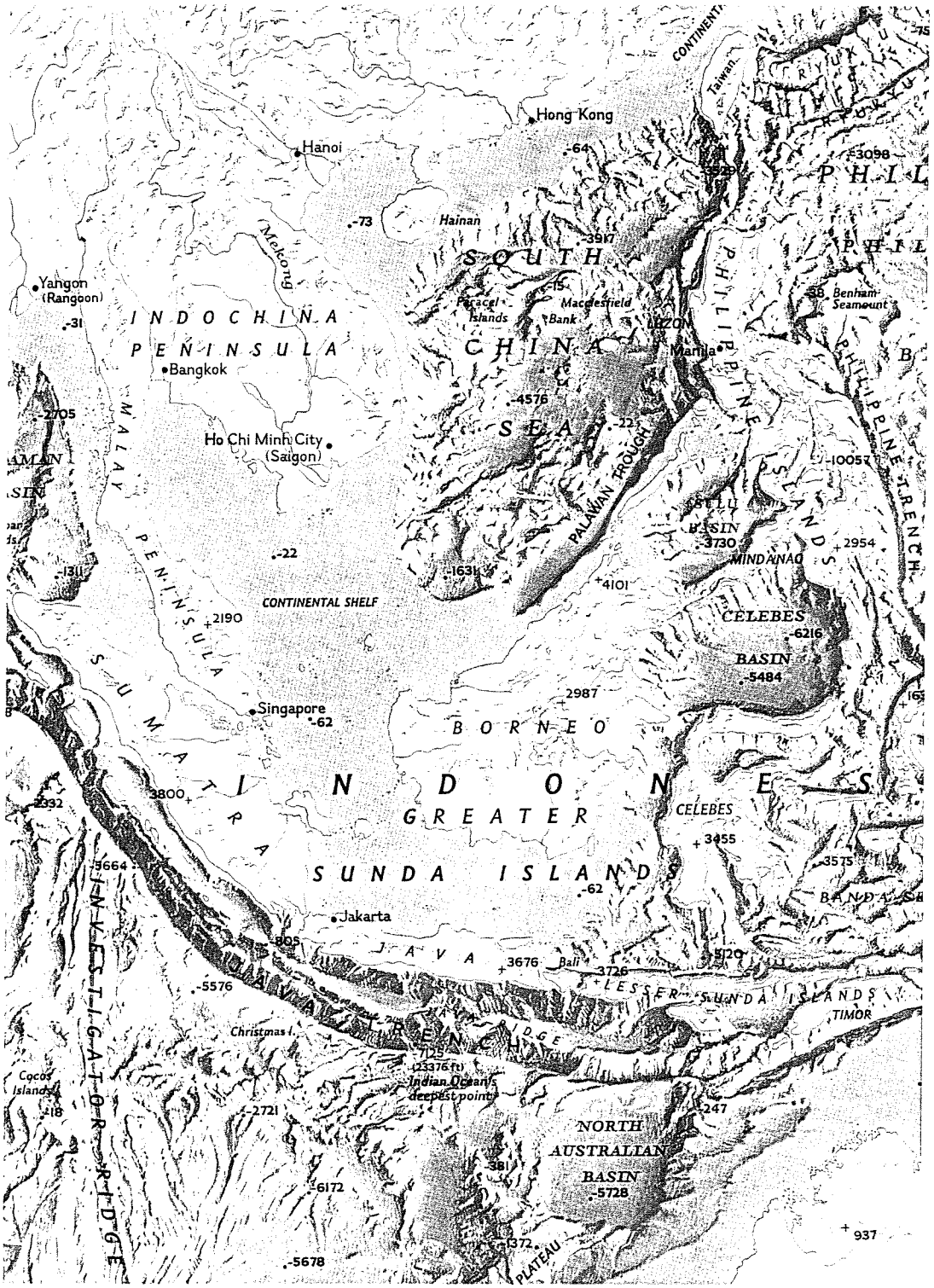

Source: National Geographic Magazine

Figure A2.2 Geography of study area

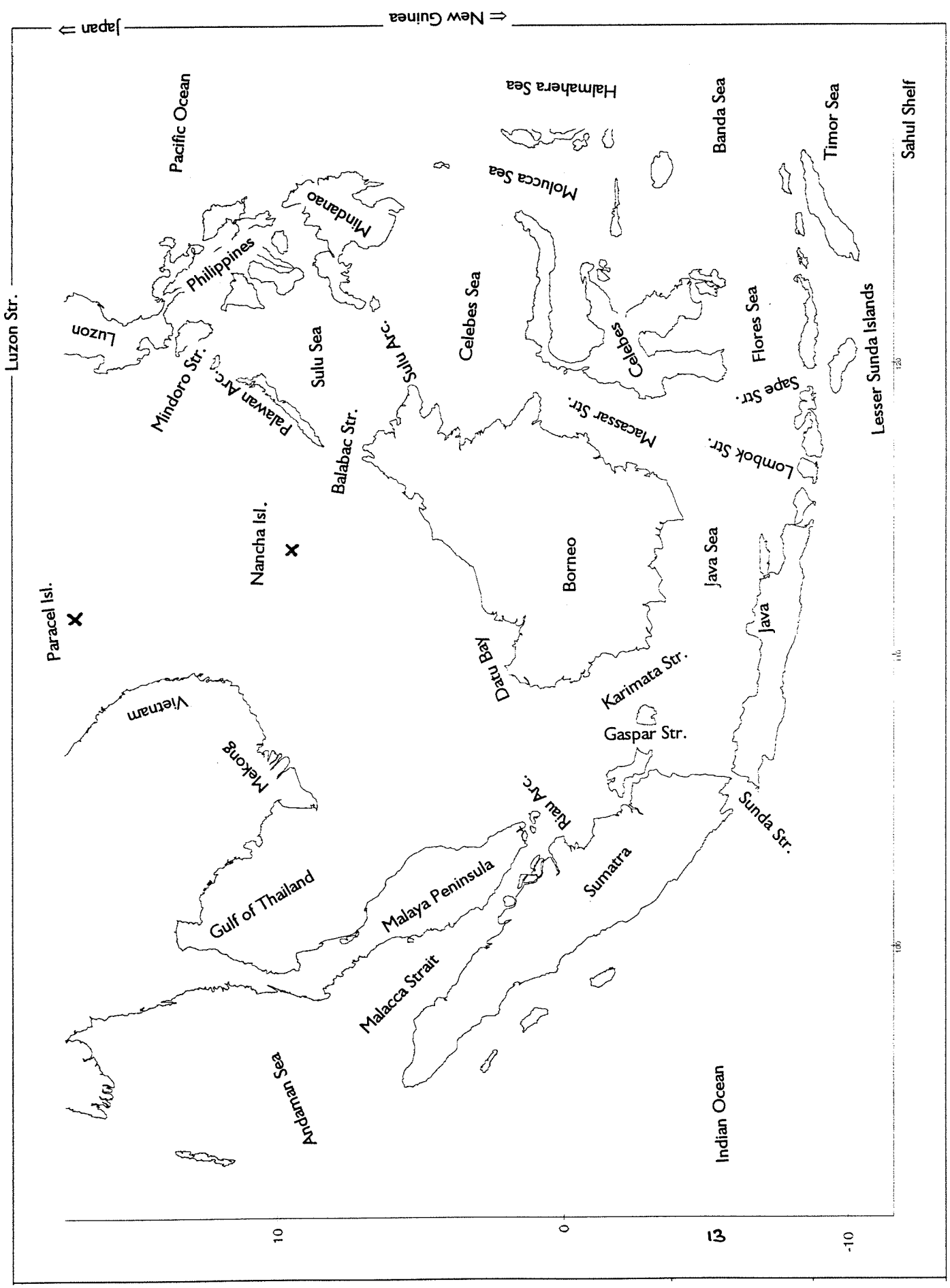

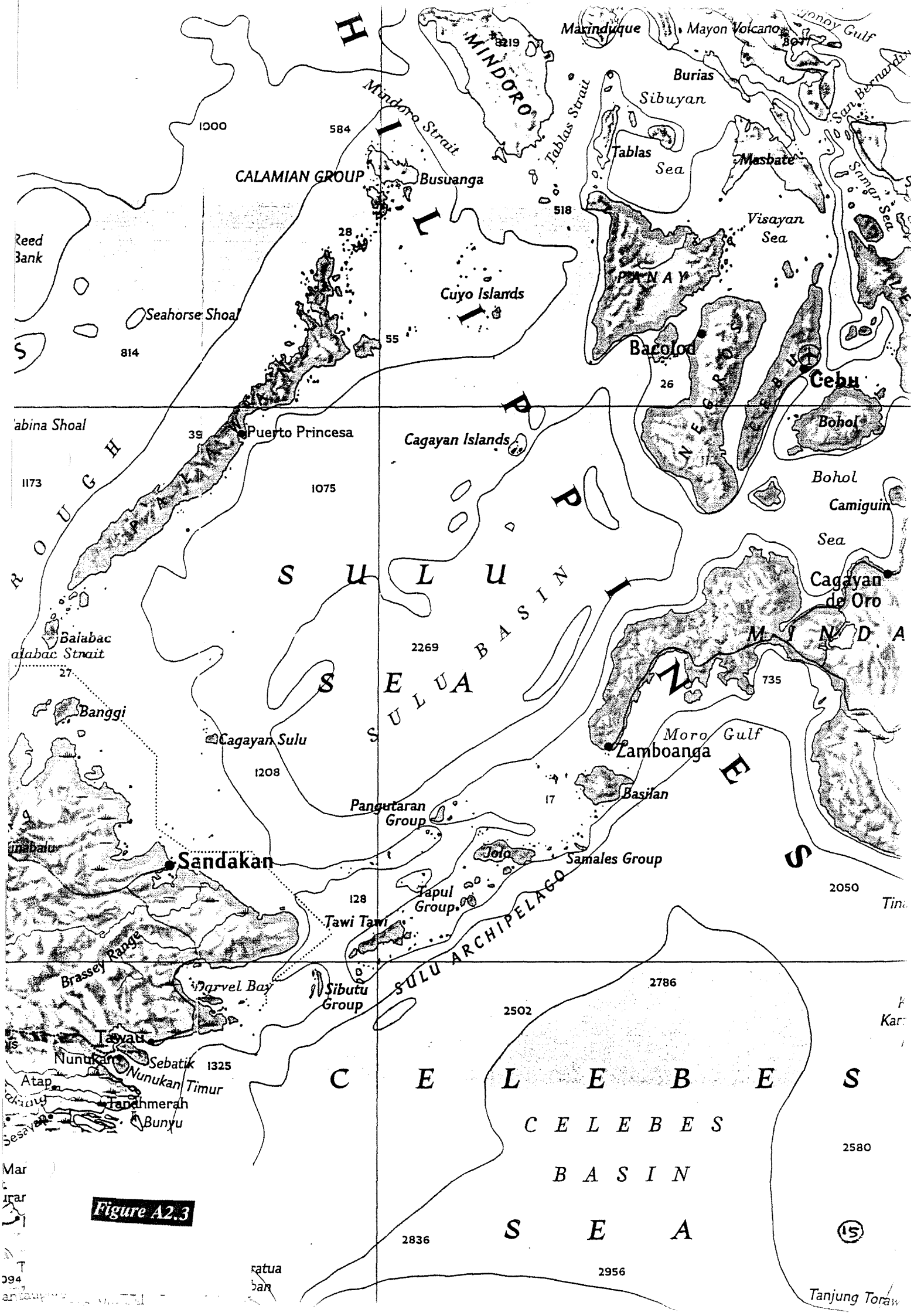

Marinduque
Mayon Volcano
Burias
Sibuyan
Tablas
Sea
Masbate
Visayan
Sea
MINDORO
Mindoro Strait
Tablas Strait
CALAMIAN GROUP
Busuanga
Reed
Bank
Seahorse Shoal
Cuyo Islands
PANAY
Bacolod
Cebu
Bohol
Camiguin
Sea
Cagayan
de Oro
Puerto Princesa
Cagayan Islands
PALAWAN
SULU
SEA
SULU BASIN
Balabac
Banggi
Cagayan Sulu
Moro Gulf
Zamboanga
Basilan
Pangutaran
Group
Jolo
Samales Group
Sandakan
Tapul
Group
Tawi Tawi
SULU ARCHIPELAGO
Brassey Range
Darvel Bay
Sibutu
Group
Tawau
Nunukan
Sebatik
Nunukan Timur
Atap
Tanahmerah
Bunyu
CELEBES
CELEBES
BASIN
SEA
Tanjung Toraw

Figure A2.3

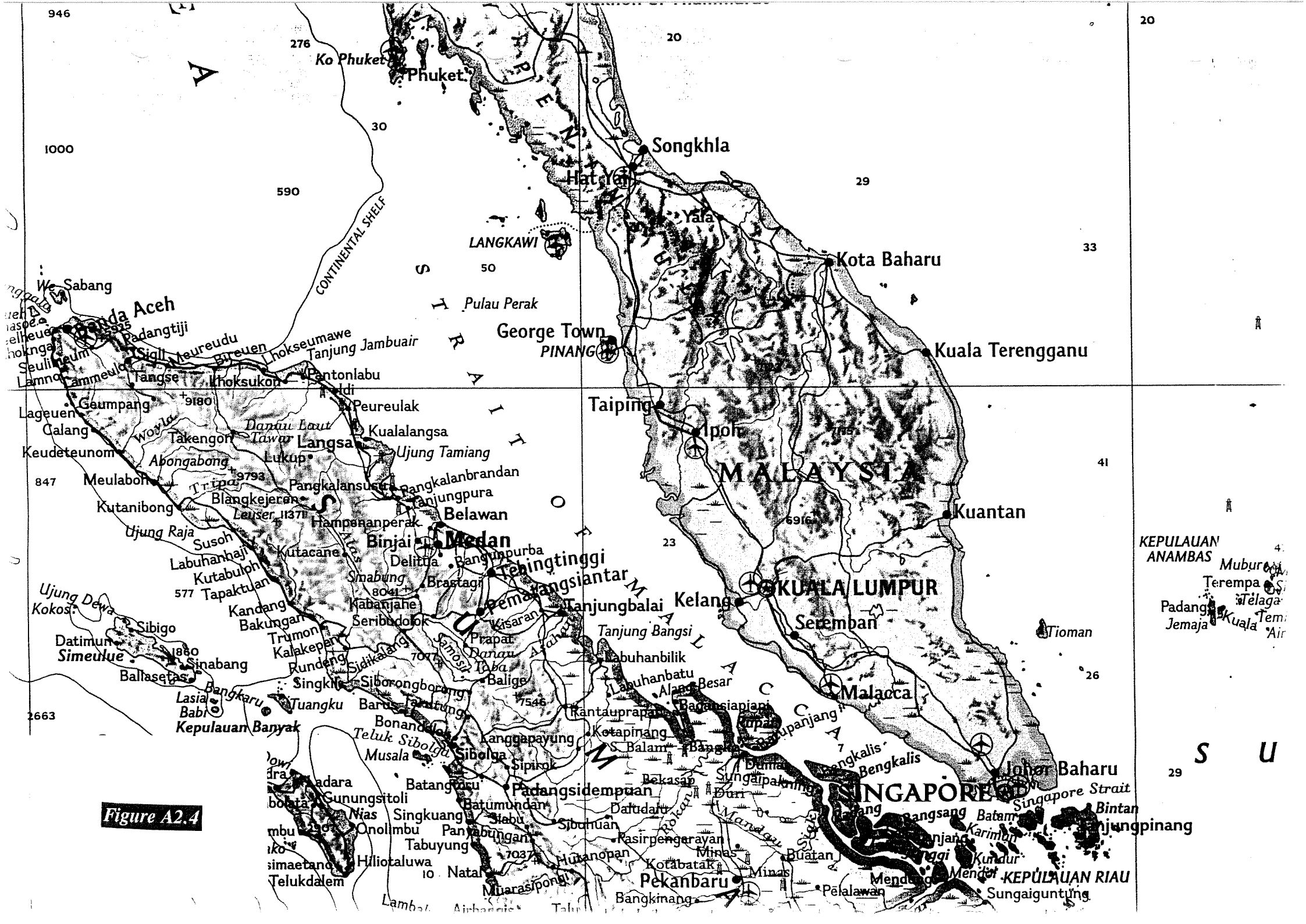

Ko Phuket
Phuket
Songkhla
Hat Yai
Yala
Kota Baharu
LANGKAWI
Pulau Perak
George Town
PINANG
Kuala Terengganu
Taiping
Ipoh
MALAYSIA
Kuantan
KUALA LUMPUR
Kelang
Seremban
Malacca
Johor Baharu
SINGAPORE
Singapore Strait
Bintan
Tanjungpinang
KEPULAUAN RIAU
Sungaiguntung
Pekanbaru
Bangkinang
Kotabatak
Minas
Duri
Bengkalis
Bangsang
Karimun
Kundur
Mendol
Pelalawan
Buatan
Pasirpengarayan
Daludalu
Sibuhuan
Padangsidempuan
Sibolga
Musala
Teluk Sibolga
Singkuang
Batumundan
Tabuyung
Natal
Muarasipongi
Hutanopan
Kotapinang
Rantauprapat
Labuhanbilik
Labuhanbatu
Alang Besar
Bagansiapiapi
Tanjung Bangsi
Tanjungbalai
Pematangsiantar
Tebingtinggi
Belawan
Medan
Binjai
Delitua
Brastagi
Kabanjahe
Seribudolok
Prapat
Danau Toba
Balige
Siborongborong
Tarutung
Barus
Singkil
Sidikalang
Rundeng
Kalakepen
Trumon
Kandang
Bakungan
Tapaktuan
Kutabuloh
Labuhanhaji
Susoh
Ujung Raja
Kutanibong
Meulaboh
Abongabong
Takengon
Danau Laut Tawar
Langsa
Lukup
Ujung Tamiang
Kualalangsa
Peureulak
Idi
Pantonlabu
Lhoksukon
Lhokseumawe
Tanjung Jambuair
Bireuen
Meureudu
Sigli
Padangtiji
Banda Aceh
Lamno
Lammeulo
Tangse
Geumpang
Lageuen
Calang
Keudeteunom
Woyla
Tripa
Blangkejeren
Leuser
Pangkalansusu
Pangkalanbrandan
Tanjungpura
Hampenanperak
Kutacane
Alas
Sinabung
Kabanjahe
Bangunpurba
Tanjung Bangsi
Kisaran
Asahan
Samosir
Sibigo
Datimun
Simeulue
Sinabang
Ballasetas
Lasia
Babi
Bangkaru
Kepulauan Banyak
Tuangku
Ujung Dewa
Kokos
Nias
Onolimbu
Hiliotaluwa
Telukdalem
Gunungsitoli
Ladara
Batangtoru
Tanjung Jambuair
CONTINENTAL SHELF
STRAIT OF MALACCA
KEPULAUAN ANAMBAS
Mubur
Terempa
Telaga
Padang
Jemaja
Kuala
Tioman
Bekasap
Rokan
Mandau
Siak
Dumai
Sungaipakning
Bangkalis
Duri
Batupanjang
Rupat
Bagansiapiapi
Kotapinang
S. Balam
Langgapayung
Sipirok
Batumundan
Siabu
Panyabungan
Hutanopan
Kotabatak
Pekanbaru
Minas
Bangkinang
Pelalawan
Mendol
Kundur
Karimun
Batam
Bintan
Singapore Strait
Sungaipakning
Dumai
Bangkalis
Tanjungpinang
946
276
1000
590
30
20
29
33
50
41
847
577
23
26
2663
10
7

Figure A2.4

Figure A2.5

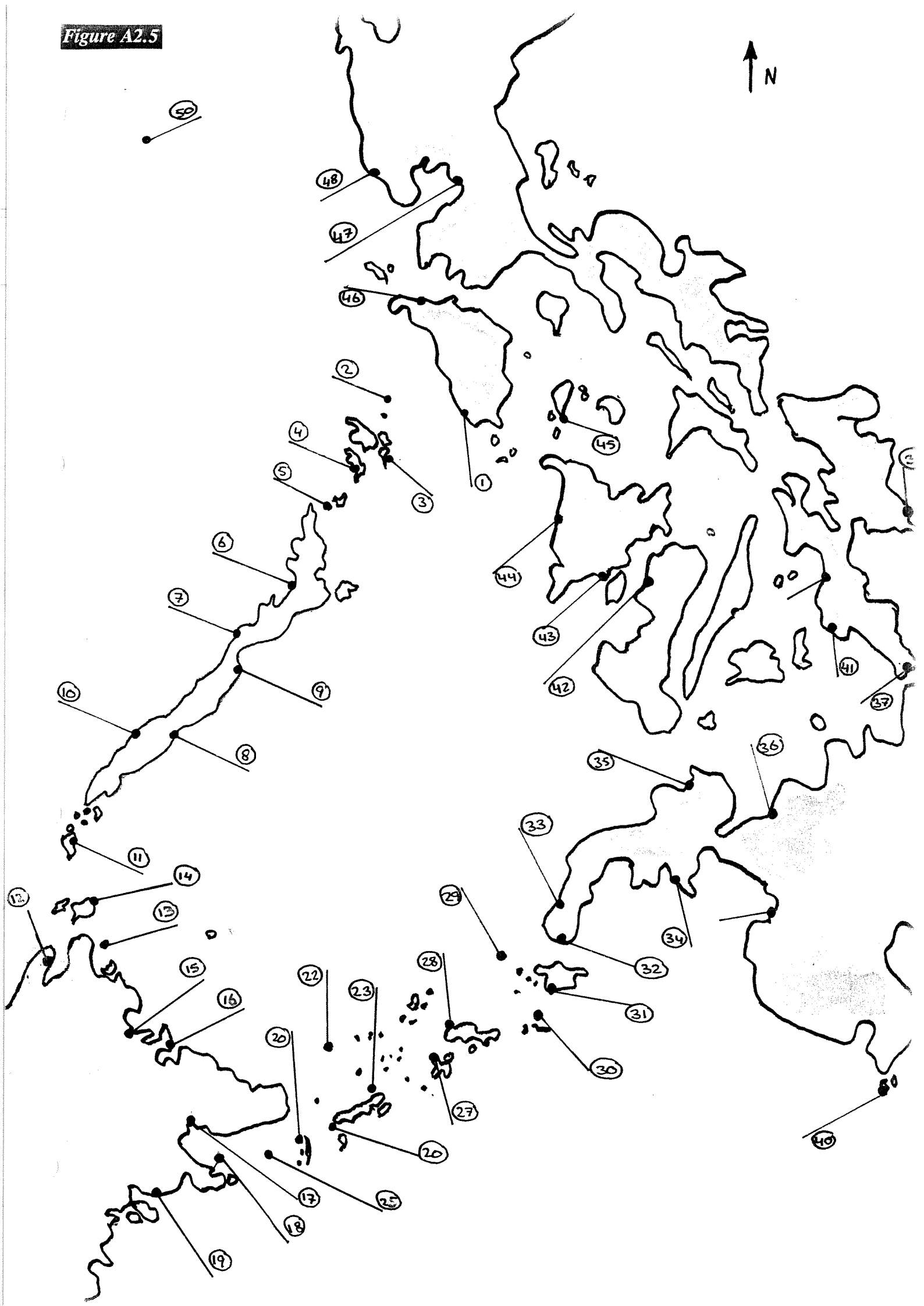
N
50
48
47
46
2
4
5
3
1
45
6
7
44
43
42
41
37
10
9
8
35
36
33
11
14
12
13
29
34
32
15
16
22
23
28
31
20
30
27
20
40
17
25
18
19

Table A2.1

Overview Of tidal Constituents in the Sulu Sea related to time zone -7

			Constituent M2		Constituent S2		Constituent K1		Constituent O1	
no	**Station**	**MSL**	**Ampl**	**Phase**	**Ampl**	**Phase**	**Ampl**	**Phase**	**Ampl**	**Phase**
1	Mangarin	0.55	0.25	272	0.11	310	0.31	305	0.26	257
2	Apo Island	0.5	0.2	269	0.1	308	0.3	301	0.3	254
3	Coron Island	0.7	0.2	274	0.1	313	0.3	302	0.3	254
4	Halsey Harbour	0.52	0.24	274	0.10	-26	0.30	303	0.30	254
5	Linapacan Island	0.6	0.2	274	0.1	310	0.3	303	0.3	254
6	Pankol	0.61	0.23	280	0.07	312	0.33	309	0.29	265
7	Ulugan Bay	0.58	0.20	275	0.08	315	0.33	302	0.28	253
8	Island Bay	0.6	0.3	276	0.2	315	0.3	307	0.3	260
9	Puerta Princesa	0.61	0.29	272	0.16	313	0.34	306	0.30	261
10	Eran Bay	0.6	0.2	281	0.1	320	0.3	305	0.3	256
11	Balabac	0.61	0.25	285	0.13	321	0.32	308	0.30	259
12	Kudat	1.22	0.29	288	0.15	329	0.44	298	0.25	250
13	Pulau Tigabu	1.19	0.33	283	0.18	323	0.37	305	0.31	266
14	Pulau Banggi	1.15	0.29	285	0.13	321	0.34	304	0.31	260
15	Labuk Bay	1.47	0.45	288	0.24	-28	0.35	313	0.35	264
16	Sandakan	1.11	0.42	287	0.23	327	0.35	308	0.32	267
17	Lahad Datu	0.98	0.53	125	0.22	172	0.16	277	0.12	248
18	Kunak	0.99	0.51	123	0.33	181	0.12	289	0.17	245
19	Tawau	1.51	0.76	132	0.43	187	0.19	245	0.22	193
20	Tumindao Island	0.49	0.42	133	0.26	181	0.15	268	0.16	246
21	Port Bongao	0.55	0.43	118	0.27	165	0.18	248	0.16	226
22	Pearl Bank	0.52	0.19	261	0.11	298	0.29	297	0.28	256
23	Basbas Channel	0.27	0.14	181	0.10	219	0.24	285	0.21	252
24	Tandlungan Channel	0.61	0.40	142	0.24	187	0.21	277	0.17	240
25	Gallo Malo Channel	0.85	0.67	136	0.38	182	0.17	248	0.15	214
26	South Ubian Island	0.46	0.32	121	0.19	165	0.18	275	0.16	242
27	Tapul Island	0.37	0.20	147	0.13	198	0.25	295	0.23	252
28	Iolo	0.34	0.17	203	0.10	243	0.25	300	0.24	261
29	Dassalan Island	0.40	0.20	214	0.12	250	0.27	292	0.22	251
30	Bulan Island	0.67	0.53	131	0.30	180	0.16	251	0.13	223
31	Port Holland	0.40	0.25	158	0.15	200	0.19	293	0.19	256
32	Zamboanga	0.43	0.3	146	0.2	188	0.2	288	0.2	254
33	Sibuko Bay	0.6	0.3	266	0.2	188	0.2	288	0.2	254
34	Mangsanubig	0.76	0.62	134	0.37	177	0.14	243	0.12	224
35	Dapitan	0.58	0.3	270	0.2	319	0.3	309	0.3	265
36	Iligan	0.6	0.3	283	0.2	-27	0.3	313	0.3	269
37	Surigao	0.52	0.21	283	0.12	-25	0.26	303	0.27	259
38	Guiuan	0.37	0.26	138	0.06	167	0.12	271	0.14	231
39	Tandag	0.7	0.6	133	0.2	170	0.2	185	0.2	168
40	Balut Island	0.73	0.57	131	0.31	170	0.18	235	0.12	204
41	Maasin	0.7	0.3	280	0.2	-30	0.3	313	0.3	269
42	Bacolod	0.9	0.50	296	0.20	-12	0.30	311	0.30	268
43	Hoilo	0.76	0.41	291	0.20	-17	0.35	309	0.31	269
44	Tibiao	0.8	0.40	275	0.20	324	0.30	306	0.30	263
45	Port Look	0.79	0.38	286	0.18	-27	0.32	307	0.30	262
46	Paluan	0.5	0.20	265	0.10	306	0.30	299	0.30	253
47	Manila	0.48	0.19	266	0.06	303	0.30	305	0.28	254
48	Olongapo	0.43	0.17	255	0.06	303	0.30	305	0.28	254
49	San Fernando	0.37	0.08	235	0.03	253	0.24	297	0,2	253
50	Scarborough Shoal	0.9	0.20	276	0.10	310	0.30	315	0.30	266
51	North Danger Reef	1.1	0.20	269	0.1	317	0,2	290	0.3	243

Table A2.2

no	Station	f	(M2/S2)M2+S2(K1/O1)K1+O1(M2-S2)(K1-O1)					
1	Mangarin	1,58	2,27	0,36	1,19	0,57	-38	48
2	Apo Island	2	2	0,30	1	0,60	-39	47
3	Coron Island	2	2	0,30	1	0,60	-39	48
4	Halsey Harbour	1,76	2,4	0,34	1	0,60	-60	49
5	Linapacan Island	2	2	0,30	1	0,60	-36	49
6	Pankol	2,07	3,29	0,30	1,14	0,62	-32	44
7	Ulugan Bay	2,18	2,50	0,28	1,18	0,61	-40	49
8	Island Bay	1,2	1,5	0,50	1	0,60	-39	47
9	Puerta Princesa	1,42	1,81	0,45	1,13	0,64	-41	45
10	Eran Bay	2	2	0,30	1	0,60	-39	49
11	Balabac	1,63	1,92	0,38	1,07	0,62	-36	49
12	Kudat	1,57	1,93	0,44	1,76	0,69	-41	48
13	Pulau Tigabu	1,33	1,83	0,51	1,19	0,68	-40	39
14	Pulau Banggi	1,55	2,23	0,42	1,1	0,65	-36	44
15	Labuk Bay	1	1,88	0,69	1	0,70	-44	49
16	Sandakan	1	1,83	0,65	1,09	0,67	-40	41
17	Lahad Datu	0,37	2,41	0,75	1,33	0,28	-47	29
18	Kunak	0,35	1,55	0,84	0,71	0,29	-58	44
19	Tawau	0,34	1,77	1,19	0,86	0,41	-55	52
20	Tumindao Island	0,46	1,62	0,68	0,94	0,31	-48	22
21	Port Bongao	0,49	1,59	0,70	1,13	0,34	-47	22
22	Pearl Bank	1,90	1,73	0,30	1	0,57	-37	41
23	Basbas Channel	1,88	1,40	0,24	1,14	0,45	-38	33
24	Tandungan Channel	0,59	1,67	0,64	1,24	0,38	-45	37
25	Cailo Malo Channel	0,30	1,76	1,05	1,13	0,32	-46	34
26	South Ubian Island	0,67	1,68	0,51	1,13	0,34	-44	33
27	Tapul Island	1,45	1,54	0,33	1,09	0,48	-51	43
28	Jolo	1,81	1,70	0,27	1	0,49	-40	39
29	Dassalan Island	1,53	1,67	0,32	1,23	0,49	-36	41
30	Bulan Island	0,35	1,77	0,83	1,23	0,29	-49	28
31	Port Holland	1	1,67	0,40	1	0,38	-42	37
32	Zamboanga	0,8	1,5	0,50	1	0,40	-42	34
33	Sibuko Bay	0,8	1,5	0,50	1	0,40	78	34
34	Margosatubig	0,26	1,68	0,99	1,17	0,26	-43	19
35	Dapitan	1,2	1,5	0,50	1	0,60	-49	44
36	Iligan	1,2	1,5	0,50	1	0,60	-50	44
37	Surigao	1,61	1,75	0,33	1	0,53	-52	44
38	Guiuan	0,81	4,33	0,32	0,86	0,26	-29	40
39	Tandag	0,5	3	0,80	1	0,40	-37	17
40	Balut Island	0,34	1,84	0,88	1,5	0,30	-39	31
41	Maasin	1,2	1,5	0,50	1	0,60	-50	44
42	Bacolod	0,86	2,5	0,70	1	0,60	-52	43
43	Hoilo	1,08	2,05	0,61	1,13	0,66	-52	40
44	Tibiao	1	2	0,60	1	0,60	-49	43
45	Port Look	1,07	1,9	0,58	1,07	0,62	-47	45
46	Paluan	2	2	0,30	1	0,60	-41	46
47	Manila	2,32	3,17	0,25	1,07	0,58	-37	51
48	Olongapo	2,52	2,83	0,23	1,07	0,58	-48	51
49	San Fernando	4	2,67	0,11	1,2	0,44	-18	44
50	Scarborough Shoal	2	2	0,30	1	0,60	-34	49
51	North Danger Reef	1,67	2	0,30	0,67	0,50	-48	47

Figure A2.6

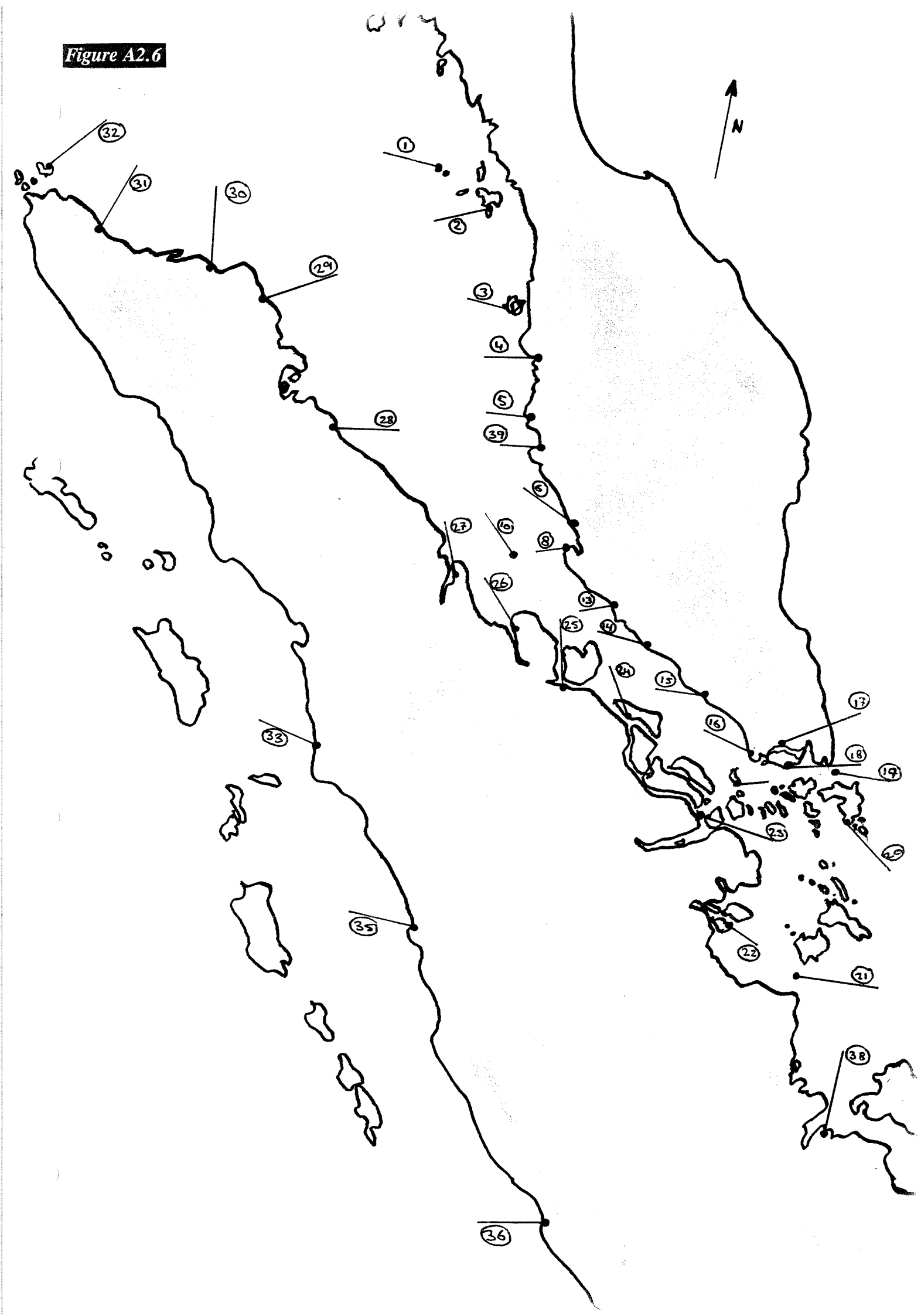
N
1
2
3
4
5
6
8
10
13
14
15
16
17
18
19
20
21
22
23
24
25
26
27
28
29
30
31
32
33
35
36
38
39

Table A2.3

Overview Of tidal Constituents in Malacca Strait related to time zone -7

			Constit M2		Constit S2		Constit K1		Constit O1	
no	Station	zone	Ampl	Phase	Ampl	Phase	Ampl	Phase	Ampl	Phase
1	Ko Butang	-8	0.7	312	0.4	-3	0.1	314	0.06	295
2	Sungai Kedah	-8	0.7	-20	0.4	24	0.2	343	0.1	282
3	Pinang (Georgetown)	-8	0.62	-4	0.37	38	0.2	342	0.05	279
4	Port Weld	-8	0.6	35	0.3	77	0.2	334	0.1	250
5	Lumut Pier	-8	0.74	85	0.35	126	0.22	-7	0.03	260
6	Selangor	-8	1.33	127	0.62	181	0.16	28	0.1	85
7	Pulau Angsa	-8	1.3	118	0.66	172	0.21	20	0.01	321
8	Pelabuhan Klang	-8	1.37	127	0.69	175	0.19	11	0.04	147
9	Pintu Gedong	-8	1.22	136	0.6	185	0.13	20	0.05	186
10	One Fathom Bank	-8	1.25	125	0.62	174	0.17	12	0.05	146
11	Pulau Jernur	-8	1.28	113	0.62	157	0.25	337	0.04	170
12	Tanjung Gabang	-8	1.01	147	0.51	196	0.08	33	0.13	136
13	Port Dickson	-8	0.83	163	0.41	211	0.05	79	0.17	135
14	Melaka	-8	0.6	210	0.28	256	0.06	129	0.21	130
15	Kuala Baru Pahat	-8	0.8	262	0.36	311	0.19	150	0.26	122
16	Kukup	-8	0.92	295	0.43	-12	0.26	147	0.25	105
17	Johor Baharu	-8	0.86	297	0.34	-7	0.3	88	0.3	36
18	Singapore	-8	0.82	298	0.35	-7	0.28	109	0.26	55
19	Horsburg Lighthouse	-8	0.56	278	0.19	-23	0.27	62	0.28	15
20	Tanjungpitnang	-7	0.36	316	0.17	26	0.34	135	0.27	63
21	Pulau Berhala	-7	0.46	61	0.14	127	0.71	153	0.59	69
22	Kuala Nipur	-7	0.78	82	0.19	120	0.67	171	0,48	96
23	Bandong	-7	1.0	321	0.56	25	0.19	166	0.42	96
24	Bengkalis	-7	0.76	213	0.36	286	0.06	123	0.26	128
25	Dumai	-7	0.84	182	0.52	229	0.12	113	0.21	133
26	Bagan Si Api Api	-7	1.7	134	0.9	184	0.18	28	0.04	198
27	Labuan Bilik	-7	1.24	135	0.61	184	0.17	16	~ 0	0.0
28	Belawan Channel	-7	0.61	32	0.32	70	0.21	347	0.04	279
29	Idi	-7	0.47	317	0.25	6	0.14	307	0.06	295
30	Lhokseumawe	-7	0.59	293	0.28	340	0.10	328	0.04	298
31	Sigli	-7	0.34	285	0.24	333	0.09	319	0.04	292
32	Sabang	-7	0.44	275	0.26	322	0.08	314	0.05	282
33	Natal	-7	0.28	178	0.13	220	0.11	281	0.07	253
34	Air Bangis	-7	0.27	165	0.15	227	0.15	274	0.05	244
35	Teluk Bayur	-7	0.24	170	0.15	217	0.11	283	0.06	250
36	Bengkulu	-7	0.32	198	0.14	242	0.11	283	0.10	259
37	Koraagung	-7	0.32	208	0.15	246	0.15	285	0.10	275
38	Sungsang	-7	0.26	191	0.13	233	0.88	156	0.6	86
39	Bagan Datoh	-8	0.79	96	0.39	143	0.21	359	0.03	280
40	Tanjungbalai	-7	0.78	300	0.43	353	0.27	145	0.2	99
41	Pelabuhan Bass	-8	0.73	332	0.41	16	0.18	341	0.05	281

Table A2.4

no	Station	f	(M2/S2	(M2+S	(K1/O	(K1+O	(M2-S2	(K1-O1)
1	Ko Butang	0,15	1,75	1,10	1,67	0,16	314	20
2	Sungai Kedah	0,27	1,75	1,10	2	0,30	-45	62
3	Pinang (Georgetown)	0,25	1,68	0,99	4	0,25	-43	64
4	Port Weld	0,33	2	0,90	2	0,30	-43	85
5	Lumut Pier	0,23	2,11	1,09	7,33	0,25	-42	-266
6	Selangor	0,13	2,15	1,95	1,60	0,26	-55	-56
7	Pulau Angsa	0,11	1,97	1,96	21	0,22	-55	-300
8	Pelabuhan Klang	0,11	1,99	2,06	4,75	0,23	-49	-135
9	Pintu Gedong	0,10	2,03	1,82	2,60	0,18	-50	-165
10	One Fathom Bank	0,12	2,02	1,87	3,40	0,22	-50	-133
11	Pulau Jernur	0,15	2,06	1,90	6,25	0,29	-45	168
12	Tanjung Gabang	0,14	1,98	1,52	0,62	0,21	-50	-102
13	Port Dickson	0,18	2,02	1,24	0,29	0,22	-49	-55
14	Melaka	0,31	2,14	0,88	0,29	0,27	-47	0
15	Kuala Batu Pahat	0,39	2,22	1,16	0,73	0,45	-50	29
16	Kukup	0,38	2,14	1,35	1,04	0,51	306	43
17	Johor Baharu	0,50	2,53	1,20	1	0,60	303	53
18	Singapore	0,46	2,34	1,17	1,08	0,54	304	55
19	Horsburg Lighthouse	0,73	2,95	0,75	0,96	0,55	300	48
20	Tanjungpinang	1,15	2,12	0,53	1,26	0,61	290	72
21	Pulau Berhala	2,17	3,29	0,60	1,20	1,30	-66	84
22	Kuala Nitur	1,19	4,11	0,97	1,40	1,15	-38	75
23	Bandong	0,39	1,79	1,56	0,45	0,61	296	70
24	Bengkalis	0,29	2,11	1,12	0,23	0,32	-73	-5
25	Dumai	0,24	1,62	1,36	0,57	0,33	-47	-20
26	Bagan Si Api Api	0,08	1,89	2,60	4,5	0,22	-50	-170
27	Labuan Bilik	0,09	2,03	1,85	170	0,17	-49	16
28	Belawan Channel	0,27	1,91	0,93	5,25	0,25	-38	68
29	Idi	0,28	1,88	0,72	2,33	0,20	311	12
30	Lhokseumawe	0,16	2,11	0,87	2,5	0,14	-47	30
31	Sigli	0,22	1,42	0,58	2,25	0,13	-48	27
32	Sabang	0,19	1,69	0,70	1,6	0,13	-47	32
33	Natal	0,44	2,15	0,41	1,57	0,18	-42	28
34	Air Bangis	0,48	1,8	0,42	3	0,20	-62	30
35	Teluk Bayur	0,44	1,6	0,39	1,83	0,17	-47	33
36	Bengkulu	0,46	2,29	0,46	1,1	0,21	-44	24
37	Kotaagung	0,53	2,13	0,47	1,5	0,25	-38	10
38	Sungsang	3,79	2	0,39	1,47	1,48	-42	70
39	Bagan Datoh	0,2	2,03	1,18	7	0,24	-48	-280
40	Tanjungbalai	0,39	1,81	1,21	1,35	0,47	-53	46
41	Pelabuhan Bass	0,2	1,78	1,14	3,6	0,23	-45	61

Appendix 3: The 1-dimensional approach

This Appendix contains the generation of the 1-D model based on harmonic analysis and a print output of one of the programmed files. Thereafter there are figures containing the results of the 1-D TRISULA test case, discussed in section 4.4. Finally the Appendix further includes some results (isoline plots and overview plots) of the programmed model and the test results of the programmed files.

Summarised this Appendix contains

A3.1 The generation of the model
A3.2 Testing the validity and reliability of the model
A3.3 Print output of one of the programmed files

— Figure A3.1 up to Figure A3.5 results of the TRISULA 1-D test model
— Figure A3.6 up to Figure A3.27 isoline plot results of the self constructed 1-D model
— Figure A3.28 up to Figure A3.41 overview plots of water levels along the length axis of basin combinations of the constructed 1-D model
— Figure A3.41, Figure A3.42, Figure A3.43 test results of the constructed model

A3.1 Construction of a 1-D model based on harmonic analysis

A3.1.1 General equations

The equations for continuity and momentum used in this model study, are of the most simple form possible. This means that the equations are 1-dimensional, the momentum equation is taken without advection, external forces like wind forces, friction and so on. Neglecting the friction is justified by the assumption that the depths are all large enough to suggest that friction will not or very little change the obtained solutions. The tidal movement can then be described with the following set of differential equations (van Rijn, 1990):

- *momentum equation:*
$$\frac{\partial u}{\partial t} + g\frac{\partial \varsigma}{\partial x} = 0 \qquad \text{(A3.1)}$$

- *continuity equation:*
$$\frac{\partial \varsigma}{\partial t} + H\frac{\partial u}{\partial x} = 0 \qquad \text{(A3.2)}$$

Taking the depth H as a constant, it can be seen that these equations are simplified forms of equations (A1.12) and (A1.13) of Appendix 1. In fact H is actually equal to the mean depth summed with water elevation (so H=h+ς), but the assumption that water elevation is much less regarded to the depth (so $\varsigma << h$) permits this simplification. The equations (A3.1) and (A3.2) can now be written alternatively as follows:

- *momentum equation:*
$$\frac{\partial u}{\partial t} + \sqrt{gH}\frac{\partial}{\partial x}\sqrt{\frac{g}{H}}\varsigma = 0 \qquad \text{(A3.3)}$$

- *continuity equation*:
$$\frac{\partial}{\partial t}\sqrt{\frac{g}{H}}\varsigma + \sqrt{gH}\frac{\partial u}{\partial x} = 0 \qquad \text{(A3.4)}$$

The tidal wave in this case is in fact a summation of two separate waves, moving in opposite directions. This wave combination can be described with the so called Riemann invariants [(Stelling&Booij, 1993), (Verspuy, 1987)] with two velocities in opposite directions:

$$u^*_{1,2} = u \pm \sqrt{\frac{g}{H}}\varsigma \qquad \text{(A3.5)}$$

Substitution of (A3.5) in equations (A3.3) and (A3.4) gives:

$$\frac{\partial}{\partial t}\left(u + \sqrt{\frac{g}{H}}\varsigma\right) + \sqrt{gH}\frac{\partial}{\partial x}\left(u + \sqrt{\frac{g}{H}}\varsigma\right) = 0 \qquad \text{(A3.6)}$$

$$\frac{\partial}{\partial t}\left(u - \sqrt{\frac{g}{H}}\varsigma\right) - \sqrt{gH}\frac{\partial}{\partial x}\left(u - \sqrt{\frac{g}{H}}\varsigma\right) = 0 \qquad \text{(A3.7)}$$

From the equations (A3.6) and (A3.7), two analytical solutions can be found. In these φ and ψ are the non-zero phases of the waves.

$$u + \sqrt{\frac{g}{H}}\varsigma = A\cos\left[\omega\left(t - \frac{1}{\sqrt{gH}}x\right) + \varphi\right] \qquad \text{(A3.8)}$$

$$u - \sqrt{\frac{g}{H}}\varsigma = B\cos[\omega(t + \frac{1}{\sqrt{gH}}x) + \psi] \qquad \text{(A3.9)}$$

From these two solution equations (A3.8) and (A3.9), after some algebra (and control of the rightness of it with the mass and momentum differential equations), the velocity and water elevation for a monochromatic wave can be found:

$$u(x,t) = A\cos[\omega(t - \frac{1}{\sqrt{gH}}x) + \varphi] + B\cos[\omega(t + \frac{1}{\sqrt{gH}}x) + \psi] \qquad \text{(A3.10)}$$

$$\varsigma(x,t) = A\sqrt{\frac{H}{g}}\cos[\omega(t - \frac{1}{\sqrt{gH}}x) + \varphi] - B\sqrt{\frac{H}{g}}\cos[\omega(t + \frac{1}{\sqrt{gH}}x) + \psi] \qquad \text{(A3.11)}$$

Note that A and B are the coefficients determining the amplitudes of the two waves and which are a unique set of coefficients only depending of the dimensions of a basin and the boundary conditions (so B is not the width!). (A3.10) and (A3.11) reveal a sinusoidal function of water velocity and elevation. They are the result of two separate, but in opposite direction moving waves, each with its own amplitude and phase.

With some algebra, different sets of (A3.10) and (A3.11) can be achieved:

(A3.12) and (A3.13)

$$\begin{aligned}\varsigma(x,t) = {} & A\sqrt{\frac{H}{g}}\cos(\omega t)\cos[\omega(\frac{1}{\sqrt{gH}}x)]\cos(\varphi) + A\sqrt{\frac{H}{g}}\cos(\omega t)\sin[\omega(\frac{1}{\sqrt{gH}}x)]\sin(\varphi) + \\ & A\sqrt{\frac{H}{g}}\sin(\omega t)\sin[\omega(\frac{1}{\sqrt{gH}}x)]\cos(\varphi) - A\sqrt{\frac{H}{g}}\sin(\omega t)\cos[\omega(\frac{1}{\sqrt{gH}}x)]\sin(\varphi) - \\ & B\sqrt{\frac{H}{g}}\cos(\omega t)\cos[\omega(\frac{1}{\sqrt{gH}}x)]\cos(\psi) + B\sqrt{\frac{H}{g}}\cos(\omega t)\sin[\omega(\frac{1}{\sqrt{gH}}x)]\sin(\psi) + \\ & B\sqrt{\frac{H}{g}}\sin(\omega t)\sin[\omega(\frac{1}{\sqrt{gH}}x)]\cos(\psi) + B\sqrt{\frac{H}{g}}\sin(\omega t)\cos[\omega(\frac{1}{\sqrt{gH}}x)]\sin(\psi)\end{aligned}$$

$$\begin{aligned}u(x,t) = {} & A\cos(\omega t)\cos[\omega(\frac{1}{\sqrt{gH}}x)]\cos(\varphi) + A\cos(\omega t)\sin[\omega(\frac{1}{\sqrt{gH}}x)]\sin(\varphi) + \\ & A\sin(\omega t)\sin[\omega(\frac{1}{\sqrt{gH}}x)]\cos(\varphi) - A\sin(\omega t)\cos[\omega(\frac{1}{\sqrt{gH}}x)]\sin(\varphi) + \\ & B\cos(\omega t)\cos[\omega(\frac{1}{\sqrt{gH}}x)]\cos(\psi) - B\cos(\omega t)\sin[\omega(\frac{1}{\sqrt{gH}}x)]\sin(\psi) - \\ & B\sin(\omega t)\sin[\omega(\frac{1}{\sqrt{gH}}x)]\cos(\psi) - B\sin(\omega t)\cos[\omega(\frac{1}{\sqrt{gH}}x)]\sin(\psi)\end{aligned}$$

(5.12) and (5.13) on their turn can further be rewritten as follows:

(A3.14) and (A3.15)

$$\zeta(x,t) = \cos(\omega\ t)\left[\begin{array}{l} A\left[\sqrt{\frac{H}{g}}\cos[\omega(\frac{1}{\sqrt{gH}}x)]\cos(\varphi)+\sqrt{\frac{H}{g}}\sin[\omega(\frac{1}{\sqrt{gH}}x)]\sin(\varphi)\right]+ \\ B\left[-\sqrt{\frac{H}{g}}\cos[\omega(\frac{1}{\sqrt{gH}}x)]\cos(\psi)+\sqrt{\frac{H}{g}}\sin[\omega(\frac{1}{\sqrt{gH}}x)]\sin(\psi)\right] \end{array}\right]$$

$$+\sin(\omega\ t)\left[\begin{array}{l} \left[A\left[-\sqrt{\frac{H}{g}}\cos[\omega(\frac{1}{\sqrt{gH}}x)]\sin(\varphi)+\sqrt{\frac{H}{g}}\sin[\omega(\frac{1}{\sqrt{gH}}x)\cos(\varphi)\right]+ \right. \\ \left. B\left[\sqrt{\frac{H}{g}}\cos[\omega(\frac{1}{\sqrt{gH}}x)]\sin(\psi)+\sqrt{\frac{H}{g}}\sin[\omega(\frac{1}{\sqrt{gH}}x)]\cos(\psi)\right]\right] \end{array}\right]$$

and

$$u(x,t) = \cos(\omega\ t)\left[\begin{array}{l} A\left[\cos[\omega(\frac{1}{\sqrt{gH}}x)]\cos(\varphi)+\sin[\omega(\frac{1}{\sqrt{gH}}x)]\sin(\varphi)\right]+ \\ B\left[\cos[\omega(\frac{1}{\sqrt{gH}}x)]\cos(\psi)-\sin[\omega(\frac{1}{\sqrt{gH}}x)]\sin(\psi)\right] \end{array}\right]$$

$$+\sin(\omega\ t)\left[\begin{array}{l} A\left[-\cos[\omega(\frac{1}{\sqrt{gH}}x)]\sin(\varphi)+\sin[\omega(\frac{1}{\sqrt{gH}}x)]\cos(\varphi)\right]+ \\ B\left[-\cos[\omega(\frac{1}{\sqrt{gH}}x)]\sin(\psi)-\sin[\omega(\frac{1}{\sqrt{gH}}x)]\cos(\psi)\right] \end{array}\right]$$

The equations of water elevation and velocity given above ((A3.14) and (A3.15))can specifically be solved in one basin with constant dimensions of depth, length and width.
When a system of four basins is considered, these formulas can still be used, but attention must be paid on the changing dimensions and x-axis positions (only 1-D movement is considered) of the basins.
In this case the equations of water elevation and velocities must be indicated with basin indices. Moreover other rewritten variables have to be introduced:

(A3.16) and (A3.17)

$$\zeta(x,t) = \cos(\omega\ t)[\alpha_j^i(x)A^i\cos(\varphi^i)+\beta_j^i(x)A^i\sin(\varphi^i)-\alpha_j^i(x)B^i\cos(\psi^i)+\beta_j^i(x)B^i\sin(\psi^i)]+$$
$$\sin(\omega\ t)[\beta_j^i(x)A^i\cos(\varphi^i)-\alpha_j^i(x)A^i\sin(\varphi^i)+\beta_j^i(x)B^i\cos(\psi^i)+\alpha_j^i(x)B^i\sin(\psi^i)]]$$

$$u(x,t) = \cos(\omega\ t)[\gamma_j^i(x)A^i\cos(\varphi^i)+\varepsilon_j^i(x)A^i\sin(\varphi^i)+\gamma_j^i(x)B^i\cos(\psi^i)-\varepsilon_j^i(x)B^i\sin(\psi^i)]+$$
$$\sin(\omega\ t)[\varepsilon_j^i(x)A^i\cos(\varphi^i)-\gamma_j^i(x)A^i\sin(\varphi^i)-\varepsilon_j^i(x)B^i\cos(\psi^i)-\gamma_j^i(x)B^i\sin(\psi^i)]]$$

in which:

$$\alpha_j^i(x) = \sqrt{\frac{H^i}{g}} \cos[\omega(\frac{1}{\sqrt{gH^i}} x)] \qquad \beta_j^i(x) = \sqrt{\frac{H^i}{g}} \sin[\omega(\frac{1}{\sqrt{gH^i}} x)]$$

$$\gamma_{ij}(x) = \cos[\omega(\frac{1}{\sqrt{gH^i}} x)] \qquad \varepsilon_j^i(x) = \sin[\omega(\frac{1}{\sqrt{gH^i}} x)]$$

To simplify the equations (A3.16) and (A3.17), the following set of variables are introduced:

$$A^i \cos(\varphi) = P^i \qquad B^i \cos(\psi) = R^i$$
$$A^i \sin(\varphi) = Q^i \qquad B^i \sin(\psi) = S^i$$

i and *j* are indices of basin number and position within the basin respectively. From left to right as it is presented in the drawing on page 4–14:

i= 1 to 4 (in case of four basins)
j= 1 or 2 to indicating the left or right side of one basin

So finally there is the following set of equations for water elevation and velocity:

$$\zeta(x,t) = \cos(\omega t)\left[\alpha_j^i(x)P^i + \beta_j^i(x)Q^i - \alpha_j^i(x)R^i + \beta_j^i(x)S^i\right] + \sin(\omega t)\left[\beta_j^i(x)P^i - \alpha_j^i(x)Q^i + \beta_j^i(x)R^i + \alpha_j^i(x)S^i\right]$$

$$u(x,t) = \cos(\omega t)\left[\gamma_j^i(x)P^i + \varepsilon_j^i(x)Q^i + \gamma_j^i(x)R^i - \varepsilon_j^i(x)R^i\right] + \sin(\omega t)\left[\varepsilon_j^i(x)P^i - \gamma_j^i(x)Q^i - \varepsilon_j^i(x)R^i - \gamma_j^i(x)S^i\right]$$

(A3.18) and (A3.19)

By writing out the boundary and transition relations of all the basins with their correct terms, the whole system can be drawn up by a matrix. This will be dealt with in the next sections.

A3.1.2 Setting up of the model

At the starting point of basin 1 and at the end of basin 4, two boundary formulations are given in the form of water elevations:

$$\text{WAVE 1:} \quad \varsigma_1^1 = |a_1|\cos[\omega t + \theta_1] = |a_1|\cos(\theta_1)\cos(\omega t) - |a_1|\sin(\theta_1)(\sin\omega t)$$
$$\text{WAVE2} \quad \varsigma_2^4 = |a_4|\cos[\omega t + \theta_4] = |a_4|\cos(\theta_4)\cos(\omega t) - |a_4|\sin(\theta_4)(\sin\omega t)$$

in which |a| is the amplitude, θ_1 and θ_4 are the resulting phases at the edges and ω is the frequency of the waves which is the same for all positions because only one tidal component (M_2) is dealt with.
The system of equations dealt with in these sections, can be solved analytically, for instance with the double sweep method (Stelling&Booij, 1993). However when lots of basins are involved and the basins differ in their dimensions, the system of equations can get quite complex to solve by hand. As it will be discussed in detail in the next paragraphs, the present four-basin system model is therefore simulated by a computer program.
Before presenting and discussing the results of the computations of self built model(s), a brief summary of the program structure in steps will be given below. After that some examples of the equations transformed into matrices will be given.

The program[10] in steps:

- Give the dimensions (length l, width b and depth h) of each basin
- Compute the wave length (L), wave number (k) and wave velocity (c) of each basin according to its dimensions (length l, width b and depth h) and given the specific wave period (ω).
- Compute the basin constants (α,β,γ and ε of equations (A3.16) and (A3.17)) of each basin at each side.
- Create the harmonic relation matrix [M], containing the transition relations of momentum and continuity and the boundary relations at the edges. This matrix consists of the basin constants of step 3, in correct order for cos(ωt) and the sin(ωt) terms in changing row orders.
- Create the boundary relations vector, (which is called vector [s] in this case) containing the boundary relations of water elevation at the begin and the end of the system. The middle terms are equal to zero because in matrix [M], the subtracted form of the transition relations is dealt with.
- Given the matrix and vector of steps 5 and 6 the basin coefficients vector containing the basin coefficients P, Q, R and S of each basin can be calculated. This vector is called vector [c]. $[c] = [M]\cdot[s]$
- Create a new matrix, called [Z], containing again the relevant basin constants of step 4 in correct order, in order to compute the water elevations at the frontier points of the basins by multiplication with vector [c].
- Now the water elevation of chosen the stations can be calculated. The solution matrix that was searched for is called matrix [Y] and it is the result of the multiplication of the matrices [Z] and [c]. $[Y] = [Z]\cdot[c]$

A3.1.3 Boundary and transition conditions

Boundary conditions:

At both edges of the system (z_0 and z_8 see drawing on page 4–14), it follows from the boundary water elevations:

$$\text{WAVE 1: } x=0:\ \zeta(0,t) = |a_1|cos(\omega t+\theta_1) \qquad \text{(A3.20)}$$
$$= cos(\omega t)\ |a_1|cos(\theta_1) - sin(\omega t)|a_1|sin(\theta_1)$$
$$\text{WAVE 2: } x=L_t:\ \zeta(L_t,t) = |a_4|cos(\omega t+\theta_4) \qquad \text{(A3.21)}$$
$$= cos(\omega t)|a_4|cos(\theta_4) - sin(\omega t)|a_4|sin(\theta_4)$$

with the total length equalling $L_t=(l_1+l_2+l_3+l_4)$ this leads to:

At **basin 1**, x=0 and WAVE 1 is valid. The basin constants are therefore:

$$\text{because } \alpha_1^1 = 1 \quad \beta_1^1 = 0 \quad \gamma_1^1 = 1 \quad \beta_1^1 = 0 \quad \varepsilon_1^1 = 0:$$
$$\zeta(0,t) = \cos(\omega t)\left[A^1\cos(\varphi^1) - B^1\cos(\psi^1)\right] + \sin(\omega t)\left[-A^1\cos(\varphi^1) + B^1\cos(\psi^1)\right] \qquad \text{(A3.22)}$$
$$\zeta_1^1 = \cos(\omega t)\left[P_1^1 - R_1^1\right] + \sin(\omega t)\left[-P_1^1 + R_1^1\right]$$

After substitution of the boundary levels, the following set of formulations can finally be achieved:

[10] *an output of one of the programs is given in at the end of this Appendix*

$$|a_1|\cos(\theta_1) = \left[P^1 - R^1\right]$$
$$-|a_1|\sin(\theta_1) = \left[-P^1 + R^1\right]$$

At **basin 4** $x=L_t$ and WAVE 2 is valid. The basin constants after application of equation (5.16) are therefore:

$$\zeta(L,t) = \cos(\omega\ t)\left[\alpha_2^4 A^4\cos(\varphi^4)+\beta_2^4 A^4\sin(\varphi^4)-\alpha_2^4 B^4\cos(\psi^4)+\beta_2^4 B^4\sin(\psi^4)\right]+ \sin(\omega\ t)\left[\beta_2^4 A^4\cos(\varphi^4)-\alpha_2^4 A^4\sin(\varphi^4)+\beta_2^4 B^4\cos(\psi^4)+\alpha_2^4 B^4\sin(\psi^4)\right] \quad \text{(A3.23)}$$

$$\zeta_2^4 = \cos(\omega\ t)\left[\alpha_2^4 P^4+\beta_2^4 Q^4-\alpha_2^4 R^4+\beta_2^4 S^4\right]+ \sin(\omega\ t)\left[\beta_2^4 P^4-\alpha_2^4 Q^4+\beta_2^4 R^4+\alpha_2^4 S^4\right]$$

After substitution of the boundary levels, the following set of formulations can finally be achieved:

$$|a_4|\cos(\theta_4) = \left[\alpha_2^4 P^4+\beta_2^4 Q^4-\alpha_2^4 R^4+\beta_2^4 S^4\right]$$
$$-|a_4|\sin(\theta_4) = \left[\beta_2^4 P^4-\alpha_2^4 Q^4+\beta_2^4 R^4+\alpha_2^4 S^4\right]$$

Transition Conditions:

At the joint boundary of two basins, for instance at the end of basin 1 and the beginning of basin 2, two transition conditions are valid:
because of continuity of momentum, the water elevations are equal on both sides:

$$\zeta_2^1 = \zeta_1^2 \qquad \text{or} \qquad \zeta_2^1 - \zeta_1^2 = 0 \quad \text{(A3.24)}$$

this implies:

cos(ω t) part: $\alpha_2^1 P^1+\beta_2^1 Q^1-\alpha_2^1 R^1+\beta_2^1 S^1-\alpha_1^2 P^2-\beta_1^2 Q^2+\alpha_1^2 R^2-\beta_1^2 S^2 = 0$

sin(ω t) part: $\beta_2^1 P^1-\alpha_2^1 Q^1+\beta_2^1 R^1+\alpha_2^1 S^1-\beta_1^2 P^2+\alpha_1^2 Q^2-\beta_1^2 R^2-\alpha_1^2 S^2 = 0$

because of mass balance, the water discharge is constant between separate basins:

$b^1h^1u^1{}_2 = b^2h^2u_2{}^1$ or $b^1h^1u^1{}_2 - b^2h^2u_2{}^1=0$ (A3.25)

this implies:

cos(ω t) part: $b^1h^1\gamma_2^1 P^1+b^1h^1\varepsilon_2^1 Q^1+b^1h^1\gamma_2^1 R^1-b^1h^1\varepsilon_2^1 S^1- b^2h^2\gamma_1^2 P^2-b^2h^2\varepsilon_1^2 Q^2-b^2h^2\gamma_1^2 R^2+b^2h^2\varepsilon_1^2 S^2 = 0$

sin(ω t) part: $b^1h^1\varepsilon_2^1 P^1-b^1h^1\gamma_2^1 Q^1-b^1h^1\varepsilon_2^1 R^1-b^1h^1\gamma_2^1 S^1- b^2h^2\varepsilon_1^2 P^2+b^2h^2\gamma_1^2 Q^2+b^2h^2\varepsilon_1^2 R^2+b^2h^2\gamma_1^2 S^2 = 0$

A3.1.4 System of equations

If there are *n basins* in a system, there are *4n unknowns*.
These are:(P, Q, R and S for each basin for each side as given in equations (A3.16) and (A3.17))

For a system of n basins there are the following conditions:

- For the 'cos(ωt) part':
  - 2 water level boundary conditions
  - 2 transition conditions of the water level
  - 2 transition conditions of flux
- For the 'sin(ωt) part':
  - 2 water level boundary conditions
  - 2 transition conditions of the water level
  - 2 transition conditions of flux

So in total: $2\ (2+n-1+n-1) = 4n$ *conditions*

So there is twice a set of eight unknowns, with twice a set of eight equations. The complete solution of this system is a summation of two solutions of cos(ωt) and sin(ωt) parts. Both these parts are within the solution matrix of water levels in changing row orders and need to be summed together at the end of calculations. Each of the both parts can be found by the multiplication of two matrices:

$$[M]\times[c]=[s] \qquad \text{(A3.26)}$$

In (A3.26) [M] is known, [s] is given and [c] is unknown.

For the case of four basins these matrices are the following:

[M] = a [16×16] matrix in which the coefficients α, β, γ and ε of each basin are ordered in correct ranks for the cos(ωt) part and sin (ωt) part in changing row orders. This is the matrix of step 5 dealt with in section A3.1.2.

An overview of this matrix for the case of four basins is:

(A3.27)

$$M:=\begin{bmatrix}
1 & 0 & -1 & 0 & 0 & 0 & 0 & 0 & & & & & & & & \\
-1 & 0 & 1 & 0 & 0 & 0 & 0 & 0 & & & & & & & & \\
\alpha_2^1 & \beta_2^1 & -\alpha_2^1 & \beta_2^1 & -\alpha_1^2 & -\beta_1^2 & \alpha_1^2 & -\beta_1^2 & & & 0 & & & & 0 & \\
\gamma_2^1 & \varepsilon_2^1 & \gamma_2^1 & -\varepsilon_2^1 & -\gamma_1^2 & -\varepsilon_1^2 & -\gamma_1^2 & \varepsilon_1^2 & & & & & & & & \\
\beta_2^1 & -\alpha_2^1 & \beta_2^1 & \alpha_2^1 & -\beta_1^2 & \alpha_1^2 & -\beta_1^2 & -\alpha_1^2 & 0 & 0 & 0 & 0 & & & & \\
\varepsilon_2^1 & -\gamma_2^1 & -\varepsilon_2^1 & -\gamma_2^1 & -\varepsilon_1^2 & \gamma_1^2 & \varepsilon_1^2 & \gamma_1^2 & 0 & 0 & 0 & 0 & & & 0 & \\
0 & 0 & 0 & 0 & \alpha_2^2 & \beta_2^2 & -\alpha_2^2 & \beta_2^2 & -\alpha_1^3 & -\beta_1^3 & \alpha_1^3 & -\beta_1^3 & & & & \\
0 & 0 & 0 & 0 & \gamma_2^2 & \varepsilon_2^2 & \gamma_2^2 & -\varepsilon_2^2 & -\gamma_1^3 & -\varepsilon_1^3 & -\gamma_1^3 & -\varepsilon_1^3 & & & & \\
 & & & & \beta_2^2 & -\alpha_2^2 & \beta_2^2 & \alpha_2^2 & -\beta_1^3 & \alpha_1^3 & -\beta_1^3 & -\alpha_1^3 & 0 & 0 & 0 & 0 \\
 & & 0 & & \varepsilon_2^2 & -\gamma_2^2 & -\varepsilon_2^2 & -\gamma_2^2 & -\varepsilon_1^3 & \gamma_1^3 & \varepsilon_1^3 & \gamma_1^3 & 0 & 0 & 0 & 0 \\
 & & & & 0 & 0 & 0 & 0 & \alpha_2^3 & \beta_2^3 & -\alpha_2^3 & \beta_2^3 & -\alpha_1^4 & -\beta_1^4 & \alpha_1^4 & -\beta_1^4 \\
 & & & & 0 & 0 & 0 & 0 & \gamma_2^3 & \varepsilon_2^3 & \gamma_2^3 & -\varepsilon_2^3 & -\gamma_1^4 & -\varepsilon_1^4 & -\gamma_1^4 & \varepsilon_1^4 \\
 & & & & & & & & \beta_2^3 & -\alpha_2^3 & \beta_2^3 & \alpha_2^3 & \alpha_1^4 & -\beta_1^4 & -\alpha_1^4 & -\beta_1^4 \\
 & & 0 & & & & 0 & & \varepsilon_2^3 & -\gamma_2^3 & -\varepsilon_2^3 & -\gamma_2^3 & -\varepsilon_1^4 & \gamma_1^4 & \varepsilon_1^4 & \gamma_1^4 \\
 & & & & & & & & 0 & 0 & 0 & 0 & \alpha_2^4 & \beta_2^4 & -\alpha_2^4 & \beta_2^4 \\
 & & & & & & & & 0 & 0 & 0 & 0 & \beta_2^4 & -\alpha_2^4 & \beta_2^4 & \alpha_2^4
\end{bmatrix}$$

[c] = a vector of [1×16] in which basin coefficients are ordered in appropriate order. This is the basin coefficients vector, which first has to be determined according to step 7. It is the vector needed to make calculations for water elevations and velocities.

For the case of four basins this vector is:

(A3.28)

$$\vec{c}:=\begin{bmatrix}
P^1 \\ Q^1 \\ R^1 \\ S^1 \\ P^2 \\ Q^2 \\ R^2 \\ S^2 \\ P^3 \\ Q^3 \\ R^3 \\ S^3 \\ P^4 \\ Q^4 \\ R^4 \\ S^4
\end{bmatrix}$$

[s] = is the [1×16] boundary relations vector of step 6. In this vector only the first two and the last two terms are non-zero values representing the given water level boundaries at both the ends. In between, all values are equal to zero because in [M]

matrix the continuity and mass balance formulations are incorporated, in subtracted form, with the result that each row (after being multiplied with [c]) equals zero.

For the case of four basins this vector is:

(A3.29)

$$\vec{s} := \begin{bmatrix} |a_1| cos(\theta_1) \\ -|a_1| sin(\theta 1) \\ 0 \\ 0 \\ 0 \\ 0 \\ 0 \\ 0 \\ 0 \\ 0 \\ 0 \\ 0 \\ 0 \\ 0 \\ |a_4| cos(\theta_4) \\ -|a_4| sin(\theta 4) \end{bmatrix}$$

When the basin coefficients have been calculated (vectors [c]), the water elevation for an arbitrary point within the system can be calculated. In this case the choice was made upon the begin and end of each basin, at the frontiers, which are calculated twice in this case. This can serve as one of the checks of the rightness of the obtained solutions because at frontier points the elevation for the two neighbouring basins must be equal.

[Z] = According to step eight, a new matrix has to be defined in order to calculate water levels at the desired stations. In this matrix the α and β coefficients of each basin are ordered in appropriate order for the cos(ωt) part and the sin (ωt) part of the solution.

For the case of four basins this matrix Z is as follows:

(A3.30)

$$Z:=\begin{bmatrix}
\alpha_1^1 & \beta_1^1 & -\alpha_1^1 & \beta_1^1 & & & & & & & & & & & & \\
\beta_1^1 & -\alpha_1^1 & \beta_1^1 & \alpha_1^1 & & & & 0 & & & & 0 & & & & 0 \\
\alpha_2^1 & \beta_2^1 & -\alpha_2^1 & \beta_2^1 & & & & & & & & & & & & \\
\beta_2^1 & -\alpha_2^1 & \beta_2^1 & \alpha_2^1 & & & & & & & & & & & & \\
 & & & & \alpha_1^2 & \beta_1^2 & -\alpha_1^2 & \beta_1^2 & & & & & & & & \\
 & & & & \beta_1^2 & -\alpha_1^2 & \beta_2^1 & \alpha_1^2 & & & & & & & & \\
 & 0 & & & \alpha_2^2 & \beta_2^2 & -\alpha_2^2 & \beta_2^2 & & & & 0 & & & & 0 \\
 & & & & \beta_2^2 & -\alpha_2^2 & \beta_2^2 & \alpha_2^2 & & & & & & & & \\
 & & & & & & & & \alpha_1^3 & \beta_1^3 & -\alpha_1^3 & \beta_1^3 & & & & \\
 & & & & & & & & \beta_1^3 & -\alpha_1^3 & \beta_1^3 & \alpha_1^3 & & & & \\
 & 0 & & & & 0 & & & \alpha_2^3 & \beta_2^3 & -\alpha_2^3 & \beta_2^3 & & & & 0 \\
 & & & & & & & & \beta_2^3 & -\alpha_2^3 & \beta_2^3 & \alpha_2^3 & & & & \\
 & & & & & & & & & & & & \alpha_1^4 & \beta_1^4 & -\alpha_1^4 & \beta_1^4 \\
 & 0 & & & & 0 & & & & 0 & & & \beta_1^4 & -\alpha_1^4 & \beta_1^4 & \alpha_1^4 \\
 & & & & & & & & & & & & \alpha_2^4 & \beta_2^4 & -\alpha_2^4 & \beta_2^4 \\
 & & & & & & & & & & & & \beta_2^4 & -\alpha_2^4 & \beta_2^4 & \alpha_2^4
\end{bmatrix}$$

The water elevations of the system is the [1×16] solution vector [Y] resulting from the multiplication between matrix [Z] and vector [c].

$$[Z]\times[c] = [Y] \tag{A3.31}$$

Once the vector [Y] has been calculated, the uneven row numbers must be multiplied by cos(ωt) and the even row numbers with sin(ωt) in order to achieve results in time. Thereafter rows 1 and 2 must be summed up in order to get the complete elevation ζ_1^1, rows 3 and 4 for ζ_2^1.....until row 15 and 16 for ζ_2^4.

The water elevations of chosen stations are then achieved in following form:

$$\zeta_n^n = a\cos(\omega t) + b\sin(\omega t) \tag{A3.32}$$

If wanted (A3.32) can be transformed in one single cosine function:

$$\zeta_n^n = a'\cos(\omega t + \phi)$$

$$\text{with:} \quad a' = \sqrt{\left(a^2 + b^2\right)}$$

$$\phi = \pm\arctan\left(\frac{b}{a}\right) \text{ or} \tag{A3.33}$$

$$\phi = \pi \pm \arctan\left(\frac{b}{a}\right)$$

In which a` represents the resulting amplitude and ϕ the resulting phase.

A3.2 Test results of the program(s)

Before drawing conclusions of the results of self-programmed files, one must be secure that the programmed file is indeed valid for the calculation of the subject it was designed for and that results of the program can be relied upon. The validity and confidence of the designed program must therefore be confirmed first. A couple of tests are needed for this.

In order to check the confidence and validity of the programmed file(s), four tests were made. The first test is the calculation of a system, of which all the basins have the same dimensions. The second test consists of two parts: part one is the calculation of four basins with varying dimensions and part two is the calculation of the same system in reversed order. The third test is the calculation of a same kind of basin system as in test 1, but this time the same calculation is also made with TRISULA, in order to see whether the results look alike. The fourth test is based on checking the representation of system of equations as given with (A3.14) and (A3.16) by the programs. This will further be explained below.

The results of these various tests were as follows:

1• Test one

All four basins have the same dimensions. These are:
length: 220000 m
depth: 800 m
width: 400000 m

Boundary conditions:
first end : $\zeta_1^1 = 0.5\cos(\omega t + 1.3963)$ $|a_1|=0.5$ and $\theta_1=80°$
second end: $\zeta_2^4 = 0.5\cos(\omega t + 2.7925)$ $|a_4|=0.5$ and $\theta_4=160°$

with: $c = \sqrt{gH} \approx 90\ ^m/_s$ over the whole length of four basins a phase lag of $L = cT \approx 4\ 10^6$ m

$\frac{4 \times 220000}{4\ 10^6} 360 \approx 80°$ should occur. That phase lag is almost the phase difference between the two outer boundary elevations. The expectation is that the elevation plots of stations from z_0 to z_8 will give a series of graphs of same amplitude following each, as if they were laid next to each other, with phase difference of 20°.
The result is indeed as expected: see Figure A3.41 of this Appendix.

2• Test two

First a run is made with the model based on following basin dimensions (computation 1):

l_1: 150000	l_2: 220000	l_3: 220000	l_4: 400000
h_1: 700	h_2: 400	h_3: 1200	h_4: 800
b_1: 200000	b_2: 100000	b_3: 400000	b_4: 600000

Boundary conditions:
$|a_1|$: 0.2 θ_1: 305
$|a_4|$: 0.5 θ_4: 160

Then after this run, a second run is made with the same boundary conditions and basin dimensions, but this time in reversed order.
(computation 2):

l_1: 400000	l_2: 220000	l_3: 220000	l_4: 150000
h_1: 800	h_2: 1200	h_3: 400	h_4: 700
b_1: 600000	b_2: 400000	b_3: 100000	b_4: 200000

Boundary conditions:
$|a_1|$: 0.5 θ_1: 160
$|a_4|$: 0.2 θ_4: 305

The expectation was the same form of plots for water elevation would be generated, but of course in reversed order. The water elevation of z_8 in the first run would be the same as the water elevation of z_0 in the second run, and so would be z_2 and z_6. The elevation of z_4 ought to be the same because it is situated in exactly the middle of the system.
The plots generated after these runs indeed agree with the expectations: see Figure A3.42.

3• Test three

Again a single basin form computation has been made, but this time the same calculation has also been made with TRISULA.

All the four basins have the same dimensions. These are:

length: 216000 m
depth: 100 m
width: 24000 m

Boundary conditions:
first end : $\zeta_1^1 = 0.2\cos(\omega t + 2.7925)$ $|a_1|$=0.2 and θ_1=160°
second end: $\zeta_2^4 = 0.5\cos(\omega t + 5.3233)$ $|a_4|$=0.5 and θ_4=305°

The same calculation has also been made with TRISULA. A rectangular grid of 12×12 km has been chosen in a basin of 2×72 grids. The time step was 4 minutes which is in accordance with CFL condition (Stelling&Booij, 1993).
The stations have been chosen at the same positions as in the programmed (MAPLE V) file. In TRISULA the calculations have been made with friction (the calculations of the programmed file are without friction). A Manning coefficient of 0.03 is chosen in order to damp out initial disturbances of the water elevation plots in TRISULA.
The results of both MAPLE V and TRISULA (Figure A3.43) look almost the same. Slight amplitudes and phase lags in TRISULA can be explained by friction effects.

4• Test four

This test is made to double-check whether the programs indeed resemble the system of equations dealt with in the former sections. This test is based on three steps:

step 1:
The second computation of test 2 is done once more (one is allowed to make any computation for this test):

l_1: 400000	l_2: 220000	l_3: 220000	l_4: 150000
h_1: 800	h_2: 1200	h_3: 400	h_4: 700
b_1: 600000	b_2: 400000	b_3: 100000	b_4: 200000

Boundary conditions:

$\|a_1\|$: 0.5	θ_1: 160
$\|a_4\|$: 0.2	θ_4: 305

The solution matrix [Y] that resulted was as follows:

```
Y:=multiply(Z,V);
```

$$Y := [-.4698474272\ \%2 \quad -.1710070032\ \%1 \quad -.5916427596\ \%2 \quad -.1953031369\ \%1$$
$$-.5916427596\ \%2 \quad -.1953031371\ \%1 \quad -.5715957841\ \%2 \quad -.1794457104\ \%1$$
$$-.5715957843\ \%2 \quad -.1794457108\ \%1 \quad -.0000346021\ \%2 \quad .1116568291\ \%1$$
$$-.0000346021\ \%2 \quad .1116568293\ \%1 \quad .1147173268\ \%2 \quad .1638289807\ \%1]$$

$$\%1 := \sin(.0001405637584\ t)$$

$$\%2 := \cos(.0001405637584\ t)$$

If the solution matrix given above, is the result of two solitary waves it should be the result of the following two computations:

step 2: computation 1 with boundary conditions:

$\|a_1\|$: 0	θ_1: 160
$\|a_4\|$: 0.2	θ_4: 305

This is a propagating wave with an anti-node prescribed at the position of Z_0.
The resulting solution matrix [Y_1] of this computation is:

```
Y1:=multiply(Z,V);
```

$$Y_1 := [-.1\ 10^{-10}\ \%2 \quad .1\ 10^{-10}\ \%1 \quad .01882525138\ \%2 \quad .02688453293\ \%1$$
$$.01882525137\ \%2 \quad .02688453296\ \%1 \quad .02687025811\ \%2 \quad .03837368890\ \%1$$
$$.0268702581\ \%2 \quad .03837368889\ \%1 \quad .1049379349\ \%2 \quad .1498629320\ \%1$$
$$.1049379349\ \%2 \quad .1498629318\ \%1 \quad .1147173267\ \%2 \quad .1638289807\ \%1]$$

$$\%1 := \sin(.0001405637584\ t)$$

$$\%2 := \cos(.0001405637584\ t)$$

step 3: computation 2 with boundary conditions:

$\|a_1\|$: 0.5	θ_1: 160
$\|a_4\|$: 0	θ_4: 305

This is a propagating wave with an anti-node prescribed at the position of Z_8.
The resulting solution matrix [Y_2] of this computation is:

Y_2=multiply(Z,V);

$$Y_2 := \begin{bmatrix} -.4698474271\,\%2 & -.1710070032\,\%1 & -.6104680110\,\%2 & -.2221876698\,\%1 \\ -.6104680112\,\%2 & -.2221876697\,\%1 & -.5984660423\,\%2 & -.2178193991\,\%1 \\ -.5984660420\,\%2 & -.2178193993\,\%1 & -.1049725369\,\%2 & -.03820610248\,\%1 \\ -.1049725368\,\%2 & -.03820610247\,\%1 & .3\,10^{-10}\,\%2 & -.65\,10^{-10}\,\%1 \end{bmatrix}$$

$$\%1 := \sin(.0001405637584\,t)$$

$$\%2 := \cos(.0001405637584\,t)$$

With a quick calculation, it can be seen that $[Y]=[Y_1]+[Y_2]$,
so the system indeed resembles the system of equations dealt with in the notes before.

A3.3 Print Output of a self-programmed file

```
restart;
          with(linalg):          with(plots):
Warning: new definition for   norm
Warning: new definition for   trace

                    h1:=300:        b1:=400000:
l2:=220000:         h2:=1000:       b2:=600000:
l3:=220000:         h3:=3500:       b3:=600000:
                    h4:=60:         b4:=300000:
l1:=seq(7000*i,i=1..15):
l4:=seq(10000*j,j=1..15):

unprotect(Pi):              Pi:=3.1416:
omega:=(2*Pi)/T:            g:=9.81:          T:=44700:

c1:=sqrt(g*h1):             L1:=c1*T:         k1:=omega/c1:
c2:=sqrt(g*h2):             L2:=c2*T:         k2:=omega/c2:
c3:= sqrt(g*h3):            L3:=c3*T:         k3:=omega/c3:
c4:=sqrt(g*h4):             L4:=c4*T:         k4:=omega/c4:

Ao:=0.2;                        theta0:=305;
A8:=0.5;                        theta4:=160;
theta0:=convert(theta0*degrees,radians):
theta4:=convert(theta4*degrees,radians):

for i from 1 to 15 do
for j from 1 to 15 do

 x0:=0:
 x1[i,j]:=x0+l1[i]:
 x2[i,j]:=x1[i,j]+l2:
 x3[i,j]:=x2[i,j]+l3:
 x4[i,j]:=x3[i,j]+l4[j]:

od:
od:

for i from 1 to 15 do
for j from 1 to 15 do

alpha11:=sqrt(h1/g)*cos(k1*x0):
beta11:=sqrt(h1/g)*sin(k1*x0):
```

```
gamma11:=cos(k1*x0):
epsilon11:=sin(k1*x0):

alpha12[i,j]:=sqrt(h1/g)*cos(k1*x1[i,j]):
beta12[i,j]:=sqrt(h1/g)*sin(k1*x1[i,j]):
gamma12[i,j]:=cos(k1*x1[i,j]):
epsilon12[i,j]:=sin(k1*x1[i,j]):

alpha21[i,j]:=sqrt(h2/g)*cos(k2*x1[i,j]):
beta21[i,j]:=sqrt(h2/g)*sin(k2*x1[i,j]):
gamma21[i,j]:=cos(k2*x1[i,j]):
epsilon21[i,j]:=sin(k2*x1[i,j]):

alpha22[i,j]:=sqrt(h2/g)*cos(k2*x2[i,j]):
beta22[i,j]:=sqrt(h2/g)*sin(k2*x2[i,j]):
gamma22[i,j]:=cos(k2*x2[i,j]):
epsilon22[i,j]:=sin(k2*x2[i,j]):

alpha31[i,j]:=sqrt(h3/g)*cos(k3*x2[i,j]):
beta31[i,j]:=sqrt(h3/g)*sin(k3*x2[i,j]):
gamma31[i,j]:=cos(k3*x2[i,j]):
epsilon31[i,j]:=sin(k3*x2[i,j]):

alpha32[i,j]:=sqrt(h3/g)*cos(k3*x3[i,j]):
beta32[i,j]:=sqrt(h3/g)*sin(k3*x3[i,j]):
gamma32[i,j]:=cos(k3*x3[i,j]):
epsilon32[i,j]:=sin(k3*x3[i,j]):

alpha41[i,j]:=sqrt(h4/g)*cos(k4*x3[i,j]):
beta41[i,j]:=sqrt(h4/g)*sin(k4*x3[i,j]):
gamma41[i,j]:=cos(k4*x3[i,j]):
epsilon41[i,j]:=sin(k4*x3[i,j]):

alpha42[i,j]:=sqrt(h4/g)*cos(k4*x4[i,j]):
beta42[i,j]:=sqrt(h4/g)*sin(k4*x4[i,j]):
gamma42[i,j]:=cos(k4*x4[i,j]):
epsilon42[i,j]:=sin(k4*x4[i,j]):

od:
od:

for i from 1 to 15 do
for j from 1 to 15 do

M[i,j]:=matrix(16,16,[(alpha11,beta11,-alpha11,beta11,0,0,0,0,0,0,0,0,0,0,0,0,
    beta11,-alpha11,beta11,alpha11,0,0,0,0,0,0,0,0,0,0,0,0,
    alpha12[i,j],beta12[i,j],-alpha12[i,j],beta12[i,j],
    -alpha21[i,j],-beta21[i,j],alpha21[i,j],-beta21[i,j],0,0,0,0,0,0,0,0,
    beta12[i,j],-alpha12[i,j],beta12[i,j],alpha12[i,j],
    -beta21[i,j],alpha21[i,j],-beta21[i,j],-alpha21[i,j],0,0,0,0,0,0,0,0,
    b1*h1*gamma12[i,j],b1*h1*epsilon12[i,j],b1*h1*gamma12[i,j],
    -b1*h1*epsilon12[i,j],-b2*h2*gamma21[i,j],-b2*h2*epsilon21[i,j],
    -b2*h2*gamma21[i,j],b2*h2*epsilon21[i,j],0,0,0,0,0,0,0,0,
    b1*h1*epsilon12[i,j],-b1*h1*gamma12[i,j],-b1*h1*epsilon12[i,j],
    -b1*h1*gamma12[i,j],-b2*h2*epsilon21[i,j], b2*h2*gamma21[i,j],
    b2*h2*epsilon21[i,j],b2*h2*gamma21[i,j],0,0,0,0,0,0,0,0,
    0,0,0,0,alpha22[i,j],beta22[i,j],-alpha22[i,j],beta22[i,j],
    -alpha31[i,j],-beta31[i,j],alpha31[i,j],-beta31[i,j],0,0,0,0,
    0,0,0,0,beta22[i,j],-alpha22[i,j],beta22[i,j],alpha22[i,j],
    -beta31[i,j],alpha31[i,j],-beta31[i,j],-alpha31[i,j],0,0,0,0,
    0,0,0,0,b2*h2*gamma22[i,j],b2*h2*epsilon22[i,j],b2*h2*gamma22[i,j],
    -b2*h2*epsilon22[i,j],-b3*h3*gamma31[i,j],-b3*h3*epsilon31[i,j],
    -b3*h3*gamma31[i,j], b3*h3*epsilon31[i,j],0,0,0,0,
    0,0,0,0,b2*h2*epsilon22[i,j],-b2*h2*gamma22[i,j],-b2*h2*epsilon22[i,j],
    -b2*h2*gamma22[i,j],-b3*h3*epsilon31[i,j],b3*h3*gamma31[i,j],
    b3*h3*epsilon31[i,j],b3*h3*gamma31[i,j],0,0,0,0,
    0,0,0,0,0,0,0,0,alpha32[i,j],beta32[i,j],-alpha32[i,j],beta32[i,j],
    -alpha41[i,j],-beta41[i,j],alpha41[i,j],-beta41[i,j],
```

```
      0,0,0,0,0,0,0,0,beta32[i,j],-alpha32[i,j],beta32[i,j],alpha32[i,j],
     -beta41[i,j],alpha41[i,j],-beta41[i,j],-alpha41[i,j],
      0,0,0,0,0,0,0,0,b3*h3*gamma32[i,j],b3*h3*epsilon32[i,j],
      b3*h3*gamma32[i,j],-b3*h3*epsilon32[i,j],-b4*h4*gamma41[i,j],
     -b4*h4*epsilon41[i,j],
     -b4*h4*gamma41[i,j],b4*h4*epsilon41[i,j],
      0,0,0,0,0,0,0,0,b3*h3*epsilon32[i,j],-b3*h3*gamma32[i,j],
     -b3*h3*epsilon32[i,j],-b3*h3*gamma32[i,j],-b4*h4*epsilon41[i,j],
      b4*h4*gamma41[i,j],b4*h4*epsilon41[i,j],b4*h4*gamma41[i,j],
      0,0,0,0,0,0,0,0,0,0,0,0,0,0,alpha42[i,j],beta42[i,j],-alpha42[i,j],beta42[i,j],
      0,0,0,0,0,0,0,0,0,0,0,0,0,0,beta42[i,j],-alpha42[i,j],beta42[i,j],alpha42[i,j]]):

od:
od:

R:=vector([Ao*cos(theta0),-Ao*sin(theta0),0,0,0,0,0,0,0,0,0,0,0,0,
          A8*cos(theta4),-A8*sin(theta4)]);

for i from 1 to 15 do
for j from 1 to 15 do

V[i,j]:=linsolve(M[i,j],R);

od:
od:

for i from 1 to 15 do
for j from 1 to 15 do

Z[i,j]:=matrix(16,16,[cos(omega*t)*alpha11,cos(omega*t)*beta11,
      -cos(omega*t)*alpha11,cos(omega*t)*beta11,0,0,0,0,0,0,0,0,0,0,0,0,
       sin(omega*t)*beta11,-sin(omega*t)*alpha11,
       sin(omega*t)*beta11,sin(omega*t)*alpha11,0,0,0,0,0,0,0,0,0,0,0,0,
       cos(omega*t)*alpha12[i,j],cos(omega*t)*beta12[i,j],
      -cos(omega*t)*alpha12[i,j],cos(omega*t)*beta12[i,j],0,0,0,0,0,0,0,0,0,0,0,0,
       sin(omega*t)*beta12[i,j],-sin(omega*t)*alpha12[i,j],
       sin(omega*t)*beta12[i,j],sin(omega*t)*alpha12[i,j],0,0,0,0,0,0,0,0,0,0,0,0,
       0,0,0,0,cos(omega*t)*alpha21[i,j],cos(omega*t)*beta21[i,j],
       -cos(omega*t)*alpha21[i,j],cos(omega*t)*beta21[i,j],0,0,0,0,0,0,0,0,
       0,0,0,0,sin(omega*t)*beta21[i,j],-sin(omega*t)*alpha21[i,j],
       sin(omega*t)*beta21[i,j],sin(omega*t)*alpha21[i,j],0,0,0,0,0,0,0,0,
       0,0,0,0,cos(omega*t)*alpha22[i,j],cos(omega*t)*beta22[i,j],
       -cos(omega*t)*alpha22[i,j],cos(omega*t)*beta22[i,j],0,0,0,0,0,0,0,0,
       0,0,0,0,sin(omega*t)*beta22[i,j],-sin(omega*t)*alpha22[i,j],
       sin(omega*t)*beta22[i,j],sin(omega*t)*alpha22[i,j],0,0,0,0,0,0,0,0,
       0,0,0,0,0,0,0,0,cos(omega*t)*alpha31[i,j],cos(omega*t)*beta31[i,j],
       -cos(omega*t)*alpha31[i,j],cos(omega*t)*beta31[i,j],0,0,0,0,
        0,0,0,0,0,0,0,0,sin(omega*t)*beta31[i,j],-sin(omega*t)*alpha31[i,j],
       sin(omega*t)*beta31[i,j],sin(omega*t)*alpha31[i,j],0,0,0,0,
       0,0,0,0,0,0,0,0,cos(omega*t)*alpha32[i,j],cos(omega*t)*beta32[i,j],
       -cos(omega*t)*alpha32[i,j],cos(omega*t)*beta32[i,j],0,0,0,0,
       0,0,0,0,0,0,0,0,sin(omega*t)*beta32[i,j],-sin(omega*t)*alpha32[i,j],
       sin(omega*t)*beta32[i,j],sin(omega*t)*alpha32[i,j],0,0,0,0,
       0,0,0,0,0,0,0,0,0,0,0,0,cos(omega*t)*alpha41[i,j],cos(omega*t)*beta41[i,j],
        -cos(omega*t)*alpha41[i,j],cos(omega*t)*beta41[i,j],
        0,0,0,0,0,0,0,0,0,0,0,0,sin(omega*t)*beta41[i,j],-sin(omega*t)*alpha41[i,j],
        sin(omega*t)*beta41[i,j],sin(omega*t)*alpha41[i,j],
       0,0,0,0,0,0,0,0,0,0,0,0,cos(omega*t)*alpha42[i,j],cos(omega*t)*beta42[i,j],
      -cos(omega*t)*alpha42[i,j],cos(omega*t)*beta42[i,j],
        0,0,0,0,0,0,0,0,0,0,0,0,sin(omega*t)*beta42[i,j],-sin(omega*t)*alpha42[i,j],
        sin(omega*t)*beta42[i,j],sin(omega*t)*alpha42[i,j]]):

od:
od:

for i from 1 to 15 do
for j from 1 to 15 do
```

```
Y[i,j]:=multiply(Z[i,j],V[i,j]):

od:
od:

for i from 1 to 15 do
   for j from 1 to 15 do
      for k from 1 to 16 do
          p:=1:
            for s from 1 to 8 do

               f[i,j][k]:=unapply(Y[i,j][k],t);
               z[i,j][s]:=(f[i,j][p](t)+f[i,j][p+1](t));
               z1[i,j][s]:=diff(z[i,j][s],t);
               p:=p+2:
             od;

      od;

   od;
od:

AMP:=matrix(15,15):
FAS:=matrix(15,15):

for s from 3 to 6 do
    for i from 1 to 15 do
       for j from 1 to 15 do

            OPL:=fsolve(z1[i,j][s](t)=0,t=0...(T/2));
            OPL2:=fsolve(z[i,j][s](t)=0,t,t=0..(T/2));
            AMP[i,j]:=abs(subs(t=OPL,z[i,j][s]));
            OPL3:=evalf(subs(t=OPL2,z1[i,j][s]));
             if type(OPL3,positive) then
                      FAS[i,j]:=(360-(90+(OPL2/T)*360))
                         else FAS[i,j]:=(270-(((0.5*T)+OPL2)/T)*360) fi;
                        while (FAS[i,j]<0) do FAS[i,j]:=360+FAS[i,j]; od;

       od;
  od;

  PL1[s]:=matrixplot(AMP);
  PL2[s]:=matrixplot(FAS);
writeto(`Loutp.txt`);
od:

interface(plotdevice=ps);
interface(plotoutput=`Hampl2.ps`):
display3d(PL1[3],axes=boxed,view=0..1,shading=ZHUE,style=contour,
        orientation=[0,1.5708],ambientlight=[1,0.3,1],
         title=`amplitude of water level at Z2`,thickness=2,
         labels=[`H1 index`,`H4 index`,`z (m)`]);
interface(plotdevice=ps);
interface(plotoutput=`Hampl4.ps`):
display3d(PL1[4],axes=boxed,view=0..1,shading=ZHUE,ambientlight=[1,0.3,1],
        style=contour, orientation=[0,1.5708],thickness=2,
         title=`amplitude of water level at Z4`,
         labels=[`H1 index`,`H4 index`,`z (m)`]);
interface(plotdevice=ps);
interface(plotoutput=`Hampl6.ps`):
display3d(PL1[6],axes=boxed,view=0..1,shading=ZHUE,ambientlight=[1,0.3,1],
         title=`amplitude of water level at Z6`,style=contour,
         orientation=[0,1.5708],thickness=2,
         labels=[`H1 index`,`H4 index`,`z (m)`]);
interface(plotdevice=ps):
interface(plotoutput=`Hpha2.ps`):
display3d(PL2[3],axes=boxed,shading=ZHUE,ambientlight=[1,0.3,1],
         style=contour, orientation=[0,1.5708],thickness=2,
```

```
        title=`phase Z2`,labels=[`H1 index`,`H4 index`,`phase (degr)`]);
interface(plotdevice=ps):
interface(plotoutput=`Hpha4.ps`):
display3d(PL2[4],axes=boxed,shading=ZHUE,ambientlight=[1,0.3,1],
          title=`phase Z4`,style=contour,
          orientation=[0,1.5708],thickness=2,
          labels=[`H1 index`,`H4 index`,`phase (degr)`]);
interface(plotdevice=ps):
interface(plotoutput=`Hpha6.ps`):
display3d(PL2[6],axes=boxed,shading=ZHUE,ambientlight=[1,0.3,1],
          title=`phase Z6`,style=contour,
          orientation=[0,1.5708],thickness=2,
          labels=[`H1 index`,`H4 index`,`phase (degr)`]);
```

DELFT HYDRAULICS

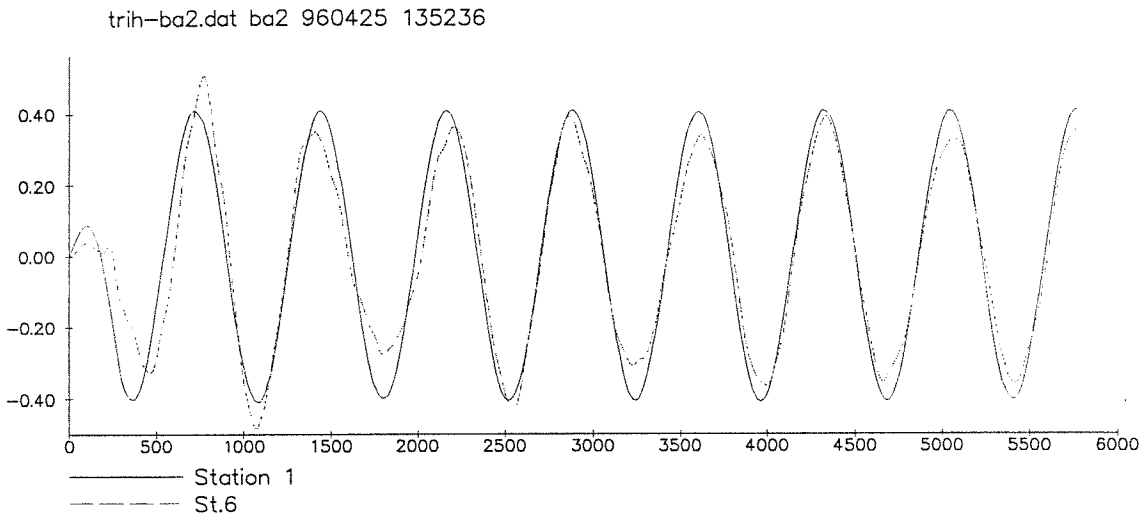

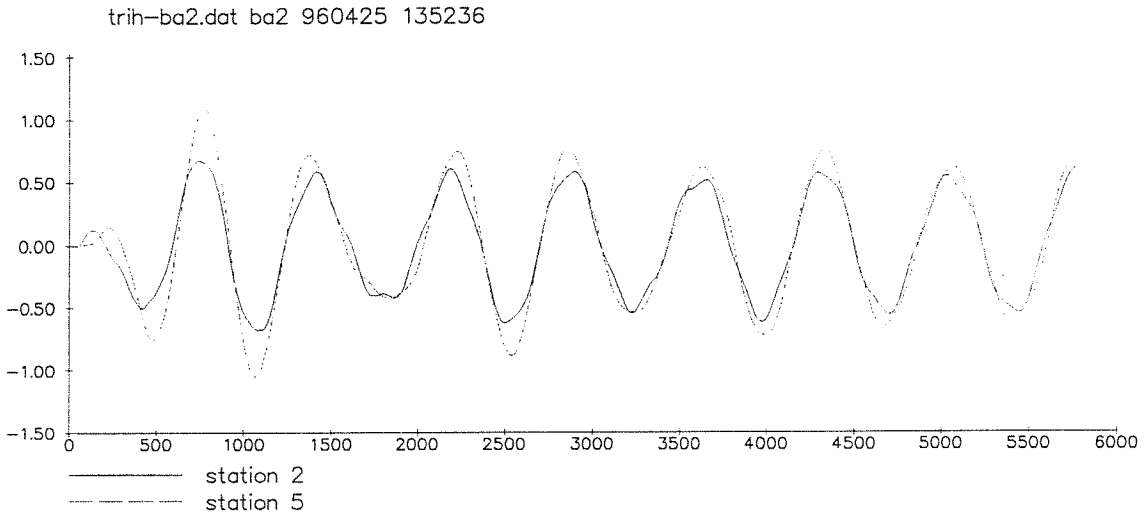

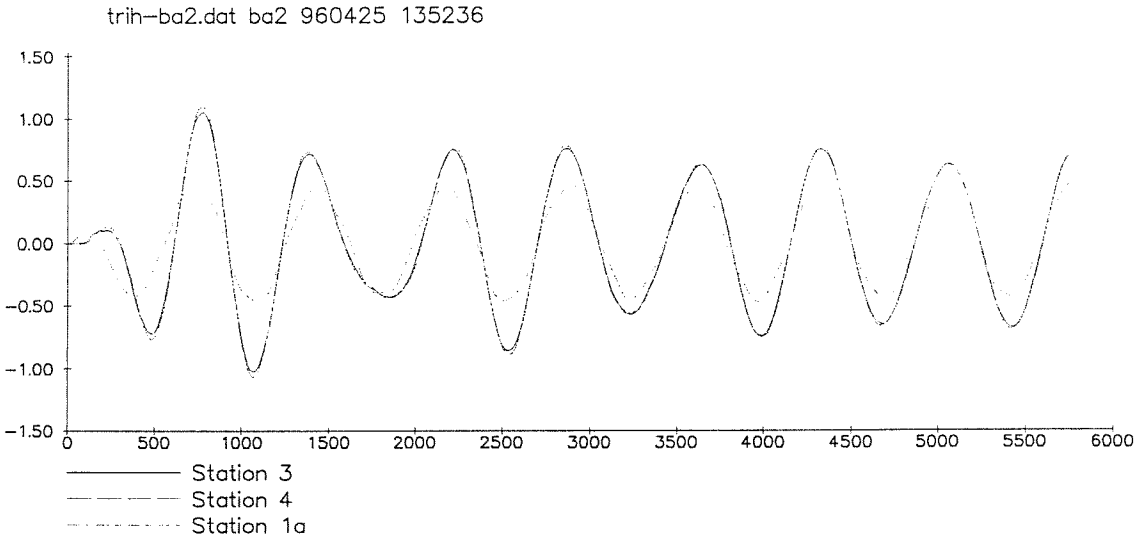

Sulu Sea 1-dimensional test case. Connection of two deep waters by a shallow passage.		1996-04-25 13:54:46
TRISULA – Delft Hydraulics (NL)		*Figure A3.1*

DELFT HYDRAULICS

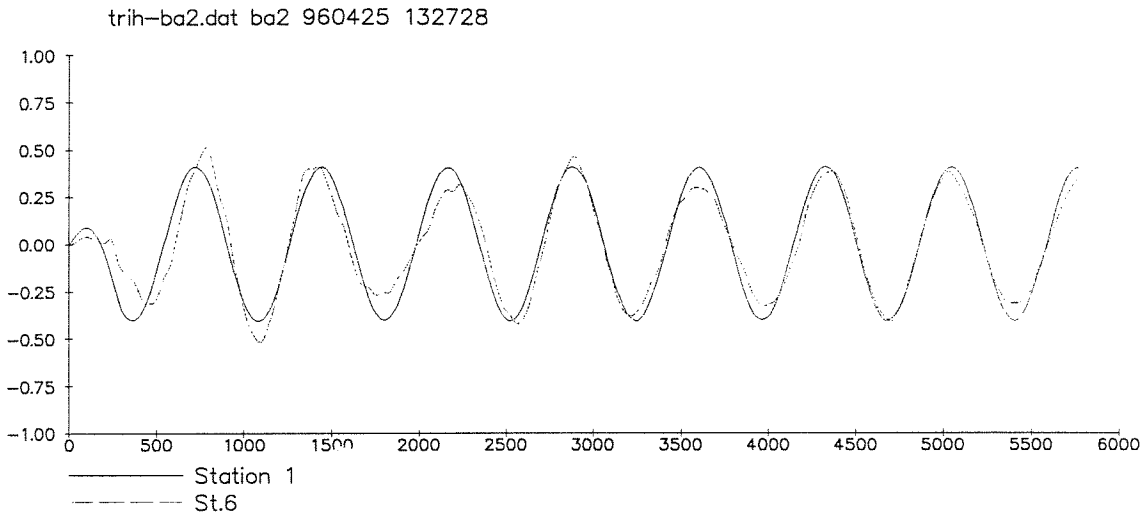

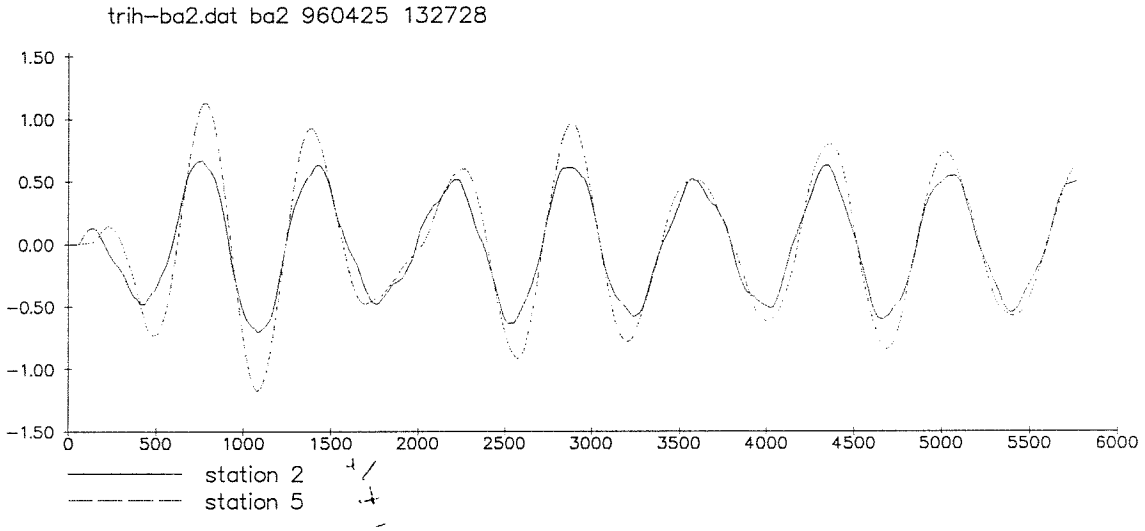

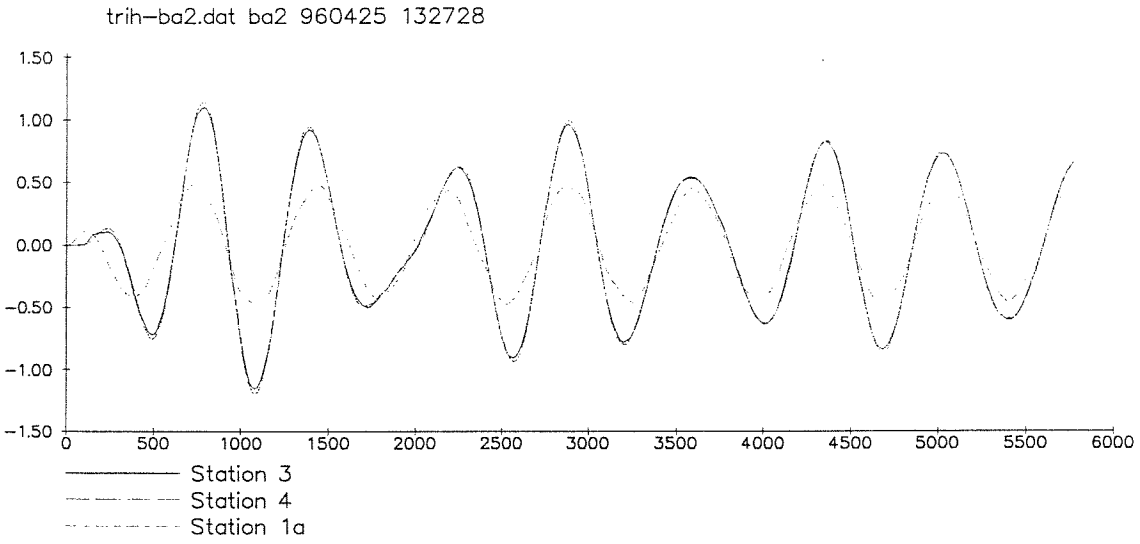

Sulu Sea 1–dimensional test case. Connection of two deep waters by a shallow passage. Pal. Pass. = 200 m Sulu Pass. = 70 m k = 0,04		1996–04–25 13:31:09
TRISULA – Delft Hydraulics (NL)		***Figure A3.2***

DELFT HYDRAULICS

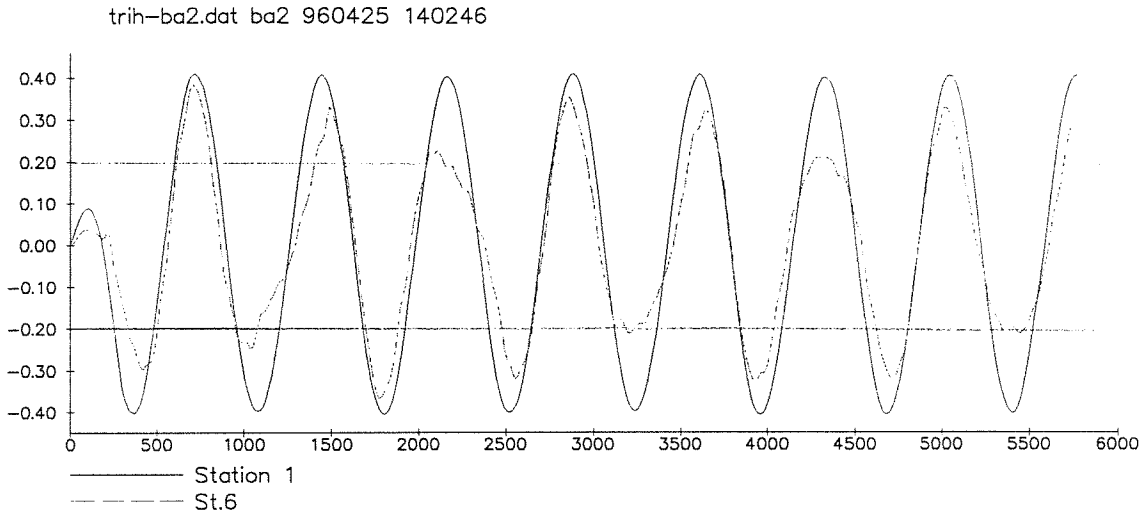

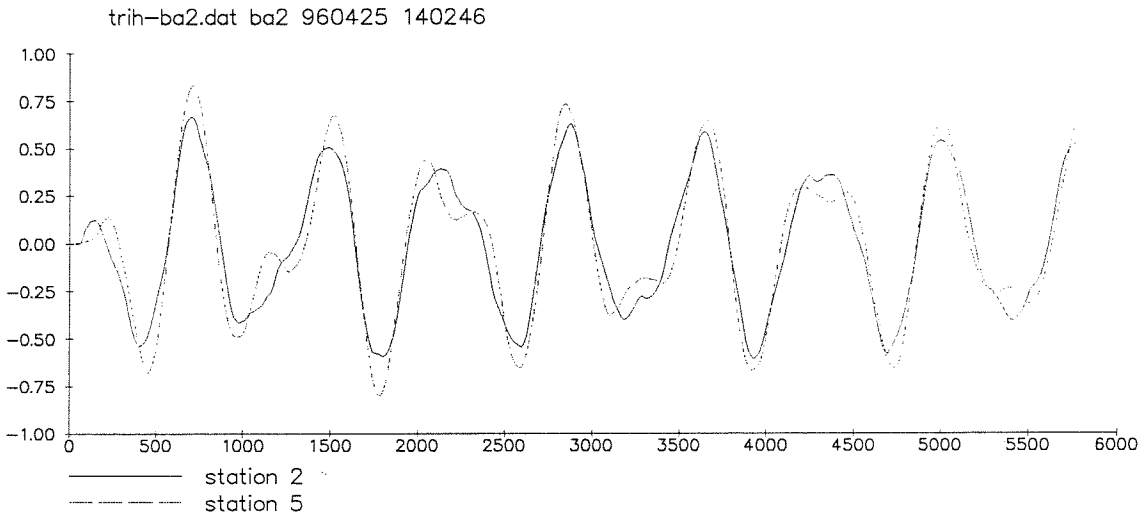

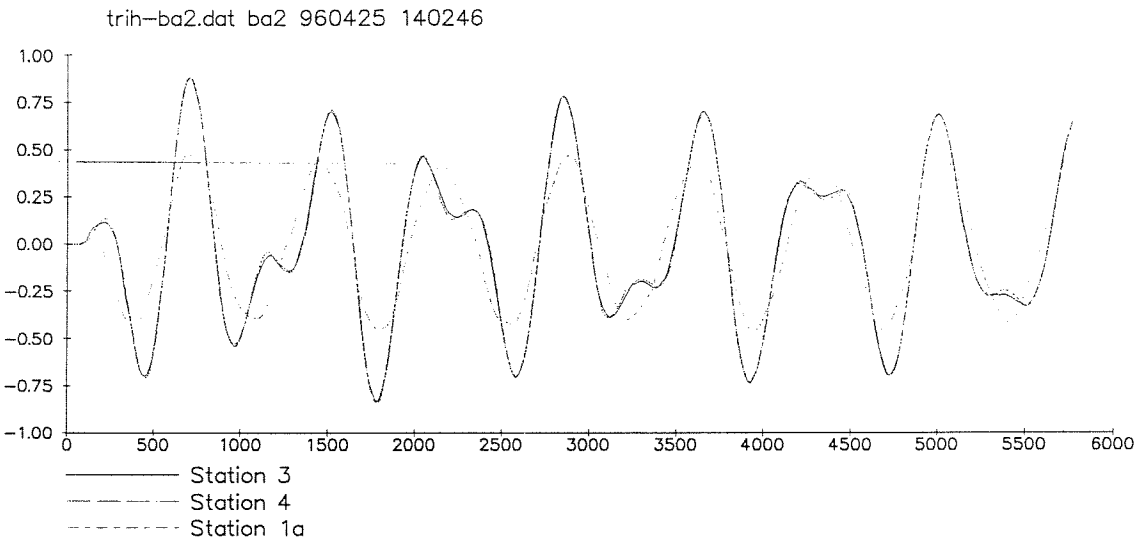

Sulu Sea 1-dimensional test case.
Connection of two deep waters by a shallow passage.
pal=250 m sul=150 m k=0.052

1996-04-25
14:07:45

TRISULA - Delft Hydraulics (NL)

Figure A3.3

DELFT HYDRAULICS

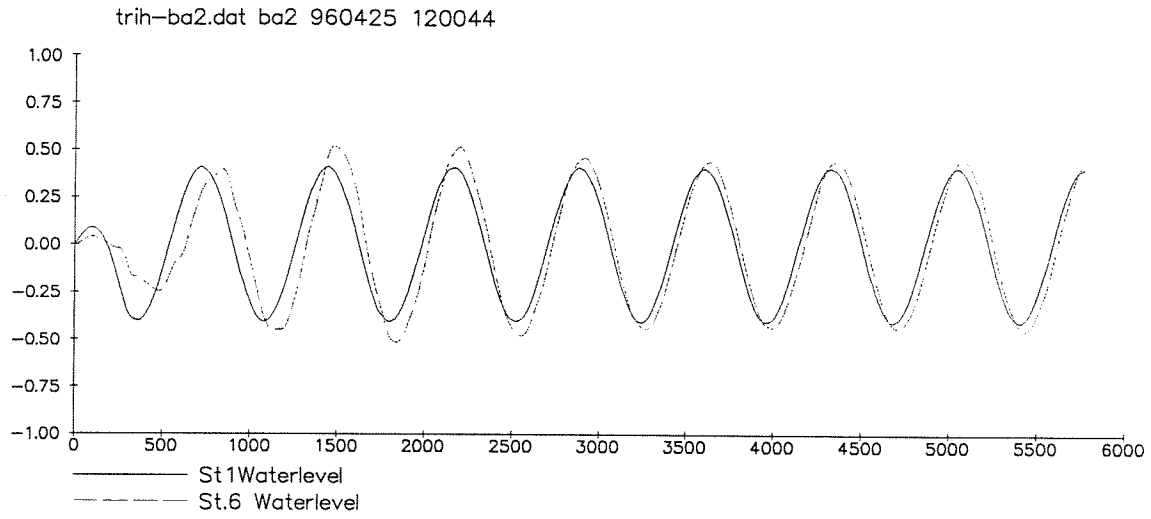

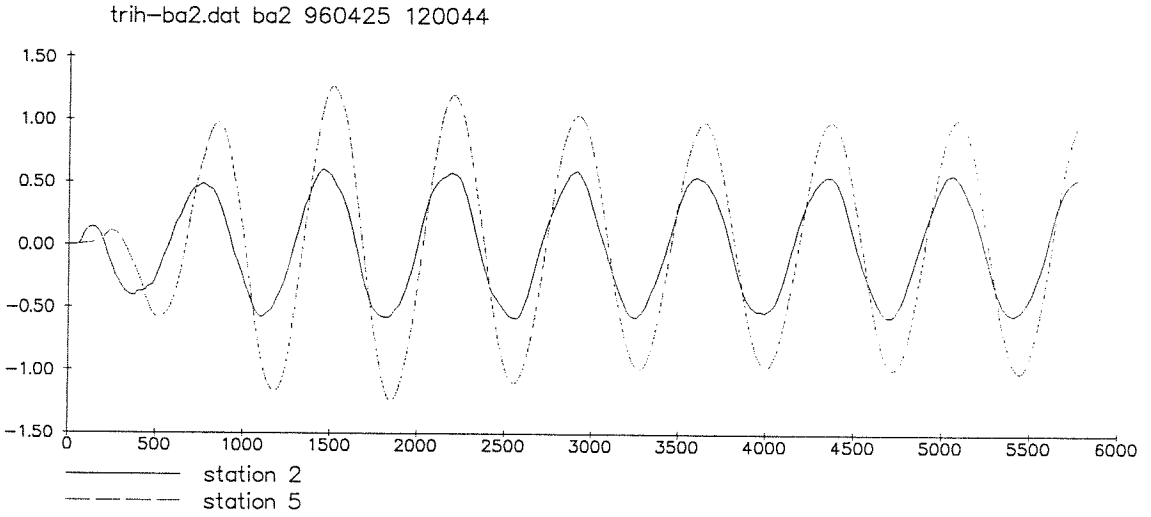

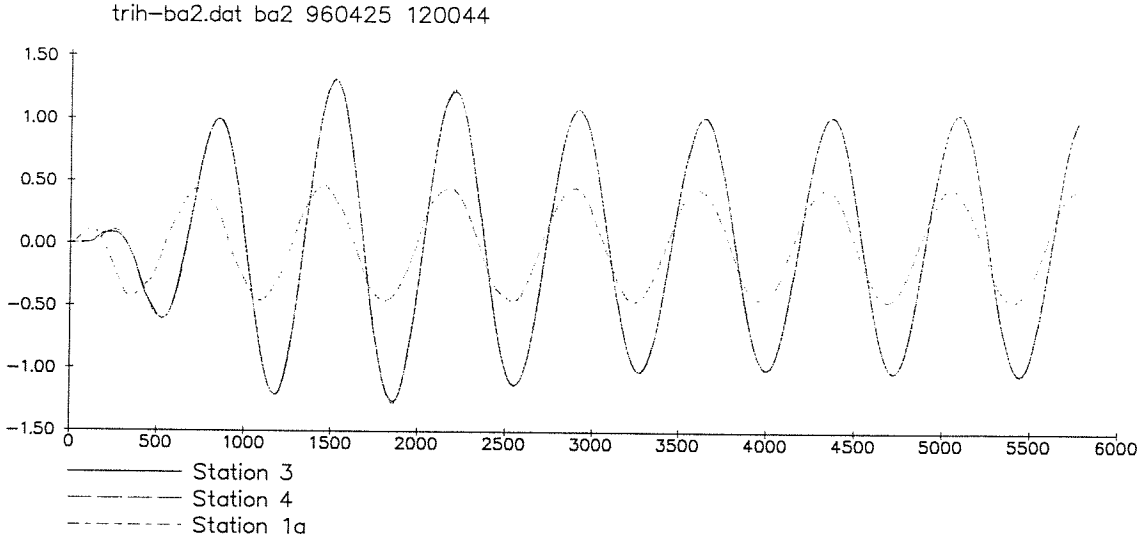

Sulu Sea 1-dimensional test case.
Connection of two deep waters by a shallow passage.
Both passages have a depth of 70 m.

1996-04-25
12:08:41

TRISULA – Delft Hydraulics (NL)

Figure A3.4

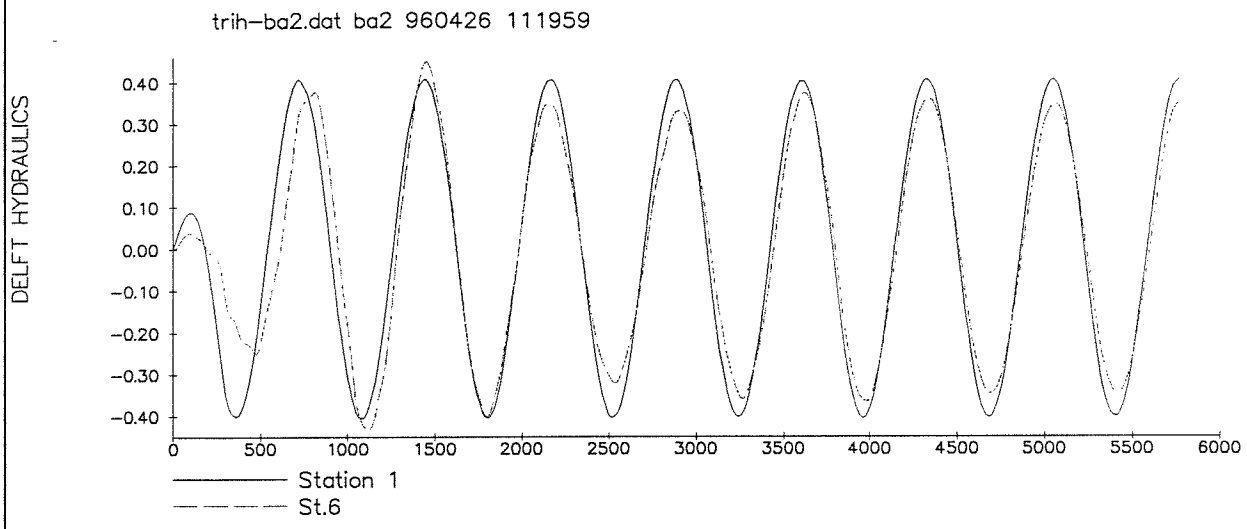

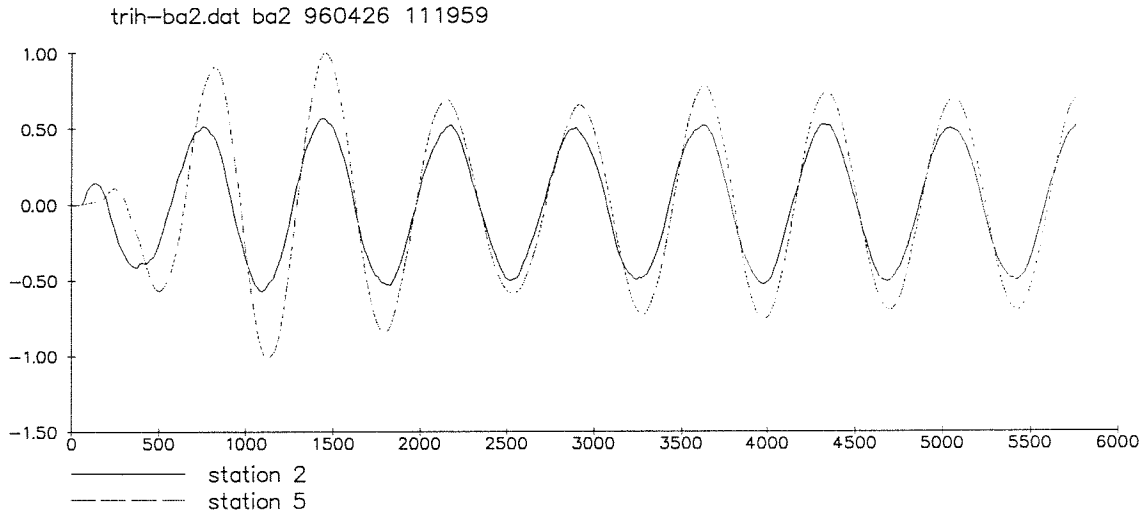

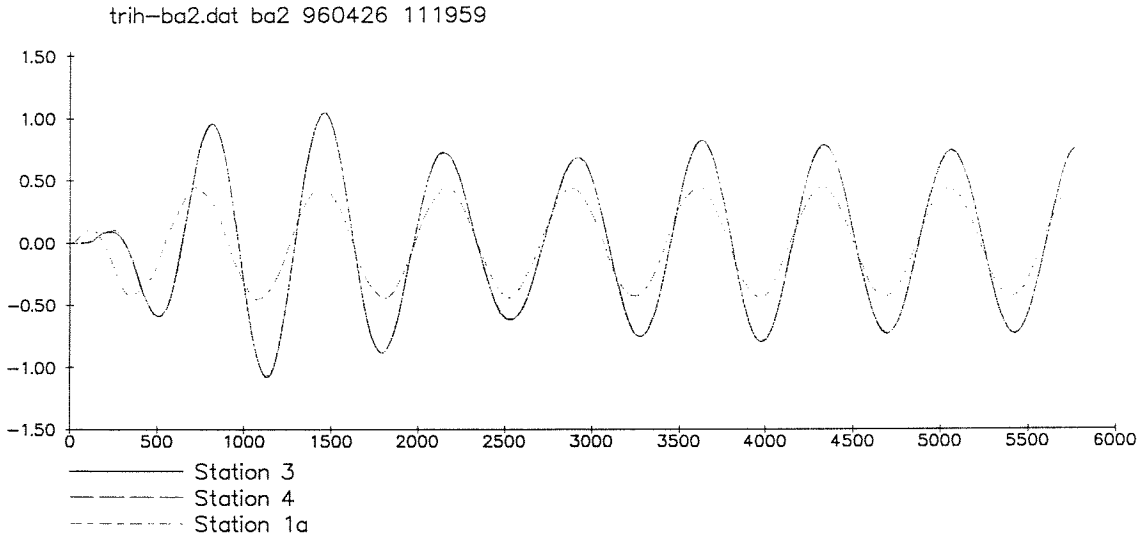

Sulu Sea 1-dimensional test case.
Connection of two deep waters by a shallow passage.
pal=70 m sul=95 m k=0.052

1996-04-26
11:23:00

TRISULA - Delft Hydraulics (NL)

Figure A3.5

Figure A3.6 amplitude of water level at Z2

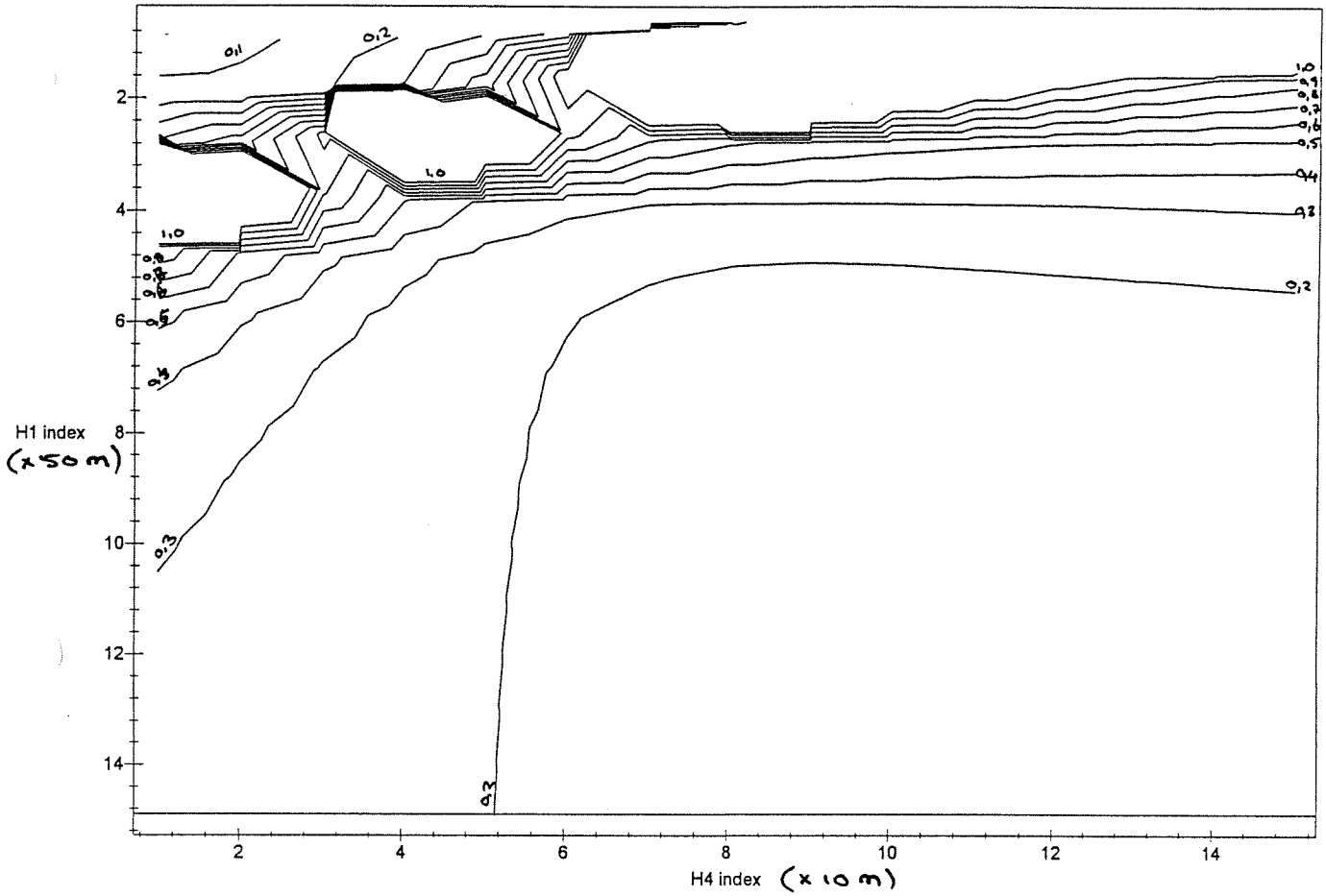

Figure A3.7 phase Z2

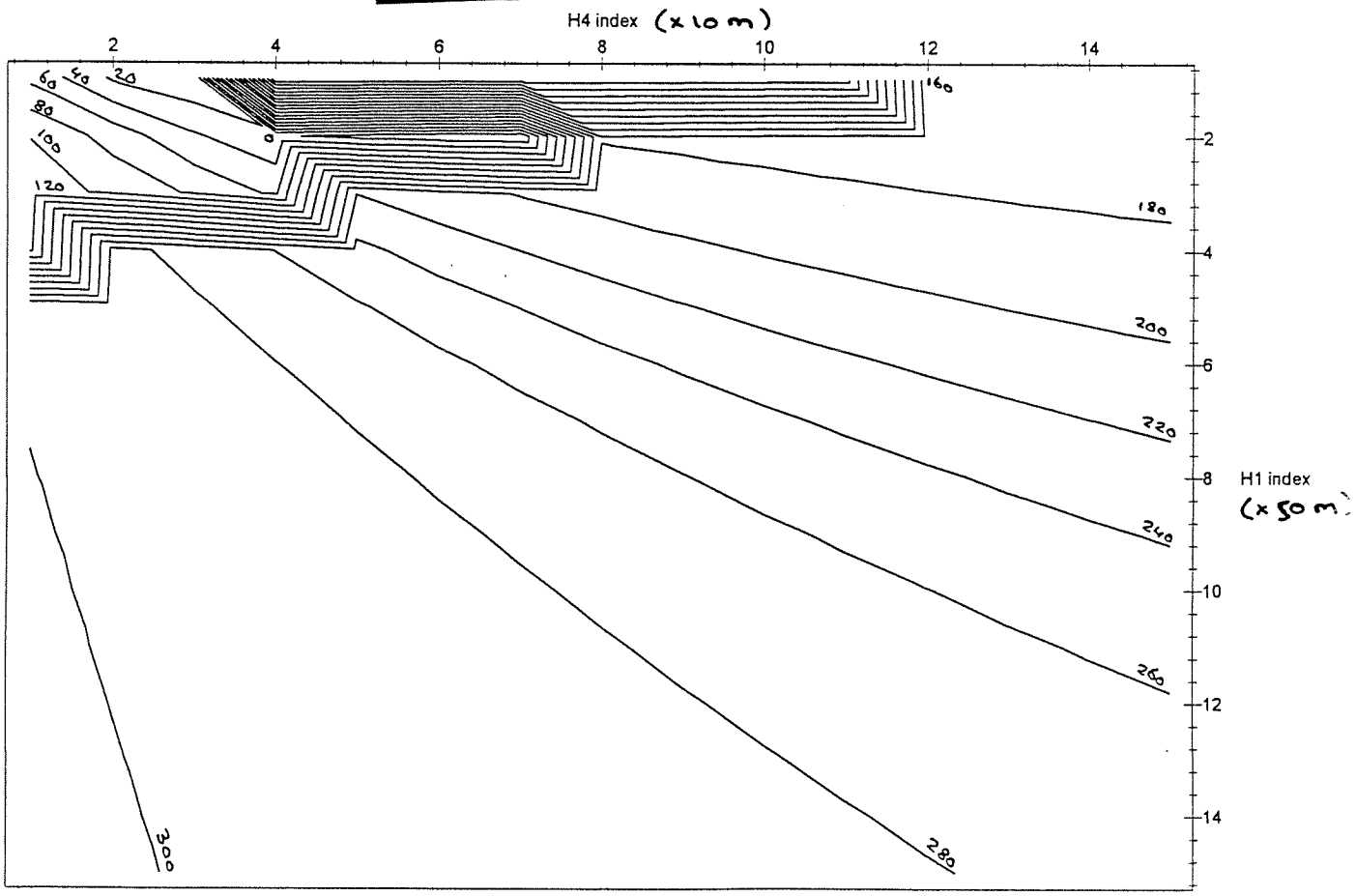

Figure A3.8 phase Z4

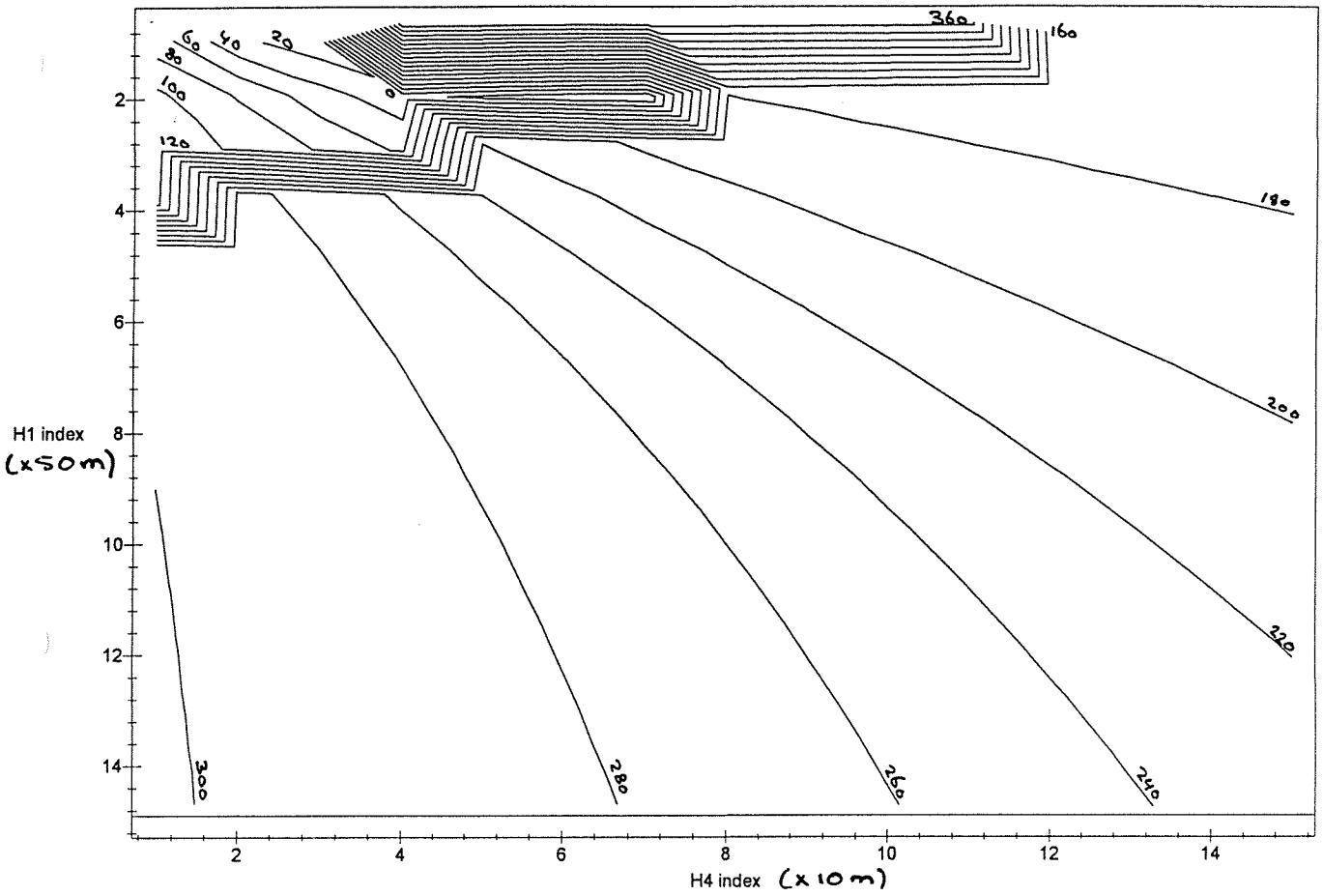

Figure A3.9 amplitude of water level at Z4

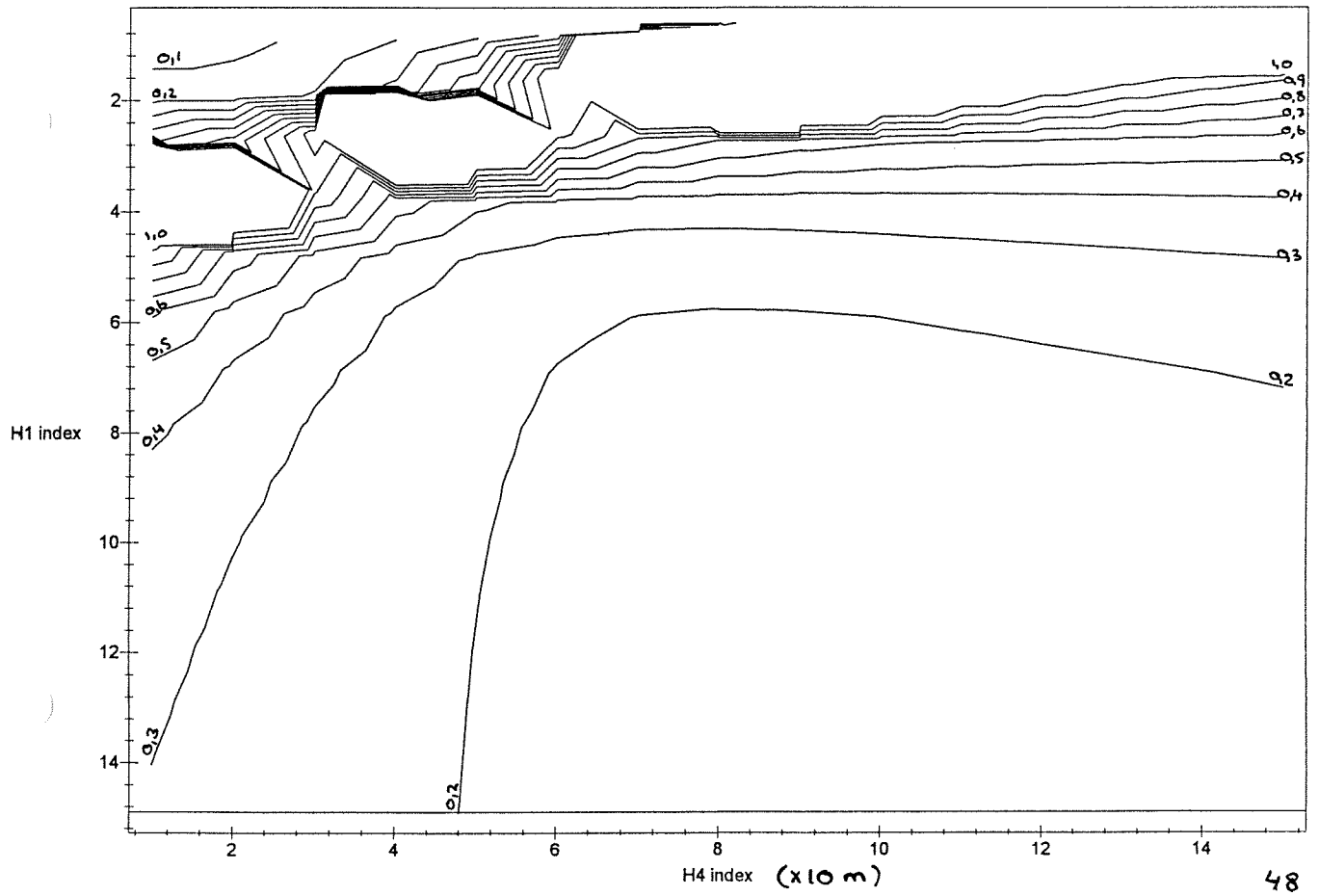

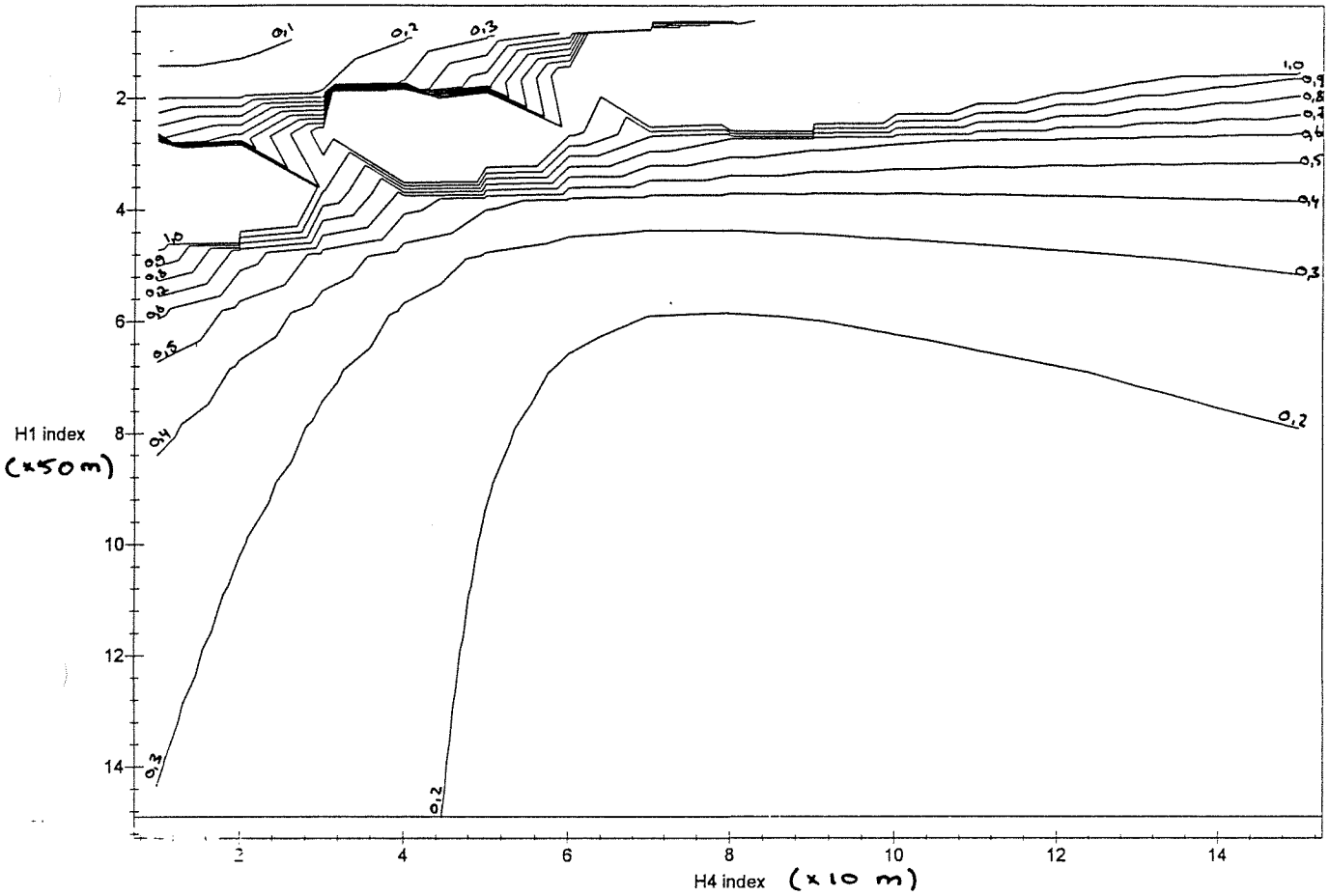

Figure A3.11 phase Z6

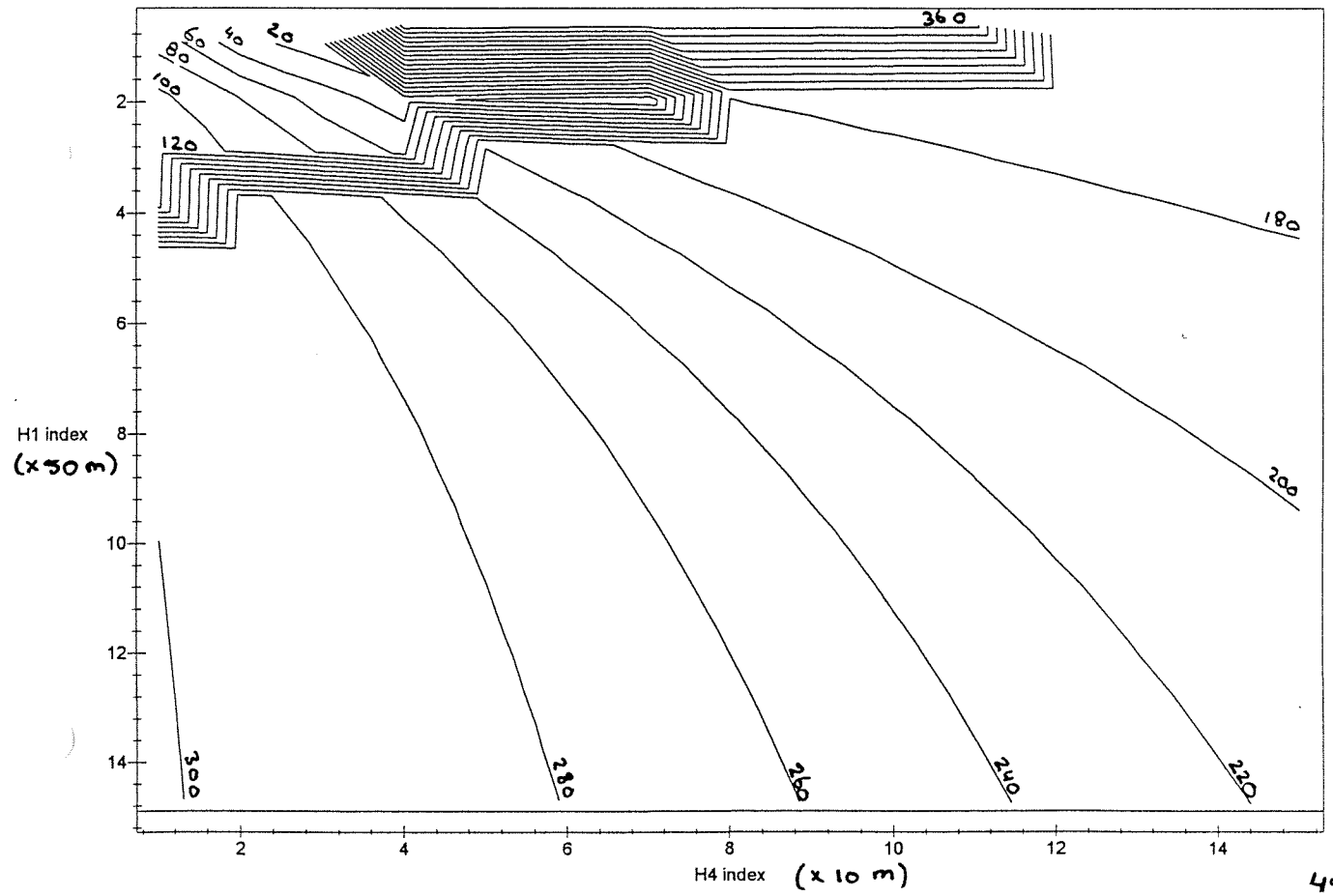

Figure A3.12 amplitude of water level at Z2

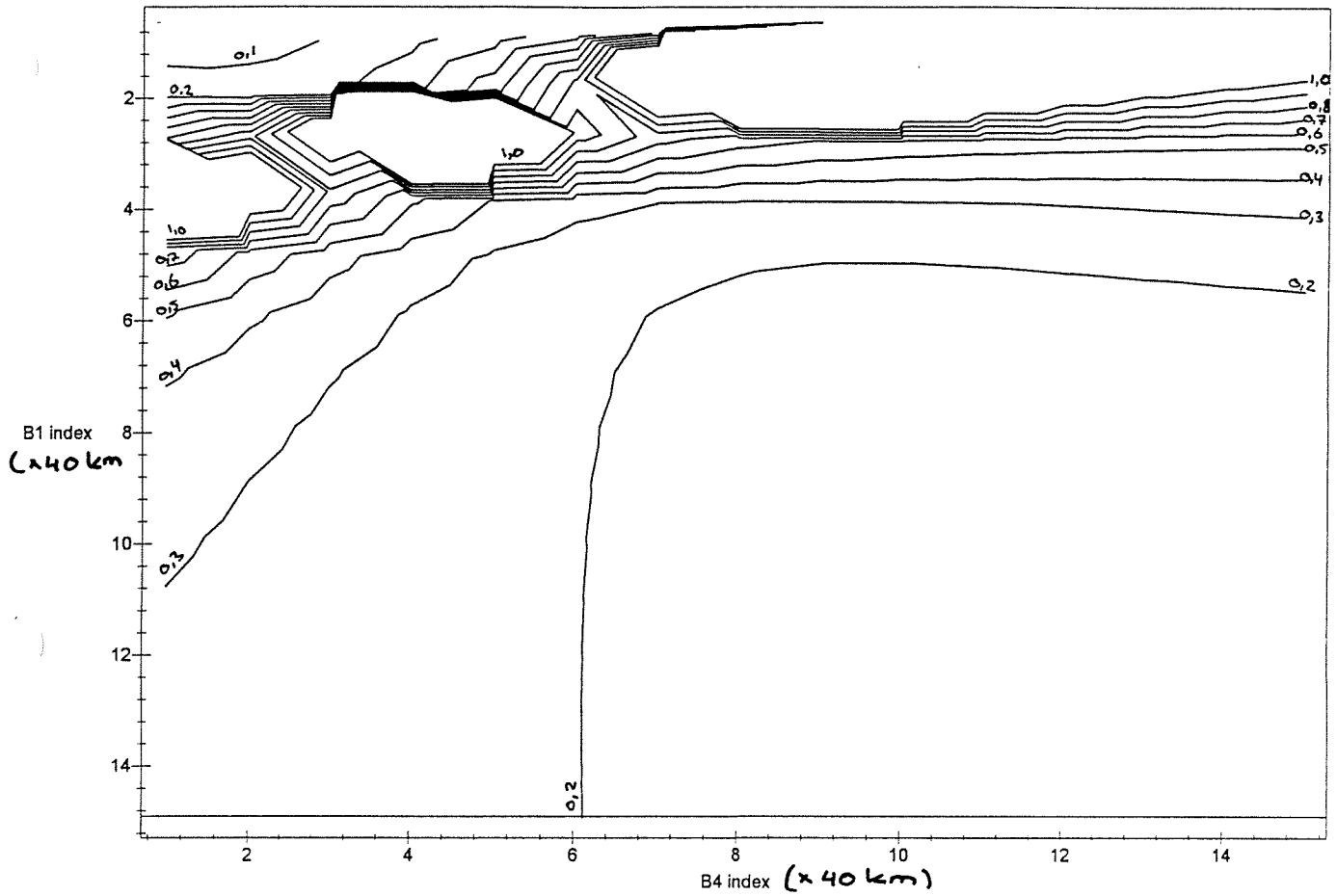

Figure A3.13 phase of Z2

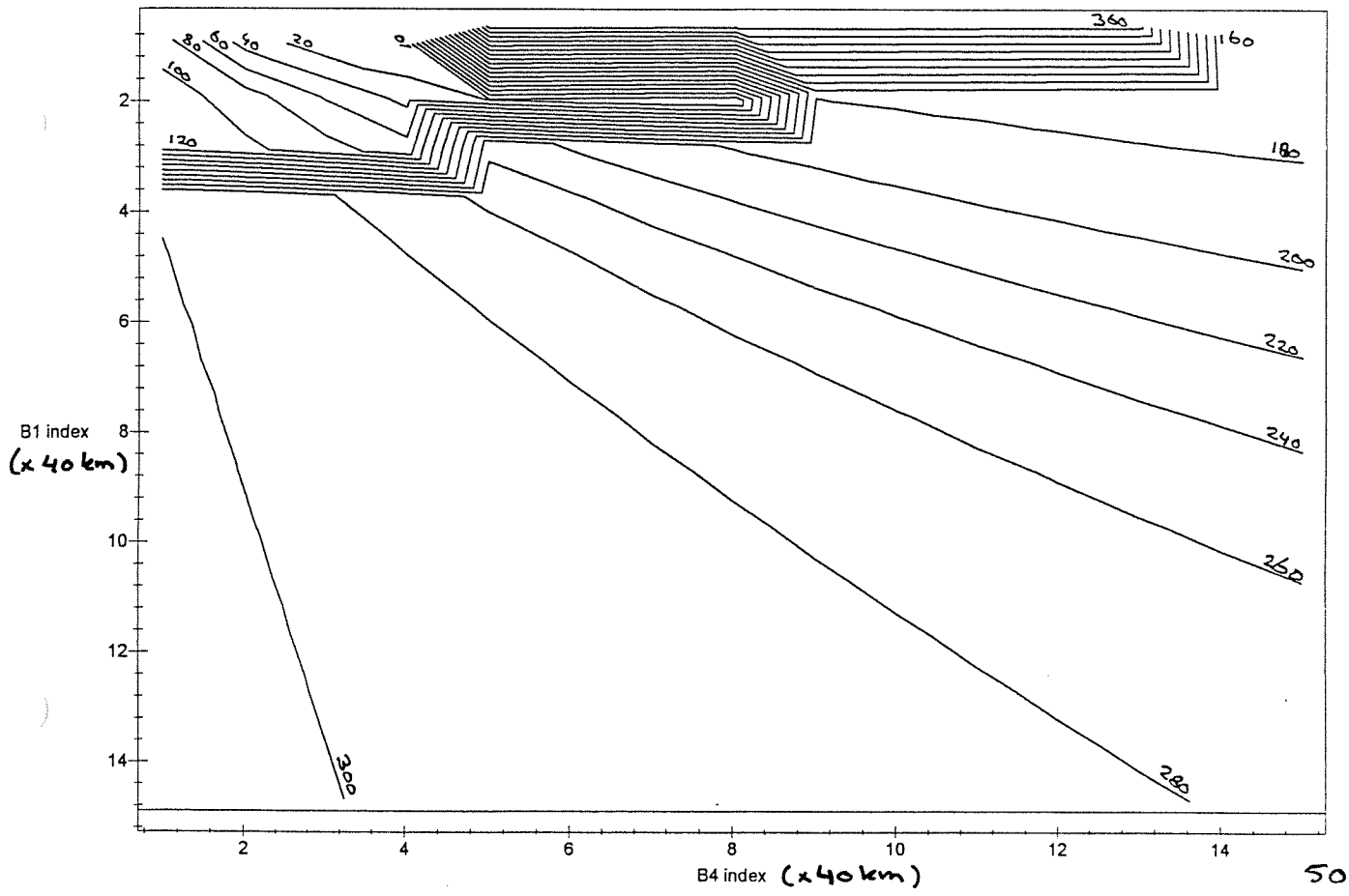

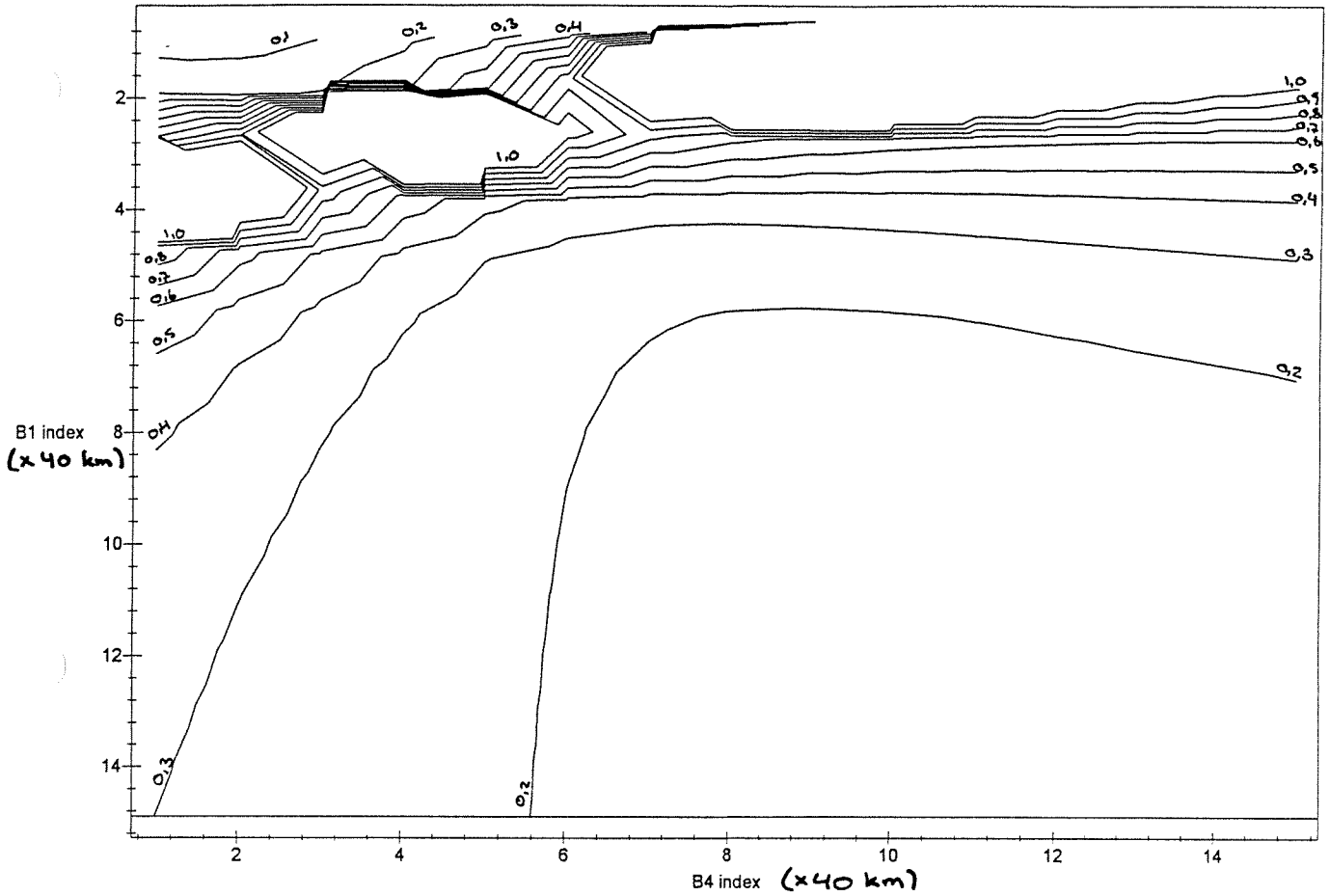

Figure A3.15 phase of Z4

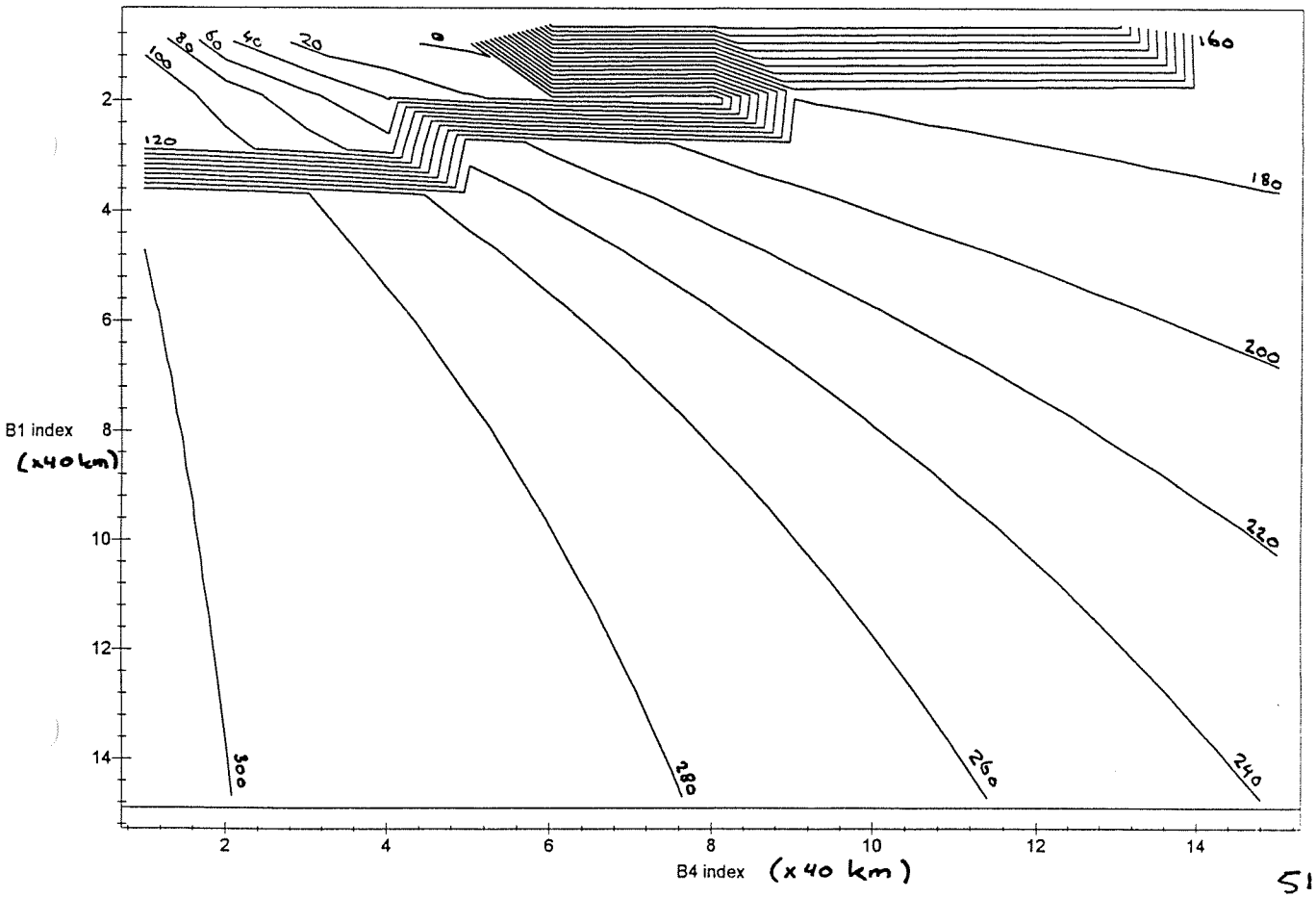

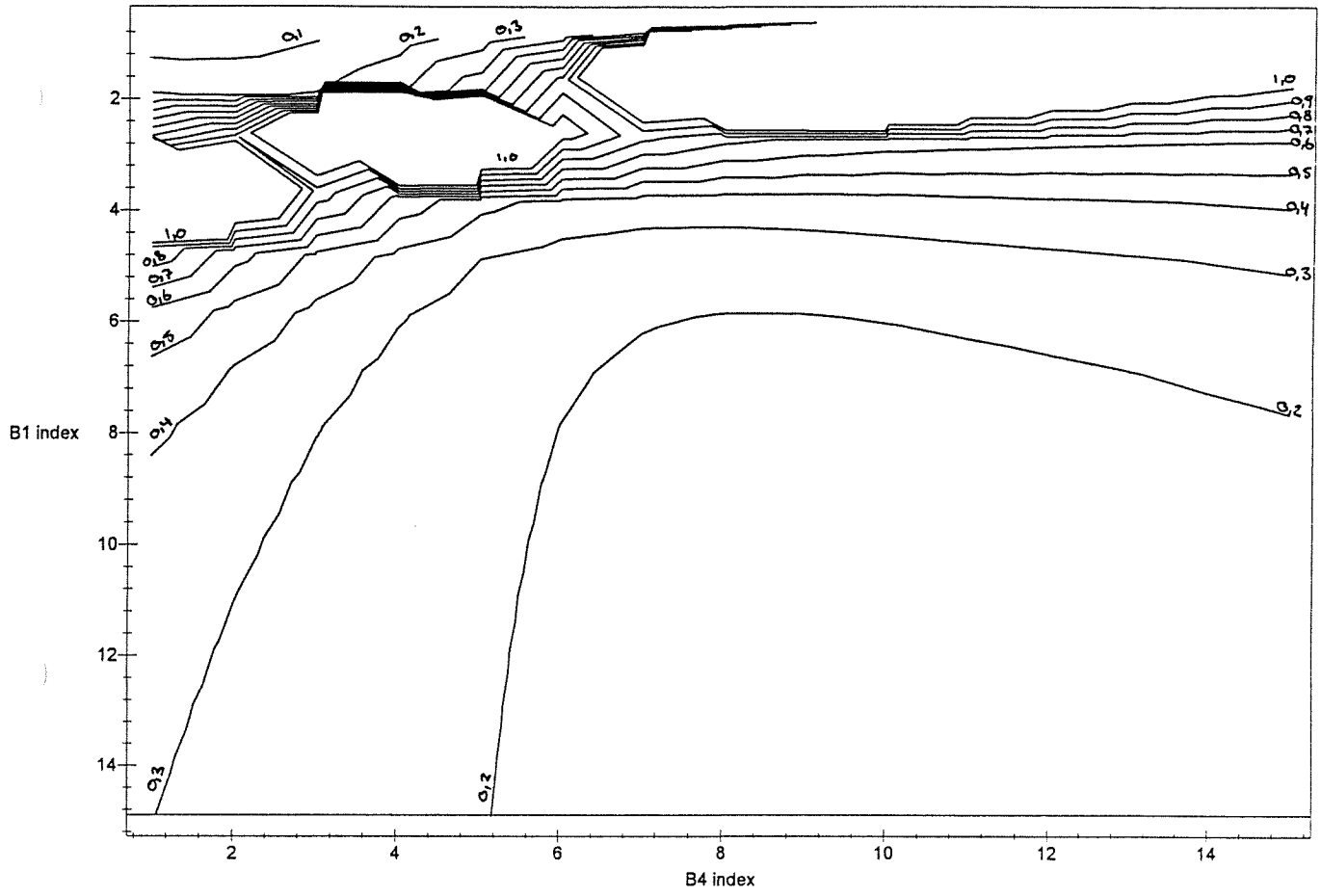

Figure A3.17 phase of Z6

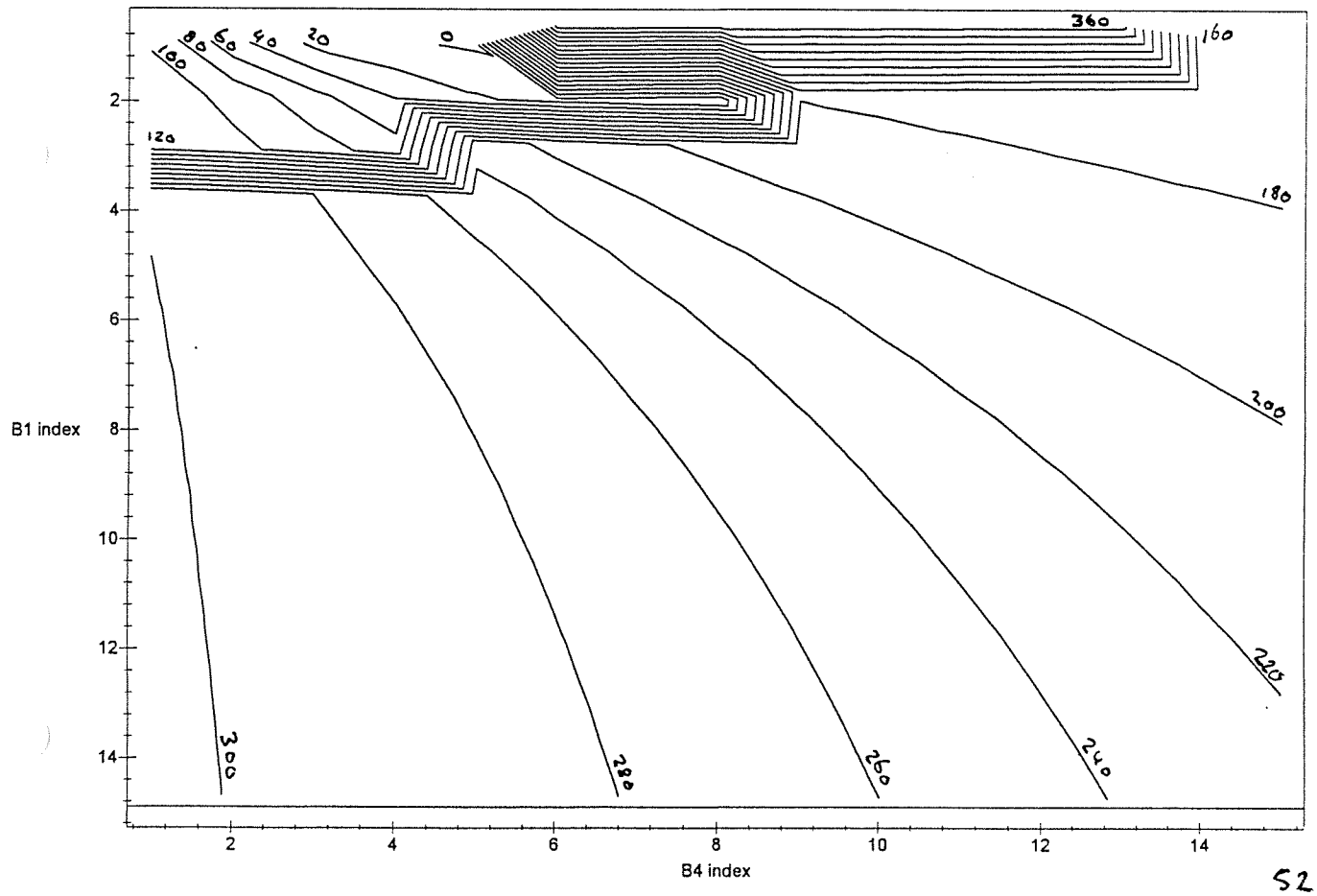

Figure A3.18 amplitude of water level at Z2 (m)

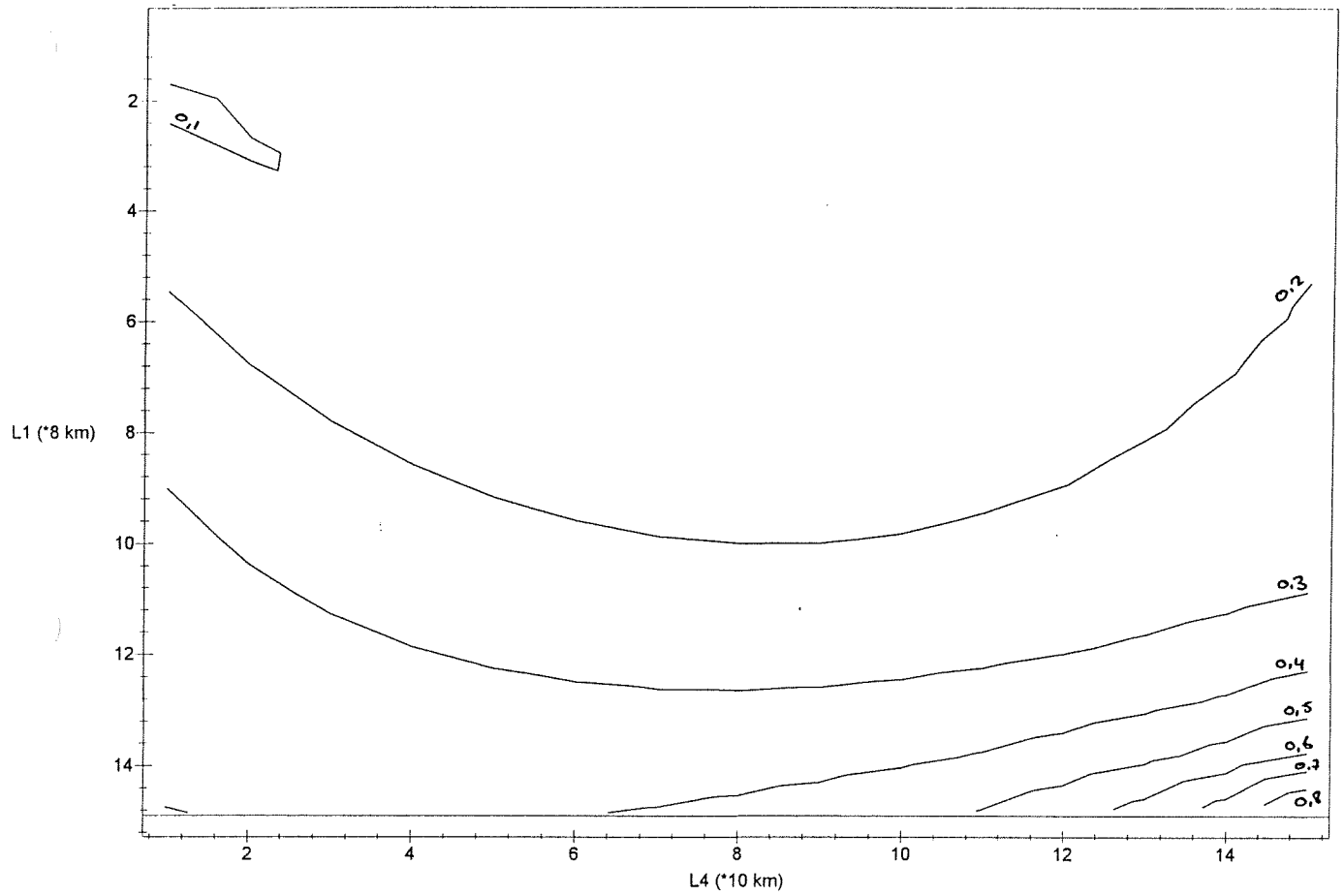

Figure A3.19 phase Z2 (degrees)

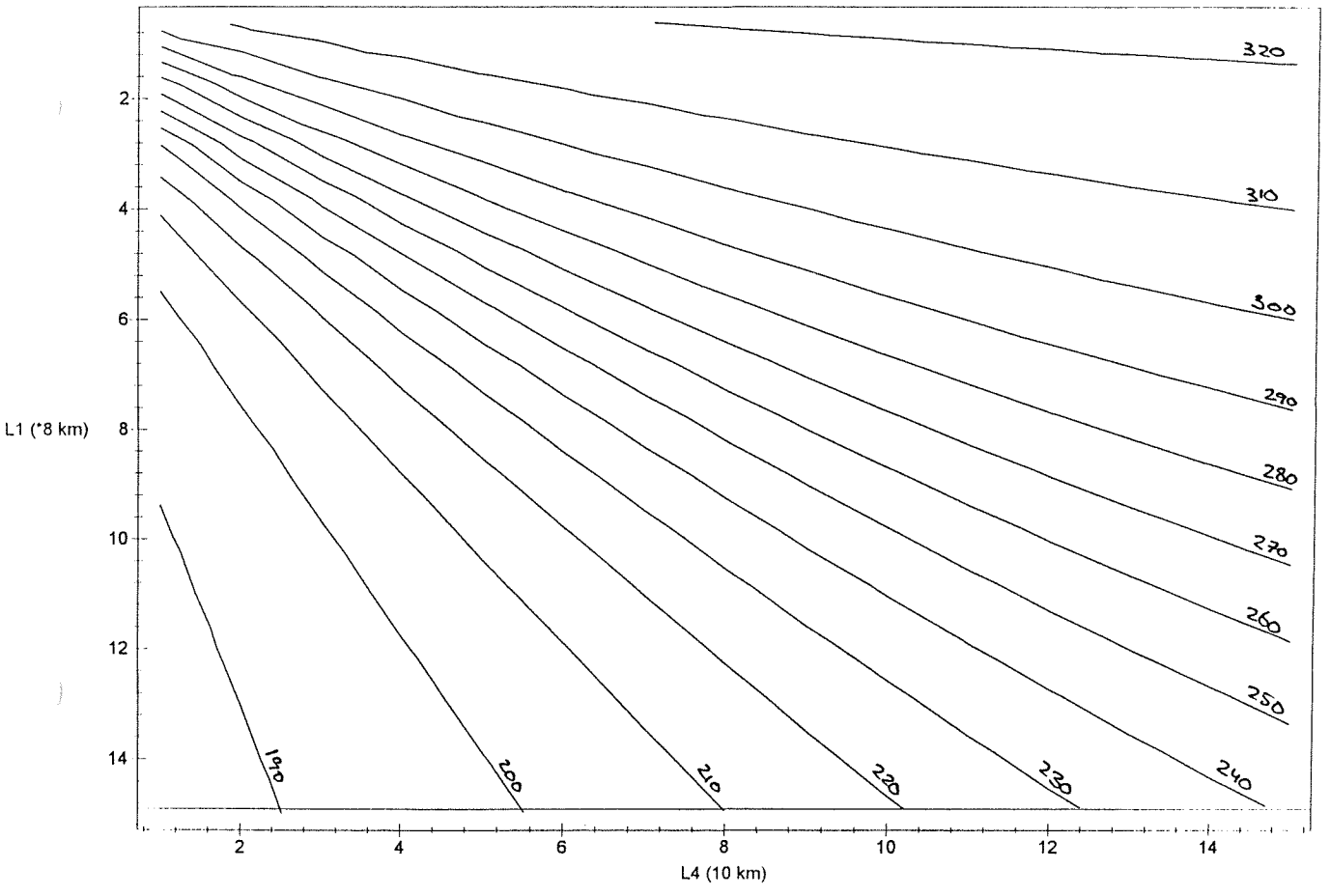

Figure A3.20 amplitude of water level at Z4 (m)

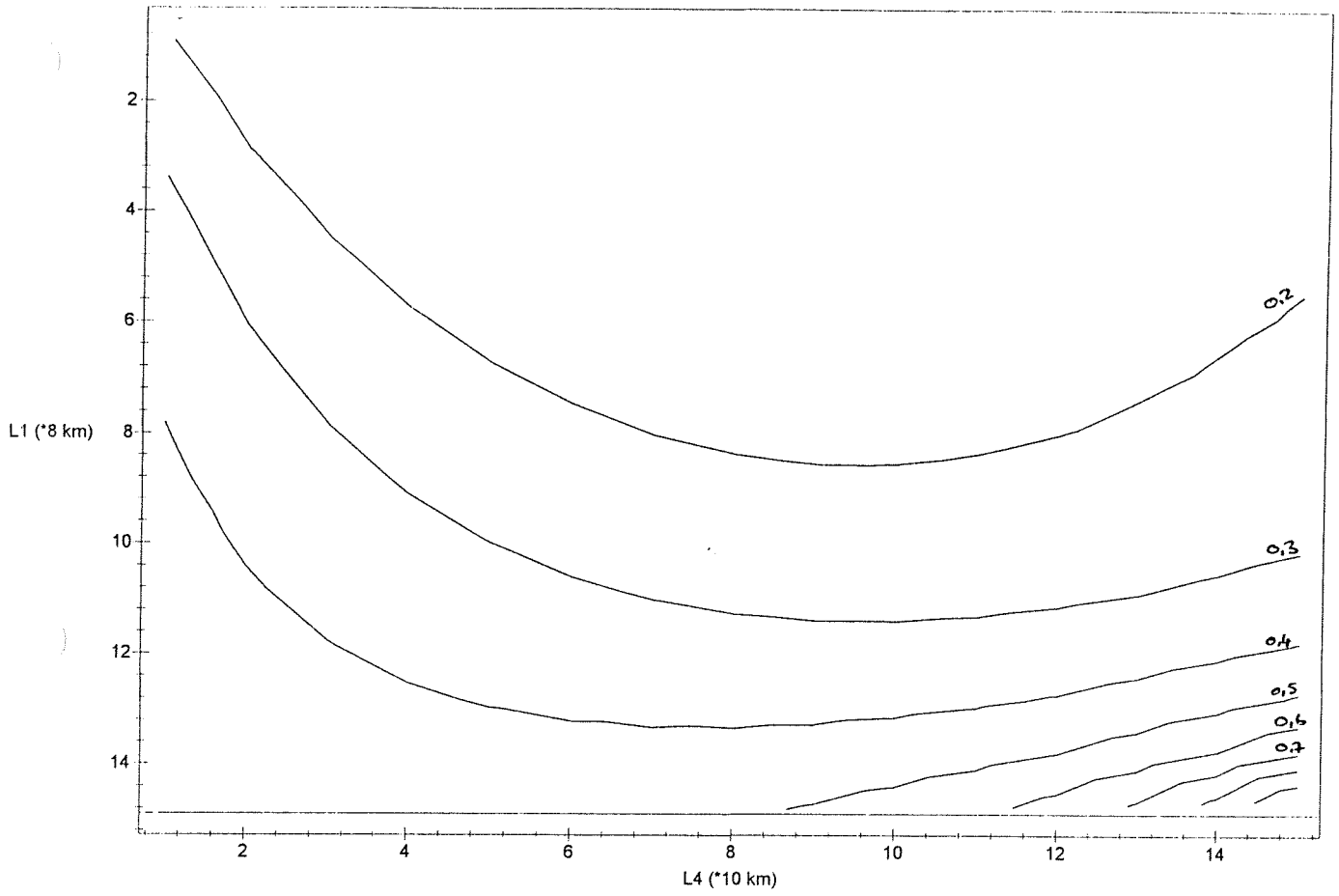

Figure A3.21 phase Z4 (degrees)

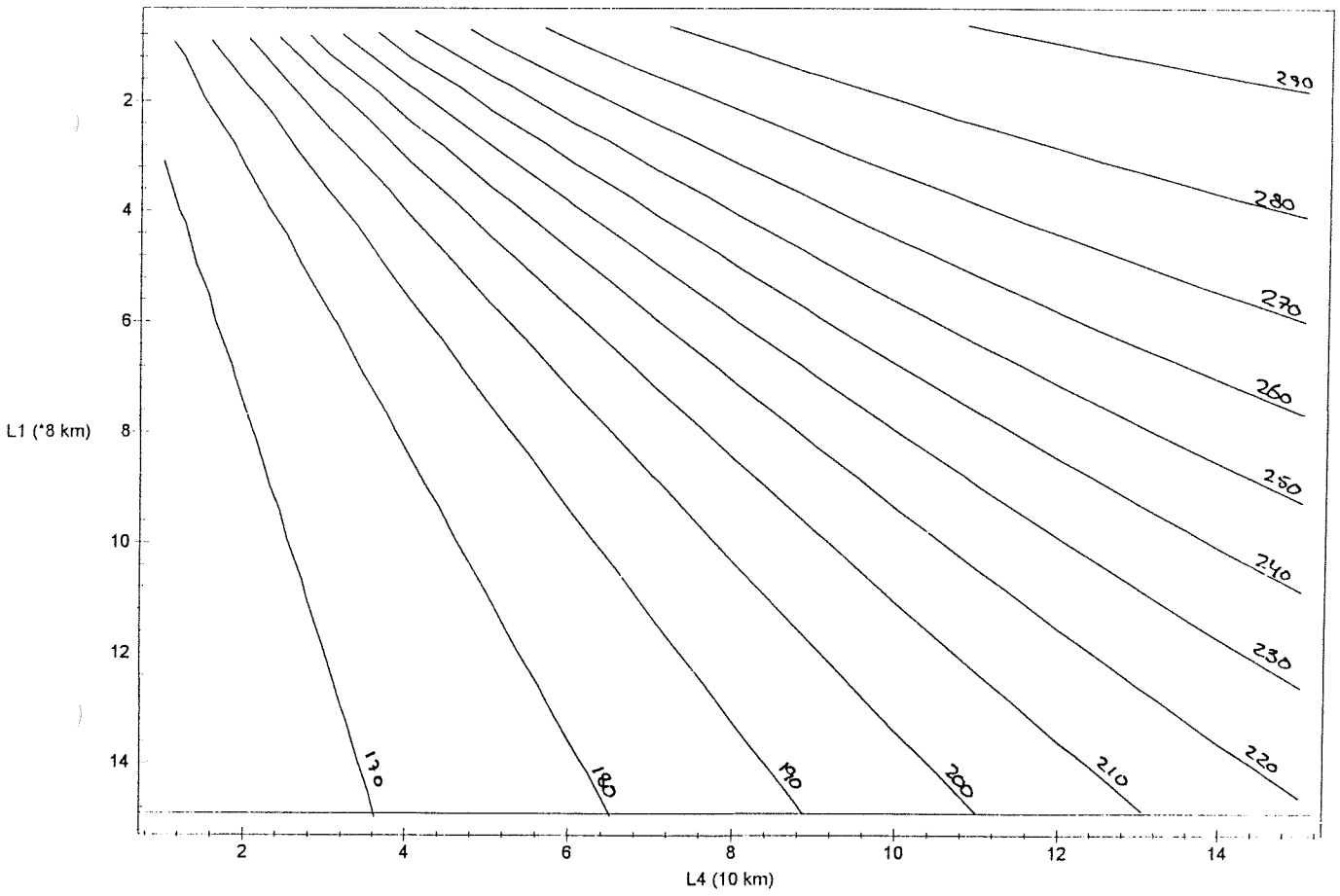

Figure A3.22 amplitude of water level at Z6 (m)

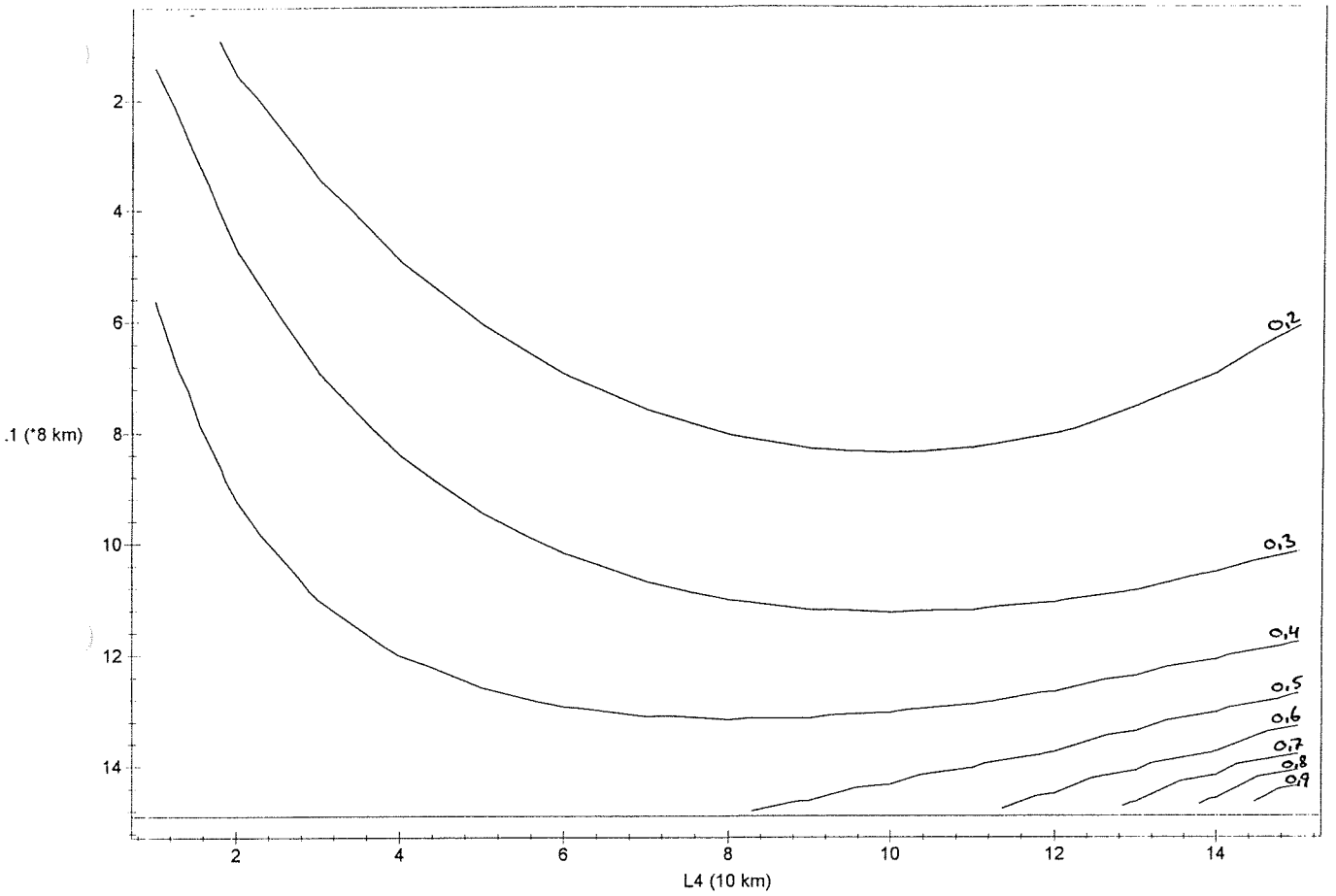

Figure A3.23 phase Z6 (degree)

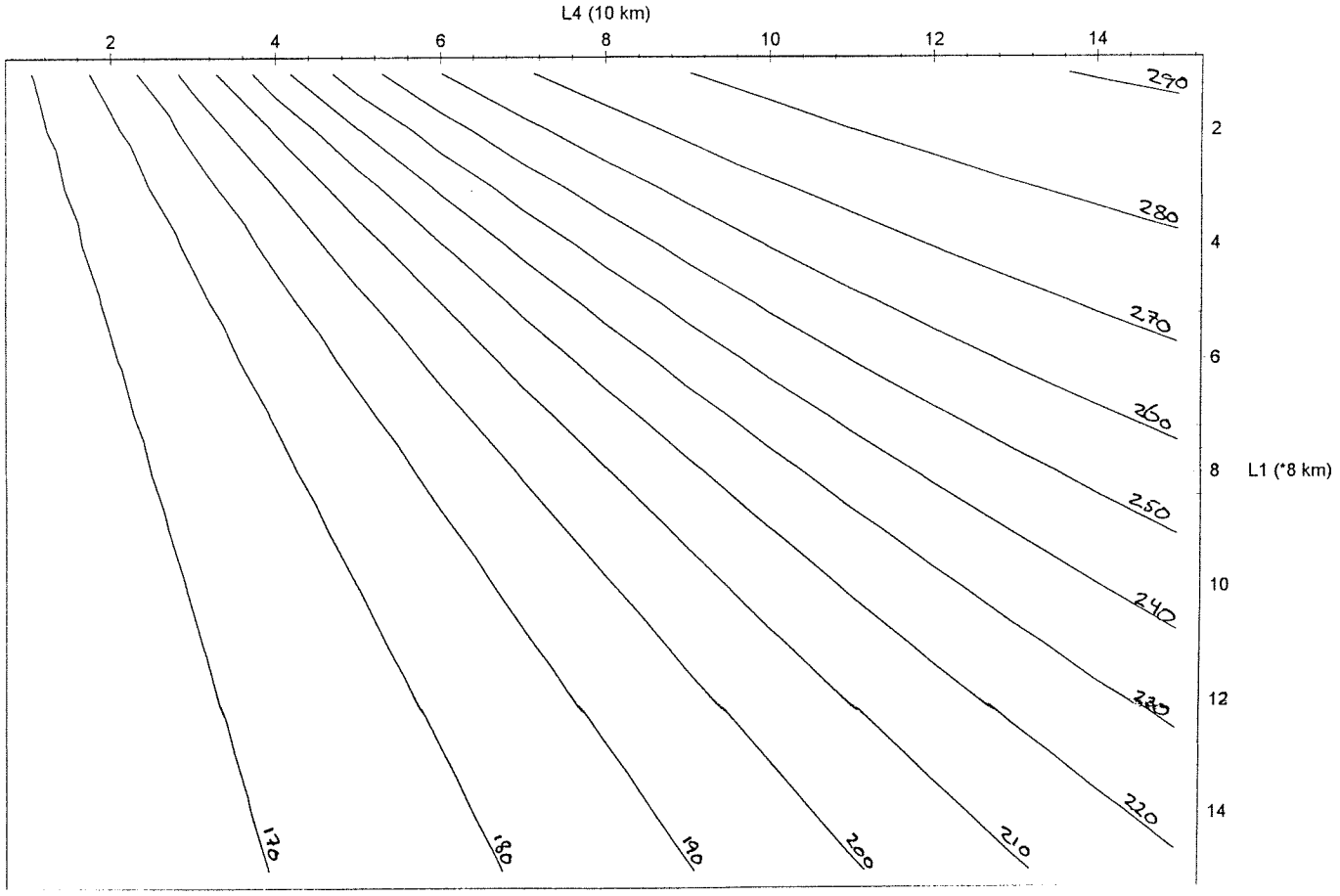

Figure A3.24 amplitude (m) of water level at Z2

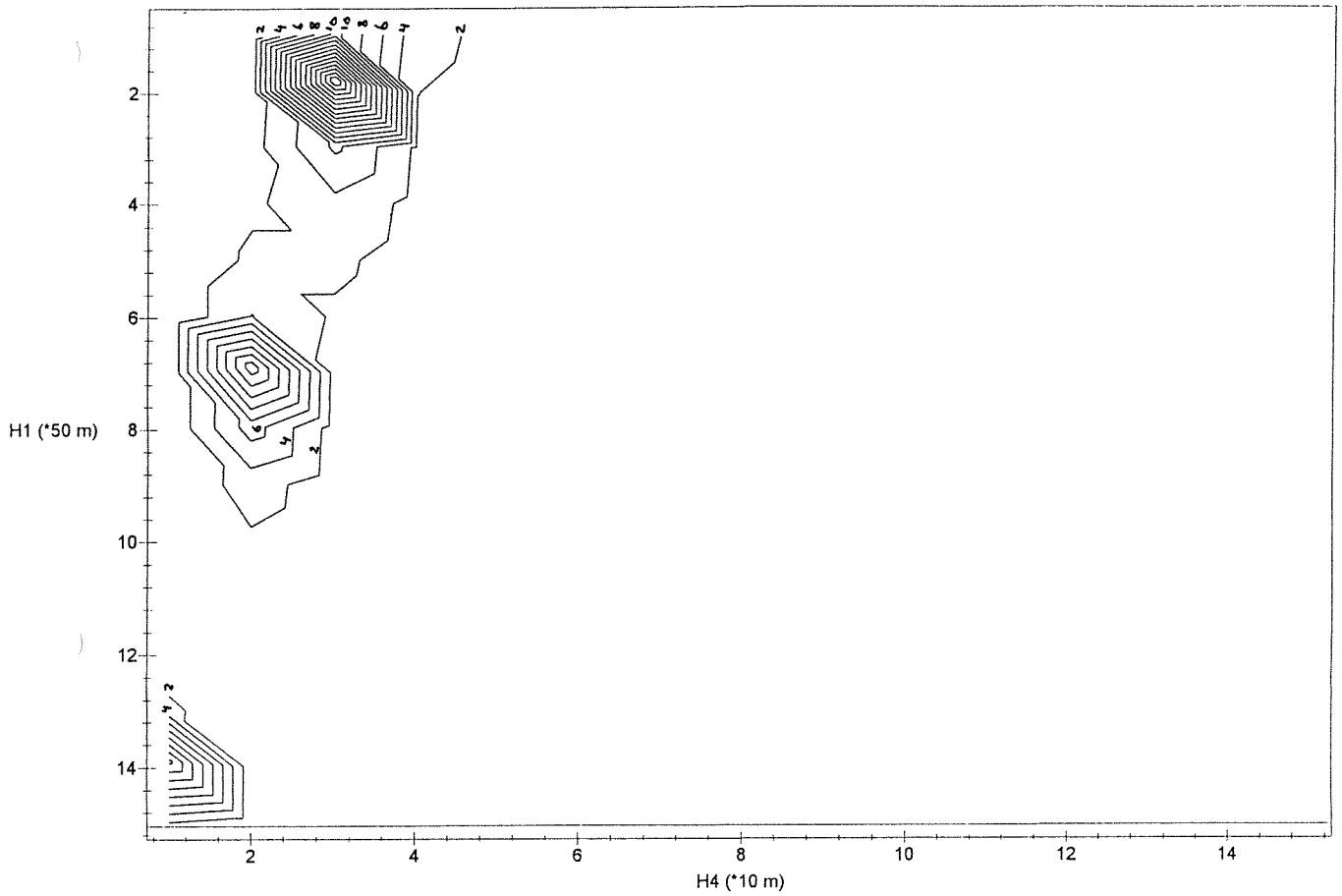

Figure A3.25 amplitude of water level at Z2 (m)

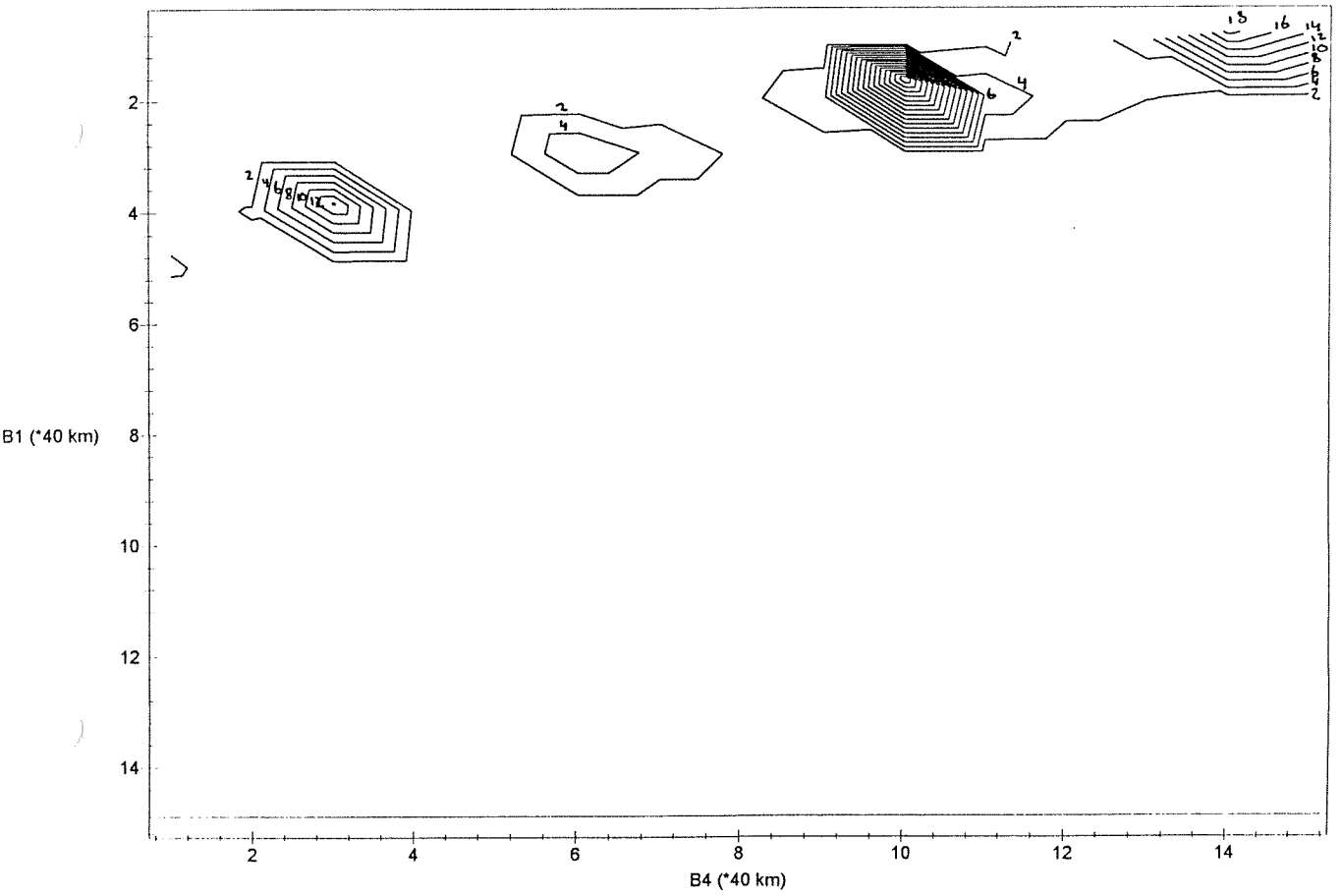

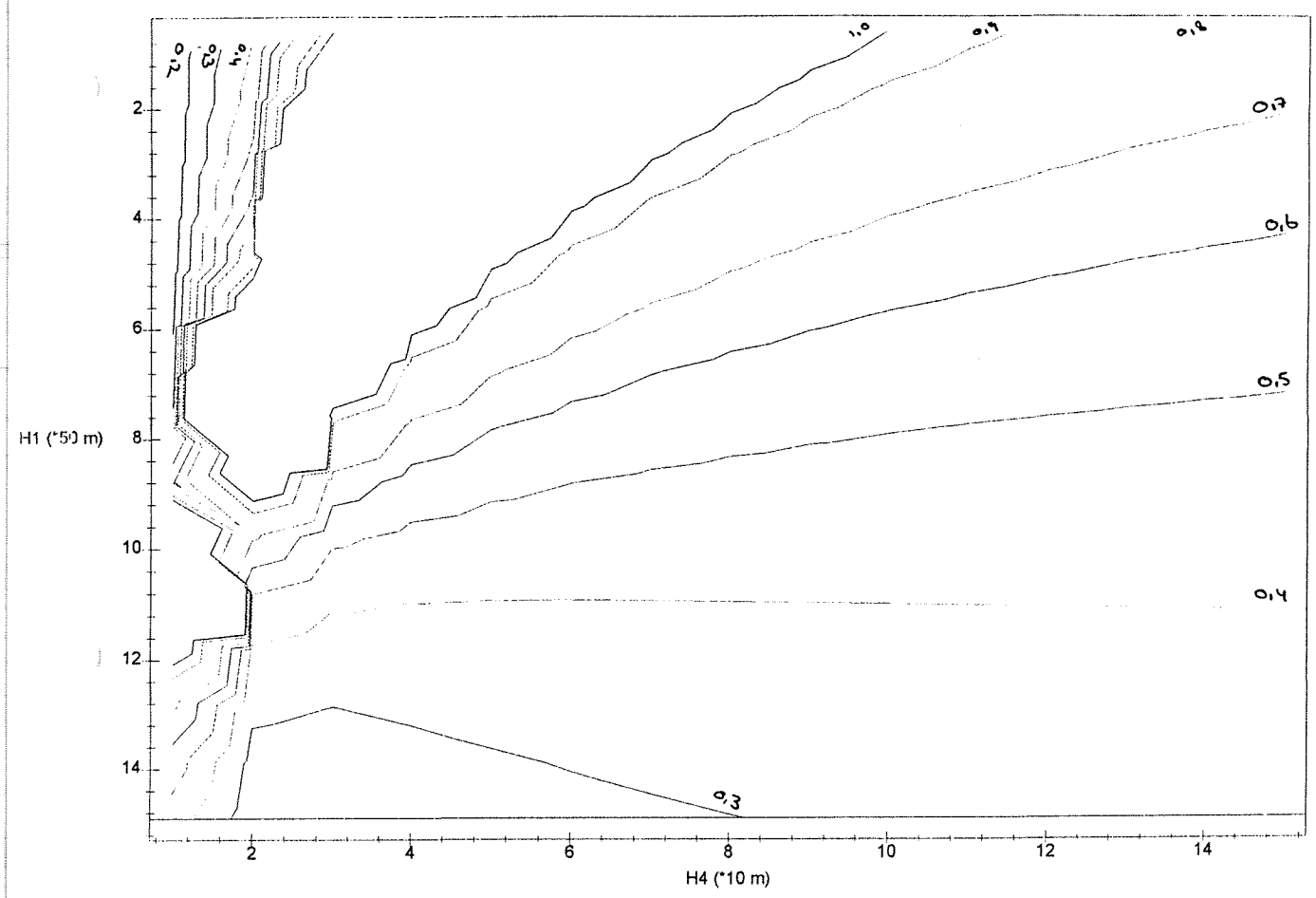

amplitude of water level at Z2 (m)

Figure A3.27

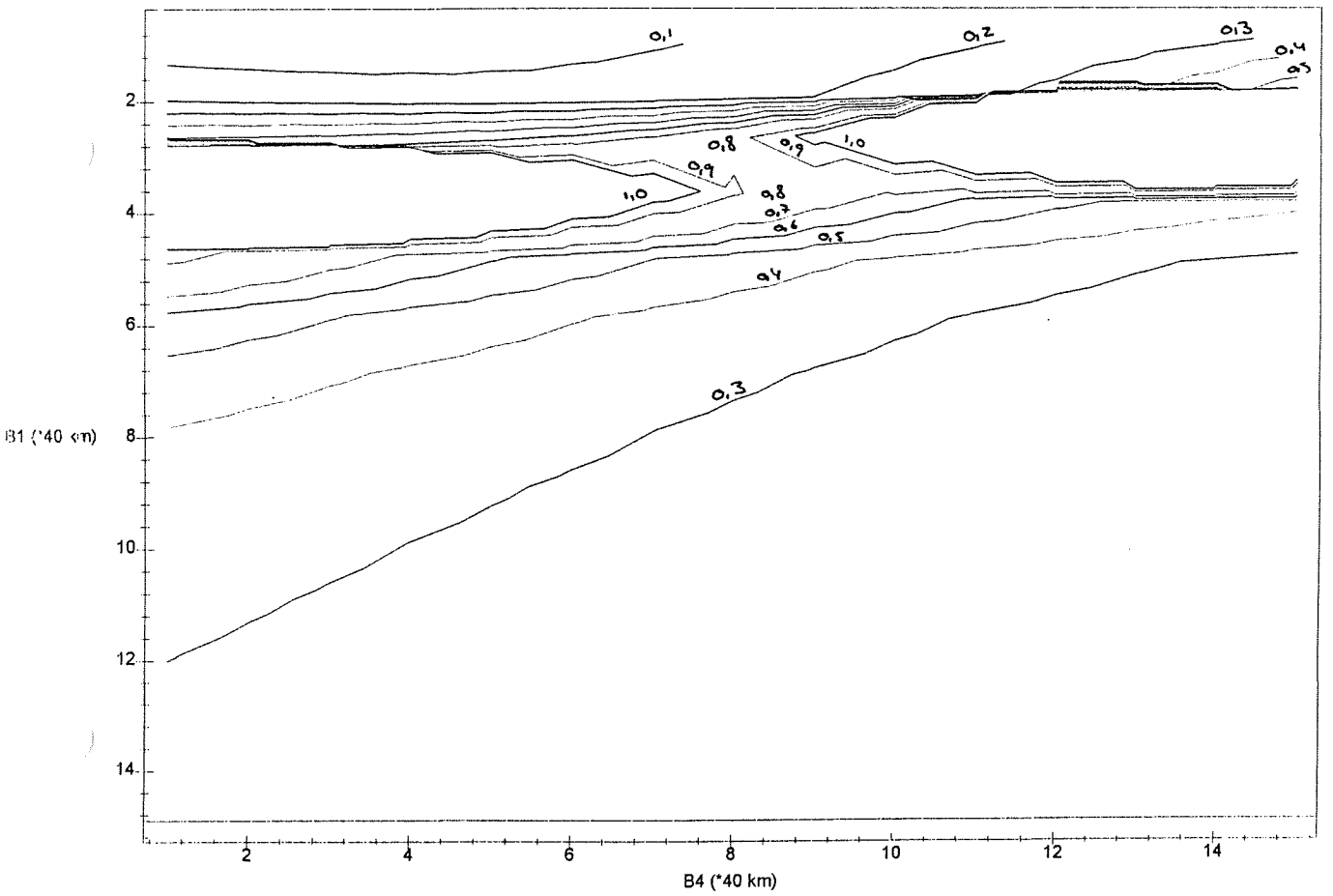

Figure A3.29

Computation 1: Solution for Z6

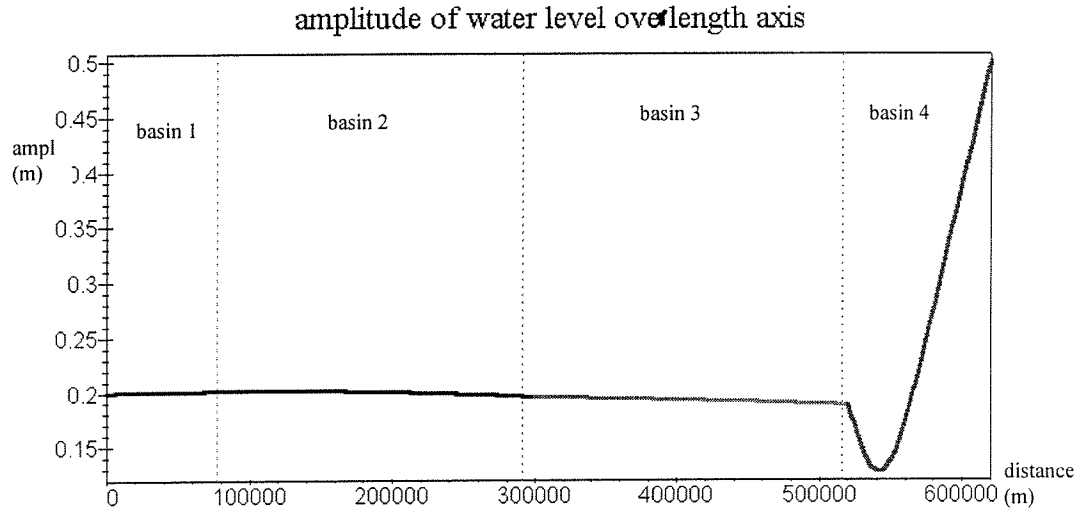

Figure A3.30

Computation 1: Soulution for Z2

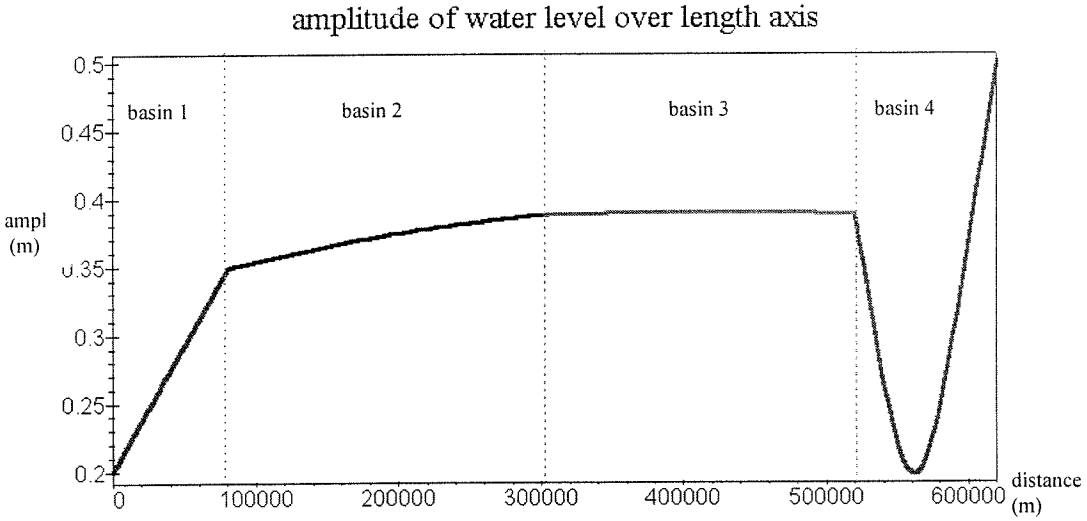

sup kenmerken toevoegen

Figure A3.31

Combination of Computations 4&5

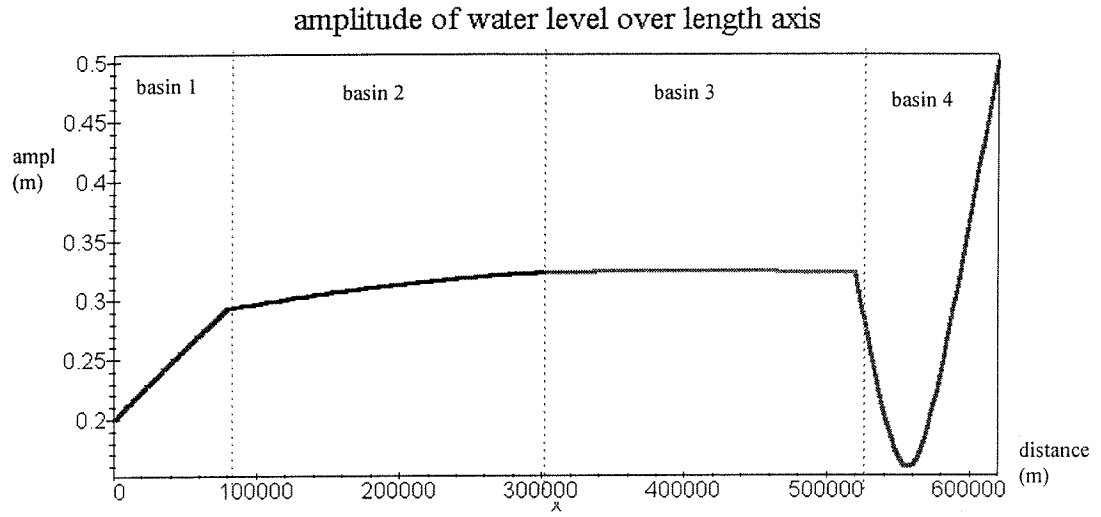

alti

Figure A3.32

Oscillation with h_1=110 m, h_4=50 m, b_1= 360 km and b_4= 240 km

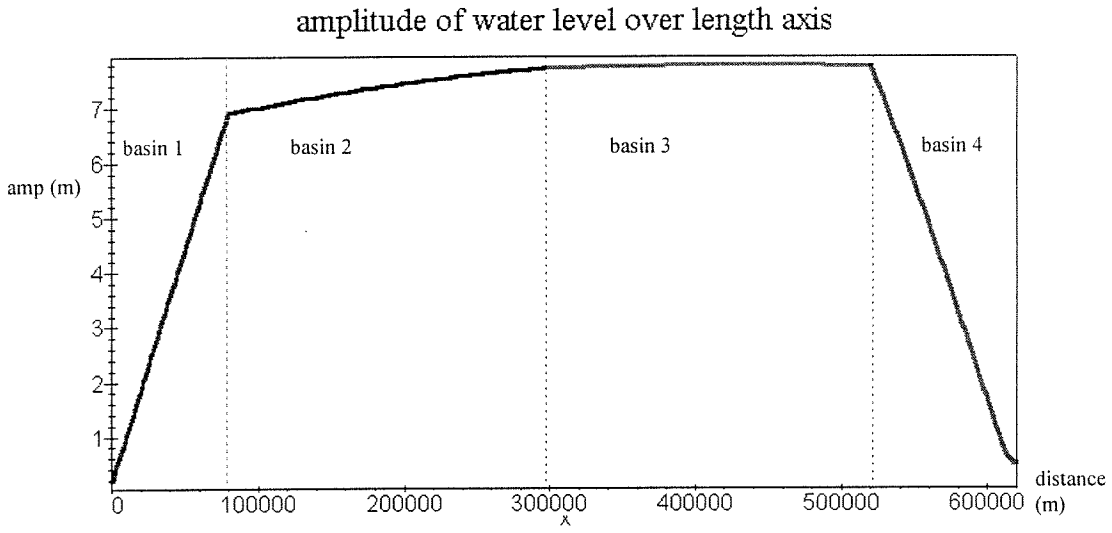

Figure A3.33

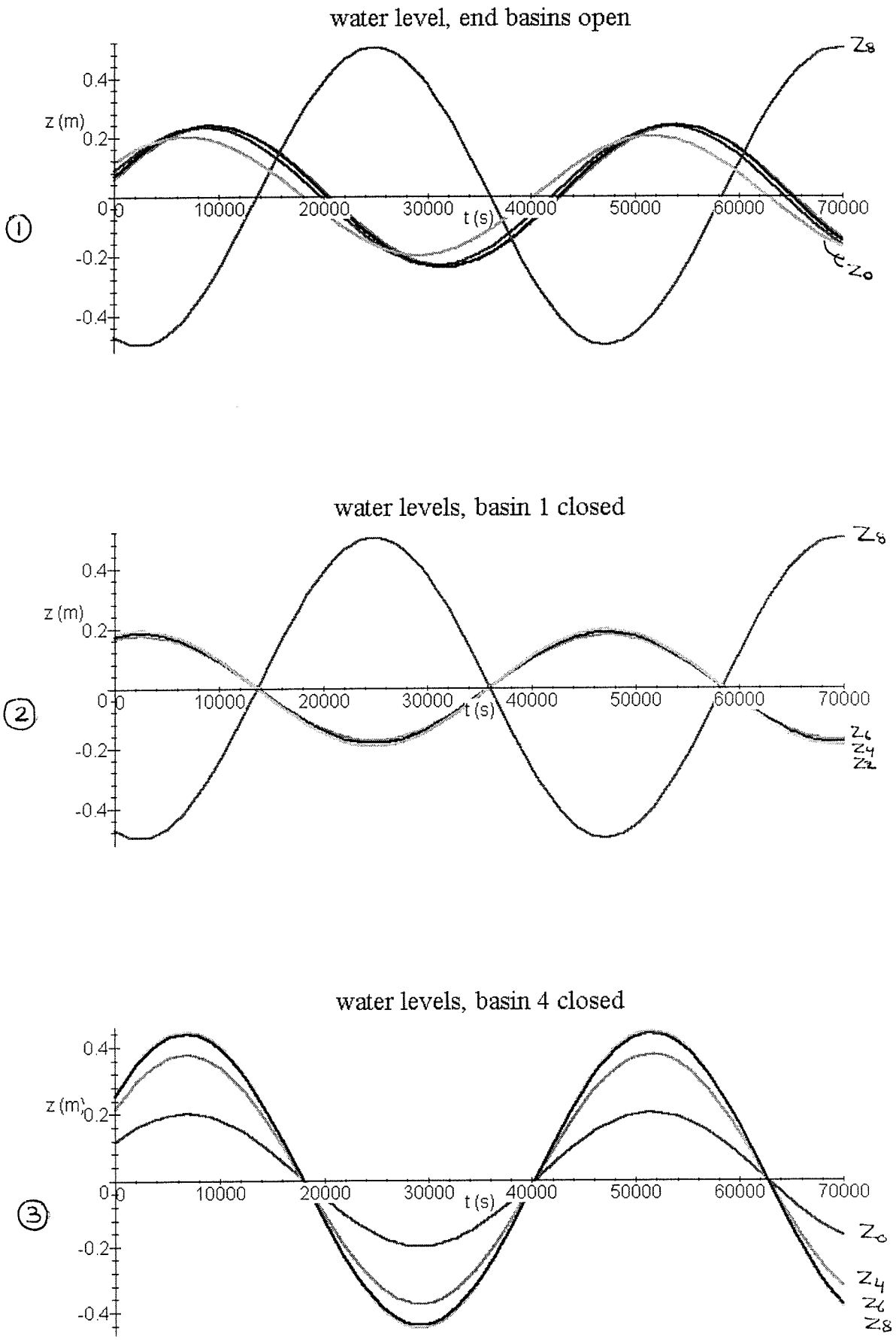
water level, end basins open
z (m)
0.4
0.2
0
-0.2
-0.4
0
10000
20000
30000
40000
50000
60000
70000
t (s)
Z8
Z0
1
water levels, basin 1 closed
z (m)
0.4
0.2
0
-0.2
-0.4
0
10000
20000
30000
40000
50000
60000
70000
t (s)
Z8
Z6
Z4
Z2
2
water levels, basin 4 closed
z (m)
0.4
0.2
0
-0.2
-0.4
0
10000
20000
30000
40000
50000
60000
70000
t (s)
Z0
Z4
Z6
Z8
3

Figure A3.34

b_1= 360 km, b_4=240 km, h_1=300 m, h_2= 60 m

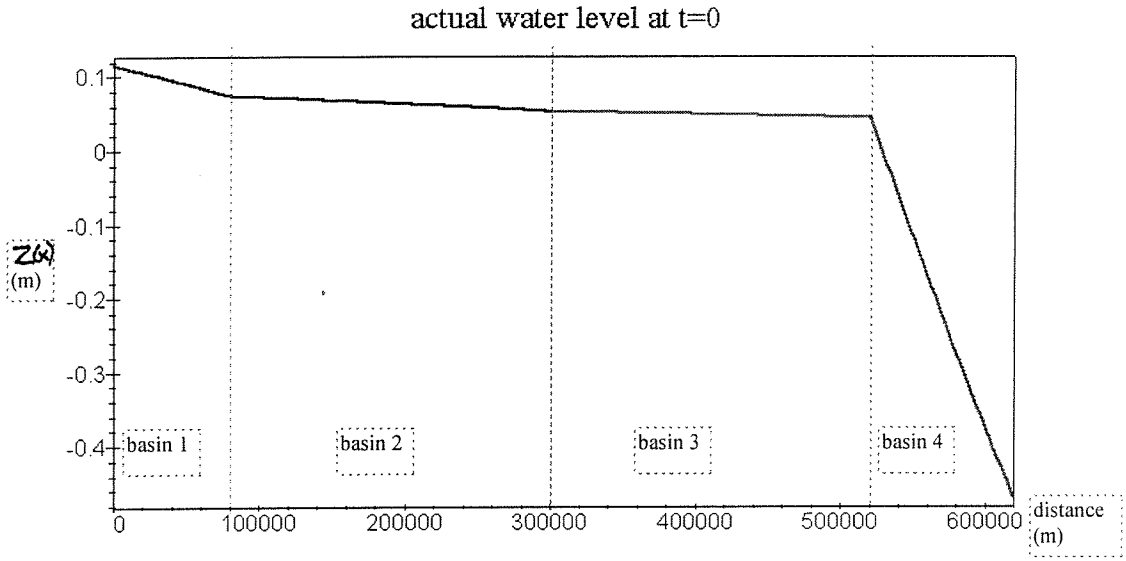

Figure A3.35

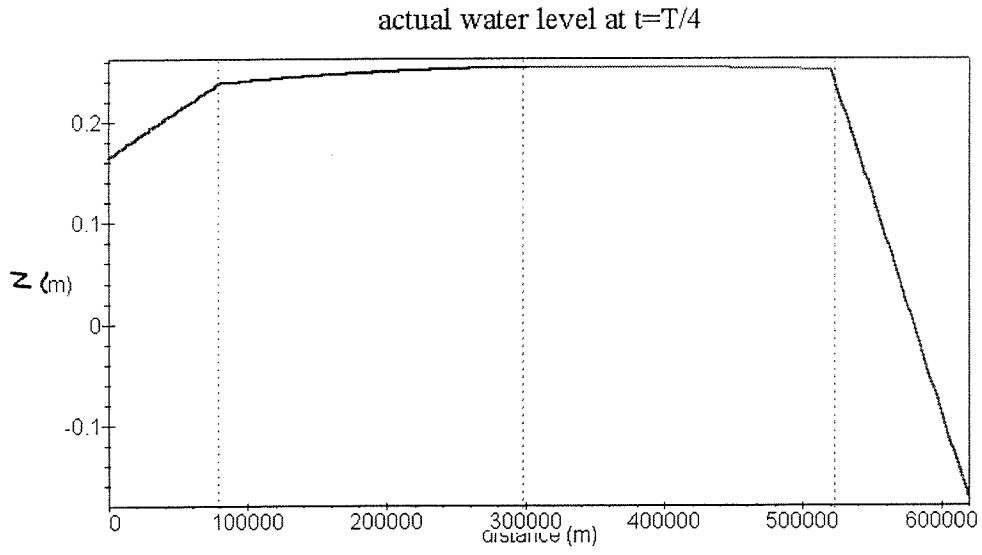

Figure A3.36

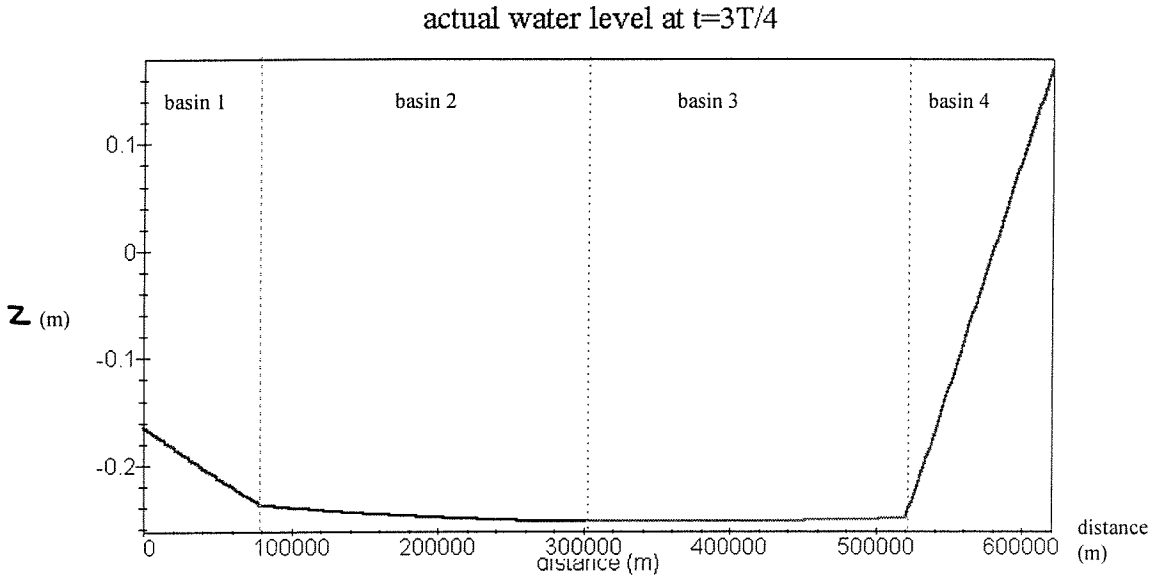

Figure A3.37

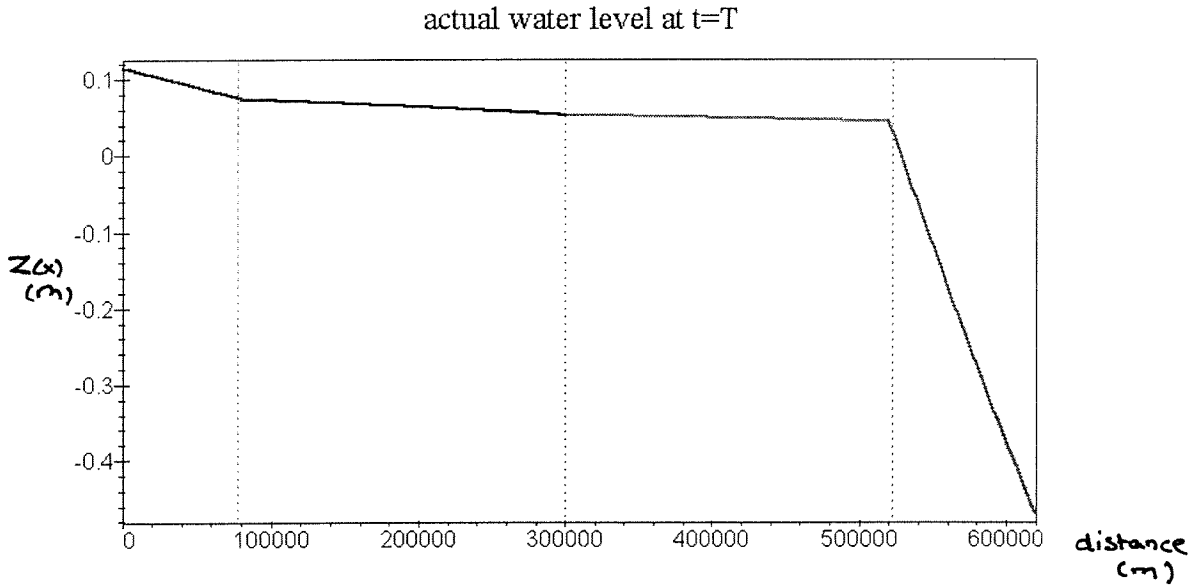

Figure A3.38

Closed boundary between basin 1 and basin 2 (v=0 prescribed)

b_4=240 km, h_1=300 m, h_2= 60 m

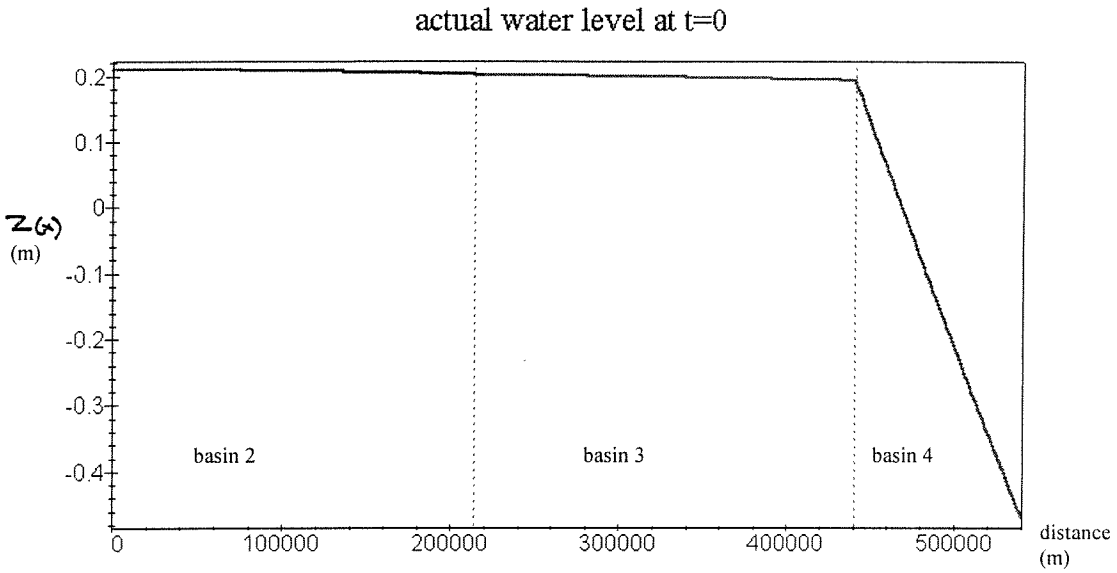

Figure A3.39

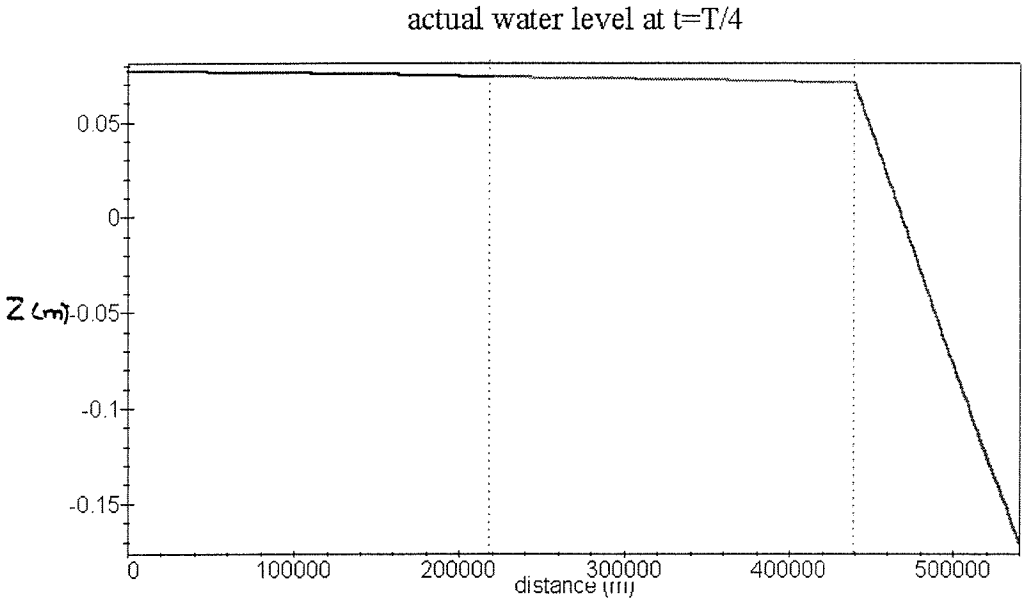

Figure A3.40

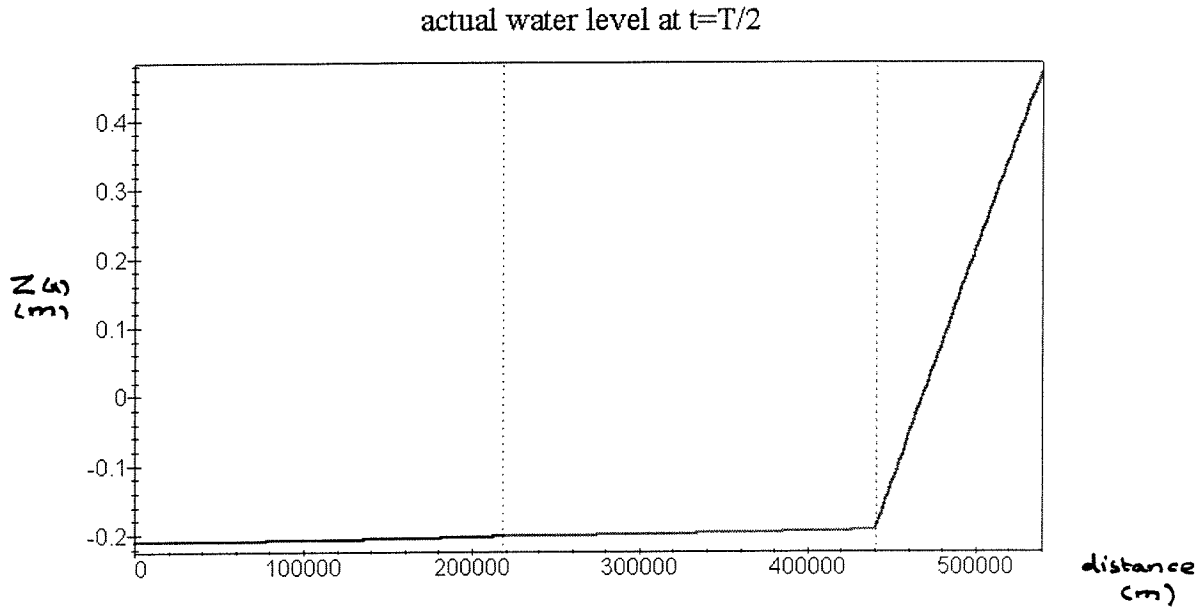

Figure A3.41

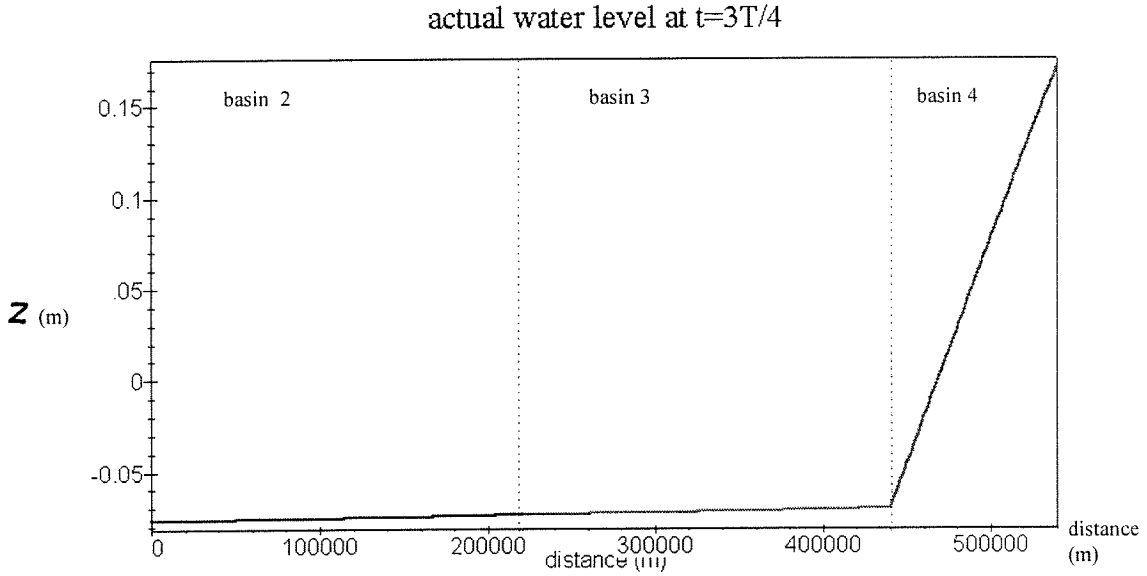

Figure A3.42 Test 1

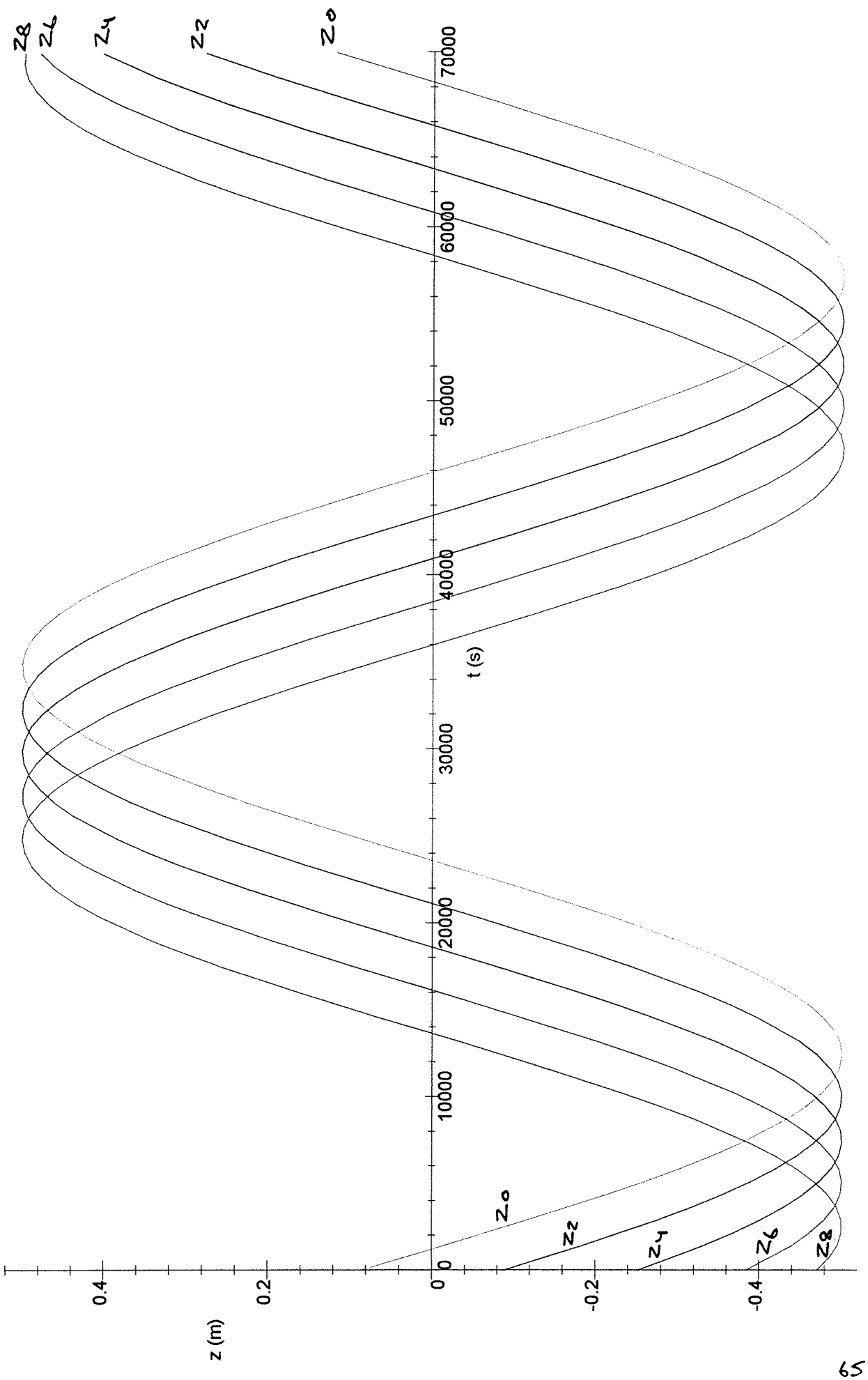

ampl ot water level:cyan=z0, red= z2,blue= z4,green= z6,magenta=z8

Figure A3.43 Test 2

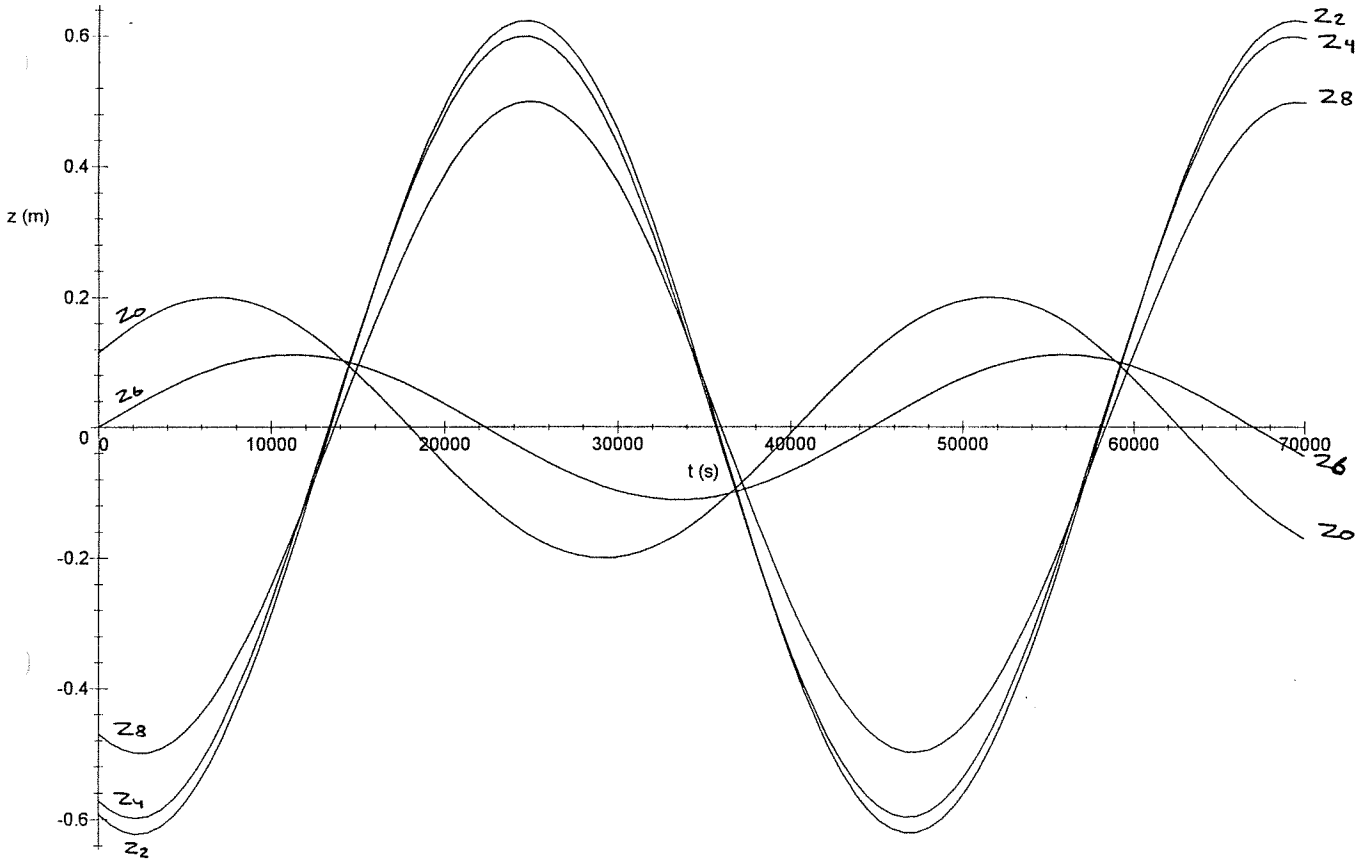

computation 1

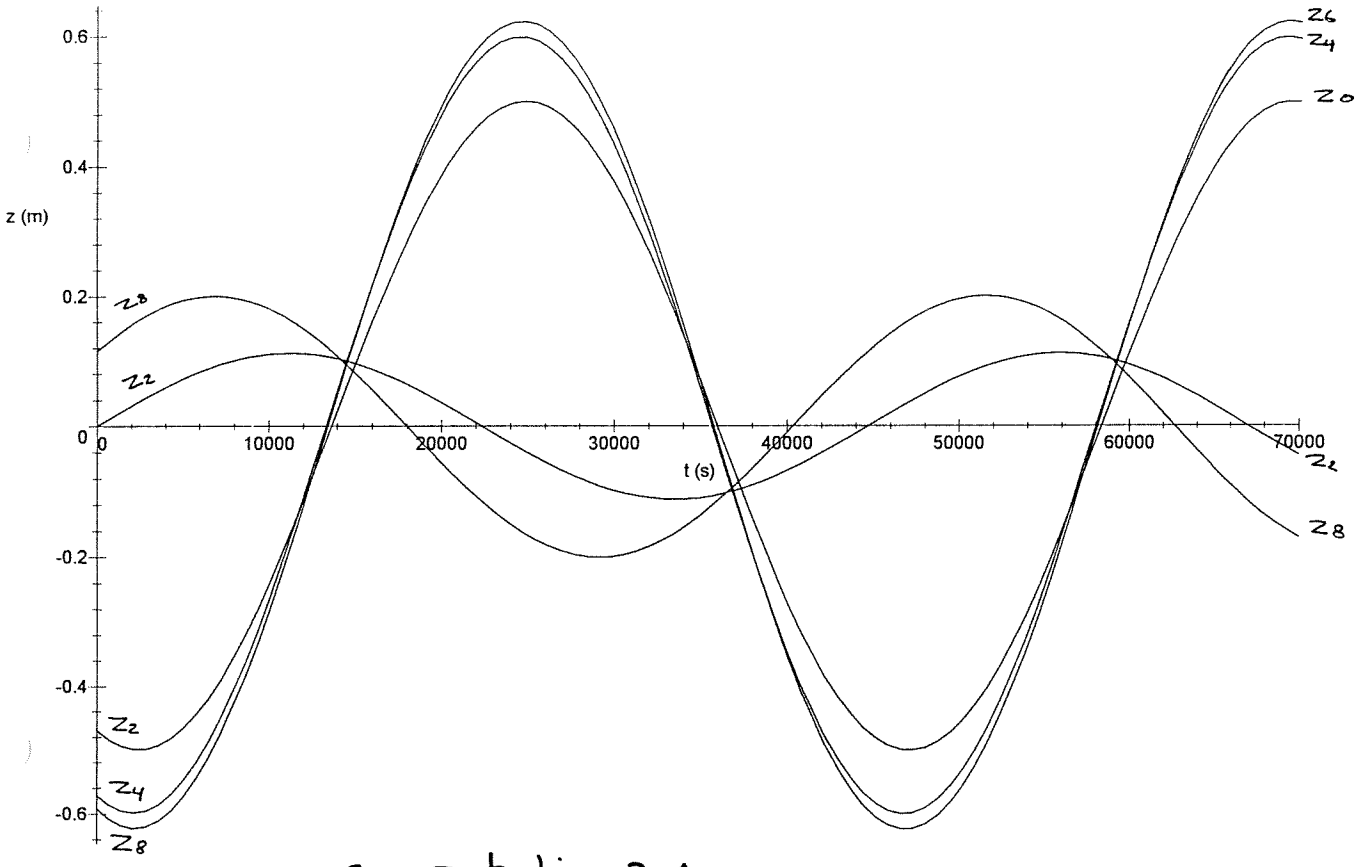

computation 2

"

Figure A3.44

Test 3

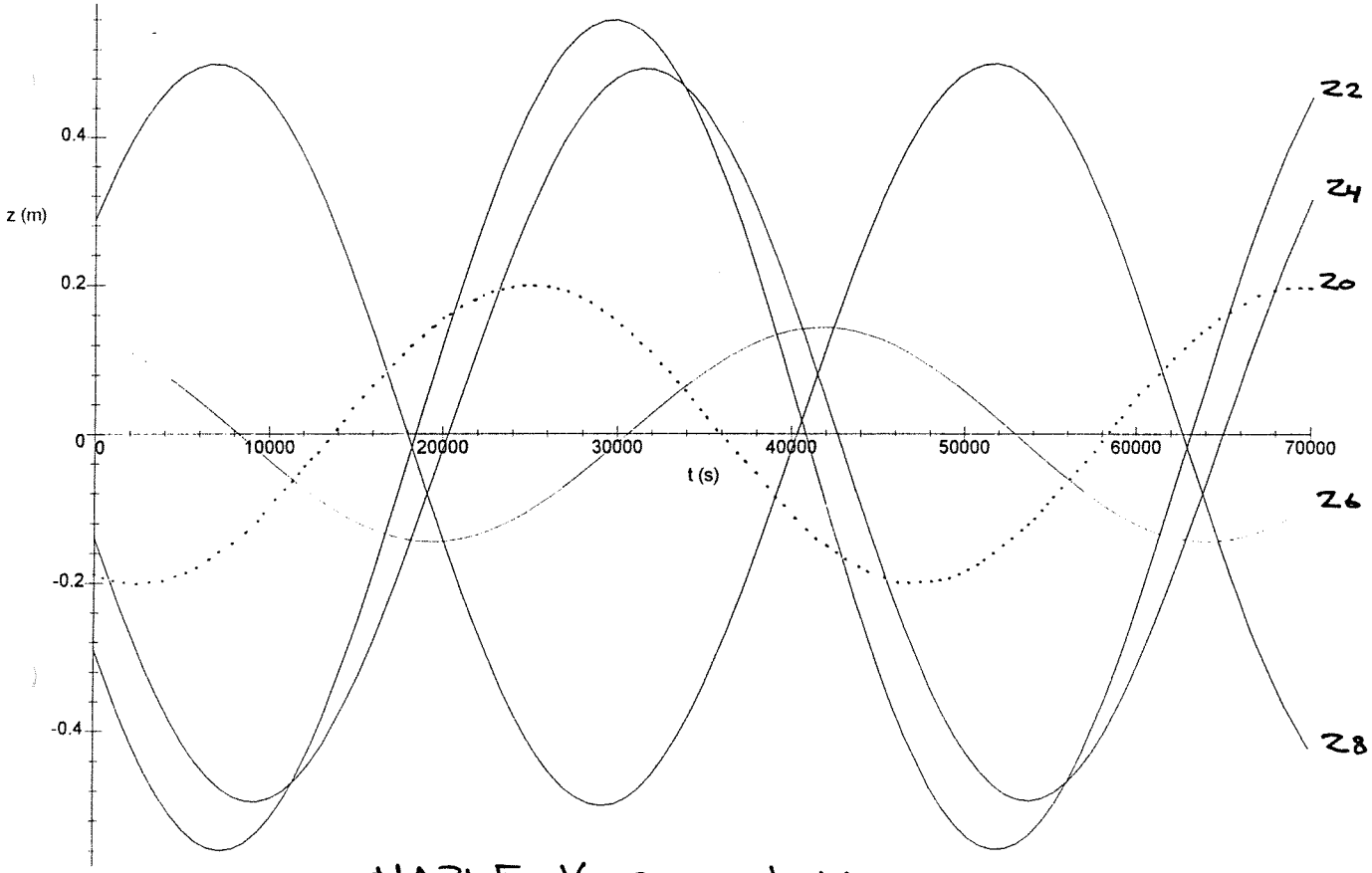

MAPLE V computation

DELFT HYDRAULICS

TRISULA computation

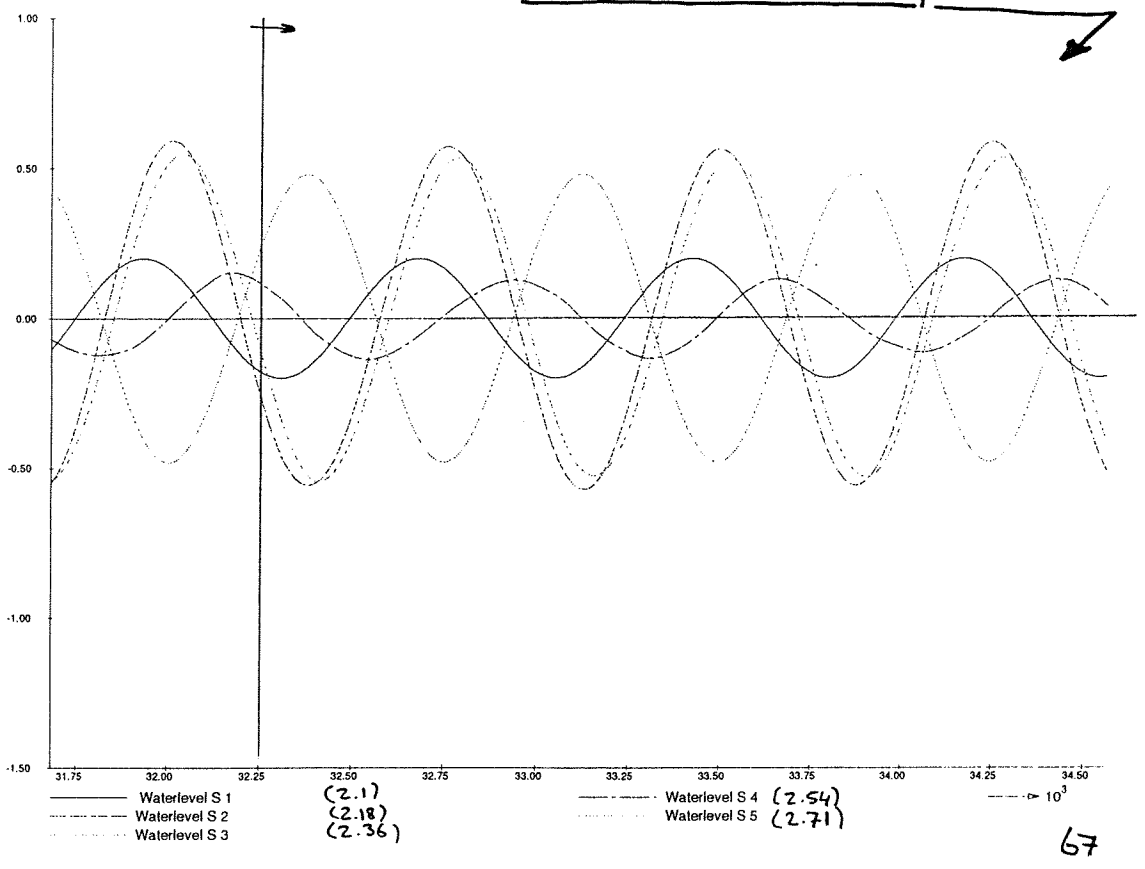

DELFT HYDRAULICS

f112

1996-08-19
11:54:46

67

Appendix 4: TRISULA computation results

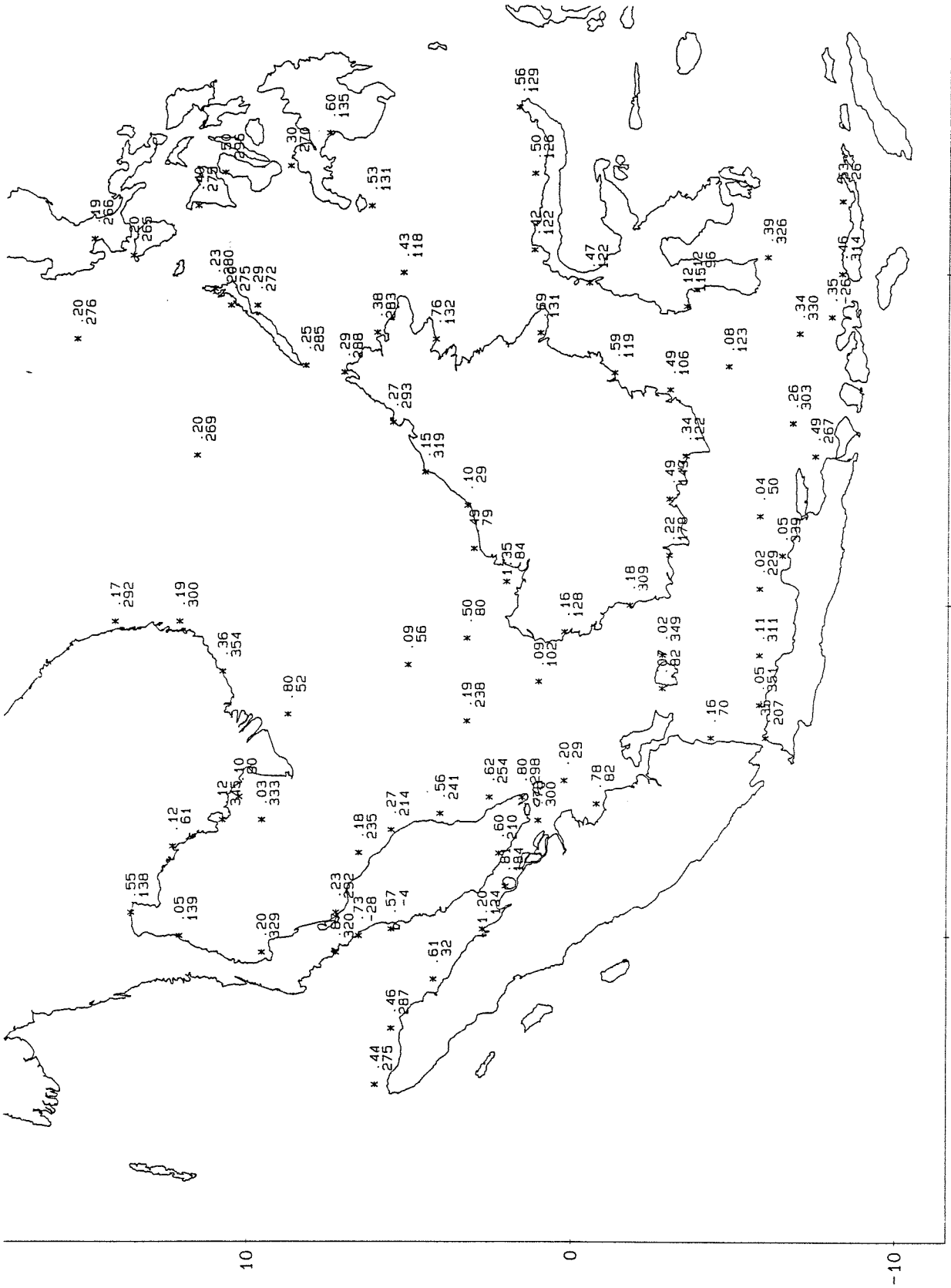

Tidal Constituent M2, in selected water level stations Observed amplitude (above) Observed phase (below)	TRISULA	
	South China Sea	
DELFT HYDRAULICS	Jun 30, 1994	**Figure A4.1**

Tidal Constituent K1, in selected water level stations
Observed amplitude (above)
Observed phase (below)

TRISULA

South China Sea

DELFT HYDRAULICS

Jun 30, 1994

Figure A4.2

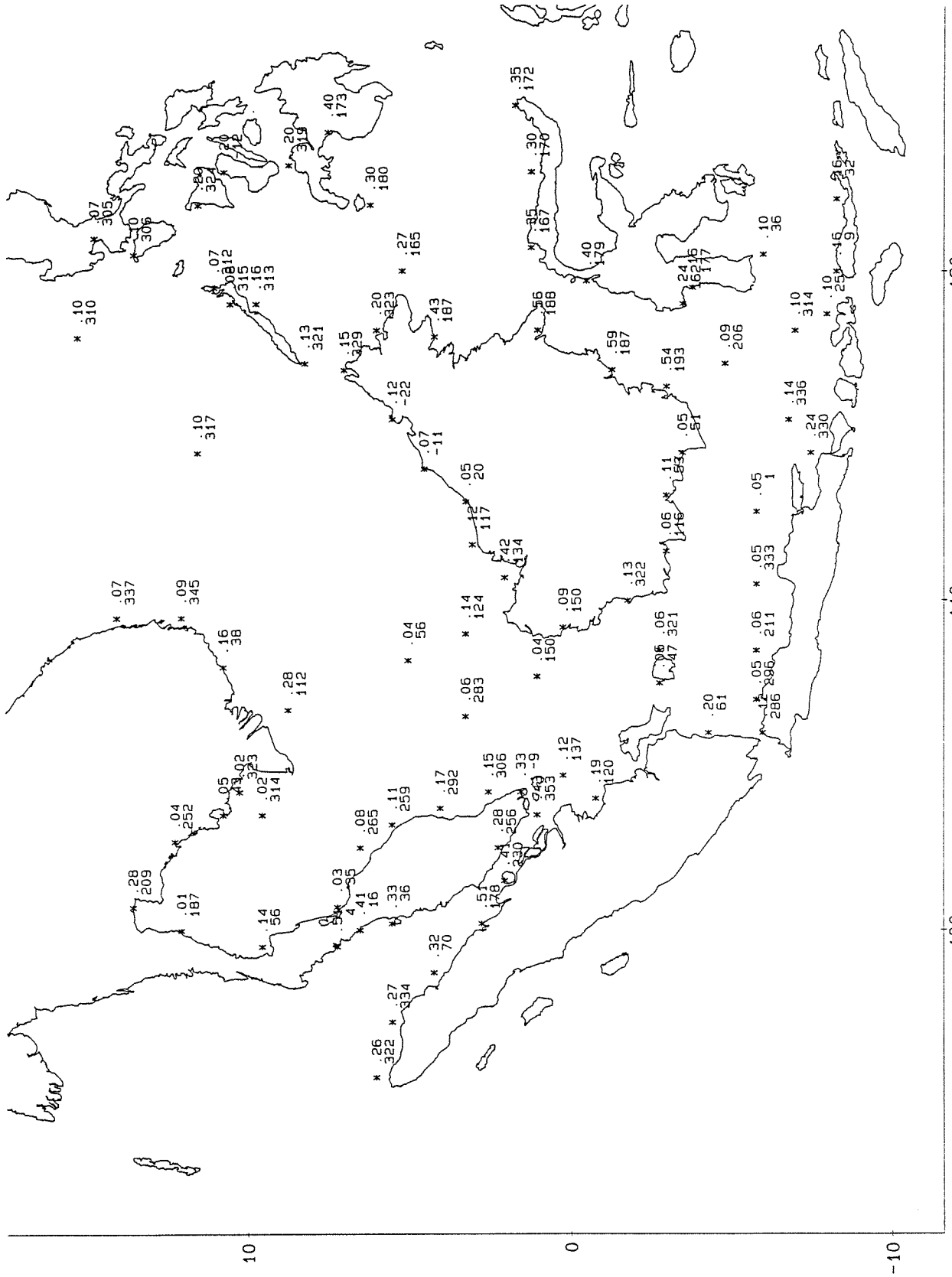

Tidal Constituent S2, in selected water level stations
Observed amplitude (above)
Observed phase (below)

TRISULA

South China Sea

DELFT HYDRAULICS

Jun 30, 1994

Figure A4.3

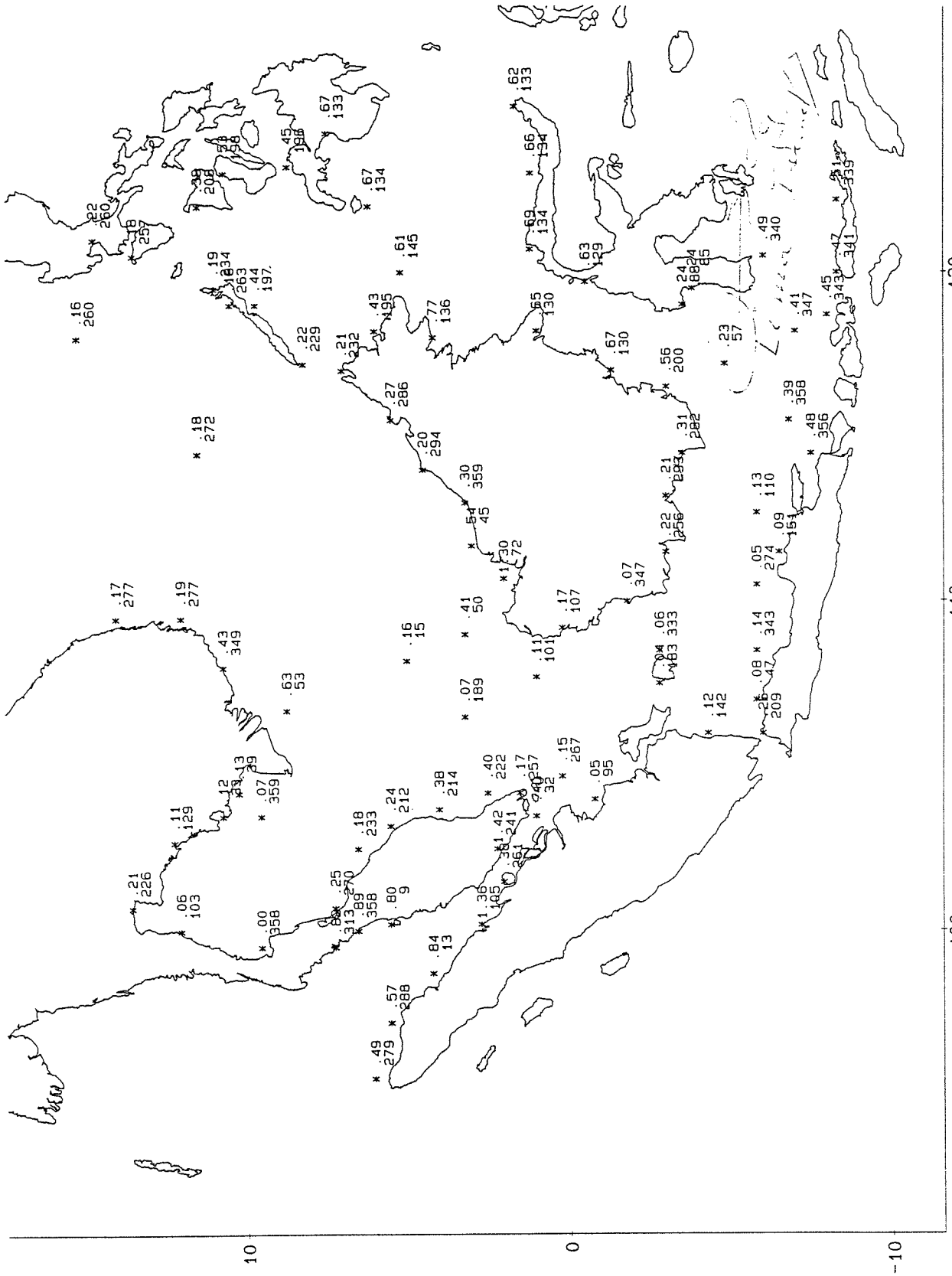

Tidal Constituent M2, in selected water level stations Computed amplitude (above) Computed phase (below)	TRISULA	g13
	South China Sea	
DELFT HYDRAULICS	Jun 30, 1994	**Figure A4.4**

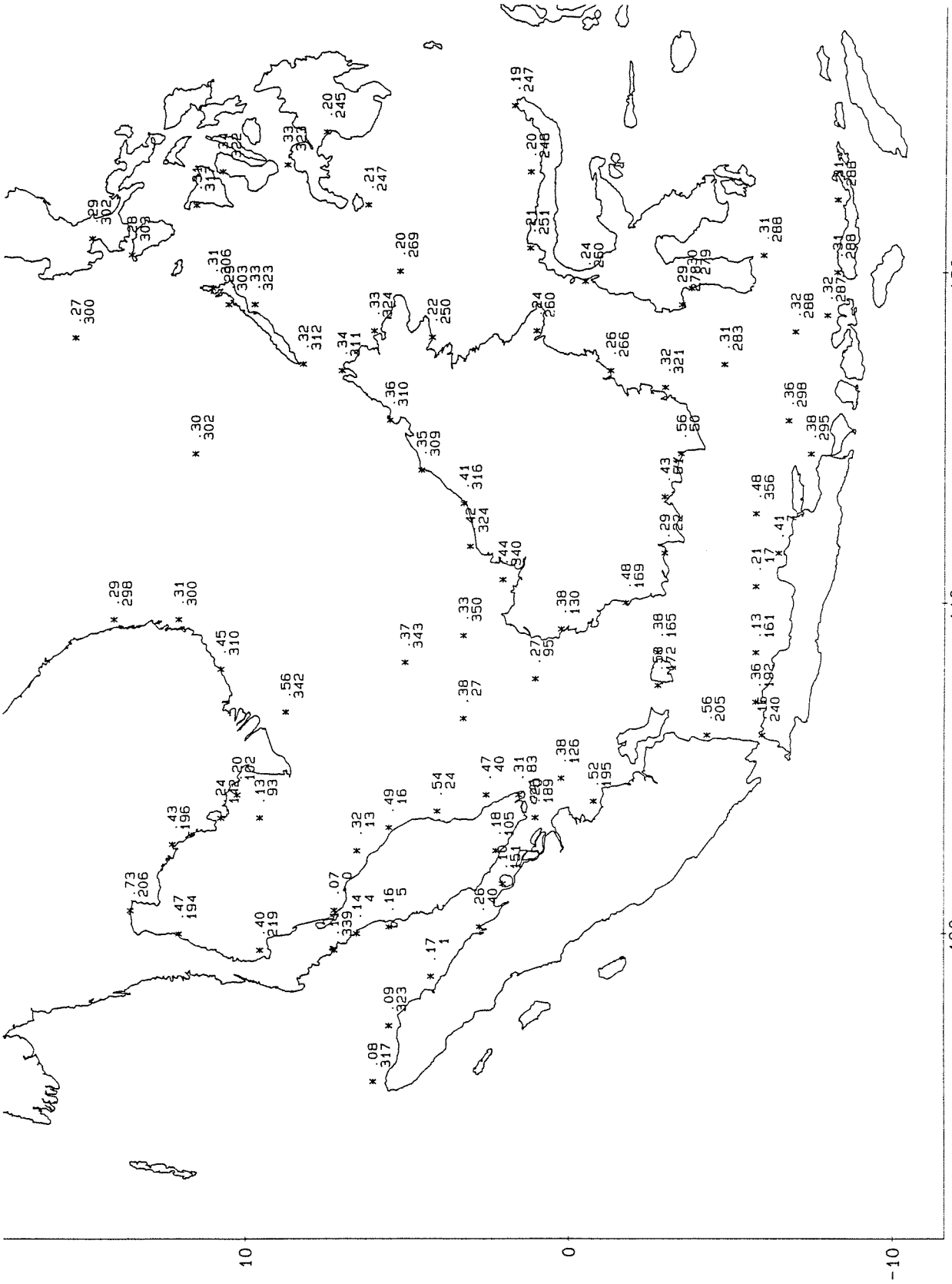

Tidal Constituent K1, in selected water level stations Computed amplitude (above) Computed phase (below)	TRISULA	g13
	South China Sea	
DELFT HYDRAULICS	Jun 30, 1994	**Figure A4.5**

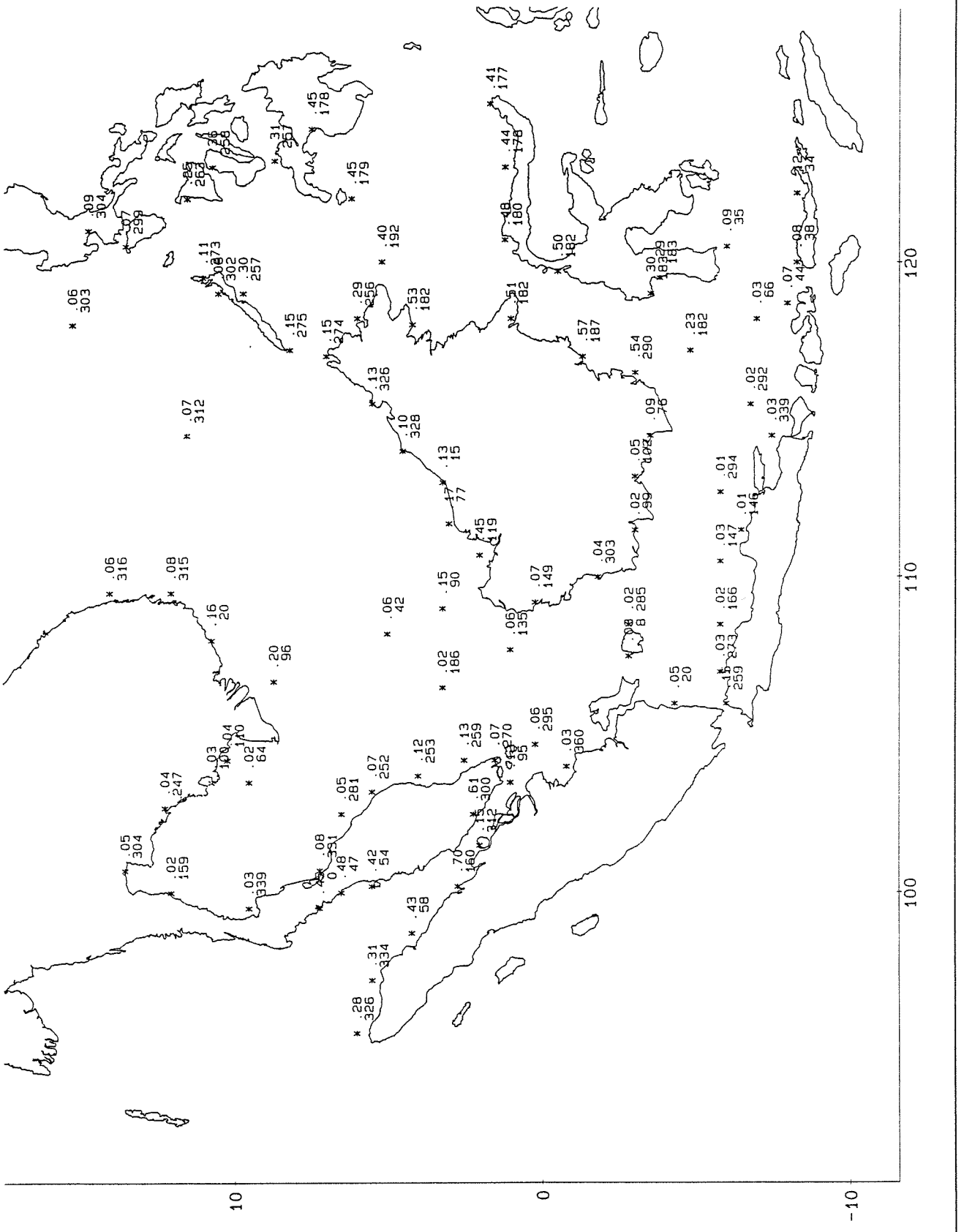

Tidal Constituent S2, in selected water level stations Computed amplitude (above) Computed phase (below)	TRISULA	g13
	South China Sea	
DELFT HYDRAULICS	Jun 30, 1994	***Figure A4.6***

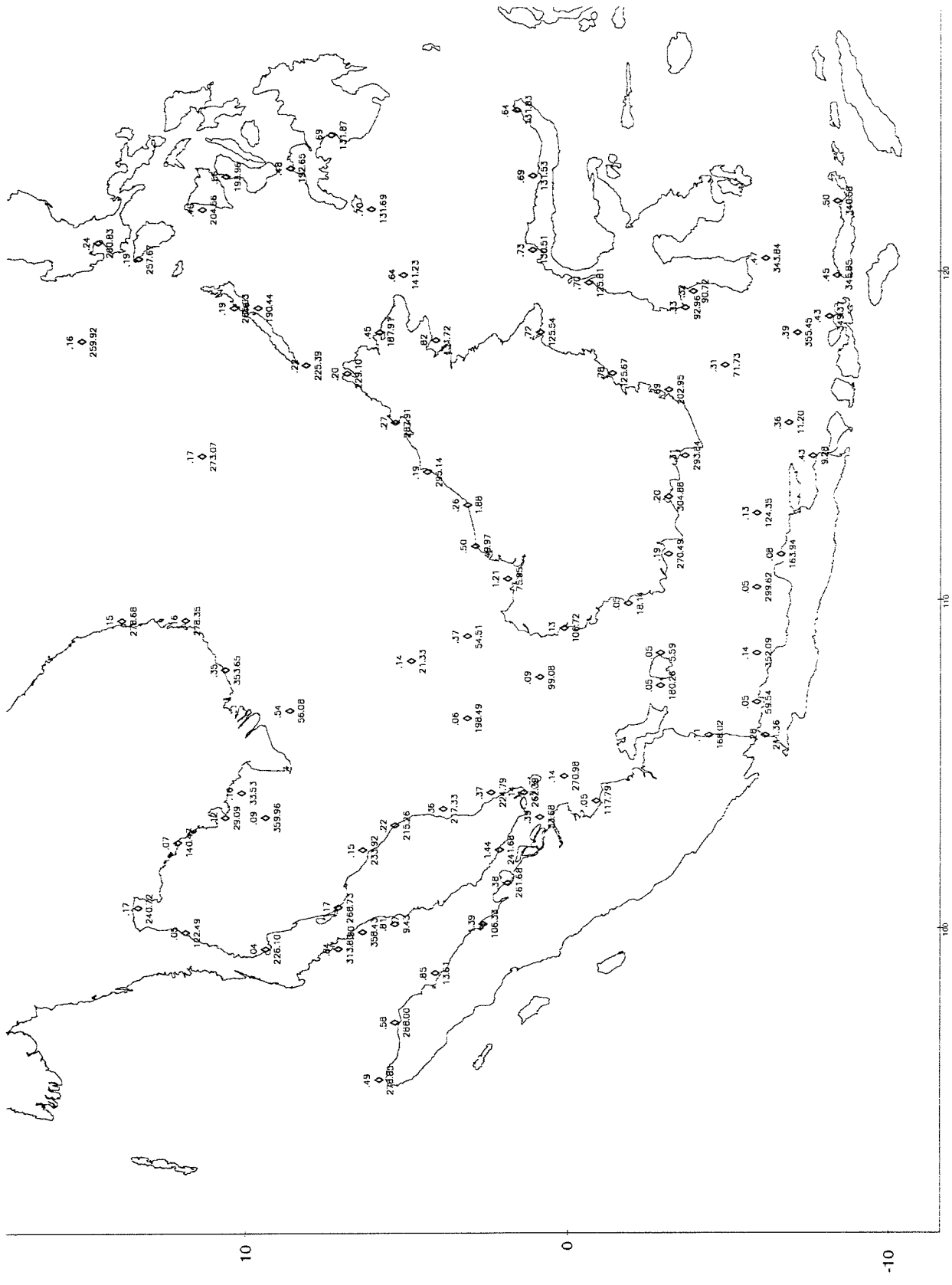

Tidal Constituent M2, in selected water level stations
Computed amplitude (above)
Computed phase (below)

TRISULA | C01

South China Sea

DELFT HYDRAULICS

Figure A4.7

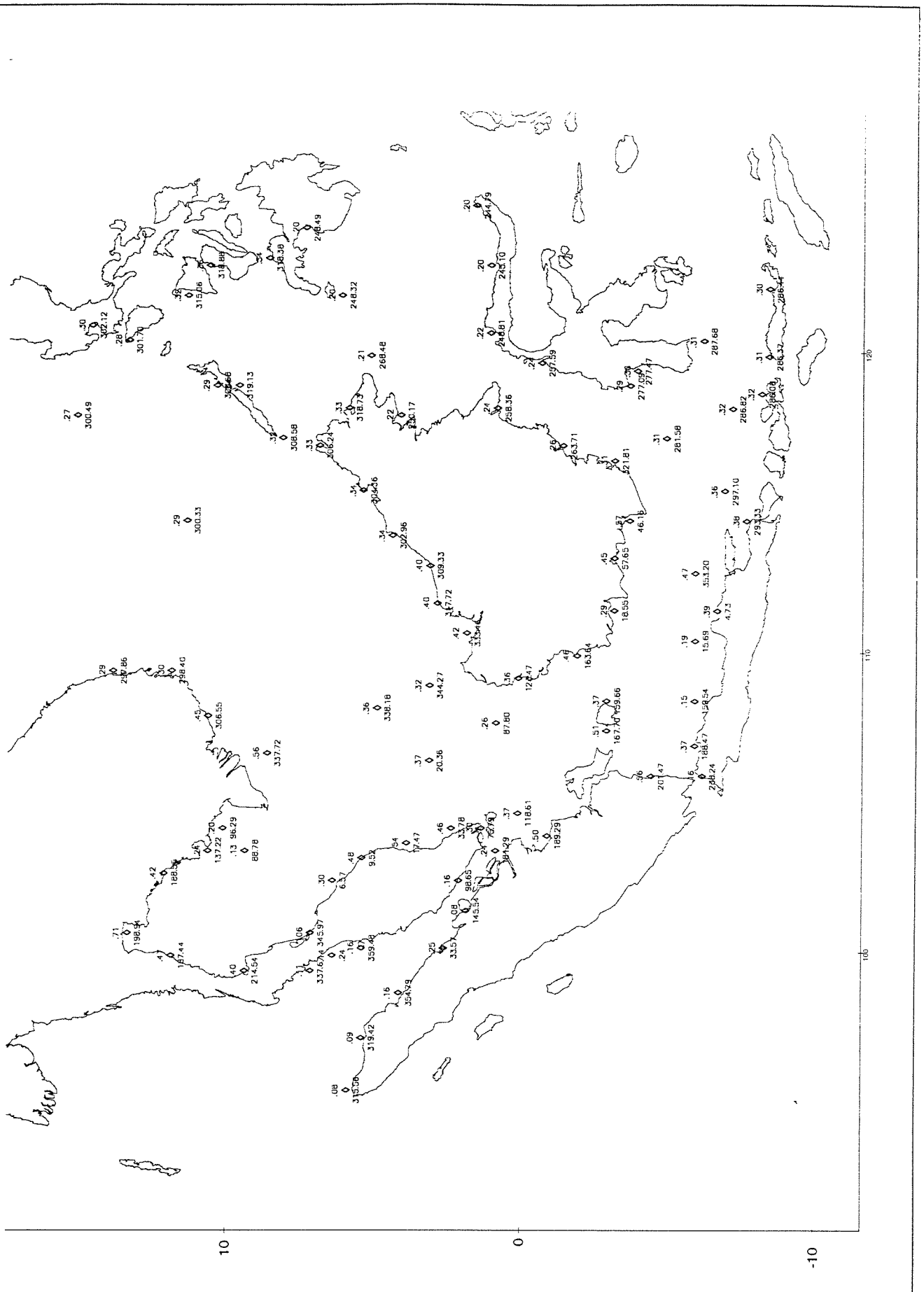

Tidal Constituent K1, in selected water level stations
Computed amplitude (above)
Computed phase (below)

TRISULA | C01

South China Sea

DELFT HYDRAULICS

Figure A4.8

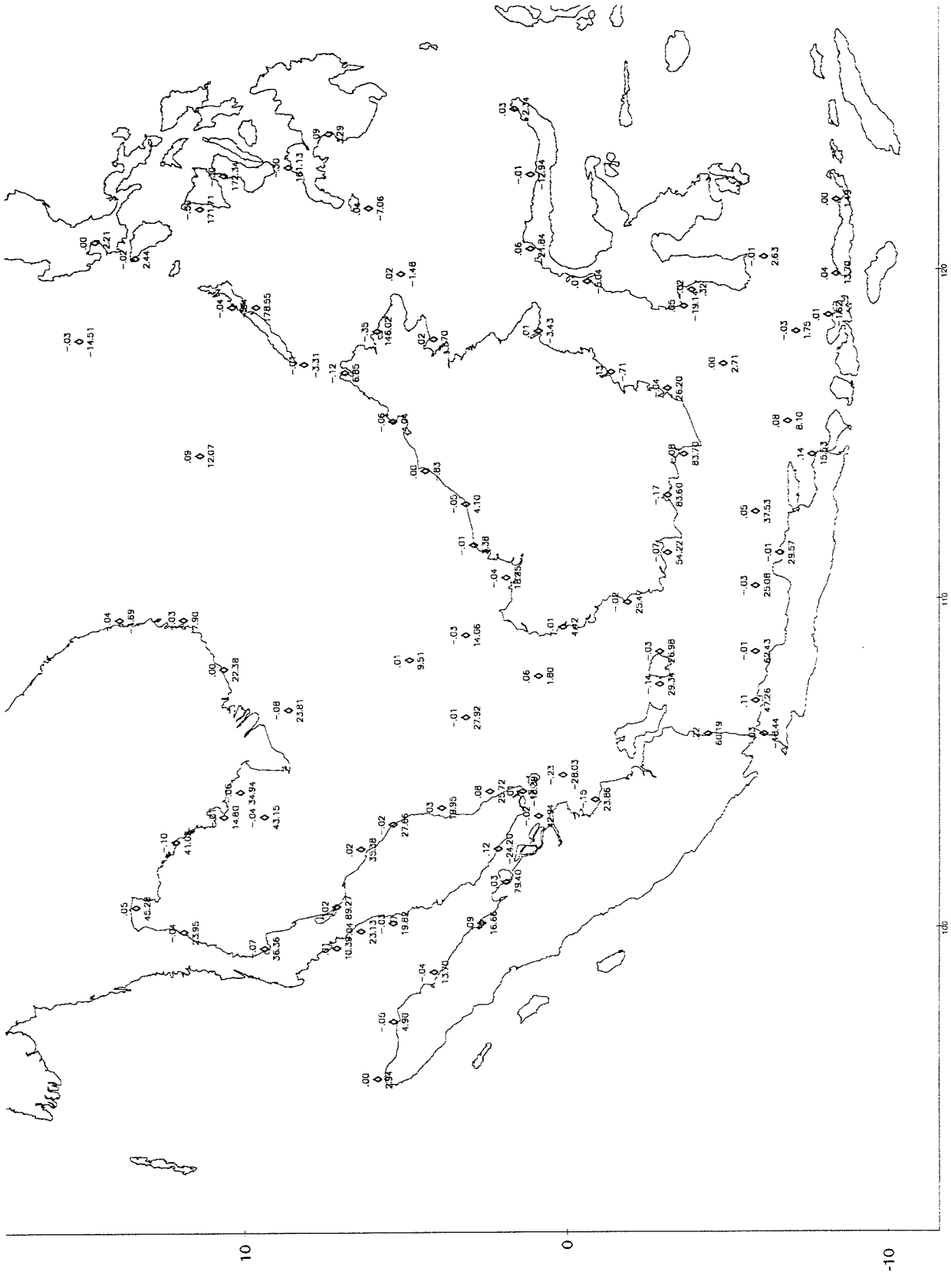

Tidal Constituent K1, in selected water level stations
Amplitude difference, computed – observed)
Phase difference (below, computed – observed)

TRISULA	*C01*
South China Sea	
DELFT HYDRAULICS	***Figure A4.9***

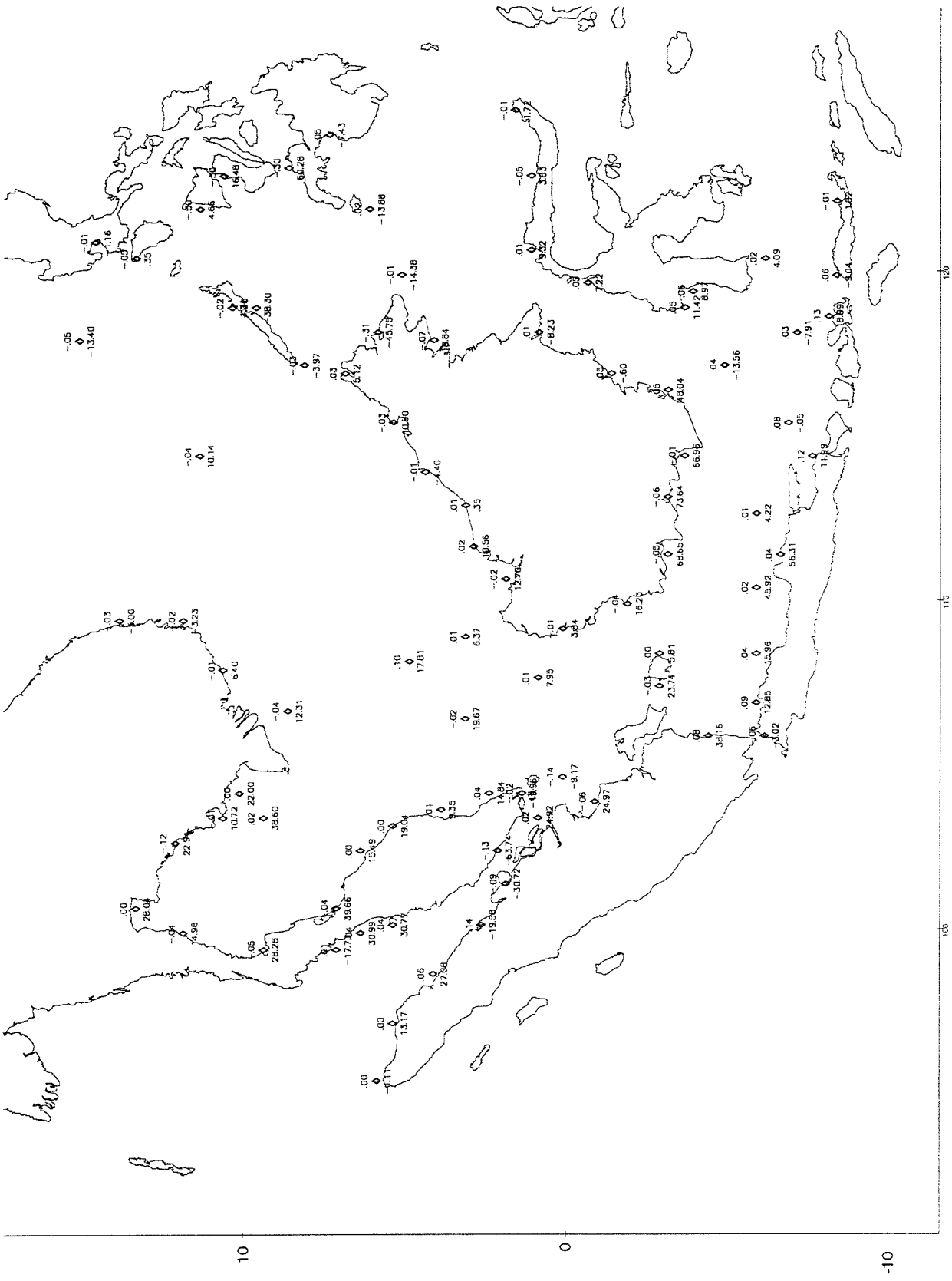

Tidal Constituent O1, in selected water level stations Amplitude difference, computed – observed) Phase difference (below, computed – observed)	TRISULA	*C01*
	South China Sea	
DELFT HYDRAULICS		***Figure A4.10***

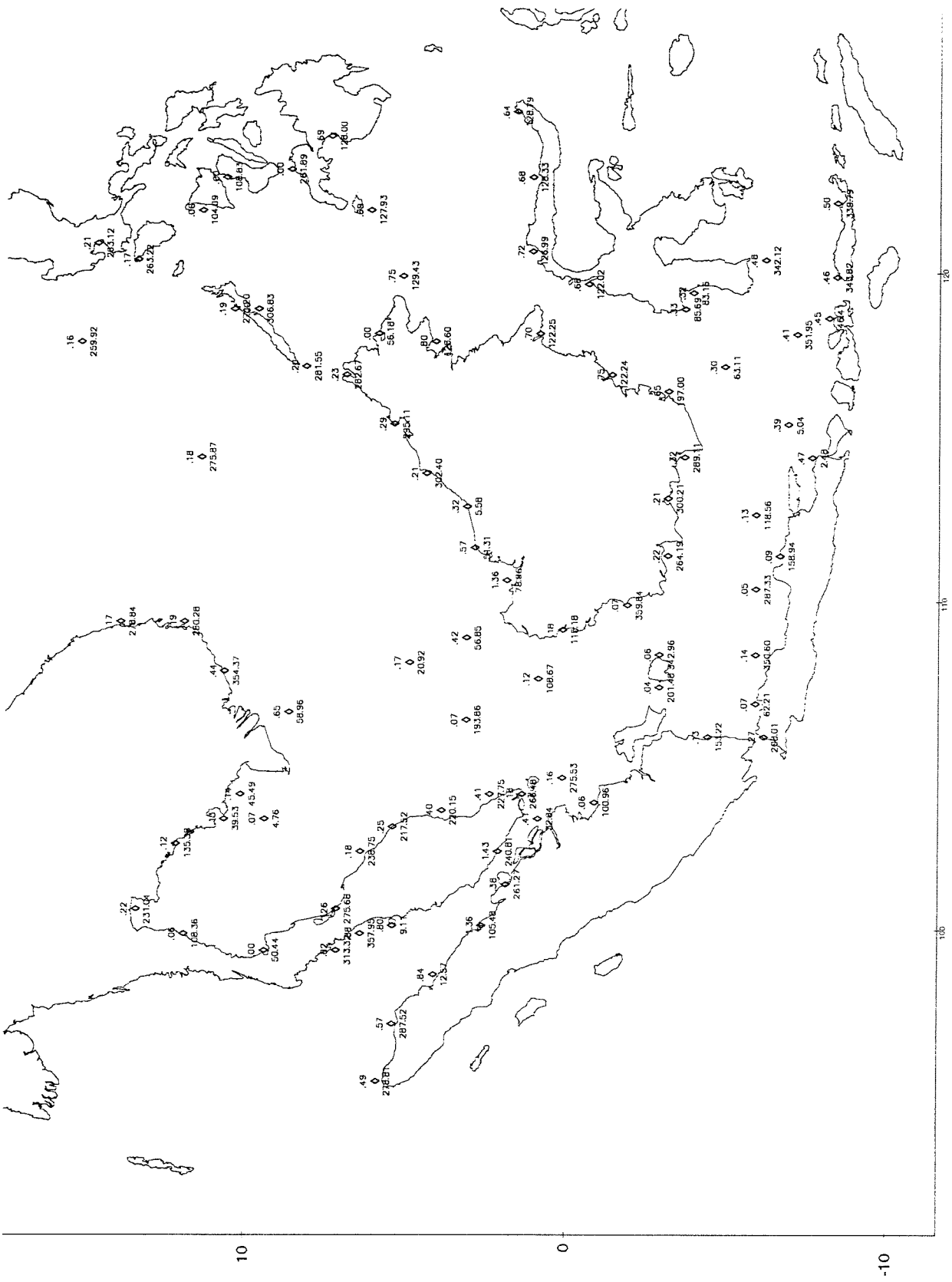

Tidal Constituent M2, in selected water level stations
Computed amplitude (above)
Computed phase (below)

TRISULA

C02

South China Sea

DELFT HYDRAULICS

Figure A4.11

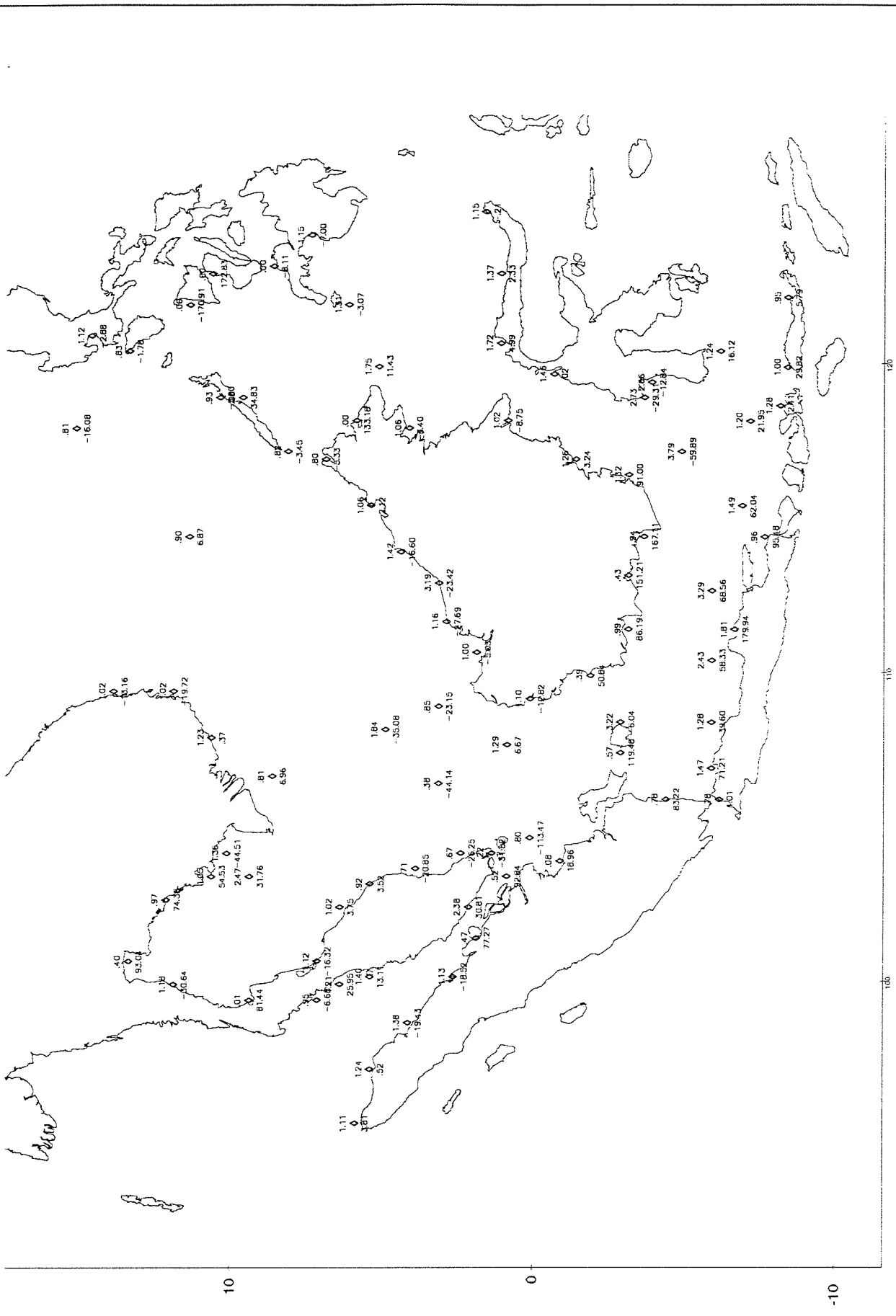

Tidal Constituent M2, in selected water level stations
Amplitude ratio (above, computed:observed)
Phase difference (below, computed – observed)

TRISULA

C02

South China Sea

DELFT HYDRAULICS

Figure A4.12

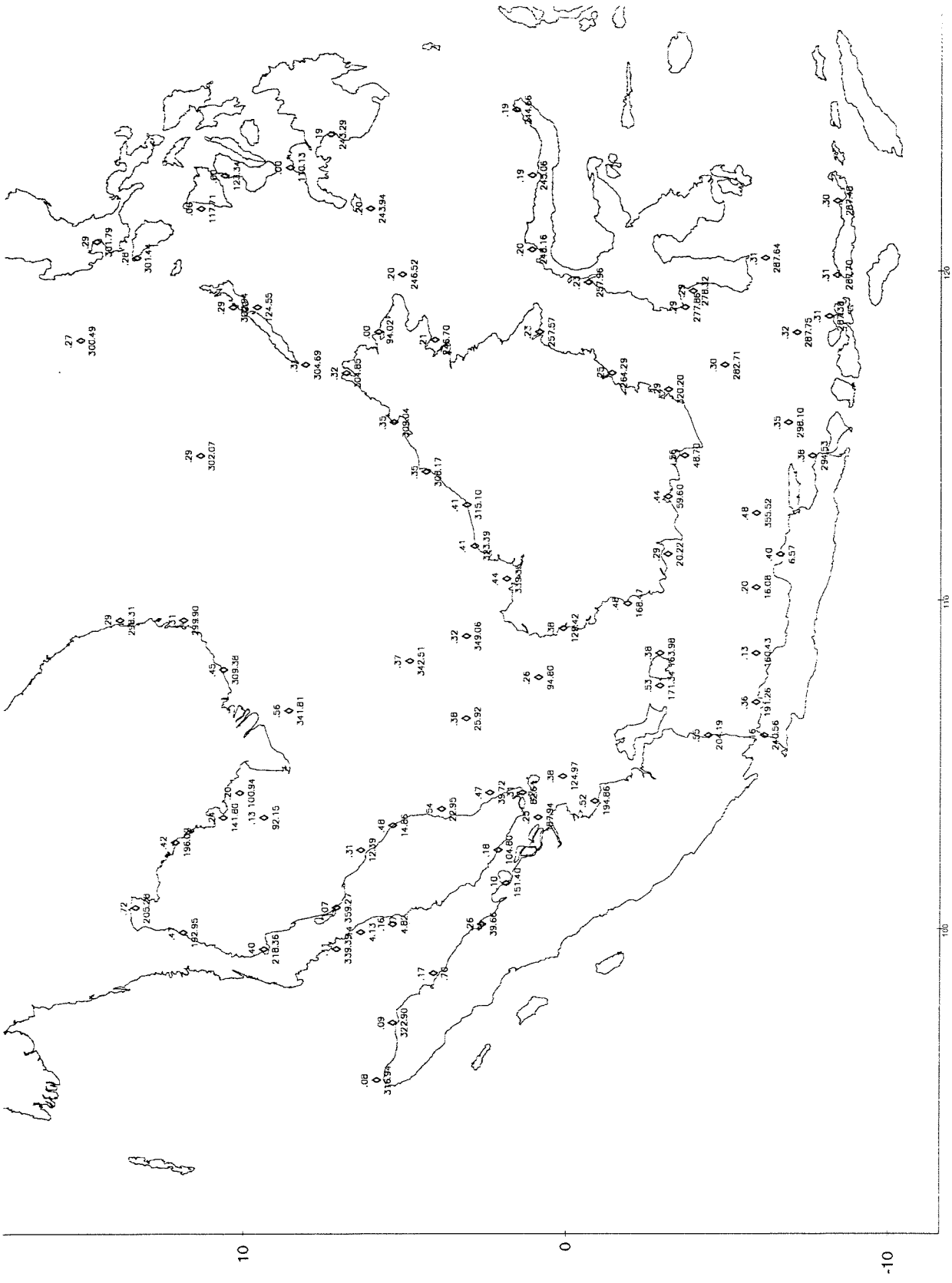

Tidal Constituent K1, in selected water level stations
Computed amplitude (above)
Computed phase (below)

TRISULA | C02

South China Sea

DELFT HYDRAULICS

Figure A4.13

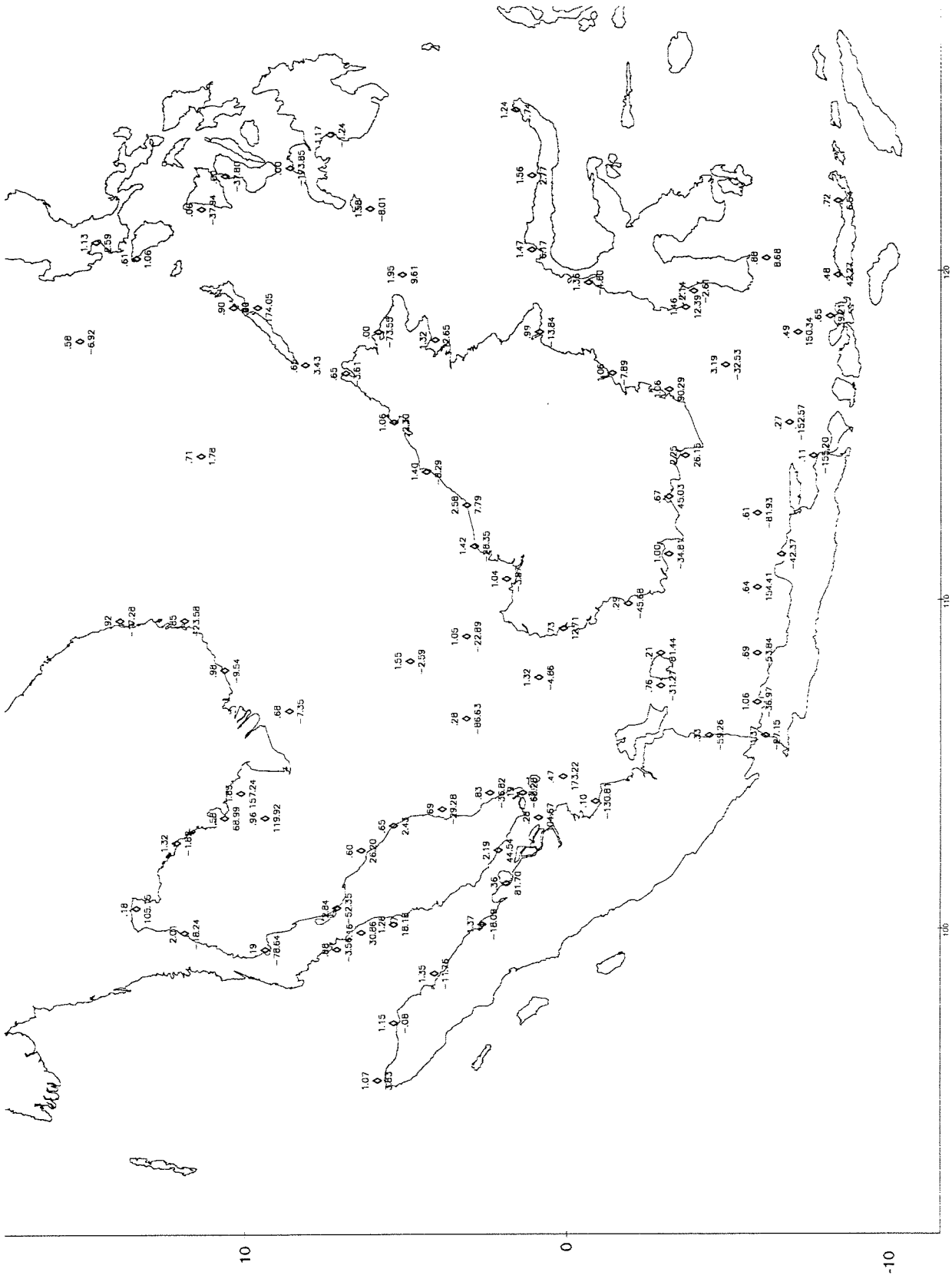

Tidal Constituent K1, in selected water level stations
Amplitude ratio (above, computed:observed)
Phase difference (below, computed – observed)

TRISULA | C02

South China Sea

DELFT HYDRAULICS

Figure A4.14

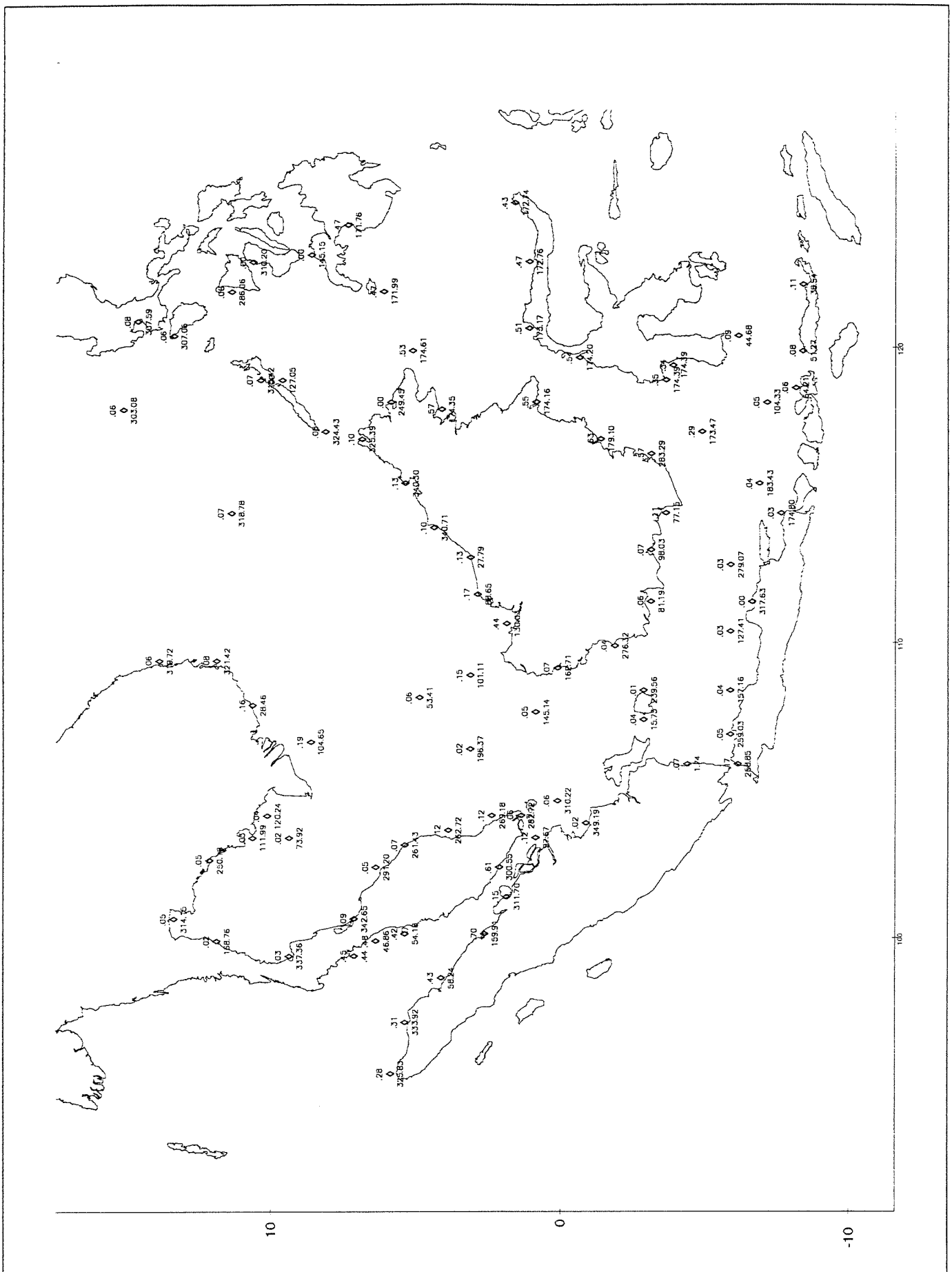

Tidal Constituent S2, in selected water level stations
Computed amplitude (above)
Computed phase (below)

TRISULA | C02

South China Sea

DELFT HYDRAULICS

Figure A4.15

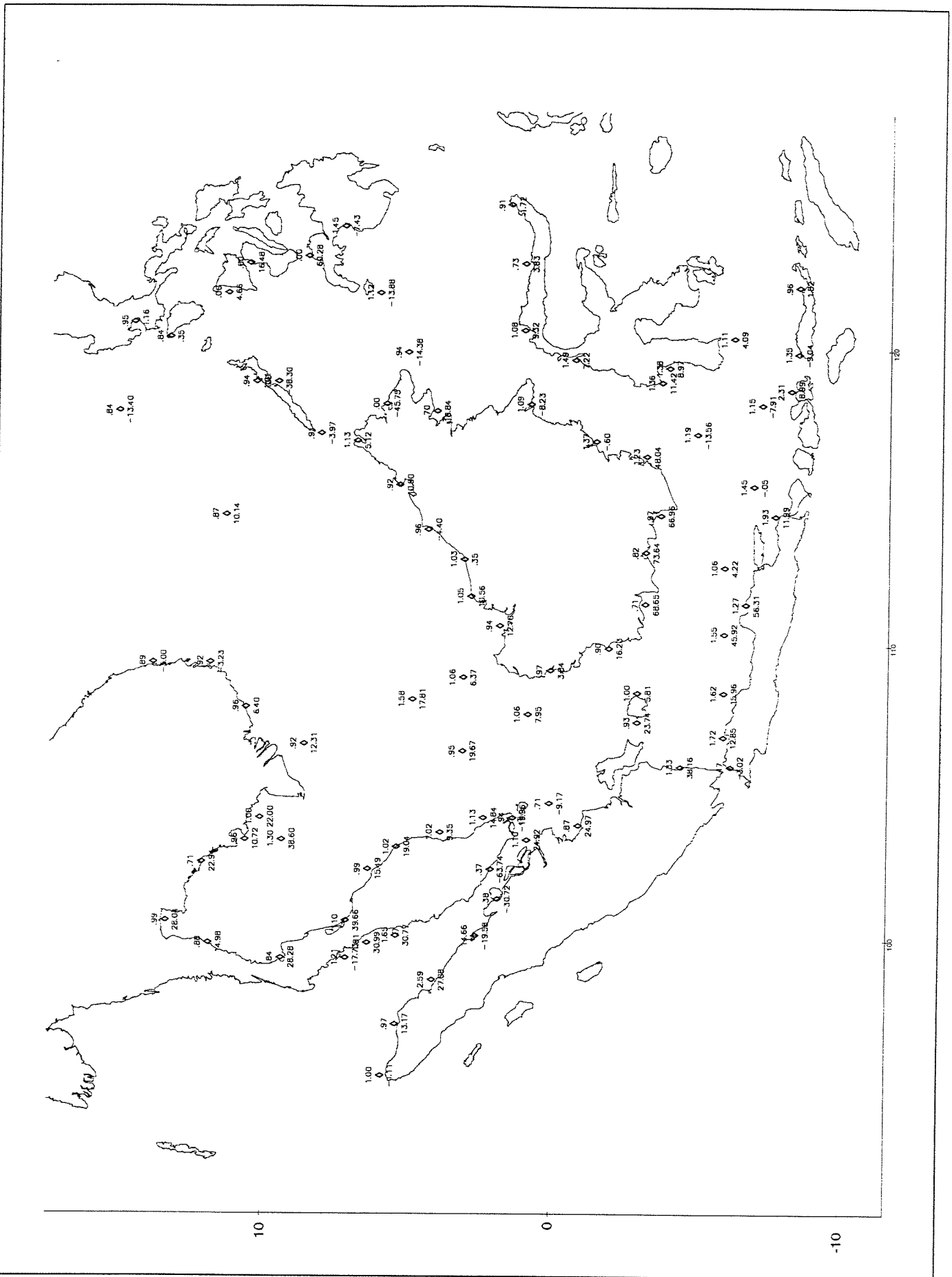

Tidal Constituent O1, in selected water level stations
Amplitude ratio (above, computed:observed)
Phase difference (below, computed – observed)

TRISULA	C02
South China Sea	

DELFT HYDRAULICS

Figure A4.16